FLUID MECHANICS OF THERMODILUTION IN CORONARY ARTERIES

WAQAR UL HASSAN

Submitted in Fulfilment of the Requirements for the Degree of
Master of Science in Mathematics (Research)

University of Glasgow
College of Science and Engineering
School of Mathematics and Statistics

31 January, 2017

Abstract

Cardiovascular disease is one of the main causes of death in the world and among various cardiovascular diseases, the coronary artery disease is considered to be the leading cause of death. Atherosclerosis is the primary cause of coronary artery disease. Different diagnostic methods have been developed for the assessment of coronary artery function. Coronary Thermodilution is one of the most recent methods used to find blood flow, temperature and assess resistance. A diagnostic coronary guidewire with a pressure and temperature sensor is used to measure temperature and pressure of blood simultaneously. For a continuous temperature signal, the rapid reduction in temperature and afterwards recovery in seconds creates a temperature curve which is displayed on the haemodynamic monitoring device.

The objectives of this study were to evaluate the thermodilution waveforms in order to understand microvascular disease of the heart. To investigate these thermodilution curves, a Matlab program was written to assess and to identify the key features of the thermodilution waveforms and different patterns of thermodilution curves were found.

In order to calculate the origin of the features of the double peaks and other thermodilution curves, a simplified computational model of tube with catheter was implemented in Fluent. We observed the temperature curves similar to the thermodilution curves when we took the measurement at the centre of the coronary artery and did not see any pulsatility due to the probe lies within the central axis and lies within the region of cold fluid and may be diffusion is too slow to absorb heat from the surroundings. Double peaks are found if the probe is off-axis. Stenosis is placed inside the coronary artery and the calculations were performed off-axis which resulted in the different shapes as we observed in the actual thermodilution data. Misalignment of the catheter may result in the errors of thermodilution data which may affect the health care cost.

Dedication

To my Mother and Father.

Acknowledgements

First of all, I would like to thank Professor Nicholas A. Hill, who was my supervisor throughout my career at the University of Glasgow; he gave me the opportunity to work with his team and introduced me to the fascinating field of computational fluid dynamics. I could not imagine having a better advisor and mentor for my MSc and without his knowledge, perceptiveness, and cracking-of-the-whip, I never would have finished. His time, encouragement, and guidance have been very important to me and to the research reported herein. I am particularly grateful to him for his continual patience and confidence in me. He has been available in every way as a resource, be it emotionally, socially, scholarly, or administratively. Without his encouragement and constant guidance, I could not have finished this dissertation.

I would like to extend my appreciation to Professor Colin Berry for helping and guiding me in my project as a cardiologist. He was always there to meet and talk about my ideas and has given new ideas to think and work on. Besides my advisor, I would like to thank Dr. David Corcoran for his valuable time and providing me data related to my project and to give particular thanks to Dr. Hao Gao, for his help and guidance in Fluent for making suitable velocity input functions and his support in Solidworks software for making 3-dimensional geometry which formed the basis of Chapter 5. Furthermore, I would also like to appreciate the advice, comments and suggestions of the students of applied mathematics group during the group meetings.

Special thanks goes to the Pakistan Air Force for sponsoring my higher education and giving me confidence and support. Without its support I would not be able to fulfil my dreams. This was the commitment of Pakistan Air Force which made me able to explore new horizons of advanced education and provided me the opportunity to exploit my intelligence and passion in a research project I desired the most.

Last but not least, I thank my family; my parents, for giving me life, for educating me, for unconditional support and encouragement to pursue my interests, even when the interests went beyond boundaries of language, field, and geography; and my fianceé, for listening to my complaints and frustrations and for believing in me.

Declaration

I declare that, except where explicit reference is made to the contribution of others, that this dissertation is the result of my own work and has not been submitted for any other degree at the University of Glasgow or any other institution.

WAQAR UL HASSAN

Contents

List of Tables

List of Figures

Chapter 1

Introduction

1.1 Introduction

Coronary heart disease (CHD) is one of the main causes of death throughout the world [1–3] and more than 73,000 people die in UK due to this disease every year [4]. The ratio of heart disease is more common in men than women and almost one out of six men and one out of ten women die due to coronary heart disease [4]. About 1% of visits have been noticed of patients having chest pain to the general practitioners [5,6], 5% to all emergency department and 40% to emergency admissions to hospitals [7]. It is estimated that about 2.3 million people living in the UK are suffering from CHD out of which 2 million people are affected by Angina, a chest pain of cardiac origin [4].

Angina happens due to insufficient supply of myocardial oxygen and is triggered by physical activity and stress. Sometimes angina is referred to obstructive coronary artery disease which may be due to the absence of flow limiting stenosis [8–13]. It is recommended by European clinical guidelines that the patients having more possibility of angina should be referred directly for invasive coronary angiography without any prior stress testing [1, 2]. Coronary disease severity is calculated with the help of coronary angiogram and most of the decisions like medical therapy, Percutaneous Coronary Intervention (PCI) or Coronary artery bypass surgery (CABG) [14], depend on graphical analysis and interpretation of coronary angiograms. These decisions may be inaccurate due to the individual's clinical judgement and interpretation of the coronary angiogram and may lead to misdiagnosis [15, 16]. Furthermore, it is difficult to make decision about the patients having multiple narrowings with the help of coronary angiogram because culprit stenosis identification and discrimination of flow limiting

from non-culprit flow disease is subjective and therefore unreliable [14–17]. Therefore, false interpretations of angiograms could result in wrong decisions, substandard health outcomes and forthcoming health care costs as these decisions are prognostically important [15–17].

Different diagnostic methods have been developed for the assessment of coronary artery function in recent years. New diagnostic possibilities have been provided by the guidewire based measurement of coronary blood pressure, temperature and resistance [18–21]. Guidewire technology has enabled the cardiologist to measure the lesion level ischaemia, coronary collateral supply and other parameters of microvascular function [21–23].

A diagnostic coronary guidewire with a pressure and temperature sensor is used to measure blood temperature and pressure simultaneously. In fact, by injecting a small (3 ml) volume of room temperature saline via the catheter into the heart artery, the mixing of the saline with the blood ($37\,^0C$) causes a transient reduction in temperature that is detected by the thermistor on the wire. This technique is known as coronary thermodilution. For a continuous temperature signal, the rapid reduction in temperature and recovery in the seconds afterwards creates a temperature curve. This thermodilution exponential decay curve is displayed on the haemodynamic monitoring device. In fact, this change in temperature is the inverse of flow velocity. The shape of the coronary thermodilution curve may also contain information as suggested by recent research [24, 25]. This research is aimed at quantifying the data (waveforms) using Matlab and providing biomarkers for clinical use, so that the disease could be specified and diagnosed easily.

1.2 Coronary Artery Disease

Sudden cardiac death is by far the most dangerous outcome of coronary artery disease and with the advancement of age it has become more common reason of death [26]. Sudden cardiac deaths, in the young, are mostly caused by hypertrophic cardiomyopathy (HCM), genetic arrhythmias and to a lesser extent, Wolf-Parkinson-White syndrome (WPW) [27–30]. An estimated 10,000 new patients of angina pectoris have been recorded every year [31]. Coronary artery disease starts developing with the formation

of pathological changes in the wall of one or more than one coronary arteries i.e. hardening of the arteries, which results into acute myocardial infarction or unstable angina pectoris [32].

1.3 Common Causes of Arterial Disease

1.3.1 Atherosclerosis

Acute coronary artery disease is mostly caused by atherosclerosis. Hardening of arteries starts from the inner most layer of wall, which is made of endothelial cells, storing of blood fats begin between the endothelial cells where inflammatory cells and macrophages ingest the fat. Lipids have been ingested by macrophages which burst and become so called foam cells. A fibrous mass starts developing around foam cell and forms a plaque. These atherosclerotic plaques appear in form of patches [33, 34]. Figures 1.1 and 1.2 are showing the accumulation of fats, cholesterol and other substances in the walls of arteries, making them less flexible and at last their breaking apart.

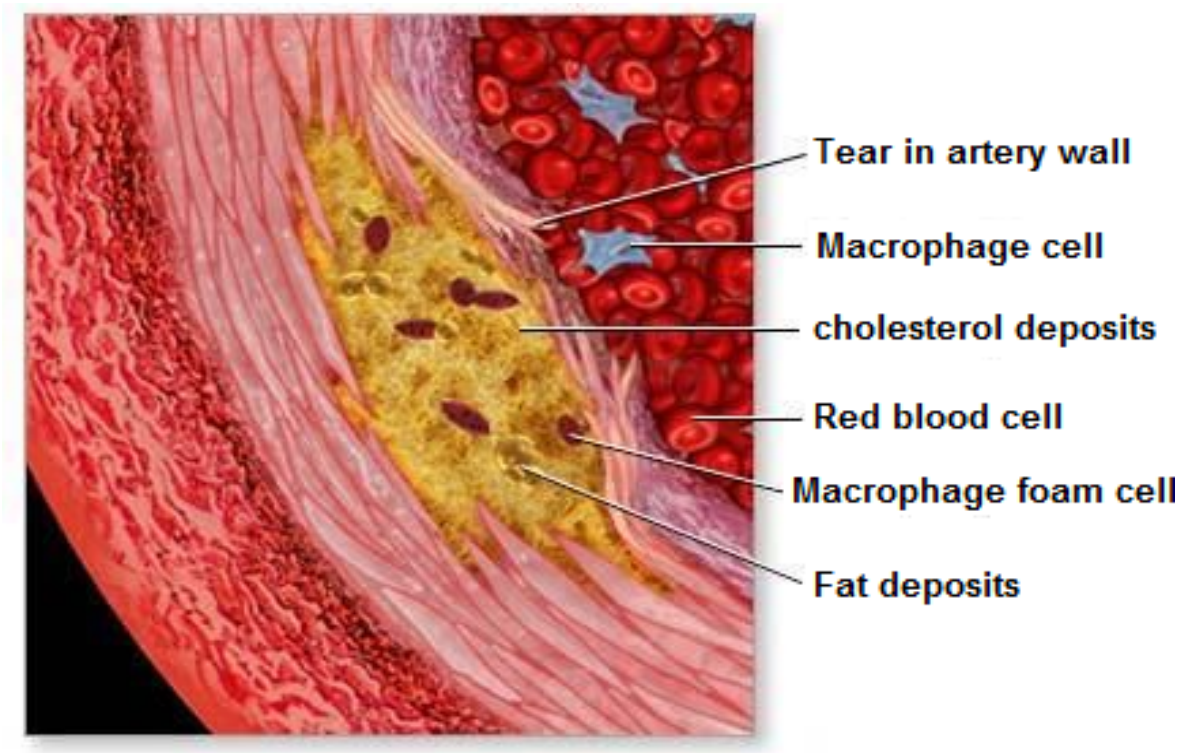

Figure 1.1: Cut-section of artery [35]

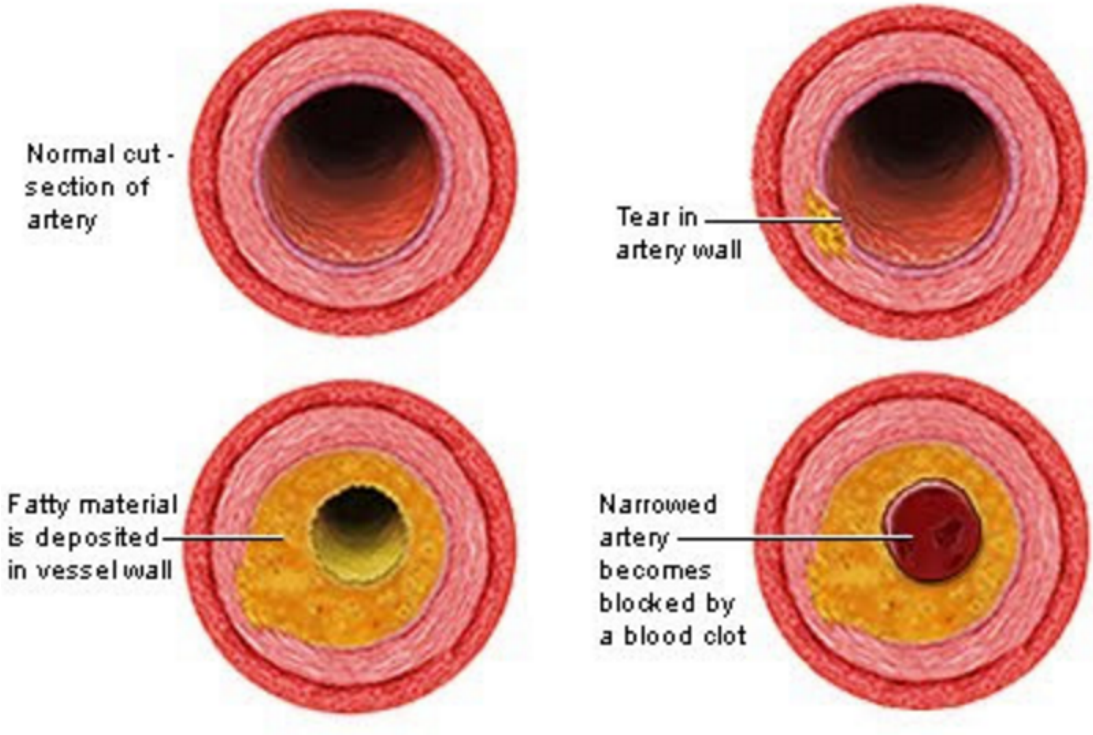

Figure 1.2: Fats deposited in artery [36]

1.3.2 Intimal Hyperplasia (Vein Graft Occlusion)

It is a phenomena associated with vein graft occlusion, reduced flow in the bypass graft due to reduced lumen and ultimate graft occlusion is attributed to the intimal hyperplasia (IH). In the first two months of implantation into the arterial circulation the bypass grafts remain open, development of IH takes place after two months of surgery [37]. It is the basic cause of vein graft atherosclerosis [37] because it blocks vein graft by abnormal proliferation of smooth muscle cells in the intimal layer of vein graft [37]. The failure of the vein and bypass graft due to intimal hyperplasia takes place between 2 and 24 months post-surgery. Intimal hyperplasia leads to vein graft atherosclerosis which leads to the occlusion of vein, it creates an emergency situation in which the CO has to be measured and often a resurgery has to be conducted to reopen the blockage. The factors triggering intimal hyperplasia are injury, inflammation, and hemodynamic factors [38]. Recurrent ischemic complaints due to vein graft occlusion have been reported by 30% to 50% [37].

1.4 Symptoms of Coronary Disease

The frequently found symptom is central chest pain and includes both unstable angina and acute myocardial infarction. Stable angina pectoris lasts for a few weeks without signs of worsening. Effort angina has been produced by physical or mental stress and ceases to exist when situation is relieved [31]. Variant angina is induced by contraction of an artery that lasts so long that heart muscles start suffering from shortage of oxygen. Variant angina can be induced even in resting position and its mixed types are not uncommon [31]. Fissuring or rupture of an atherosclerotic plaque in a coronary artery is the cause of the acute element of coronary artery disease [33]. Then the activation of thrombocytes and coagulation of blood leads to formation of a blood clot that completely or partially blocks the artery. On the complete or partial blockage of an artery that supplies blood, the ischaemia occurs and it leads to reduced availability of oxygen and nutrients. A gradual change towards cardiac death cell occurs in a blocked artery that depends on the degree of ischaema and how long it remains [39].

1.5 Diagnosis

Many tests are used to diagnose possible heart disease. The choice of which tests to be performed depends on the patients risk factors, history of heart problems, and current symptoms. Usually diagnosis begins with the simplest test and progresses to the more complicated ones. According to American Heart Association there are different methods for diagnosing heart disease and cardiac output monitoring, the non-invasive methods, e.g. ECG, oesophageal Doppler, trans-oesophageal echocardiography, lithium dilution, pulse contour, partial CO_2 rebreathing and thoracic electrical bioimpedance whereas invasive methods are Fick method and thermodilution [40].

1.6 Computational Fluid Dynamics

The properties and flow of blood are very vital areas to be focused while studying the atherogenesis and intimal hyperplasia haemodynamics [41]. Numerical simulations of fluid flow have been carried out in computational fluid dynamics. Simulated outputs are the result of numerical solution of the differential equations which have been derived from physical conservation laws for flows [42]. CFD is used to resolve many problems concerned to haemodynamics. Apart from this, CFD can also be used in scrutiny of

time-varying, 3-D flow patterns in a complex geometrical model. CFD also helps in studying atering Model and flow parameters like inlet velocity and wall conditions. If boundary condition information is correct, high resolution results can be produced by CFD [42].

Performing a Computational Fluid Dynamics (CFD) analysis is the option other than constructing a physical experiment. It generally involves taking a meshed geometry and simulations resembling the real world flow are created by using CFD software package. There can be diversified differences between the use of CFD analysis and physical experiment when any type of flow is analysed [42, 43]. Despite all the advancements of CFD Package, there are certain limitations of the same because it cannot deal with the physical variables playing a role in a real world simulation. The results of CFD present the idealized state of fluid flow behaviour in contrast to their actual behaviour in the real world simulation. Resultantly, a variation is found in the results produced in a physical experiment and the those found in CFD analysis. Hence, in order to authenticate the validity of CFD analysis, both results found in CFD simulation and during actual experiment are generally compared [42, 43].

However, benefits of CFD analysis are more as compared to that of physical experiment because the former is much cheaper and faster and various CFD Models can be run at a time due to its lesser cost. The saving of time and cost at the same time allows applying CFD approach in the conduct of research questions requiring substantial data for analysis of various problems. The analysis of CFD results is much easier than those of experiment. Moreover, CFD enables to monitor detailed physical behaviour of flow at any location within the flow making it easier to observe the effects of geometry on the behaviour of flow. Those physical properties which are difficult to be analysed experimentally, can easily be carried while using CFD such as turbulance, shear stress and flow patterns of stream lines [43].

A solid 3D-coronary artery was designed in CFD software to measure the blood flow, pressure and temperature at different positions in the coronary artery. The purpose of using CFD analysis was to identify the reasons of different shapes of the thermodilution curves.

1.7 Purpose of the Study

Thermodilution is used clinically to assess coronary circulation after an adverse event but is assessed visually. The principal aim of this research project is to quantify the data (waveforms) using Matlab and provide biomarkers for clinical use. For this purpose, we will

1. Assess the shape of the coronary thermodilution waveforms in patients with ST-elevation Myocardial Infarction, NSTEMI and stable angina as given in Section 4.4.

2. Determine whether there are different patterns of thermodilution curves as given in Section 4.6.

3. Relate the shape of the coronary thermodilution waveforms to the coronary physiology parameters used by clinicians (CFR, FFR, IMR) as given in Section 4.4.

4. CFD studies of flow in a simplified model artery undergoing the thermodilution procedure as given in Chapter 5.

Chapter 2

Background

2.1 Cardiovascular System

The cardiovascular system consists of the heart and circulatory system. The heart works as a pump to keep the blood circulating in the body. It expands and contracts to send and receive blood respectively. The components that take part in distribution and receiving of blood are arteries, capillaries, venules and veins [44]. There are three types of blood vessels: arteries, veins and capillaries. Blood is carried away from the heart by arteries and it is sent back to the heart by veins. Capillaries are small blood vessels used for transferring oxygen from the blood to the body tissues. The walls of blood vessels are elastic and porus, due to these characteristics they can expand and contract and can transfer nutrients from the blood to the surrounding tissues [45].

Cardiovascular system has two major circulatory paths; the system circulating blood between the heart and lungs is pulmonary circulatory system and the system carrying blood away from the heart, through the body and then bringing it back to the heart is called systemic circulatory system. Pulmonary veins provide oxygenated blood to the left atrium which is then transferred to the left ventricle. Left ventricle transfers blood to the largest artery of the body aorta and veins bring back the blood to the right atrium [44].

The continuous expansion and contraction of heart creates pulsatile blood flow, moving blood through the body in form of pressure waves. In each heartbeat heart completes a cardiac cycle, which consists of two types of motions; the contraction of heart is called systole whereas expansion is called diastole [44].

2.2 Blood

An average human body contains more than 5 litres of blood, it transports oxygen and nutrients to all living cells of the body. Blood is a precious fluid, providing immune cells to the infections and adopting to the body needs of a man; platelets help to form a plug in a damaged cell of body to prevent bleeding. Blood has three types, the straw coloured fluid is called plasma, it is mainly water but contains proteins (used for clotting), sugars and fats that form 60% of the blood by volume. The other types are red blood cells, white blood cells and platelets. Red blood cells are responsible for transport of oxygen, their deficiency causes a condition called anemia. White blood cells play a vital role in body's immune system; they detect the signals of any damage to the body and begin healing process. An increased risk of bleeding is caused by the thrombocytopenia, a condition of low level of platelets and high levels of platelets (thrombocythemia) can increase the risk of formation of blood clots which can block blood supply to heart and brain causing heart attack and stroke respectively [46].

2.3 Morphology of Coronary Arteries

The two coronary arteries emanate from the ascending aorta. Further LCA is divided into the left anterior descending (LAD) and circumflex artery (CX). The blood is provided to the heart muscles by these arteries and myocardial infarction or heart attack are due to the blockage in these arteries [47]. Figure 4.25 shows the different types of coronary arteries.

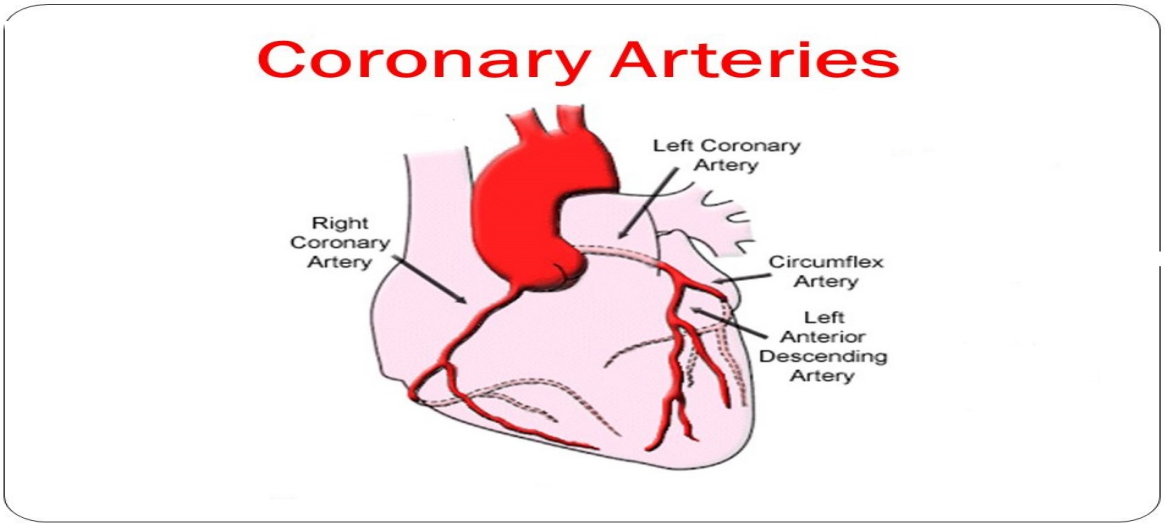

Figure 2.1: Coronary Arteries [48]

Numerous studies had been conducted to analyse the morphology of the coronary arteries. Arterial wall consists of three main layers of tissues as shown in Figure 2.2. These are known as tunica intima, tunica media, and tunica adventitia [49, 50].

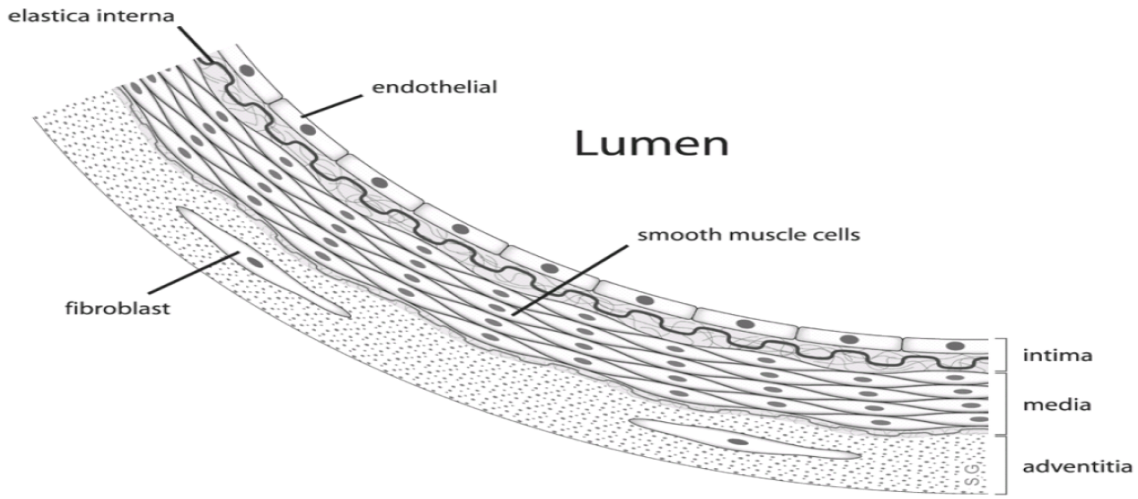

Figure 2.2: Anatomy of arterial wall [51]

2.3.1 Tunica Intima

This is the inner layer which is directly in contact with the blood flow and covers the complete surface of arteries. It is made up of an elastic membrane and endothelial cells and its function is to exchange the compounds between blood and underlying tissues [49, 50].

2.3.2 Tunica Media

This middle layer consists of smooth muscles which are capable to contract and their function is to mediate vasoconstriction and vasodilatation so that the blood pressure is maintained [49, 50].

2.3.3 Tunica Media

This is the strong outer layer which is composed of mostly fibroblasts [49, 50].

2.4 Right Coronary Artery

Right coronary artery has a large right dominance when three branches arise beyond the distal bifurcation of the right coronary artery (RCA) which supplies the septum and the

inferior-posterior walls. The three branches of RCA are the right posterior descending artery, which supplies the inferior septum, the second branch is right inferior branch which supplies the infero-posterior wall. The third branch is called the right posterior and it supplies the infero-posterior wall [52]. Figure 2.3 shows the branches of large right dominance of right coronary artery.

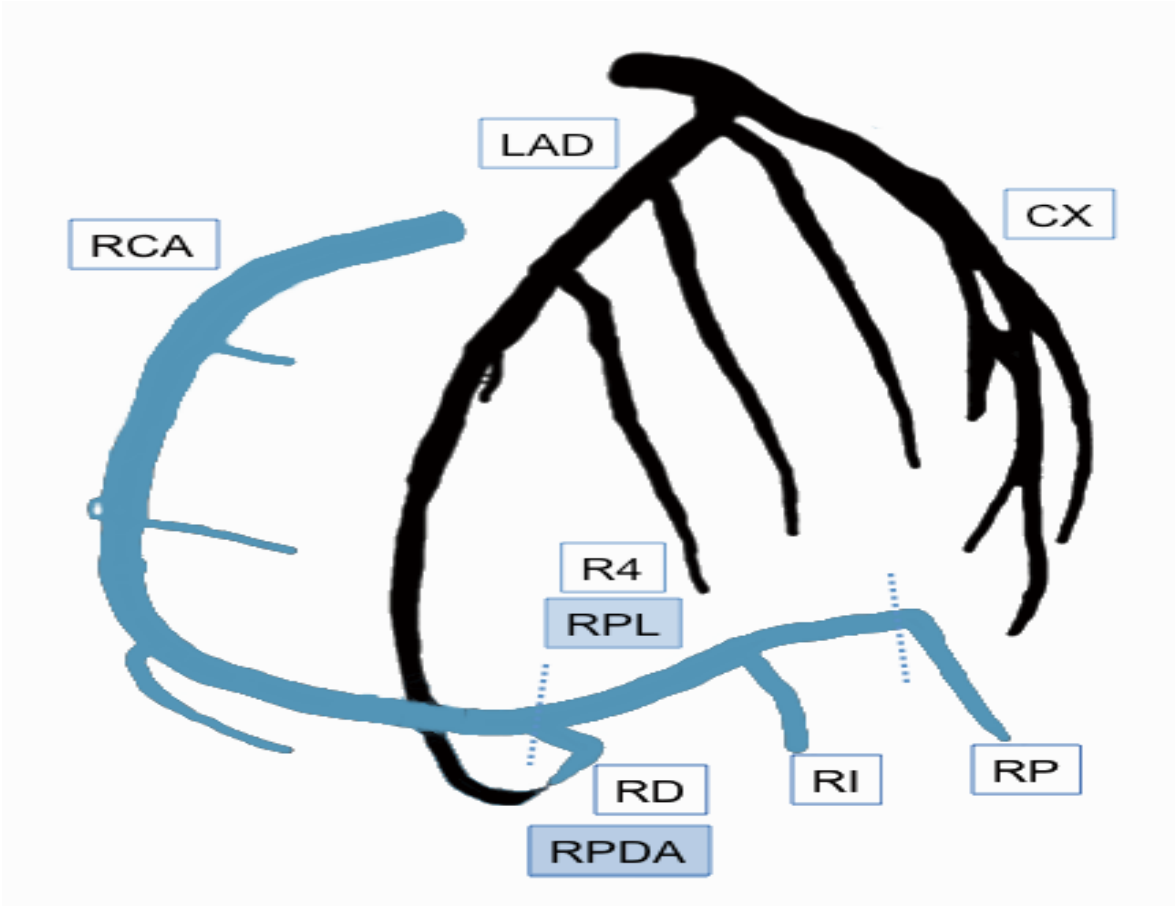

Figure 2.3: Large right dominant coronary artery [52]

2.5 Left Anterior Descending Artery

At first it passes behind the pulmonary artery and then comes between that vessel and the left auricula. There it reaches the anterior interventricular sulcus then it descends to the incisura apicis cordis. It branches out into two parts, septals and diagonals. This can be divided into four segments (L1, L2, L3 and L4). At 90^0 from the surface of heart, septal originates from LAD, supplying the intraventricular septum. The three largest septal arteries that branch from LAD are S1, S2 and S3.The 2nd branch of the LAD runs along the surface of the heart .The lateral wall of the LV and the anterolateral papillary muscle have been supplied by diagonal arteries. The three longest diagonal

arteries are D1, D2 and D3 [53]. The septal and diagonal branches of the LAD are shown in Figures 2.4 and 2.5.

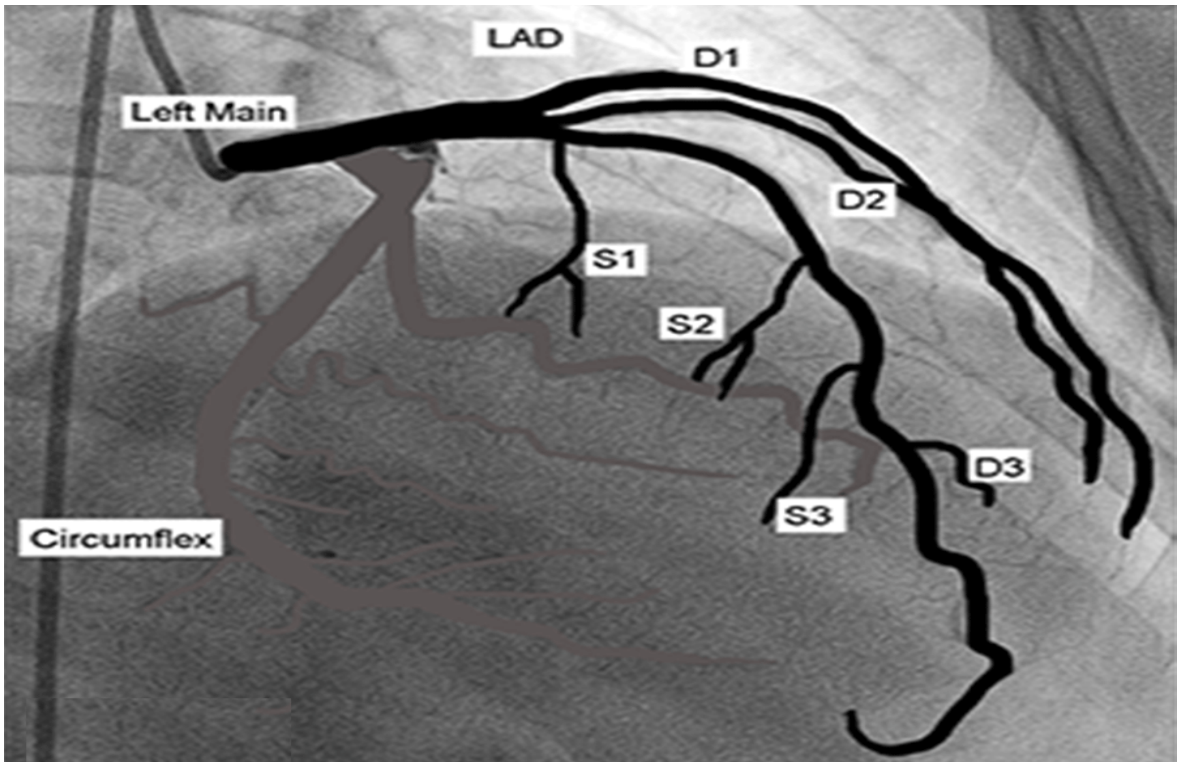

Figure 2.4: Left Anterior Descending Artery [53]

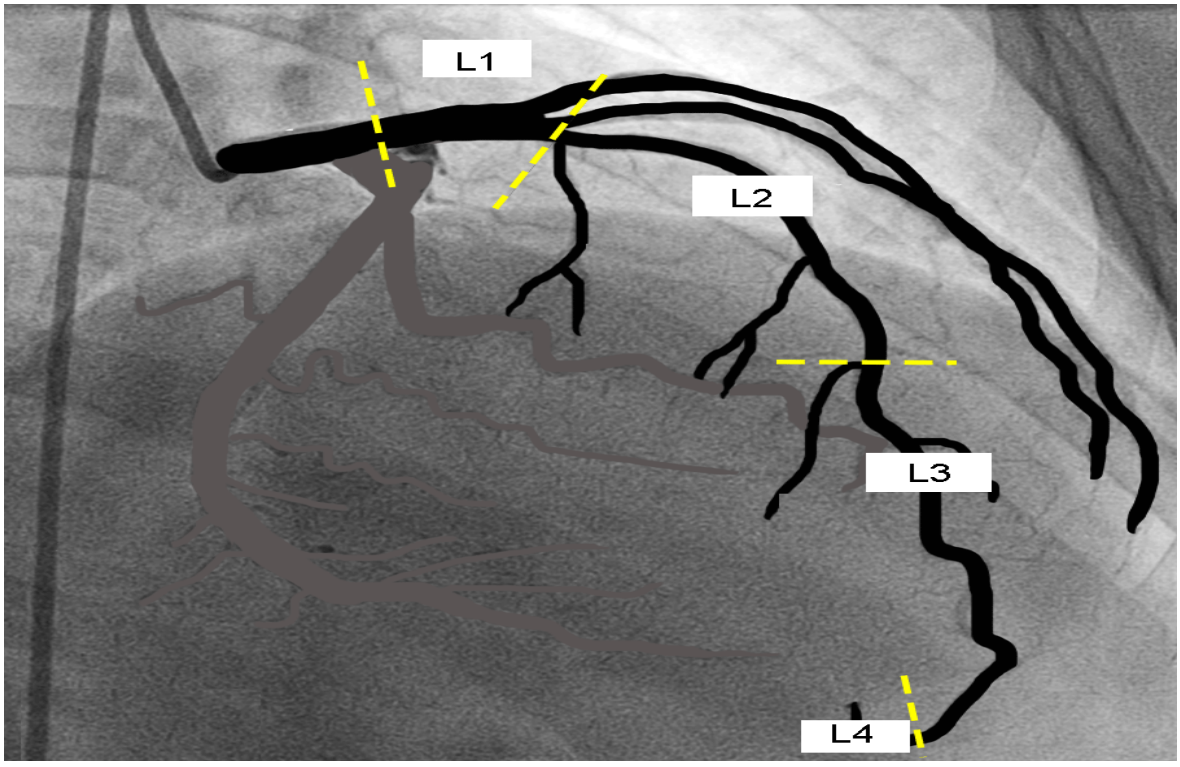

Figure 2.5: Different segments of the LAD [53]

2.6 Circumflex Artery

From the left coronary artery branches off the circumflex artery; it supplies to the left atrium. A variable number of left marginal branches is given off by the circumflex artery to supply the left ventricle. The largest of all branches is the terminal branch; the posterior wall of the left ventricle and the posterior papillary muscle of the bicuspid valve are more likely to be supplied by the circumflex artery through the AV sulcus [54].

2.7 Blood Pressure

The contraction of the left ventricle generates an axial pressure gradient. The pressure gradient along vessels drives the circulation of blood in the whole body and transports oxygen to every part of it. The oxygenated blood passes through arteries which are elastic and can with stand even high pressure but for the healthy arteries blood pressure should remain within a healthy limit [55]. High blood pressure means higher pressure of blood on the vessels. Blood pressure consists of two numbers, systolic and diastolic; systolic reading is the pressure measurements when heart beats and diastolic is when the heart rests. A blood pressure more than 139 mmHg systolic or 89 mmHg diastolic is considered as a high blood pressure. High blood pressure increases the chances of a heart attack, angina, heart failure, kidney failure and peripheral artery disease [56].

High blood pressure damages the arteries and increases the work load of heart, work load often leads to enlargement of heart and eventually a damage to the whole circulatory system. Atherosclerosis, the hardening of arteries due to deposits of fats, is also a condition caused by high blood pressure [55].

2.8 Angina

Angina is a symptom of an underlying problem; when heart muscle does not get enough oxygen-rich blood, the person feels pressure in chest which indicates a coronary heart disease (CHD). The pressure and pain is often felt in shoulders, arms, neck, jaw or back. It usually happens when one or more of the coronary arteries are blocked, which is called ischemia [57].

Besides coronary arteries blockage, angina can be a sign of coronary microvascular disease (MVD). It damages the smallest coronary arteries [52]. Angina has many

types, three of which are stable angina / angina pectoris, unstable angina and variant (Prinzmetal) angina [57].

2.8.1 Stable Angina

This situation is created by an imbalance between the oxygen rich blood the heart requires and the amount available. It happens every time due to same causes and its symptoms are also same every time, therefore, it is called stable angina. Rest and oral medication relieve the pain. Stable angina is a signal alarming about heart disease, a doctor should be consulted in case of angina attack. If there occurs any change in the symptoms and patterns then this can progress to unstable angina [57, 58].

2.8.2 Unstable Angina

It can be a changed form of stable angina. This occurs frequently and occurs when person is at rest; it lasts for a longer period. Oral medications often relieved the pain but it is an alarm of a heart attack and intense care is needed for medical treatment [57, 58].

2.8.3 Variant Angina (Prinzmetal's Angina or Coronary Spasm)

A coronary artery can lead to spasm which causes blockage of blood flow to the heart muscle. About two third of the people having variant angina have spasm at the site of blockage. This angina often happens when a person is taking rest and the risk of disease increases if one has a coronary artery disease or one is using stimulants or drugs. A heart attack can be a potential danger when coronary artery spasm is intense and lasts for longer time [57, 58].

2.9 Stenosis

Stenosis is used to describe an abnormal narrowing in a blood vessel or other tubular organ, stricture is also a name given to it. When narrowing is the result of contraction of smooth muscles, it is called a stricture. When narrowing is the result of lesion which reduces the space of lumen (e.g. atherosclerosis), it is called a stenosis [59]. Unusual blood sounds resulting from the turbulent flow in the narrowed blood vessel is associated with the vascular type of stenosis. A stethoscope can help detect this

sound. Beside other causes, atherosclerosis is the biggest cause of stenotic lesions in arteries. Vascular stenotic lesions include the intermittent claudication, Angina, and Carotid artery stenosis. Heart valves suffer four types of stenosis, pulmonary valve stenosis, Mitral valve stenosis, Tricuspid valve stenosis and Aortic valve stenosis [60]. Figure 2.6 shows Coronary Stenosis in which a coronary artery has become partially blocked by cholesterol or fat [61].

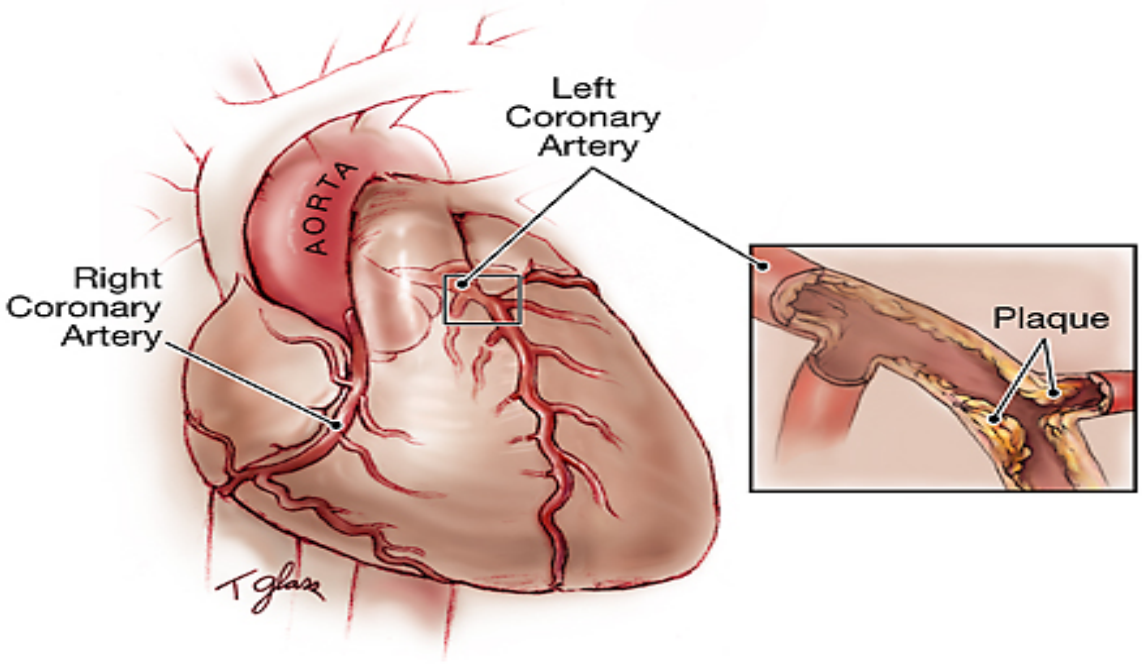

Figure 2.6: Left Coronary Artery Stenosis

2.10 Non-ST-Segment Elevation Myocardial Infarction

Non-ST Segment Elevation Myocardial Infarction (NSTEMI) is a medical emergency just like STEMI. It happens when a plaque ruptures in a coronary artery. The ruptured plaque partially blocks the artery and the heart muscle supplied by the artery starts dying; in STEMI the cardiac enzyme blood tests are abnormal, which indicates that some heart muscles have actually been damaged. The patient of NSTEMI has greater risk of a "full" myocardial infarction [62]. The electrocardiogram of NSTEMI does not show any change in the ST segment elevation. Patient suffering NSTEMI tests positive for a protein troponin which is released by the heart muscle which is damaged [63]. The

diagnosis of NSTEMI can be made when a patient has symptoms of unstable angina and non ST-segment elevation but has troponin in blood [63].

2.11 ST-Segment Elevation Myocardial Infarction

When one of the arteries supplying blood to the heart muscles is completely blocked, a serious heart attack is caused, which is called ST-Elevation Myocardial Infarction. It is often a result of atherosclerosis. Patients suffering STEMI have greater risk of arrhythmias like ventricular fibrillation causing sudden cardiac arrest. Cardiopulmonary resuscitation (CPR) and defibrillation, a shock is used to restore the heart rhythm of the patient [64]. STEMI causes a full- blown heart attack and due to its seriousness, it is called STEMI alert. This heart attack has a particular EKG heart-tracing pattern [65]. ST-elevation is an abnormality detected on the 12-lead ECG [64] as shown in Figure 2.7.

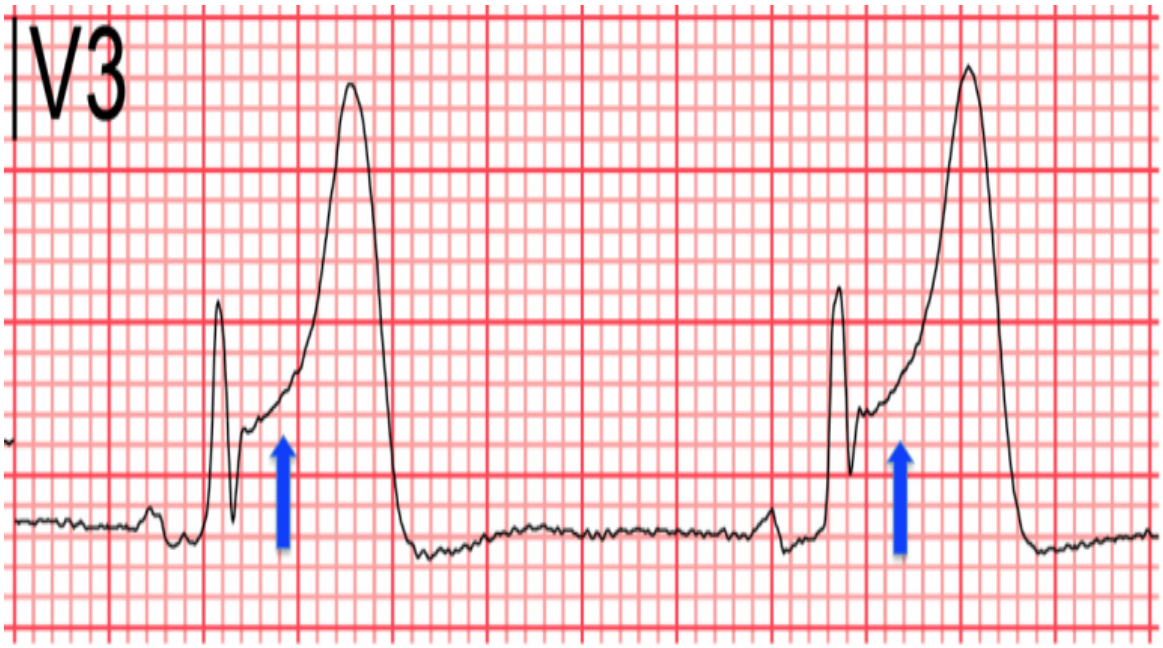

Figure 2.7: ST-Segment Elevation Miocardial Infarction [64]

2.12 Percutaneous Coronary Intervention

This process is used to improve blood flow to the heart, it is a non-surgical procedure and requires cardiac catheterization. A catheter tube and injection of contrast dye is inserted into the coronary artery; this method is used to unblock narrowed or blocked coronary arteries. It is also helpful in reducing damage after a heart attack. During

PCI, the patient stays awake. The patient receives medicines through an intravenous (IV) line in arm to prevent blood clots. A catheter is inserted into a blood vessel, live x-ray helps the doctor guide the catheter into the heart, where doctor injects special contrast dye which highlights the blockage. After locating the blockage, the doctor inserts another catheter and inflates a balloon at the tip of the catheter to unblock the blockage and then put a stent to keep the artery opened. PPCI and STEMI are associated with microvascular damage e.g. due to oedema and microvascular spasm [66]. The purpose of this study was to assess the thermodilution waveforms of three groups of patients with different haemodynamic conditions, i.e. ST-elevation Myocardial infarction (STEMI), Non-STEMI and stable angina, and divide them into different groups on the basis of waveforms.

Chapter 3

Cardiac Output Measurement

Cardiac Output (CO) monitoring is an important tool for measuring cardiac output in critically ill patients in whom large fluid shifts are expected along with bleeding and haemodynamic instability [67]. An ideal CO should be continuous, minimally or non-invasive, reproducible, cost effective, have fast response time and reliable during various physiological states [68]. There are various methods of CO monitoring based on Fick's principle, thermodilution, Doppler, pulse contour analysis and bioimpedance. Each method has its own merits and demerits.

3.1 Non-Invasive Methods

3.1.1 Electrocardiogram

According to the American Heart Association, electrocardiogram is the most commonly used non-invasive method to record the electrical activity of the heart but up to half of people suffering from angina or ischemia have normal ECG. The record of depressed or horizontal ST wave by Electrocardiogram suggests some blockage and existence of artery disease even if there is no angina present but this wave pattern can occur even without heart problems. The most important wave patterns in diagnosing and determining heart disease are ST elevations and Q waves. ST segment elevations imply that an artery to the heart is blocked, however, they do not always a sign of heart attack [69].

According to the American Heart Association, echocardiogram uses ultrasound images of the heart. It is used to identify whether there is damage to the heart muscle and the extent of heart muscle damage. But ECG shows even in the asymptomatic people

the characteristic signs of Hypertrophic cardio myopathy [70], long QT-syndrome [71], short QT- syndrome, arrhythmogenic right ventricular cardiac myopathy [72], Brugada syndrome [73], early repolarization [74] or Wolf-Parkinson-White syndrome [75]. Figure 3.1 shows the ECG tracing and equipement used for the measuring cardiac output.

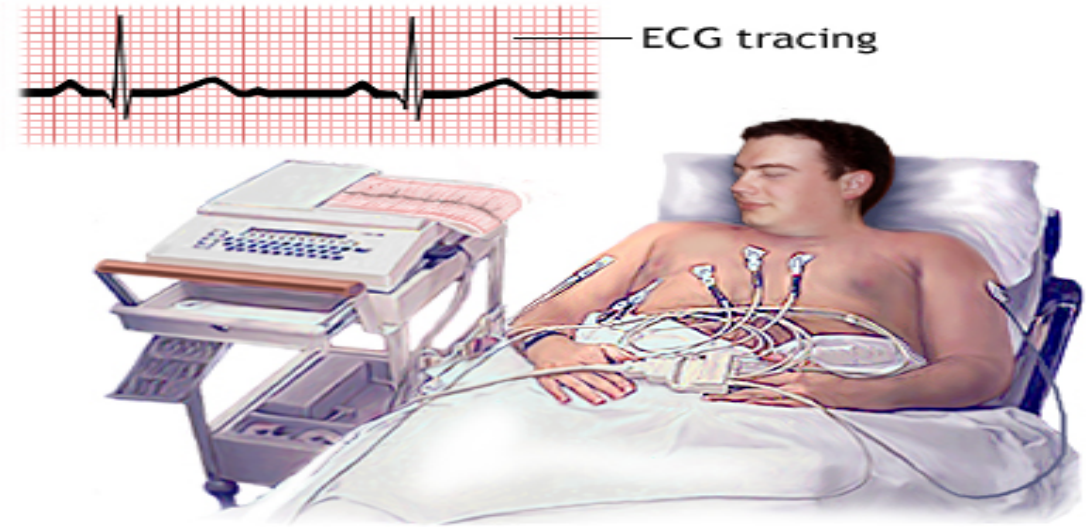

Figure 3.1: Electrocardiogram (ECG) [76]

3.1.2 Pulse Power Analysis

The principle that change of blood pressure about the mean is directly related to SV is the base of this method. The accuracy of this method is affected by many factors like wave reflection, compliance of the arterial tree, aortic systolic flow and dampening of the transducer [77]. This minimally invasive technique was first described in 1993 [77]. In venous line, a bolus of lithium chloride is injected and arterial concentration is find by thinning blood across disposable lithium sensitive sensor having an ionophore selectively permeable to Li. The calculation of CO is based on the dose of Li and area according to the concentration time circulation [78]. Pearse et al, after studying this method revealed fewer complications [79].

3.1.3 Pulse Contour Analysis

Erlanger and Hooker first described this method in 1904 [80]. The basic principle on which this method is based is that the area lying under the systolic part of the arterial pressure waveform is proportional to the SV [81]. The area in this method is measured post diastole to end of ejection phase that is divided by aortic impedance measuring SV. SVV and pulse pressure variation is also measured by this method. The

maximum and minimum difference between the SV over the respiratory cycle is called SVV and the changes in preload with alteration in intrathoracic pressure produces this difference [81].

3.1.4 Esophageal Doppler

A flexible probe with transducer at the tip is used in this process. This flexible probe can be placed for longer periods in intubated patients. As it is presumed to be parallel to the descending aorta it measures flow at the midthoracic level. SV is measured by Doppler ultrasound. After obtaining an optimal flow profile the velocity of blood flow is determined from the shift in frequency of red blood cells. Ultrasound processor performs this action by using the Doppler equation [82, 83].

$$V = \frac{f_d\, c}{2 f_0 \cos\Theta}$$

V = velocity of blood, f_d = Doppler shift in frequency, c = speed of ultrasound in tissue ($1540\,\mathrm{m\,s^{-1}}$), f_o= initial ultrasound frequency, and Θ = the angle of ultrasound beam in relation to the blood flow. Figure 3.2 displays the nasal and oral positioning of oesophageal probe in relation to aorta [83].

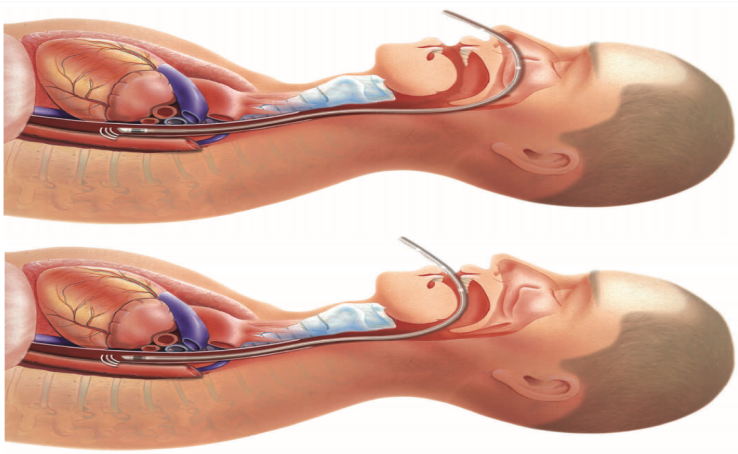

Figure 3.2: Nasal and oral positioning of oesophageal probe in relation to aorta [83]

A Meta analysis reveals ED as a reliable method having low bias and limited efficacy [84]. ED was also used in GDT and it showed greater improvement in SV and CO with faster recovery and shorter length of stay [85]. The use of ED has also decreased hospital and ICU stay with decreased incidence of gut mucosal perfusion [86]. This device was studied in patients undergoing OPCAB and it was found that in comparison

with PAC, ED cannot be used as a sole method for monitoring cardiac output [87].

3.1.5 Partial Gas Rebreathing

This method is used in patients under mechanical ventilation. Amount of CO_2 entering the lungs, at steady rate, is proportional to the cardiac output and the CO_2 exiting the lungs. CO is calculated according to this formula [88].

$$\text{Cardiac Output} = \frac{VCO_2}{C_vCO_2 - C_aCO_2}$$

VCO_2 is a Carbon dioxide elimination and is calculated by adding the product of carbon dioxide concentration and flow during each breathing cycle and C_vCO_2 and C_aCO_2 represent mixed venous and arterial carbon dioxide content respectively. Its major limitation is requirement of tracheal intubation with fixed ventilator setting. It does not produce accurate results in patients suffering severe chest trauma, significant intrapulmonary shunt, high CO states and low minute ventilation [88]. Thus, its use as compare to PAC is limited.

3.1.6 Thoraic Bioimpedance

This method was first used by astronauts in 1960s [89]. In this method the thorax is considered as a cylinder filled with fluid with specific resistivity. The electrical resistance of the thorax to a high frequency is measured by it [88]. However, many limitations affect its accuracy. Inaccurate readings in the post operative periods have been found due to presence of sternal wires and orarrythmia [90]. Furthemore, it has been found as trend analysis monitor rather than a diagnostic one [91].

3.1.7 Thoracic Bioreactance

The changes in the phase of electrical voltage signal to the current applied across the thorax have been analysed in this method. Two dual electrodes are placed on either side of the thorax. One electrode transmits sine-wave high frequency (75 kHz) current into the body and the other electrode is used by the voltage input amplifies. The final value will be found by the mean of two [92]. Good correlation has been found between this method and PAC with minimal bias [90].

3.1.8 Endotracheal Cardiac Output Monitoring (ECOM)

Electrodes are attached to endotracheal tube shaft and cuff and current is passed through them. Current passes from electrode on the shaft of endotracheal tube (ETT) and change in impedance secondary to aortic blood flow is detected by electrode on the cuff of ETT. Aortic blood flow affects impedance [93]. Its accuracy is affected by electrocautery and coronary blood flow is not calculated.

3.2 Invasive Methods

3.2.1 The Fick Method

Adolph Fick in 1870s founded the principles on which cardiac output determination is based. He proposed that the substance released by an organ is the product of the blood flowing through the organ and the difference between the same substance's arterial and venous values. In Fick method the oxygen is used as substance and lungs are taken as organ. To obtain the difference ($a - VO_2$), the arterial and venous oxygen contents are measured. Inspired minus expired oxygen content and ventilation rate can be used to calculate consumption of oxygen. This formula can help determining the cardiac output [94].

$$\text{Cardiac Output} = \frac{\text{Oxygen Consumption in ml/min}}{(a - VO_2 \quad \text{Difference in vol \%})}$$

$$\text{volume} \quad \% = \frac{1 \quad \text{ml} \quad \text{oxygen}}{100 \quad \text{cc}}$$

Normal (CaO_2) arterial oxygen content: 20 volume %

Normal (CvO_2) mixed venous oxygen content: 15 volume%

Normal (VO_2) oxygen consumption: 250 ml/min

Inserting these values into the equation:

$$CO = \frac{250}{(20 - 15) \times 100} = \frac{250}{5 \times 100} = 5000 \quad \frac{\text{ml}}{\text{min}} = 5 \quad \frac{\text{l}}{\text{min}}$$

Accurate measurement of oxygenation variables is required to calculate cardiac output with Fick equation. Large errors in the oxygen consumption results can be produced by slight errors in the content values. Ranging between (200-250) ml/min is the normal consumption of oxygen. (110-130) ml/min/m^2 is the indexed normal value of VO_2. Critically ill patients have abnormal consumption of oxygen and putting the normal

values of oxygen consumption in Fick equation can give out errors in cardiac output values [94].

3.2.2 Dye Indicator Dilution Method

Stewart in 1890s proposed the principles for the indicator dilution method and later Hamilton refined it. The basic principle of dye dilution is addition of a known concentration of an indicator to a body of fluid. After allowing the dye to adequately mix, an amount of fluid will be produced by the diluted indicator to which it was added. The concentration of indicator and dye in the blood after injecting a known sample upstream can be found by densimeter. A time-concentration plot can be found by taking continuous blood samples. Once the time-concentration plot has been found, the cardiac output can be found by using the Stewart-Hamilton equation [94].

$$\mathrm{CO} = \frac{I \times 60}{(C_m \times t)} \times \frac{1}{k}$$

where CO= cardiac output(I/min), I = amount of dye injected (mg)
60 = 60 sec/min), C_m = mean indicator concentration (mg/l)
t = total curve duration (sec), k = calibration factor (mg/ml/mm)
Indicator dilution curve is shown in Figure 3.3.

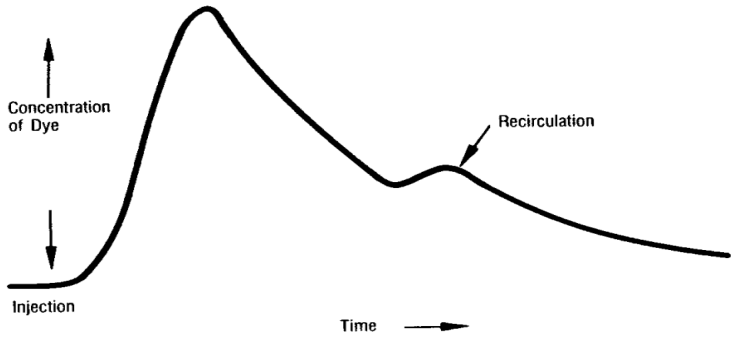

Figure 3.3: Indicator Dilution Curve [36]

3.2.3 Cardiac Output Measurement by Pulmonary Artery Catheter

Dexter developed Pulmonary artery catheter as a monitor to measure flow and pressure [95] and later Swan modified it [96] to measure central filling pressures and CO. Since 1970s, it is considered as gold standard monitor to measure CO [97]. However, many complications leading to embolism have been associated to it, like pneumothorax,

arrhythmia, infection, pulmonary artery rupture, valve injury, knotting and thrombosis [98, 99]. Furthermore, various technical errors are associated with this process like loss of injectate, variability of temperature, thermistor malfunction, clot over catheter tip, coiling of catheter or timing of injectate [98, 99].

3.2.4 Continuous CO Measurement by PAC

The modification in Pulmonary artery catheter (PAC) with copper filament in the catheter that remains in the right ventricle is called Continuous CO. The filament intermittently heats the blood in right heart and thermistor lying near the tip of catheter captures the resultant signals. Avoidance of repeated boluses thus reduces the infection risk and operator errors making CCO preferable over PAC [98]. The use of PAC involves both benefits and risks. Gore et al [100] revealed that the use of PAC increased mortality after myocardial infarction. Due to complications, many authors called for complete ban on the use of PAC [101]. Later on, the Escape trial showed functional improvement in patients of congestive heart failure due to the use of PAC guided therapy [102]. Despite risks PAC is still considered as the Gold Standard for monitoring of CO.

3.3 Theories of Thermodilution Method

3.3.1 Fractional Flow Reserve

FFR is a method of calculating an absolute value that is an indication of the pressure difference between the flow of blood downstream and upstream of the stenosis. Stenosis causes narrowing of the vessel which impedes the oxygen delivery to the heart muscles resulting in a drop in blood pressure. FFR accounts for the accurate region of lesions responsible for the ischemia in the blood vessels which are generally not detected or correctly evaluated by angiography or intravascular ultrasound [103].

FFR is independent of pressure changes and the interpreted pressure values are supported by the collateral flow and myocardial perfusion. The theoretical normal value of FFR equivalent to 1 is well defined and can be assigned to any patient without the need of a normal distribution data. The numerical index of FFR has been validated after several experiments and therefore has a reliable scientific basis [104].

The ratio of the perfusion pressures can be calculated by the following equation:

$$\mathrm{FFR}_{\mathrm{cor}} = \frac{p_d - p_w}{p_a - p_w}$$

where p_d is the distal coronary pressure in the stenotic artery and the p_a is the aortic pressure in the normal artery. p_w is the wedge pressure and its value is calculated when the balloon inflates and occludes the artery. The pressure stabilizes in front of the balloon after several seconds and the recorded pressure is the same as the distal branches of the occluded artery. $\mathrm{FFR}_{\mathrm{cor}}$ can only be calculated during percutaneous transluminal coronary angioplasty (PTCA) due to its direct relation to p_w [104, 105]. Figure 3.4 shows the position of measuring the distal and aortic pressure.

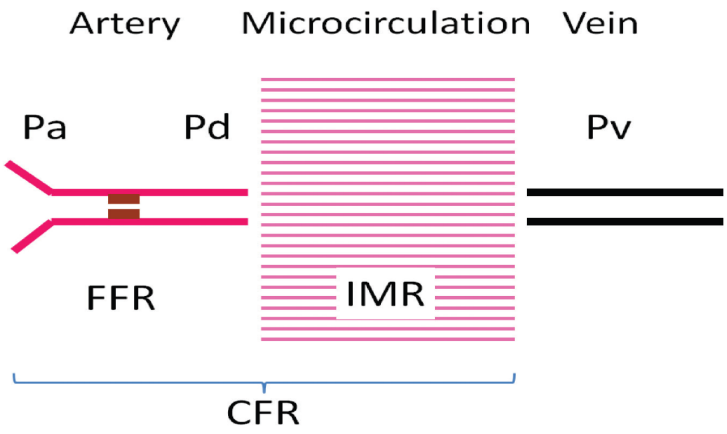

Figure 3.4: CFR = coronary flow reserve; FFR = fractional flow reserve; IMR = index of microvascular resistance; Pd = pressure distal to the lesion; Pa = pressure proximal to the lesion; Pv = the central venous pressure [105].

At maximum Hyperaemia (i.e. increased blood flow)

$$\mathrm{FFR} = \frac{p_d}{p_a}$$

FFR < 0.8 is an indication of obstructive coronary artery and requires percutaneous coronary intervention (PCI). FFR > 0.8 requires no PCI. The ratio of FFR_{myo} defines the maximum myocardial blood flow distal to an epicardial stenosis againt the myocardial blood flow in the absence of the stenosis [104].

$$\mathrm{FFR}_{\mathrm{myo}} = \frac{p_d - p_v}{p_a - p_v}$$

p_v is venous pressure, the right atrial pressure, measured at maximum vasodilation. It

is an important parameter which determines the filling pressure of the right ventricle. FFR_{myo} is an important flow index from clinical perspective as it exhibits both antegrade and collateral contribution to maximum myocardial perfusion. Also when wedge and venous pressure are not available [106] then

$$FFR_{cor} = 1.34 \times FFR_{myo} - 0.32$$

3.3.2 Coronary Flow Reserve

Coronary Flow Reserve (CFR) is the ability of the coronary flow to increase with metabolic demands of the body. By definition it is the ratio between maximum coronary blood flow to the resting blood flow. It is evaluated by measuring coronary flow or flow velocity at catheter. Relative CFR is the ratio of the stress flow in a diseased artery and stress flow in a normal artery. CFR has the potential to detect symptoms of balanced ischemia and possible condition of microvascular dysfunction. Attempts have been made to identify the effect of epicardial coronary stenosis and to assess the results of angioplasty and coronary artery bypass surgery [107, 108].

$$CFR = \frac{Qmax}{Qrest}$$

We know that Flow $= \frac{\text{volume}}{\text{Time}}$, therefore

$$CFR = \frac{[\frac{\text{volume}}{T_{mn}}]Hyp}{[\frac{\text{volume}}{T_{mn}}]Rest}$$

As epicardial volume is considered to be unchanged, therefore, CFR is measured by the ratio of mean transit time during rest to mean transit time in vasodilation.

$$CFR = \frac{[T_{mn}]Hyp}{[T_{mn}]Rest}$$

Figure 3.5 indicates the mean transit time on thermodilution curve.

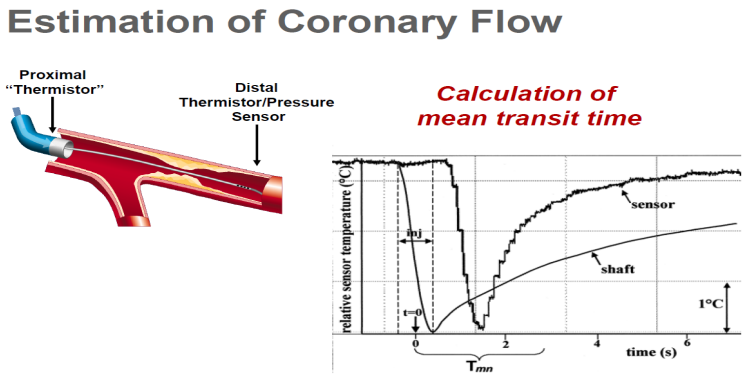

Figure 3.5: Calculation of mean transit time (Tmn) from thermodilution curve (sensor) and injection signal (shaft) [109]

Figure 3.6 shows the diagnosis and treatment based on FFR and CFR values [105].

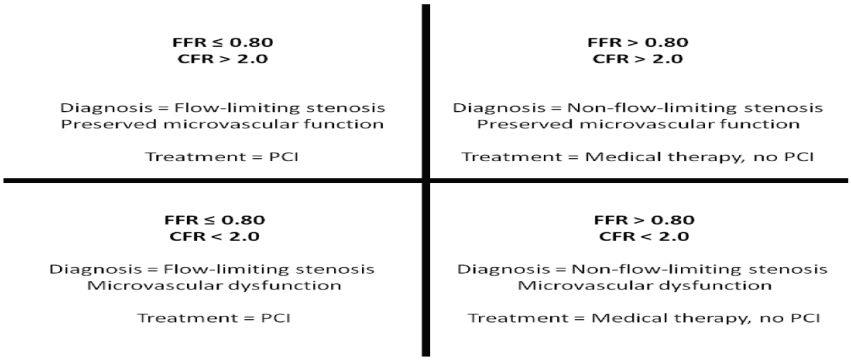

Figure 3.6: Diagnosis and treatment based on FFR and CFR values [105]

The mean transit time T_{mn} is calculated by the following equation [110].

$$T_{mn} = \frac{\int_0^\infty t.C(t).dt}{\int_0^\infty C(t).dt}$$

where $C(t)$ represents the thermodilution curve shown by the distal thermistor and $t = 0$ is defined as the time halfway the injection as shown in Figure 3.5.

3.3.2.1 Limitations of CFR

During measurement of CFR, basal and maximal flows are assessed. Due to major shortcomings of the measuring methods remains doubtful the accuracy that whether the maximal flow has been achieved or not.

Replica of flow is created to overcome the uncertainty; the flow velocities are evaluated by the Doppler Wire and mean transit time assessed by the Pressure Wire.

Regardless of the method used to measure CFR, this technique has following limitations [107].

1. Resting flow is highly variable.
2. Hyperaemic flow is in direct relation to the systemic blood pressure.
3. The hyperaemic and resting calculations are made successively and not simultaneously.
4. CFR value depends on both epicardial vessels and microcirculation and is not specific for an epicardial stenosis. At low CFR value it is impossible to differentiate whether this value is related to an epicardial artery stenosis or microcirculatory dysfunction alone, or a combination of both.

3.3.3 Index of Microvascular Resistance

Index of Microvascular Resistance measures the coronary microvascular function and can be used to study the pathophysiology of microvascular function in both stable and acute MI patients. IMR < 20 lies in the normal range and IMR > 30 indicates microvascular dysfunction [105] as shown in Figure 3.7.

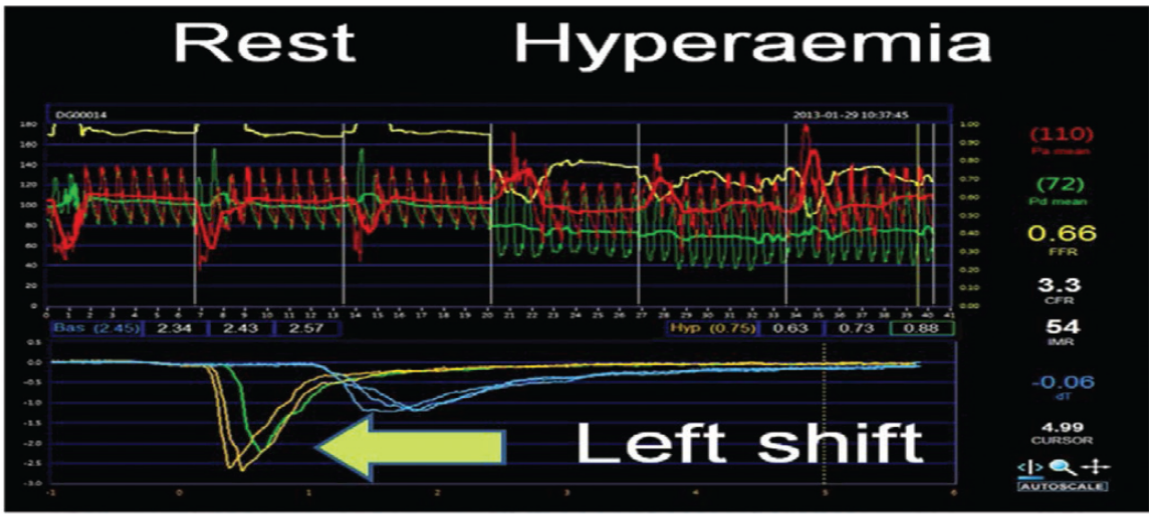

Figure 3.7: Index of Microvascular Resistance [105]

Myocardial resistance is mainly determined by the microcirculation. IMR is a coronary guidewire-based measure of coronary microvascular function [111, 112]. IMR provides information on microvascular dysfunction that could be informative both in stable patients and also in patients with acute or recent MI. The resistance of the

vascular system is defined as the ratio of the pressure gradient to the flow across that particular system [112].

$$\text{IMR} = \frac{\Delta\text{Pressure}}{\text{Flow}}$$

Resistance R is equivalent to $\text{R} = \left(\frac{p_d - p_v}{Q}\right)$ where p_d represents distal coronary arterial pressure, p_v represents the venous pressure, or pressure in the right atrium and Q denotes the blood flow through the myocardial vascular bed [107].

IMR can be derived by a simplified formula when there is no presence of epicardial disease. IMR_{app} is equivalent to the ratio between distal coronary pressure divided by coronary flow while assuming collateral flow is negligible [112].

$$\text{IMR}_{\text{app}} = \frac{\text{Distal Coronay Pressure}}{\text{Coronary Flow}}$$

$$\text{IMR}_{\text{app}} = \frac{(p_d - p_v)}{Q}$$

$$\text{IMR}_{\text{app}} = \frac{(p_d - p_v)}{\frac{1}{T_{mn}}}$$

$$\text{IMR}_{\text{app}} = p_d \times T_{mn}$$

Thus apparent IMR is calculated by multiplying the distal coronary pressure by the mean transit time of a 3 ml bolus of saline at room temperature during coronary hyperaemia as shown in Figure 3.8.

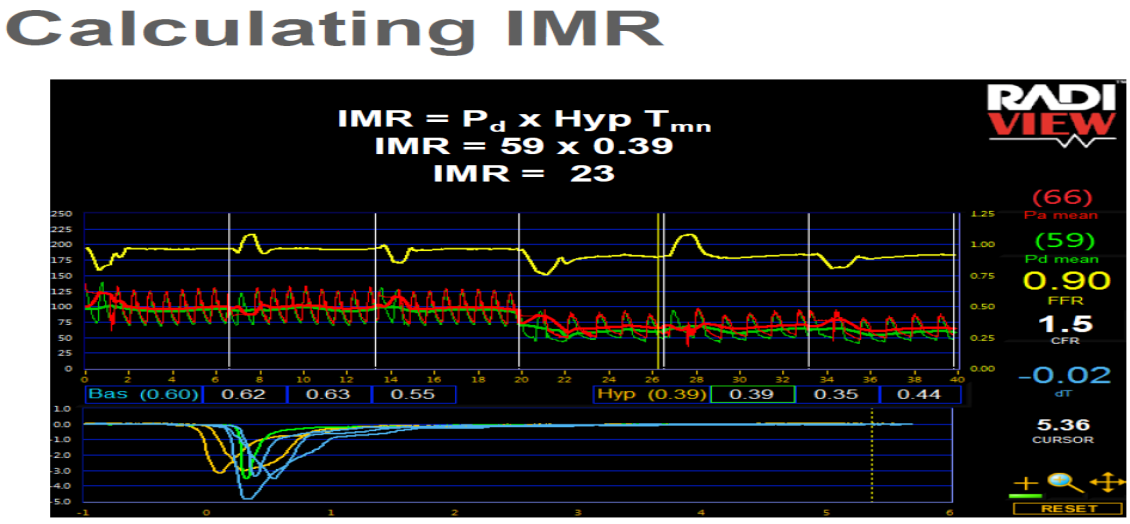

Figure 3.8: The Index of Microcirculatory Resistance Measurement [113]

When the blood flows through an epicardial stenosis myocardial flow is backed by the collateral flow while the coronary flow decreases. Collateral flow also increases the distal coronary pressure and hence in the presence of significant epicardial stenosis IMR_{app} will overemphasize the microcirculatory resistance. Additional calculations of the coronary wedge is mandatory for the calculation of the IMR and requires balloon inflation within the coronary arteries. Hence IMR measurement in patients diagnosed with epicardial stenosis is generally confined to those who are undergoing percutaneous coronary intervention (PCI) [114–117].
Calculation of IMR [117] in obstructive coronary artery is given by:

$$\text{IMR}_{\text{app}} = [(p_a - p_v) \times T_{mn}] \times \frac{(p_d - p_w)}{p_a - p_w}$$

When wedge and venous pressure are not available, IMR may be estimated using this equation [52].

$$\text{IMR} = p_a \times T_{mn} \times \text{FFR}_{\text{cor}}$$

where

$$\text{FFR}_{\text{cor}} = 1.34 \times \text{FFR}_{\text{myo}} - 0.32$$

3.4 Thermodilution Curves

When cardiac output is low, the temperature takes more time to reach to the base line which results in larger area under the curve because the thermistor senses this change in temperature over a long period of time. Similarly in case of high cardiac output, the blood flows faster through the heart and less time is required for the temperature to return to the base line which results in smaller area under the curve [94, 118]. The thermodilution curve normally has a rapid smooth upstroke and a gradual exponential decay [119]. The last portion of the curve is not used in finding the area due to the recirculation [118]. The curve varies with the health condition of patients and according to the techniques used to find the cardiac output. Figure 3.9 shows the different types of curves according to the variation in the shape of curves [119].

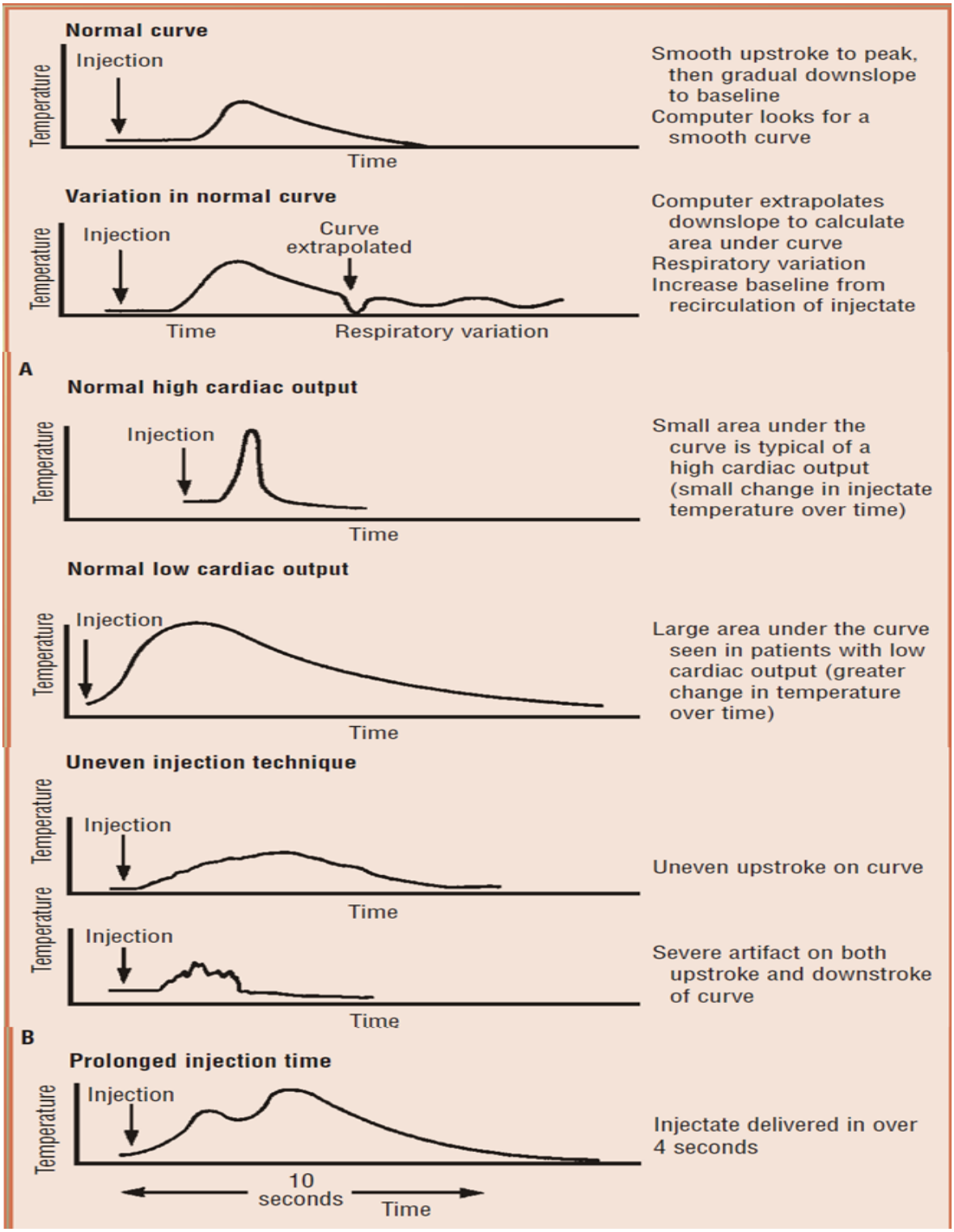

Figure 3.9: Variation in normal cardiac output curve [118]

.

3.4.1 Thermodilution Method

Different techniques are used to measure the cardiac output [120]. Thermodilution is one of the methods that are used now days by the clinicians to determine the cardiac output. This method calculates the blood flow by using the same techniques as used by

other indicator dilution methods [118]. A special thermistor tipped catheter which is known as Swan-Ganz balloon flotation catheter is used in this technique. The catheter is inserted into the pulmonary artery from the peripheral vein [120]. An injection of known quantity (volume and temperature) of cold saline solution that is colder than the blood temperature is injected into the right atrium with the catheter [118, 120]. Due to this injectate blood temperature decreases and this change in temperature is recorded as it flows over the thermistor located 3 cm from the end of the catheter tip [119]. The thermistor then sends this recorded information to the computer that displays this information in the shape of curve which shows the change in temperature over time [94, 120] and calculates the area under the curve [119]. This area is inversely proportional to the flow rate and this flow rate is taken to be the cardiac output if there are no intracardiac stunts [94]. An ideal thermodilution curve is shown in Figure 3.10. The characteristics of the administration of injectate are determined by a rapid upward slope to a peak, a stepwise downslope and an exponential-like deterioration of the thermal signal. Integration of the area under the thermodilution curve begins at the instant of injection and the cardiac output computer terminates the integration when a value of about 30% has been reached by the exponential decay. Then the decay is extrapolated by the computer to baseline. In this way, artifacts introduced by recirculation of indicator can be minimised as shown in Figure 3.10 [118].

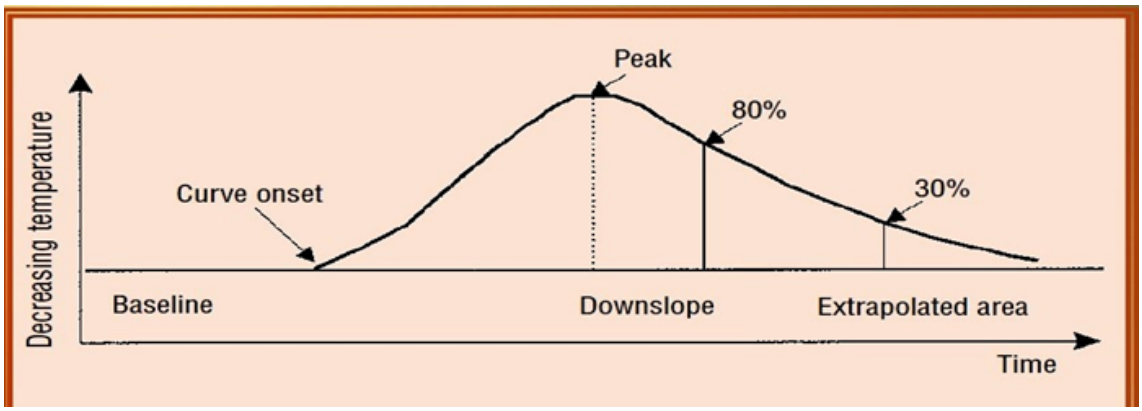

Figure 3.10: An ideal thermodilution curve [118]

.

3.4.1.1 Radi Analyser/Pressure Wire System

Radi analyser which is a commercial system is used to display the thermodilution results sent by the guide-wire catheter. The guide wire is almost the same as the conventional guide wire but with an exception of three microsensor elements which

are located at 3cm away from the distal tip at the transition of the radiopaque and radiolucent segments. The functions of each of these three sensors are specific. For instance, one measures the pressure /FFR, the second sensor measures the thermodilution derived CFR whereas the third one is designed to measure the temperature [121].

The piezoresistive pressure sensor is made of silicon and is coupled in a Wheatstone bridge having range of -30 to 300 mmHg. The Radi pressure wire having length of 170 cm or 300 cm is connected to Radi Analyser by a 6 foot adapter or a contact cable during pressure measurements and can easily be disconnected during the placement of wire and manipulation [121].
A portable computer system, Radi Analyser, is mounted on an IV pole and interfaces with the CCL haemodynamic system. The purpose of this computer is to collect and interprets the information sent by the guide wire catheter. Furthermore, it also displays the arterial waveform and pressure waveform on Radi Analyser and the catheter lab hemodynamic system simultaneously. A remote control is used for input of patients data and operation of the system. A thermal printer is also attached for printing the hardcopy of the patients measurement in the form of chart. A number of Patients recording is stored in the Radi Analyser system. The digital information is transferred by optional Radiview software into the personal computers for visualising, reporting and testing for future use [121] as shown in Figure 3.11.

Figure 3.11: Radi Analyser Monitor for displaying reports [122]

A lightweight and durable instrument, Radi Analyser, is very easy to use which not only helps in clinical decision making in everyday life but also supports the advanced

research. Radi Analyser is integrated with the catheter lab table and provides a quick access to FFR measurements without any delay. Radi Analyzer along with the Pressure WireTM CertusTM enables the assessment of FFR, CFR, IMR and intravascular temperature by using only one wire [122].

3.4.2 Thermodilution Measurement Errors

Thermodilution cardiac output measurement method has many advantages over other methods with respect to accuracy. However, there may be measurement errors due to technical reasons and pathological condition of patients.

3.4.2.1 Temperature and Volume of Injectate

In 1961, Evonuk et al. stated there is a closed correlation between the cardiac output values determined by thermodilution and dye dilution by using injectate at $23\,^0C$ to $26\,^0C$. According to them, accurate temperature of the supplied iced injectate is not only difficult to maintain and determine but also affect heart and other cardiopulmonary haemodynamic variables [123]. In 1971, the clinical use of 10 ml iced injectate in adults containing 5% dextrose in water was reported by Ganz et al. for the first time and this has been used for more than ten years [124]. Mostly [125–131] but not all [132–134] reports showed no difference in accuracy or reproducibility (ratio of standard deviation to mean value of multiple measurements) between the uses of iced or room temperature injectate. The cardiac output values were estimated by using injectate of different volume and temperature i.e 5 ml, iced, 10 ml, room-temperature, or 10 ml, iced and comparable reproducibility was reported by Elkayam et al [125]. The use of 10 ml iced or room temperature injectate is recommended because it produces less variability than 3 or 5 ml injectate [126]. The blood flow is not affected by the small volume of the injectate [135, 136]. However, an increased blood flow is reported in the region of thermistor [137]. Furthermore, due to the cold injectae, the change in systemic and pulmonary arterial pressures, right arterial pressure and pulmonary blood flow (right ventricular output) is shown in clinical practice [138–140] and the amount of change is depending upon the temperature and volume of the cold injectate [141].

3.4.2.2 Rewarming Injectate

Errors in measurement can be introduced due to rewarming the injectate before it is injected [142] and by heat transfer as it is passed through the catheter [124, 143–145].

The temperature of the 10 ml iced injectate syringe will be increased by $1\,^0C$ in every 13 seconds when it is held in warm hands having temperature $36\,^0C$ which results in overestimation of cardiac output by 2.86% for each ^0C. Cardiac output can be overestimated due to the indicator loss during the passage of the injectate through the pulmonary artery catheter. 17% of the potential signal is assumed to be lost before the 10 ml injectate leaves the catheter at $0\,^0C$ and the factor of 0.83 for the correction of this loss is used in the thermodilution equation [146].

3.4.2.3 Timing of Injection and Respiration

The accurate assessment of the area under the thermodilution curve is affected by the fluctuation of the baseline temperature in the pulmonary artery with respiration $(0.01 - 0.1\,^0C)$ [147–153] which is also called physiological noise [124, 151] as shown in Figure 3.12.

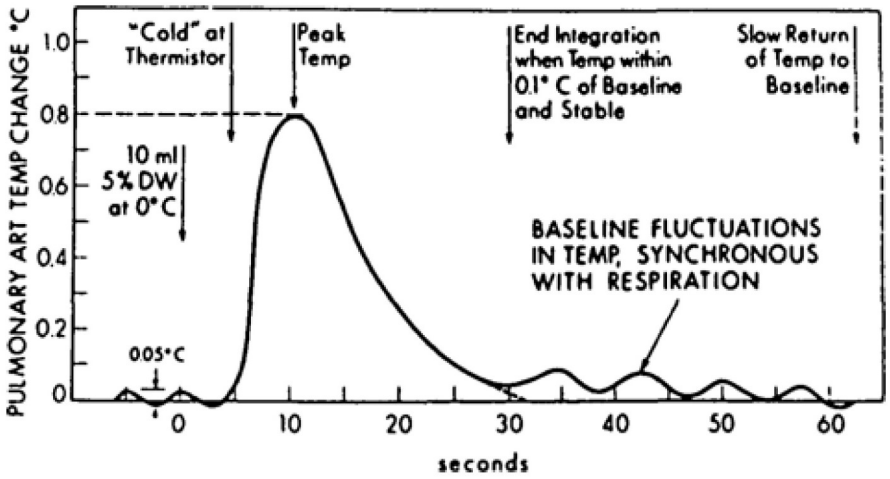

Figure 3.12: Timing of injection and respiration

The production mechanism of these temperature variations has not been fully clarified; the direction of the change in temperature may be influenced by humidity [153], the variation in blood flow and temperature changes during the respiratory cycle in the superior and inferior vena cava or it may be due to the unintentional effects of respiration on the system of circulation [152].

The cardiac output will be underestimated because of increase in baseline temperature in the pulmonary artery during spontaneous breathing and overestimated because

of decrease in temperature during intermitted positive pressure ventilation (IPPV) [150, 152, 153] at expiration which is shown in some animal experiments. However, the risk of baseline temperature drift due to the respiration is alleviated by cardiac output computers by taking the average of blood temperature for a short period of time before indicator injection [150, 154].

3.4.2.4 Speed and Mode of Injection

For an injectate volume of 5 or 10 ml the injection time of 4 seconds may be acceptable. If the injection time prolongs, poor thermdilution curves may render the CO values unreliable [155]. Automatic injector may work effectively [156,157] but small variations can occur in the time, flow and consistency in the injection powered by gas. Manually reproducing the CO values using an experienced operator may not be fruitful. Speed of injection is secondary when the consistency of injection is being measured [158].

3.4.2.5 Intravenous Fluid Administration

After cardiopulmonary bypass the calculation of CO in adults may be underestimated if a rapid peripheral intravenous infusion of 90 ml to 220 ml fluid is injected before measuring [159]. This is mainly caused by the change in temperature which is a direct consequence of the infusion augmenting the area of the thermodilution curve. Constant infusion of fluid should either be maintained or discontinued half a minute before recording the CO value [159]. During CO calculations of fluids through the side-port should be stopped [160].

3.4.2.6 Low Flow

To check the correctness of thermodilution, the values of CO have been noted in Vitro experiments when the CO is low even less than 1 to 2 $\mathrm{l\,min^{-1}}$ [161,162]. Before the completion of computed analysis, the recirculation of indicator occurs and a considerable loss of thermal indicator happens which may contribute to the variable cardiac output values. If the thermodilution curve and variations in clinical variables are observed the risk of clinical errors can be reduced [163].

3.4.2.7 Catheter Dysfunction and Position

PA catheter dysfunction is caused by the formation of thrombus around the catheter and the obstruction of the proximal lumen [164]. With the increase in the size of

catheter thrombus the value of CO is progressively underestimated, which is the result of the overestimation of thermodilution curve area by rewarming thermistor for a protracted period [165]. The catheter should be removed when improper perfusion obstructs the proximal lumen opening of the PA catheter. The injection of cold injectate into the lower portion of the superior vena cava through a central venous catheter is helpful in finding the measurements of CO [164]. It can be done by using PA catheter's right ventricular port whose original function is introduction of pacemaker or fluid administration [166]. There are three reports in which overestimation of CO is attributed to the use of the proximal port within the introducer sheath, it happens because of the reflux of thermal indicator within the introducer and failed to properly mix with venous blood flow [167–169]. To avoid this problem and to allow a useable length of catheter, the sheath should be withdrawn [169,170]. When non-dependent lung contains the PA catheter's thermistor during thoracotomy then less may be warmed the injectate on the side of the thoracotomy [171] and in pulmonary circulation around vessels in the non-dependent zone occurs a different rate of thermal dissipation [172].

3.4.2.8 lntra and Extra-Cardiac Shunts

Recirculation occurs early in a patient with left-to-right intracardiac shunt and this recirculation can be seen on the downslope of the thermodilution curve which interrupted. By obtaining the ratio of the area under the entire thermodilution curve to the area under the first portion of the curve, we can calculate the shunt ratio [173, 174]. The values found with the Fick technique($r = 0.89$), correlate with the values found by this method [173]. In infants and children with atrial septal defects and with transposition of the great arteries, the output of the left and right ventricles can be measured by the process of thermodilution [175]. The ratio of the calculations of pulmonary systematic flow made by this method correlates with the values found by Fick method ($r = 0.91$). So the magnitude of left to right intracardiac shunts can be accurately determined by thermodilution conditioned that the indicator mixes well in the main stream of blood [176–178]. Measuring CO with this method suggests the presence of left to right shunting, which shows falsely high values of CO in patients with congestive heart failure [179]. But if there is an additional shunt at the ductus level or in the presence of a right to left shunt then this method cannot be used [174]. Unless the thermodilution curve appears, the existence of a left-to-right shunt may be missed [163]. The computed CO can be similar to systematic blood flow when due to high shunt flow

recirculation may not be seen on the thermodilution curve [180]. When there exists a right to left shunt, thermistor is bypassed by indicator to reach the left side of the heart and it results in overly estimated cardiac output [181].

3.4.2.9 Valvular Heart Diseases

There is a report that shows the pulmonary valve insufficiency due to the surgical valvectomy but in dogs the measurement of CO was not affected by it, however, there occured a change in the magnitude of peak temperature and a decrease also happened in the downslope of the thermodilution curve due to mixing of indicator with a larger volume of blood and the transit time of indicator had prolonged [182]. However, the association of pulmonary regurgiration with a low CO makes impossible the determination of the area under the thermodilution curve [182]. The determination of cardiac output by thermodilution was reported as an impossibility or an unreliable action in patients with tricuspid regurgitation [183–185]. A recent animal investigation [186] reveals that there is a correlation in the values of CO estimated by thermodilution and the blood flow measured in dogs with tricuspid regugiration by an electromagnetic flowmeter and it suggests that thermodilution is more accurate method for determining CO, especially in low CO states. However, in the presence of tricuspid regurgitation, Fick method for determining CO appears to be superior to the thermodilution technique [183–185]. The indicator dilution technique may be rendered inaccurate due to aortic or mitral regurgitation [187–190]. Sampling dye in the right heart can alleviate the distortion of the dye dilution curves in people suffering severe aortic or mitral regurgitation [188–190]. However, no disparity could be found by a recent investigation between the measurements calculated by Fick method and thermodilution and investigation suggested that in patients with aortic or mitral regurgitation, thermodilution should be preferred to dye dilution [187].

3.4.2.10 Paediatric Patients

Values of CO excellently correlates when it is found by thermodilution using iced injectate of 1 ml to 3 ml with values determined by using Fick technique in new born and children [181, 191–194]. Before injection, the withdrawl of blood into the injection lumen of the catheter may lead to overestimated value of CO because the small volumes of cold injectate gains heat while passing through the catheter [195]. Pre-aspiration of blood should be avoided if accurate measurement has to be found in infants and

children [195] and the liquid filled in the catheter lumen should be at the injectate's temperature [195]. Also, a factor [195–197] should be used which rectifies the loss of thermal indicator when injectate is passing through the intravascular portion of the injectate catheter.

3.4.2.11 Electrocautery

The electrical noise created by electrocautery affects the pulmonary artery baseline temperature, so values should not be determined while electrocautery is applied [163].

3.4.2.12 Pressure Measurement Errors in Vessels

The measurement accuracy of blood pressure in the cardiovascular system is important because it provides sufficient information to identify the severity of many heart diseases [198]. In spite of so many advancements in non-invasive techniques, catheterization is the most common method to measure the pressure in the blood vessels [198]. However, the accurate measurement of cardiac output by the catheter can be affected by technical factors like pressure wave reflection at the tip and wave distortion in fluid-filled catheter [198, 199]. Distortion effect is due to the columns of fluid that fills the catheter, which is required to pass on the pressure to the external transducer [200, 201]. This design can cause the inertial artifacts due to which the shape of the waveforms is changed as it goes downstream inside the catheter. The dynamic response of the cathetertransducer system is becoming a matter of great concern because it is required to reproduce the realistic pressure waveforms [202]. The catheter usually serves as a low-pass filter to reduce all frequencies above normal frequencies and also the system starts giving errors when the signal frequency becomes equal to natural frequency. Therefore, the catheter must have an accurate amalgamation of diameter, length and the compliance of the material to increase the accuracy in the signal upto maximum level. The properties and dimensions of catheters must be carefully selected to supply the highest possible natural frequency which results in maximizing the flat frequency response essential to give an accurate measurement [203–205]. Generally, stiffer catheters add to the accuracy of the measurements. However, for better navigation in complex structures, more compliant materials are required. Air bubbles can be present if the catheter is too long or the diameter of the catheter is very small which also weakens the dynamic response [202]. The signal distortion which is derived from the pulse wave velocity (PWV) and the ratio of the stroke volume to the pulse pressure has significant

potential to compromise important clinical markers [206]. Abnormal pulse pressure, waveform shape, and pulse wave velocity are the factors that can contribute to increase cardiovascular risk [207]. A high value of the radius ratio between the catheter and the vessels (a comparatively large catheter size as compared to the vessel) is also considerable source of measurement error which can create partial hindrance of the lumen. As a result of this obstruction, pressure in comparatively smaller vessels including coronary arteries, peripheral circulation, and pediatric cases is overestimated [208, 209]. It is shown in the analytical flow models of a straight catheterized tube that, for the radius ratios from 0.3 to 0.7, the flow resistance increases by a factor of 3 to 33 due to the partial blockage [210]. This also effects the disease evaluation relying on the catheter data. Pressure measurements play an important role for risk stratifications in pulmonary hypertension patients who need the heart transplantation in which pulmonary vascular resistance, pulmonary artery systolic pressure, and transpulmonary pressure gradient are major factors for preoperative evaluation [211, 212]. The measurement errors of these parameters not only affect the cost but also the treatment options.

3.4.3 Technical Considerations

3.4.3.1 Patient Position

In the supine position, cardiac arrest is 30% more as compared to in the semierect setting. Hence, the consecutive cardiac results should be registered with the patient in a static position or the position of the patient should be recorded with each cardiac results [213].

3.4.3.2 Indicator Solution

5% dextorse in water or normal saline (0.9% sodium chloride) injection gives the most relevant assessments. Various others solutions give variable outputs (due to their different specific heats) and are not endorsed [213].

3.4.3.3 Volume and Temperature of the Injectate

The solution can be injected at room temperature or cooled in ice before administering in 5 ml or 10 ml volume. Generally, low temperature and high volume solutions injected bring about highest signal to noise ratios and therefore the most precise calculations. On the other hand, injectates administered at room temperature produce more reliable

outputs in most critically ill patients. Indicator fluid at room temperature produces reliable outcome when administered in large volume (10 ml) whereas iced injectates when injected in small volume give better results. Small volume of injectates at room temperature are not recommended due to inaccurate outcomes [213].

3.4.3.4 Injection Timing

Randomly obtained thermodilution outcomes in different respiratory cycles can differ, but timing the bolus injections with the respiratory cycle can enhance the reproducibility of the values of cardiac output obtained by the thermodilution technique [214]. Patients suffering with rapid breathing can have longer injection times than the respiratory cycles. Therefore, the indicator solution should be injected with each respiratory cycle for better results [213].

3.4.3.5 Alternative Injection Ports

The injectate can be expired through an alternative infusion port on the catheter If the proximal (right atrial) port of the PA catheter is blocked [213].

3.4.4 Recommendations

1. The volume and the temperature of the injectate is selected according to the age and pathological condition of the patients. In adults, the use of 10 ml injectate at room temperature is preferred to 10 ml iced injectate [125, 126] under most circumstances and for maintenance of temperature [129, 131]. 5 ml injectate can be used in patients suffering with pulmonary oedema secondary to congestive heart failure or renal failure to prevent the volume overload [125, 126]. Furthermore, approximately 0.15 $\mathrm{ml\,kg^{-1}}$ injectate is recommended for infants and children [181, 191, 192].

2. A single standardized syringe which is designed to supply known and constant volume of injectate should be used instead of disposable plastic syringes [215].

3. The uniform cooling of the injectate must be maintained for an accurate estimate of cardiac output [216].

4. The temperature of the injectate should be observed at the point of entry into the circulation [135, 217].

5. Room temperature injectate is preffered to iced injectate because it does not need cooling of syringe before use and negative heat loss can be minimised during the passage through the catheter.

6. Two to four calculations may be made at equal interval of ventilation cycle i.e. at end-inspiration [218], mid-inspiration [219, 220] or end-expiration [220, 221] during the intermitted positive pressure ventilation [157,218–223] as the injections timing increases the reproducibility of cardiac output values with the respiratory cycle [133, 150, 157, 218–221, 223].

Chapter 4

Statistical Analysis of Thermodilution

4.1 Data Collection

We analysed ethically-approved clinical data of coronary thermodilution of 12 patients (Berry,C.(2016).RadiView data[DAT file extension]) from Prof. Colin Berry (University of Glasgow). DAT files contain generic data which stores the information specific to the referred application and require a specific program to open. There is no specific program through which all the DAT files can be opened. For viewing the DAT file, it is required to find out which program created the file [224]. All patients presented with stable angina were subsequently referred for invasive coronary angiography. Any patient with an epicardial stenosis of 40% to 90% underwent pressure wire and thermodilution measurement as per the study protocol. Furthermore, there is a mixture of patients with evidence of obstructive epicardial coronary disease (FFR < 0.80), evidence of increased microvascular resistance (IMR > 25), evidence of reduced vasodilatory capacity (CFR < 2.5), and those with normal coronary physiology parameters.

4.2 Data Analysis

The data sets of 12 patients having DAT file extension were converted in spread sheets through Radiview software (see section A) so that we can better understand the read out data and can analyse it in the best possible way.

4.2.1 Thermodilution Records

The spreadsheet file for a thermodilution recording contains first 12 columns of sensor and cable temperature, one pair for each of three injections at room temperature saline respectively as shown in Figure 4.1. For a full Coronary Flow Reserve (CFR), there are 3 injections in baseline and 3 injections in hyperaemia, i.e. 6 injections which result in 6 pairs of sensor and cable temperature thermodilution data respectively. The following 5 columns contain pressure data, including aortic pressure (p_a), p_a average, resting distal coronary pressure (p_d), p_d average and resting distal coronary pressure to aortic pressure ratio ($\frac{p_d}{p_a}$) as shown in Figure 4.1.

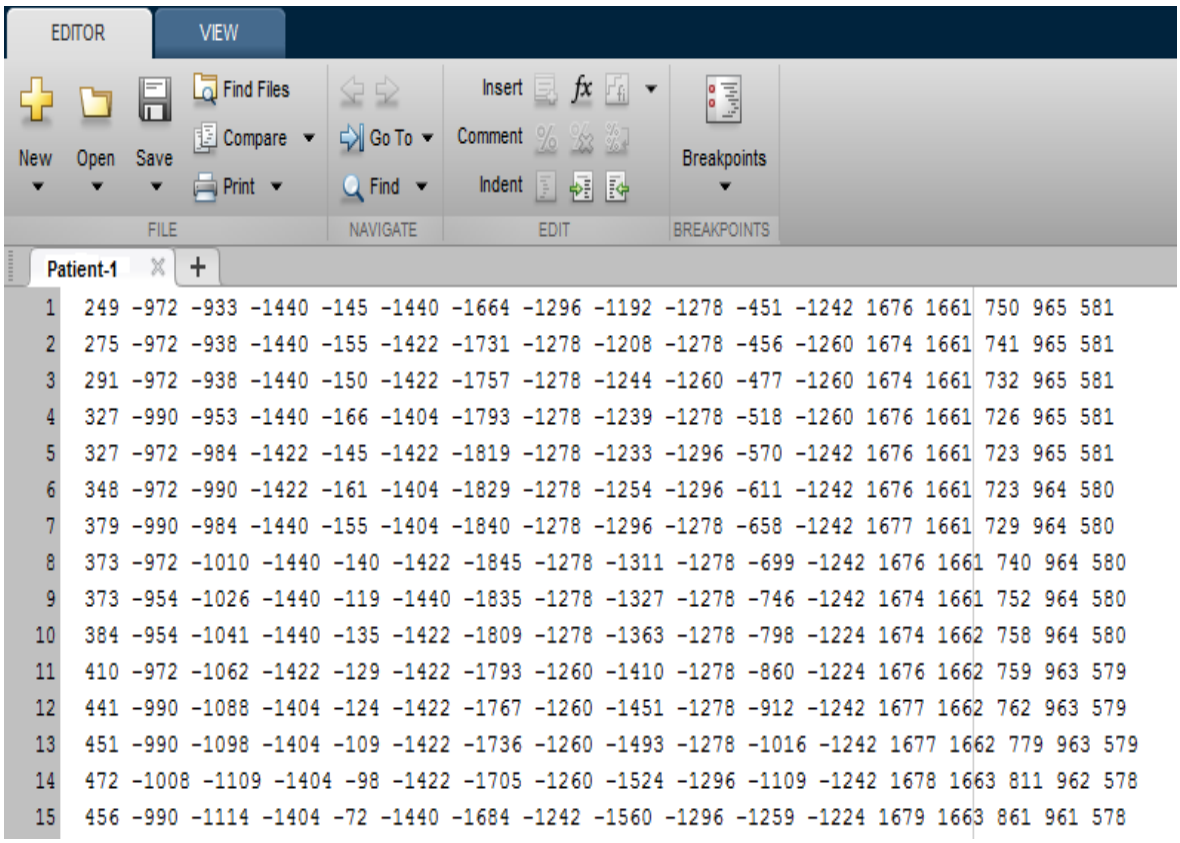

Figure 4.1: Spread sheet of thermodilution data having 12 columns of sensor and cable temperature followed by 5 columns of pressure

Figure 4.2 shows the display of thermodilution curve on Radiview software window.

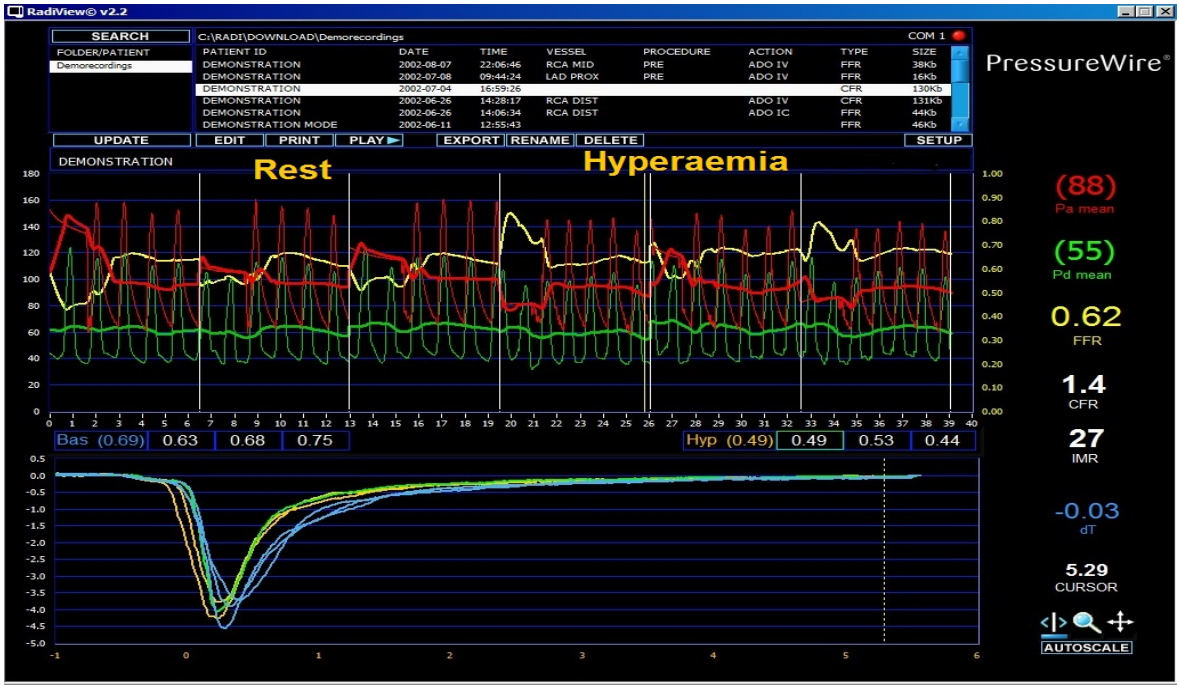

Figure 4.2: Radiview software window displaying the thermodilution data

Cable temperature refers to the temperature in the wire shaft used to detect the temperature when an injection occurs and trigger recording and mean transit time (T_{mn}) calculation whereas Sensor temperature is the temperature from the distal sensor itself, this is the classical thermo-dilution tracing recorded at the wire tip and is seen as a light blue tracing on the Xpress system. T_{mn} is calculated as the time between the trigger point in the cable temperature and the mid-point of the temperature decline in the sensor temperature as shown in Figure 4.3.

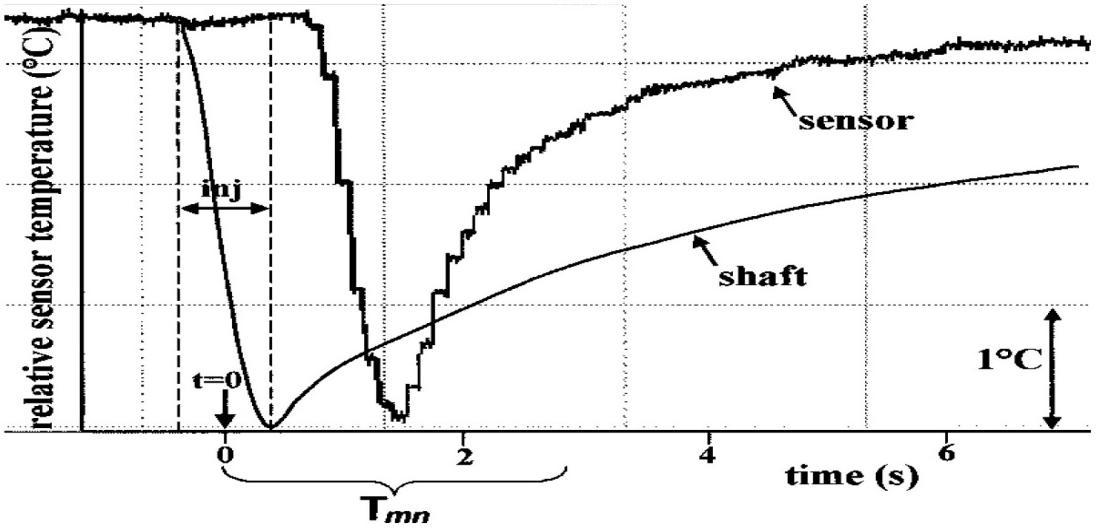

Figure 4.3: Calculation of mean transit time (T_{mn}) from thermodilution curve (sensor) and injection signal (shaft). Inj indicates injection of saline; t=0 is defined halfway injection [105].

4.3 MATLAB Programming

A program in Matlab software was designed to analyse the spreadsheet data of thermodlilution curves and to identify its key features. The program was written in such a way which not only read the spreadsheet data of one patient but also counted the number of rows after culminating the program if the consecutive number of zeros in a column exceeds from 20 by using 'Load' command and conditional statement respectively (Appendix B). Furthermore, we also plotted sensor and cable temperature (^0C) against time (ms) by using 'plot' command. The first plot of sensor and cable temperature of first patient is shown in Figure 4.4 and Figure 4.5.

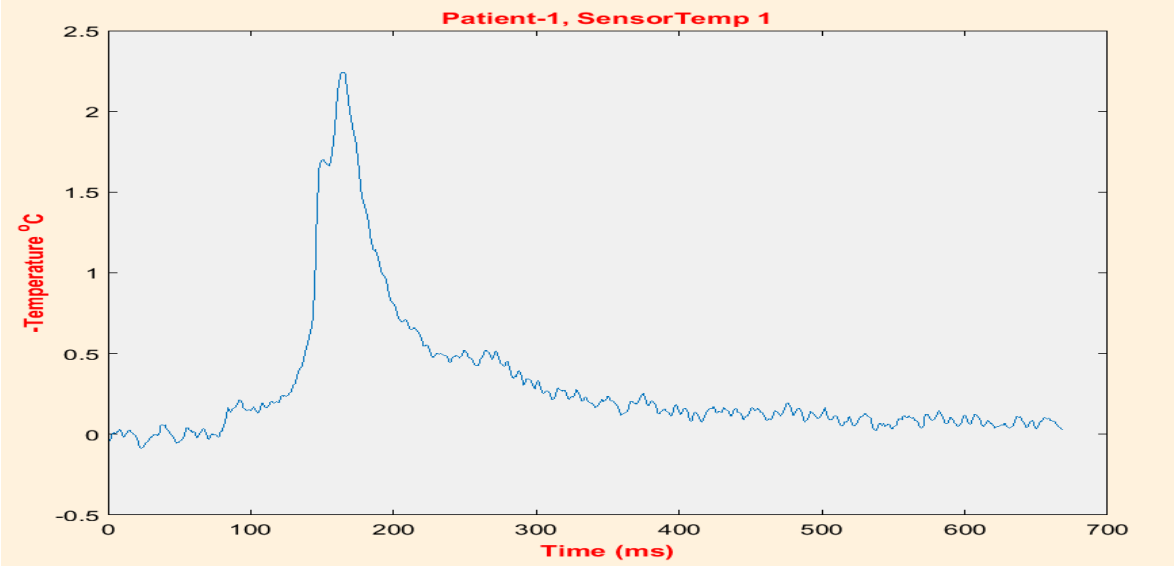

Figure 4.4: Sensor temperature-1 of patient-1

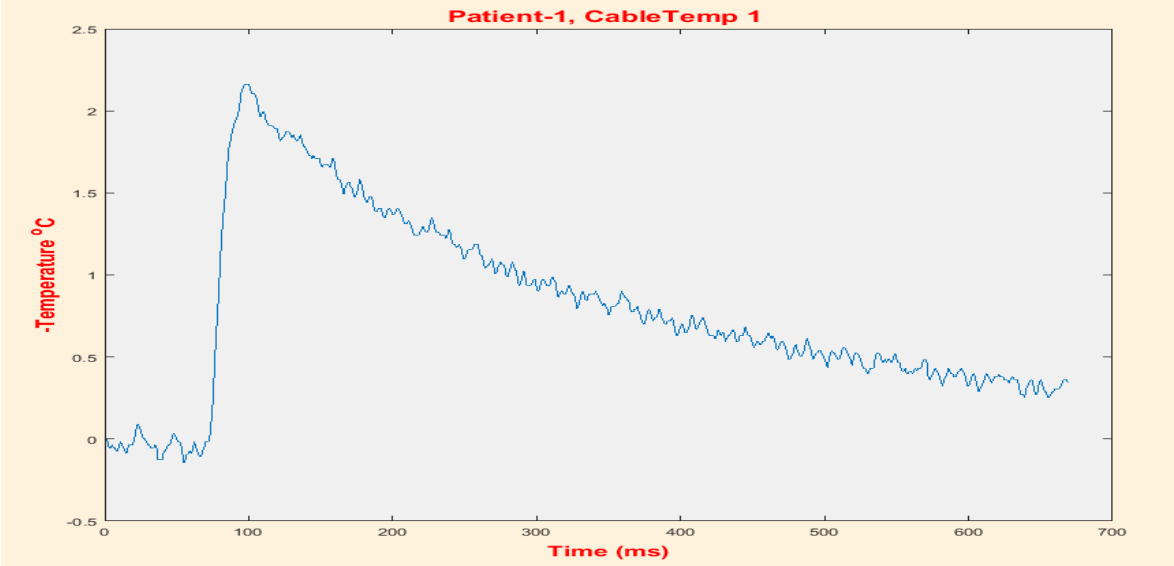

Figure 4.5: Cable temperature-1 of patient-1

After checking the functionality of the program for one patient, we then modified it in such a way that it can load the data of 12 patients at a time and can display their results to see the difference between the curves of each patient for further analysis. The next aim after plotting the results was to fit the best suitable curve on the actual sensor and cable temperature data of twelve patients to find the peak value of the curve. So, in order to find the best fit curve for a series of data we used the Least Squared curve fitting approach which will help us analyse the actual mathematical function, after which we can find the peak and other significant values of the curve easily. So, with the help of the Matlab curve fitting tool, we found that the Gaussian function of degree 8 (see Figure 4.9) is the most suitable fit function on all the sensor and cable temperature thermodilution data. The procedure for curve fitting is as follows.

1. Load the data through Matlab program on which you want to fit the curve.

2. After loading, go to the 'Curve Fitting' tool of Matlab Apps Menu. When you will double click on the curve fitting tool, a window appears as shown in Figure 4.6.

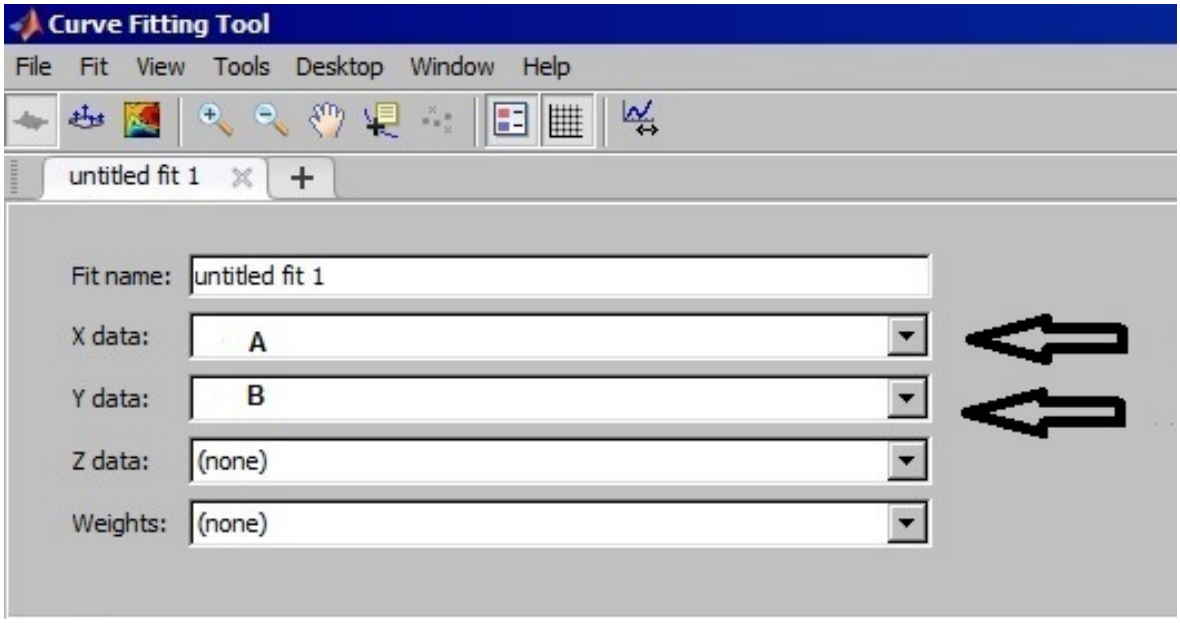

Figure 4.6: Curve fitting procedure-1

3. Choose the value of X data and Y data (see Figure 4.6).

4. When you choose the values, Matlab program will show the plotted result on the same screen as shown in Figure 4.7.

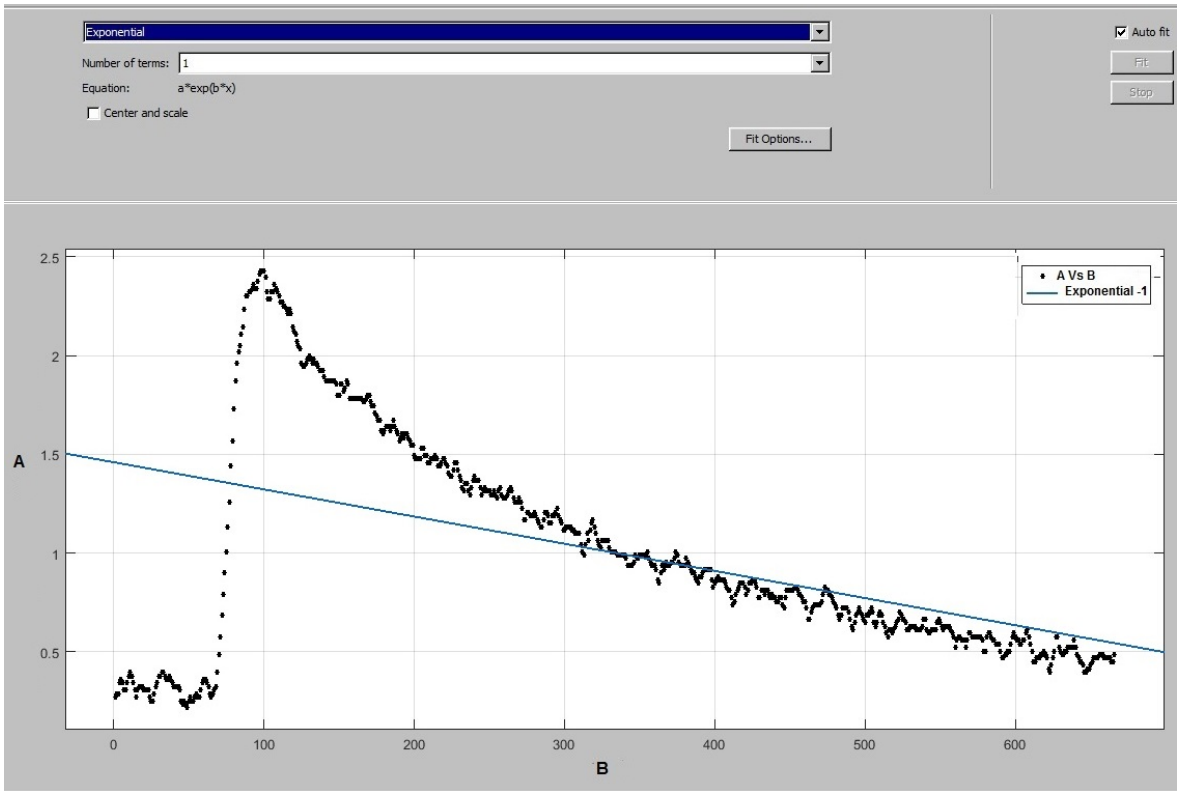

Figure 4.7: Curve fitting procedure-2

5. Choose the best suitable function and degree that fits on the curve as in my case Gaussian function of degree 8 is the best fit function as shown in Figure 4.8.

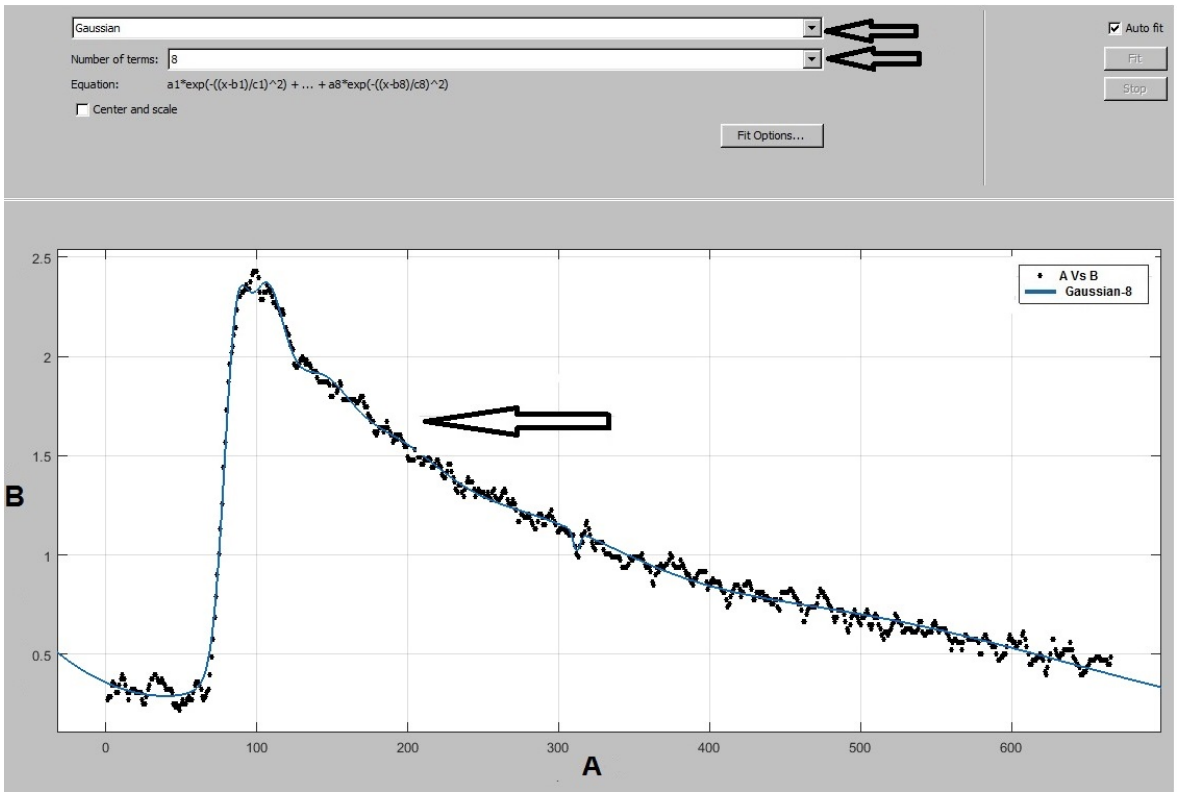

Figure 4.8: Curve fitting procedure-3

6. After fitting the function one can see the mathematical form of the fitted function along with the values of the constants appears on left side of the same screen as shown in Figure 4.9.

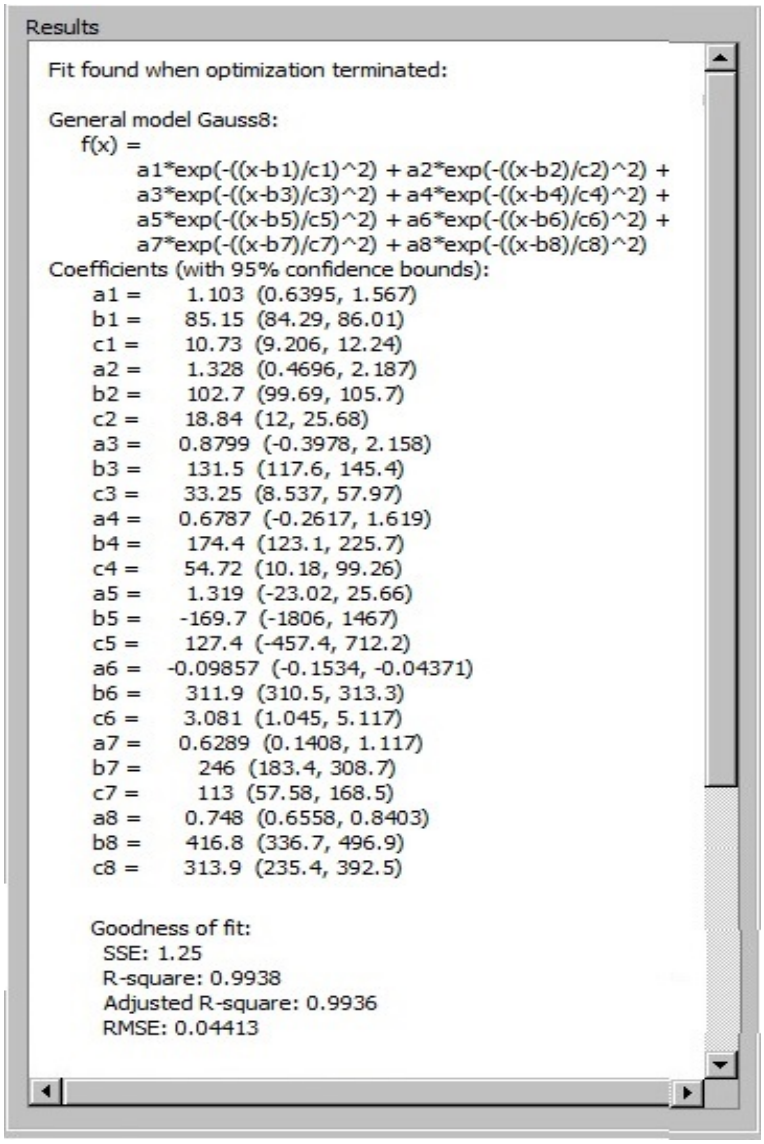

Figure 4.9: Curve fitting procedure-4 guess the definition of the Gaussian curve of degree 8

The general Gausian model fits the peak is defined as

$$y = \sum_{i=1}^{n} a_i e^{[-(\frac{x-b_i}{c_i})^2]} \quad , \tag{4.1}$$

where a_i is the amplitude of each peak, b_i is the centroid, c_i is related to the peak width and n is the number of peaks where $1 \leq n \leq 8$ [225].

The values of a_i, b_i and c_i are calculated such that the error for the data points are

minimum which can be achieved by using non-linear Least Squares procedures with tolerance function 10^{-6}. The interval shows lower and upper bound of fitting co-efficients with the confidence interval of 95% [225].

$$\text{Sum Squared Error} = \sum_{i=1}^{n}(y_i - y)^2 \qquad , \tag{4.2}$$

where y_i are the data points and y are the values of the function at that point. If the value of SSE is close to 0, it indicates that the model has smaller random error component and the fit is useful. In Figure 4.9, SSR is 1.25 shows the usefulness of the fit [226].

R^2 can be defined as the square of the correlation between the response values and the predicted response values.

$$R^2 = \sum_{i=1}^{n}(\hat{y}_i - \bar{y})^2 \qquad . \tag{4.3}$$

A value of R^2 close to 1 shows that a greater proportion of variance is accounted for by the model. In our case of Gausian 8 fit, the value of R^2 is 0.9938 means that the curve fit explains 82.34% of the total variation in the data about the mean [226].

The adjusted R^2 is useful when a series of models have to compare that are nested and its value closer to 1 indicates the best fit and the root mean squared error $\bar{R}$ estimates the standard deviation of random component in the data and is known as standard fit error.

$$\bar{R} = \sqrt{\bar{R^2}} \qquad , \tag{4.4}$$

which is the mean square error which is also known as the residual mean square. A value of $\sqrt{\bar{R^2}}$ closest to 0 indicates the best fit as shown in Figure 4.9 [226].

Overfitting of a curve fitting technique occurs when a statistical model describes random error or noise instead of the underlying relationship. Overfitting generally occurs when a model is excessively complex, such as having too many parameters relative to the number of observations. It is a modeling error which occurs when a function is too closely fit to a limited set of data points [227, 228].

Cross-validation is a technique, among many others, to evaluate predictive models

for overfitting. It is carried out by partitioning the original sample into a training set to train the model, and a test set to evaluate it. In k-fold cross-validation, the original sample is randomly partitioned into k equal-sized subsamples [227, 228].

Another facet of overfitting is the biasvariance tradeoff. It is the problem of simultaneously minimizing two sources of error that prevent supervised learning algorithms from generalizing beyond their training set. The bias is error from erroneous assumptions in the learning algorithm [227, 228].

We then generated the Matlab program code of the fitted curve through 'Generate Code' command in the file menu of the same curve fitted screen, to include that code in the same program instead of doing all the procedure again and again (Appendix B).

The main purpose of the curve fitting was to find the peak, prominence, width (half prominence) and the time at which the peak occurs in the sensor and cable temperature of the thermodilution data. Therefore, in order to find these values of the fitted function, we then added Malab function 'findpeaks'. Furthermore, we also included the 'xlswrite' command in the program to save data directly in the form of spread sheets for further analysis. Additionally, we also made a separate function for subplot to get rid of 12 separate plots which are used to be displayed on twelve different screens. We used 'subplot' Matlab function to display 6 plots (before hyperaemia) on one screen and remaning 6 plots (after hyperaemia) on another screen for better visualisation of results. The first two results of each before and after hyperaemia of the 1st patient are shown in Figures 4.10 and 4.11 respectivily.

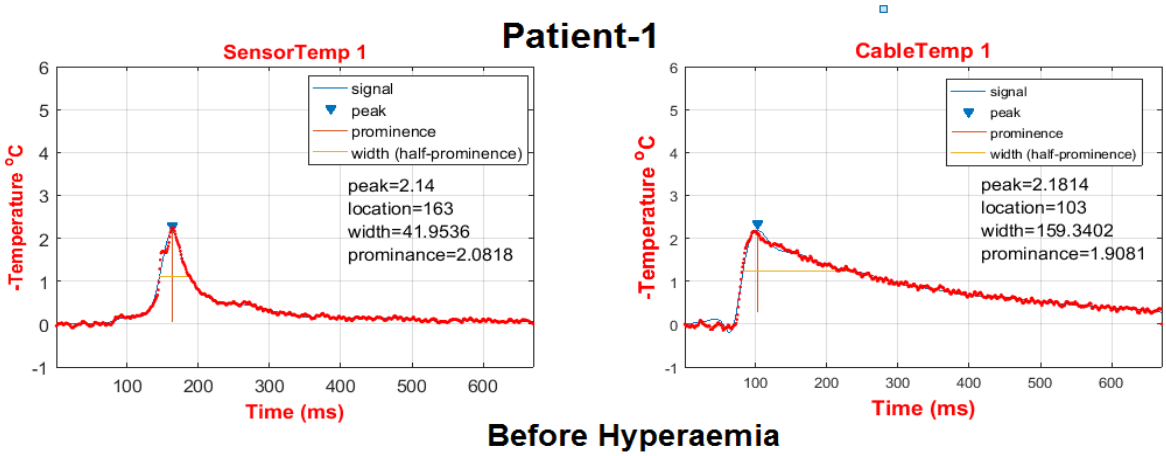

Figure 4.10: Subplot of patient-1 before hyperaemia

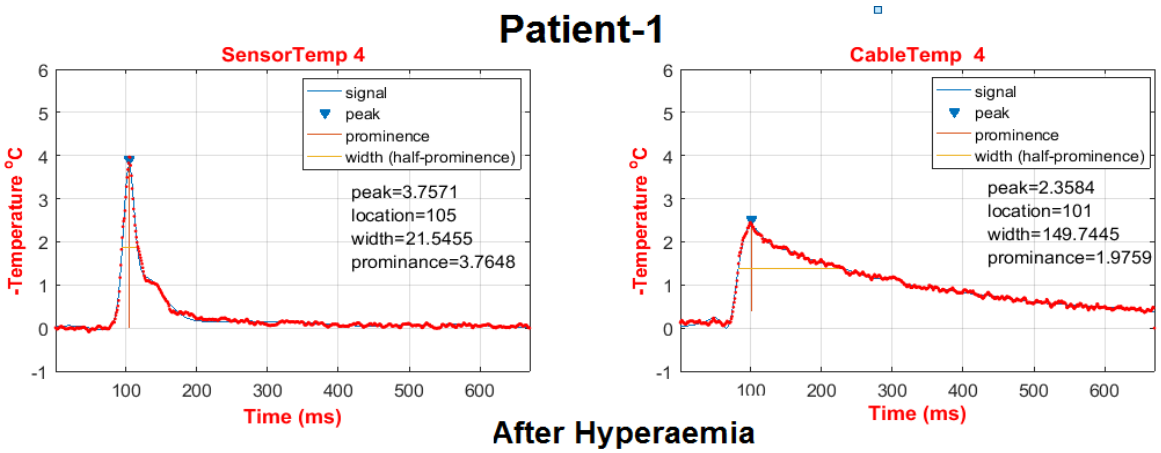

Figure 4.11: Subplot of patient-1 after hyperaemia showing the sudden increase in the peak value of sensor temperature whereas the cable temperature remains the same.

Cable temperature curve remains the same because it detects the temperature within the catheter but we can clearly observe that arrival of the peak of sensor data in hyperaemic condition which is due to increase in flow rates as shown in Figure 4.10 and Figure 4.11.

4.4 Thermodilution Curve Analysis

The next step after finding the values of peaks, prominence, width (half prominence) and the time of the peak occurrence of the sensor and cable temperature data curves of the thermodilution recordings of the twelve patients, was to analyse the spread sheet data during basal and hyperaemic conditions separately. In order to find the correlation between the data before and after hyperaemia, we calculated the mean and the percentage difference of sensor and cable temperature of patient-1 separately and plotted the results as given in Figure 4.12. Spreadsheet given in Table 4.1 shows the first three readings of sensor and cable temperature during basal conditions and the remaining three during hyperaemia.

Thermodilution Data Analysis									
Patient-1									
Sr No	Description	peak	%age Difference	width	%age Difference	Time (Peak Occurs)	%age Difference	prominence	%age Difference
1	SensorTemp 1	2.242	20.33%	42.083	25.21%	164.000	0.20%	2.217	19.47%
3	SensorTemp 2	1.692	7.75%	66.256	19.98%	161.000	1.64%	1.732	5.16%
5	SensorTemp 3	1.551	16.41%	54.328	0.19%	166.000	1.42%	1.522	18.03%
	Mean	1.828		54.222		163.667		1.824	
2	CableTemp 1	2.160	1.10%	160.000	0.01%	97.000	1.03%	1.908	3.10%
4	CableTemp 2	2.268	3.77%	163.188	1.99%	97.000	1.03%	1.998	1.51%
6	CableTemp 3	2.124	2.79%	156.750	2.04%	100.000	2.02%	1.998	1.51%
	Mean	2.184		159.979		98.000		1.968	
7	SensorTemp 4	3.967	13.46%	21.492	9.01%	105.000	1.26%	3.974	14.16%
9	SensorTemp 5	4.036	11.75%	24.292	3.23%	104.000	2.22%	4.087	11.37%
11	SensorTemp 6	5.616	21.20%	24.772	5.19%	110.000	3.39%	5.678	21.41%
	Mean	4.540		23.519		106.333		4.580	
8	CableTemp 4	2.448	0.25%	144.417	0.02%	100.000	0.67%	2.088	0.29%
10	CableTemp 5	2.448	0.25%	143.833	0.38%	100.000	0.67%	2.124	2.00%
12	CableTemp 6	2.430	0.49%	144.900	0.36%	98.000	1.35%	2.034	2.33%
	Mean	2.442		144.383		99.333		2.082	

Table 4.1: Spreadsheet of mean and percentage difference of Patient-1 data

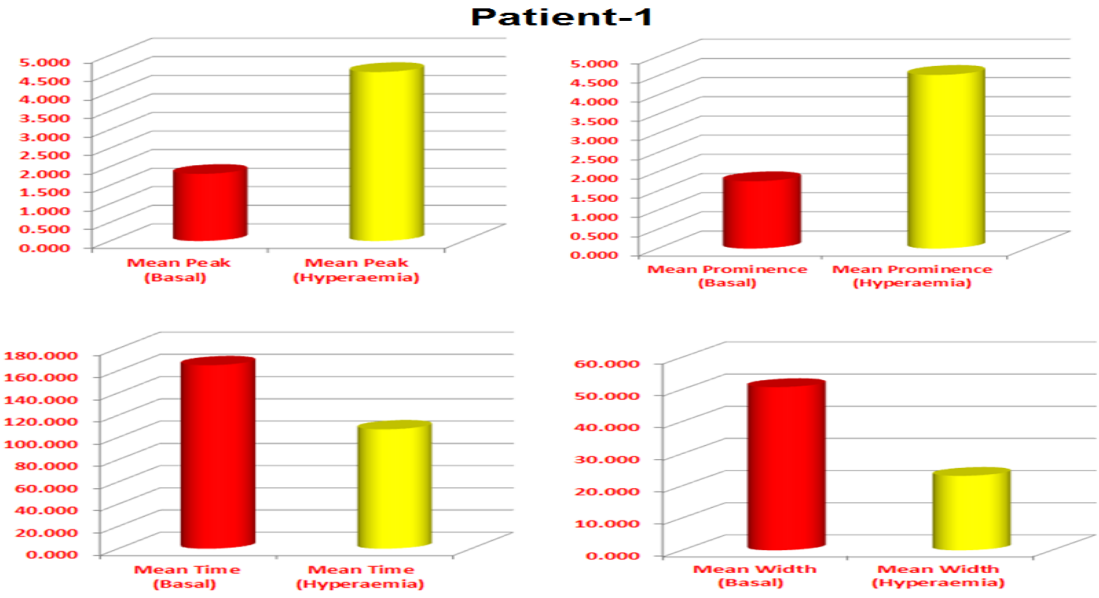

Figure 4.12: Plotted results of mean peak, prominence, width and time before and after hyperaemia showing the relationship between them.

Furthermore, in order to find significant differences between the peak values, as well as the width values before and after hyperaemia, the best suitable statistical approach "Paired T-Test" was used. For this purpose, we calculated the mean values of peak and width of twelve patients' sensor data before and after the hyperaemia, as shown in Table 4.2.

Mean Values of Peak and Width of 12 Patients				
Patient #	Before Injection		After Injection	
	Peak	Width	Peak	Width
1	1.81	50.76	4.55	23.16
2	1.20	127.08	2.23	36.66
3	2.14	97.63	4.94	42.76
4	4.41	36.77	4.53	24.59
5	11.05	33.62	12.13	32.74
6	3.64	44.52	4.02	27.08
7	5.54	33.70	5.27	35.38
8	3.94	35.66	5.01	27.60
9	1.48	100.01	2.90	42.80
10	1.87	79.06	6.03	41.03
11	1.18	102.77	2.50	43.03
12	4.06	43.08	3.99	33.61

Table 4.2: Spreadsheet of mean values of peak and width of 12 patients

The collected data was tested statistically under paired t-test with the following hypotheses;

Null Hypothesis: There is no significant difference between the peaks of two samples $\mu_1 - \mu_2 = 0$.

Alternate Hypothesis: There is significant difference between the peaks of two samples $\mu_1 - \mu_2 \neq 0$.

Using the sample size n = 12 patients, the following results were obtained:

Mean Values of Peak and Width of 12 Patients						
Patient #	Before	After	Peak Difference	Before	After	Width Difference
	Peak	Peak		Width	Width	
1	1.81	4.55	2.74	50.76	23.16	-27.60
2	1.20	2.23	1.03	127.08	36.66	-90.43
3	2.14	4.94	2.80	97.63	42.76	-54.87
4	4.41	4.53	0.12	36.77	24.59	-12.18
5	11.05	12.13	1.08	33.62	32.74	-0.87
6	3.64	4.02	0.37	44.52	27.08	-17.44
7	5.54	5.27	-0.27	33.70	35.38	1.68
8	3.94	5.01	1.07	35.66	27.60	-8.06
9	1.48	2.90	1.41	100.01	42.80	-57.21
10	1.87	6.03	4.15	79.06	41.03	-38.02
11	1.18	2.50	1.31	102.77	43.03	-59.74
12	4.06	3.99	-0.07	43.08	33.61	-9.47

Table 4.3: Spreadsheet of mean difference values of peak and width of 12 patients

We then calculated the mean and standard deviation of the differences of peak and width values using SPSS Statistics Data Editor as shown in Figure 4.13

Paired Samples Statistics

		Mean	N	Std. Deviation	Std. Error Mean
Pair 1	peak_basal	3.5267	12	2.77367	.80069
	peak_hyp	4.8417	12	2.56569	.74065
Pair 2	width_basal	65.3883	12	33.69873	9.72799
	width_hyp	34.2033	12	7.32532	2.11464

Paired Samples Correlations

		N	Correlation	Sig.
Pair 1	peak_basal & peak_hyp	12	.880	.000
Pair 2	width_basal & width_hyp	12	.719	.008

Paired Samples Test

		Paired Differences					t	df	Sig. (2-tailed)
		Mean	Std. Deviation	Std. Error Mean	95% Confidence Interval of the Difference Lower	Upper			
Pair 1	peak_basal - peak_hyp	-1.31500	1.32357	.38208	-2.15595	-.47405	-3.442	11	.006
Pair 2	width_basal - width_hyp	31.18500	28.88391	8.33807	12.83304	49.53696	3.740	11	.003

Figure 4.13: Paired T-Test results of the mean peak and width values of 12 patients

The data has been tested at the 0.05 significance level. The p-value of the paired t-test is less than the 0.05; it leads to rejection of null hypothesis. Consequently, it is concluded that there is a significant difference between the peak values as well as the width values of 12 patients before and after the hyperaemia. On the other hand, the Pearson Correlation (0.88) shows that the peaks have strong relationship as compared to the widths whose Pearson Correlation is 0.72 as shown in Figure 4.13.

To find the change in the complete thermodilution waveforms, we calculated the mean hyperaemic over mean control ratios of the peaks, width and the time at which the peak occurs of sensor temperature data with the help of Matlab program. The program was designed to separate even and odd columns data where even columns represent the cable temperature and odd ones represent the sensor temperature. After making them separate, we then calculated the mean values of the first and last three odd and even columns respectively by using 'mean' command because first and last three columns of each even and odd columns represent the values taken before and after hyperaemia. The purpose was to find the mean hyperaemic to control or basal ratio. For this pur-

pose, we used the Matlab command 'Ratio' for finding the required ratios and saved the required data in the form of two spread sheets; one for sensor and the other one for cable temperature (Appendix B.3). Table 4.4 shows the mean hyperaemic to basal ratios of peak, width, time and prominence of the sensor temperature data of twelve patients.

Thermodilution Data Analysis 12-Patients Data Sensor Temperature Data					
Sr No	Description	Peak	Width	Time	prominance
1	Patient-1	2.517	0.651	0.456	2.581
2	Patient-2	1.853	0.477	0.288	2.051
3	Patient-3	2.308	0.563	0.438	2.336
4	Patient-4	1.026	0.929	0.669	1.038
5	Patient-5	1.098	1.007	0.974	1.100
6	Patient-6	1.103	0.740	0.608	1.119
7	Patient-7	0.952	0.887	1.050	0.954
8	Patient-8	1.271	0.745	0.774	1.281
9	Patient-9	1.953	0.804	0.428	2.044
10	Patient-10	3.214	0.711	0.519	3.322
11	Patient-11	2.111	0.554	0.419	2.280
12	Patient-12	0.983	0.691	0.780	0.989

Table 4.4: Mean hyperaemic to basal ratios of peak, width, time and prominence of the sensor temperature data of 12 patients

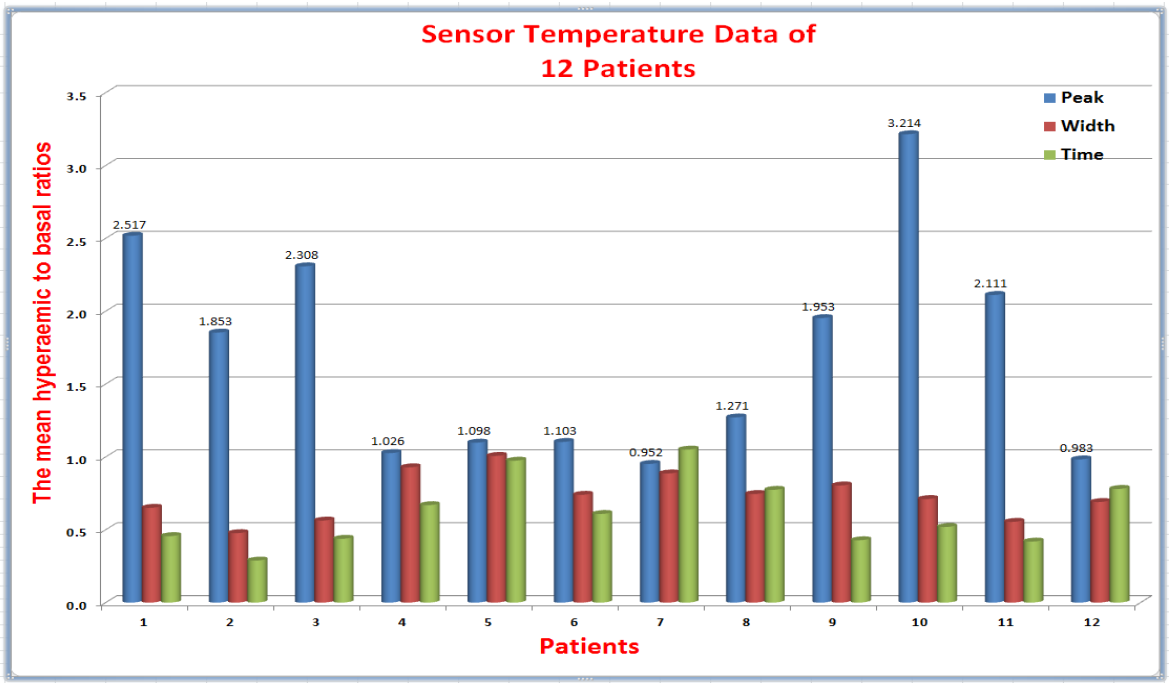

Figure 4.14: Plotted results of mean hyperaemic to basal ratios of peak, width and time of 12 patients data

From Figure 4.14 one can easily observe that there is a significant difference in peak values with respect to width ratios. We then rearranged the data into descending order with respect to peak values as shown in Figure 4.15, from which we can visualize that in almost half of the data the peak value is more than the double value of the width. On the basis of this analysis, we split the data mutually into two groups with peak values $>$ or $<$ 1.5.

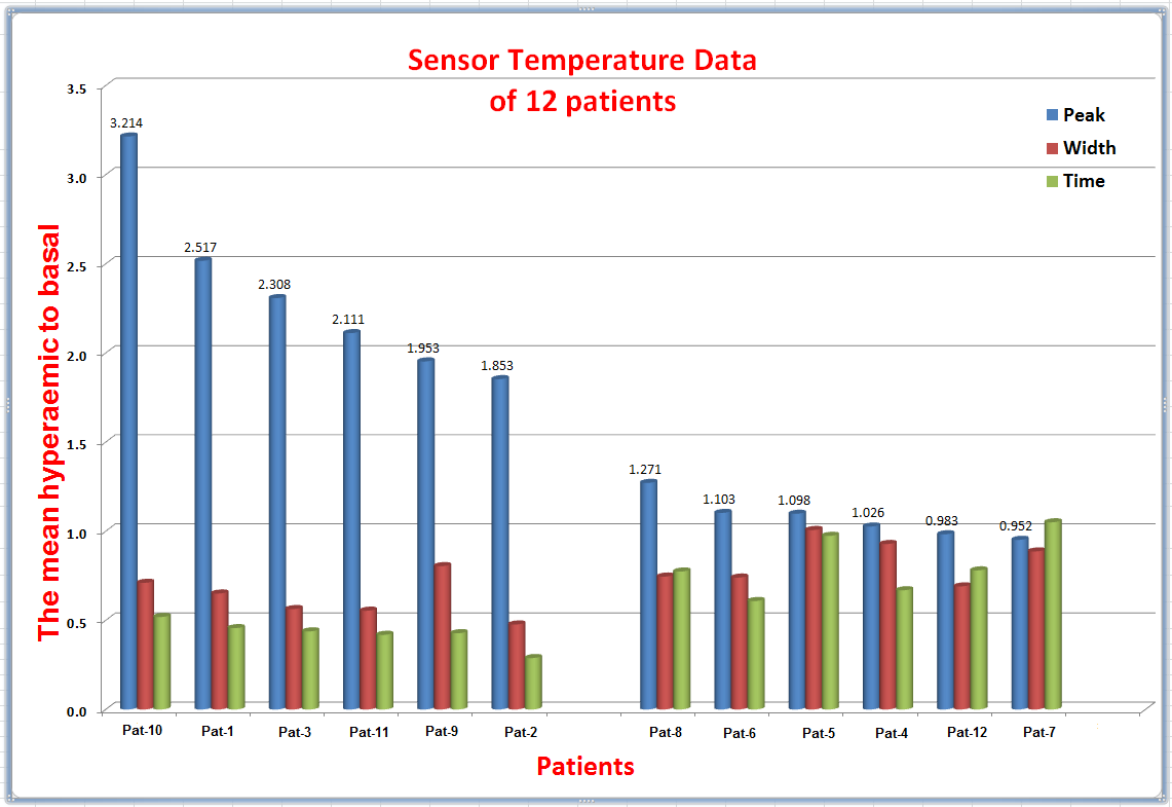

Figure 4.15: Results plotted in descending order of mean hyperaemic to basal ratios of peak, width and time

The next we found the correlation (strength of relationship) between the peak and width so that we can better understand if there is some relation which might be useful for the clinical purpose. The formulae for finding the correlation coefficient (r) are shown in equation (4.5).

$$r = \frac{\sum(x-\bar{x})(y-\bar{y})}{\sqrt{[\sum(x-\bar{x})^2][\sum(y-\bar{y})^2]}} = \frac{n\sum(xy) - \sum x \sum y}{\sqrt{[n\sum(x^2) - \sum(x)^2][n\sum(y^2) - \sum(y)^2]}} \tag{4.5}$$

where

r= sample correlation coefficient

n = number of patients

x = peak value

y = width value

We calculated the correlation coefficient between peak value and the width value using equation (4.5).

Thermodilution Data Analysis						
Sensor Temperature data of 12 Patients						
Sr No	Description	Peak (x)	Width (y)	xy	x2	y2
1	Patient-1	2.517	0.651	1.637	6.337	0.423
2	Patient-2	1.853	0.477	0.883	3.434	0.227
3	Patient-3	2.308	0.563	1.300	5.325	0.317
4	Patient-4	1.026	0.929	0.953	1.053	0.862
5	Patient-5	1.098	1.007	1.105	1.205	1.013
6	Patient-6	1.103	0.740	0.816	1.216	0.547
7	Patient-7	0.952	0.887	0.844	0.905	0.786
8	Patient-8	1.271	0.745	0.947	1.615	0.556
9	Patient-9	1.953	0.804	1.570	3.812	0.646
10	Patient-10	3.214	0.711	2.284	10.333	0.505
11	Patient-11	2.111	0.554	1.170	4.458	0.307
12	Patient-12	0.983	0.691	0.679	0.966	0.477
Total		**20.388**	**8.757**	**14.188**	**40.659**	**6.668**

Table 4.5: Spreadsheet showing the calculations for finding the correlation coefficient

$$r = -0.533894$$

$$r^2 = 0.2850$$

If the value of r is +1 or -1, it means both variables have a perfect positive or negative relationship. For instance, if one variable increases or decreases, the other variable will also increase or decrease and vice versa. The closer the value of r to +1 or -1, the stronger the relationship between two variables and the value of r equal to 0 shows that there is no relationship. The value of r in our case is -0.53 which signifies a weak relationship between peak and width values and can also be visualised in the scattered plot (Figure 4.16).

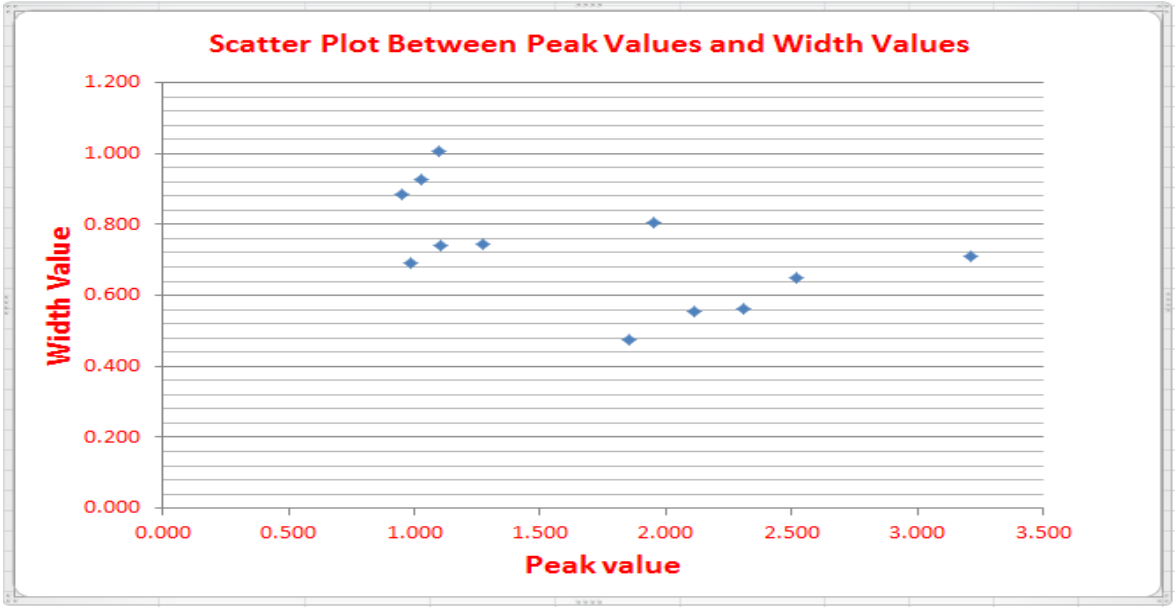

Figure 4.16: Scatter plot between peak and width values of 12 patients

Another simple method is to find the correlation with the help of Microsoft spreadsheet directly without any mathematical calculations.

1. Open the Microsoft spreadsheet and go to the data menu.
2. Click on the data analysis short cut and select the correlation.
3. Select the pair of data to find the correlation between them.

The result is shown in Figure 4.17.

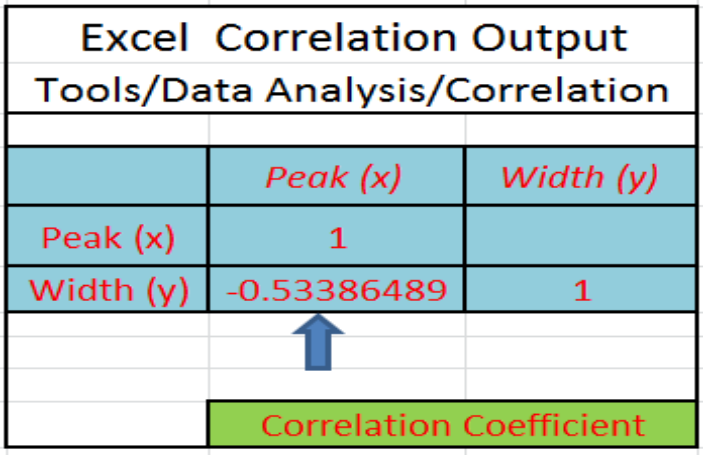

Figure 4.17: Spreadsheet showing the value of correlation coefficient

It was observed from the above calculations that there was a weak relationship between peak and width values of the sensor temperature thermodilution data. However,

visual inspection of Figure 4.16 shows that we can qualitatively assign the data into two cluster groups as shown in Figure 4.18, which is useful for further analysis.

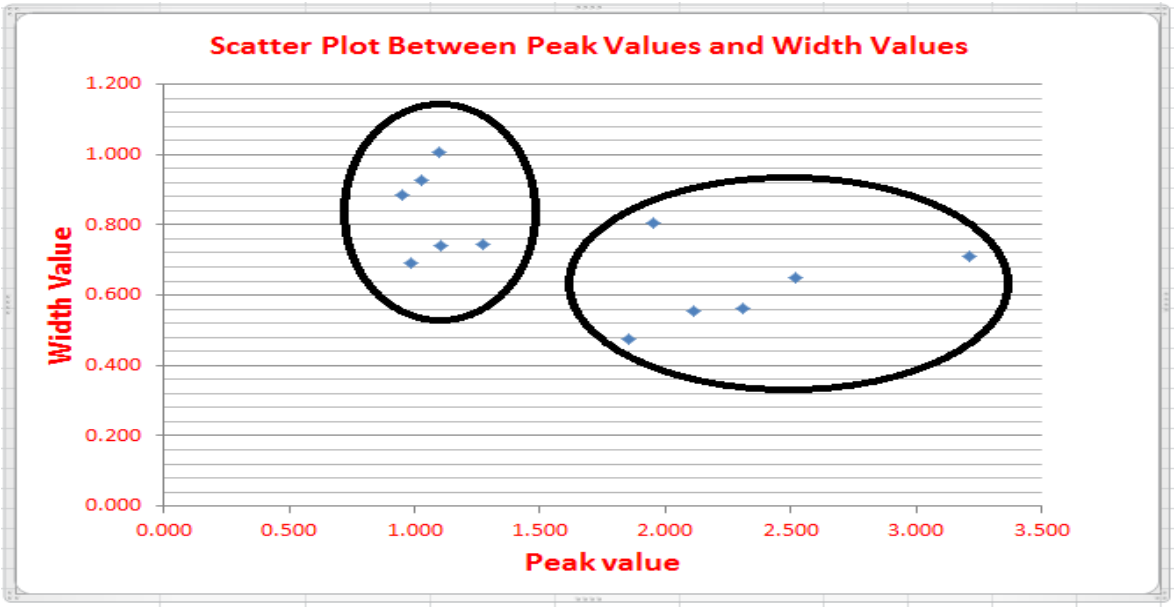

Figure 4.18: Cluster data plot between peak and width ratios of sensor temperature

After observing the scatted plot between peak and width values, next step was to compare the peak values with CFR, FFR, IMR. For this purpose we noted the values of CFR, FFR, and IMR from Radiview software screen for each patient and made a separate spreadsheet for these values. We then put the values of mean hyperaemic to basal ratio of peak in the next column to IMR for further analysis of data as shown in Table 4.6.

Thermodilution Data Analysis						
12 Patients						
Patient #	CFR	FFR	IMR	Peak	Width	Time
1	4.60	0.78	15.00	2.52	0.65	0.46
2	4.50	0.40	34.00	1.85	0.48	0.29
3	4.00	0.78	17.00	2.31	0.56	0.44
4	2.40	0.70	9.00	1.03	0.93	0.67
5	1.10	0.86	11.00	1.10	1.01	0.97
6	3.60	0.17	11.00	1.10	0.74	0.61
7	2.00	0.80	17.00	0.95	0.89	1.05
8	3.40	0.87	15.00	1.27	0.75	0.77
9	2.00	1.00	69.00	1.95	0.80	0.43
10	2.70	0.86	27.00	3.21	0.71	0.52
11	3.30	0.66	54.00	2.11	0.55	0.42
12	3.40	0.84	24.00	0.98	0.69	0.78

Table 4.6: Comparison table of CFR, FFR and IMR with peak, width and time ratios

The plotted results of CFR, FFR and IMR against peak values are shown in Figures 4.19, 4.20 and 4.21 respectivily.

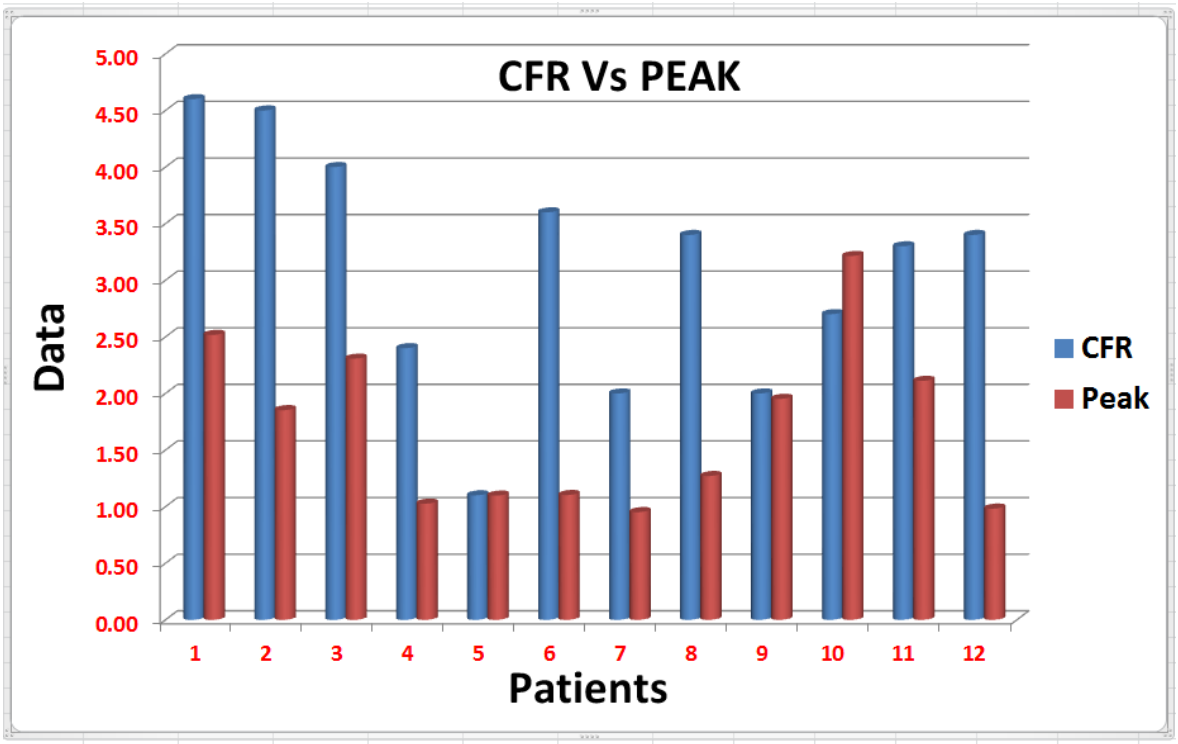

Figure 4.19: CFR Vs Peak

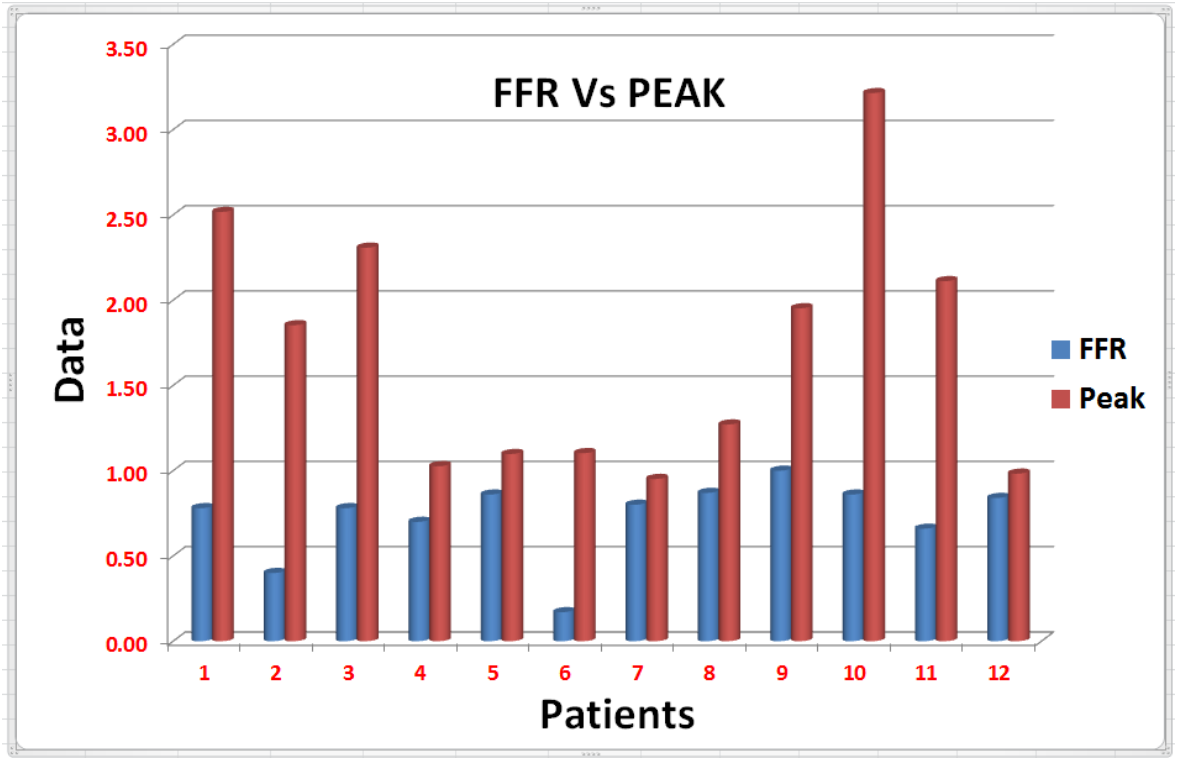

Figure 4.20: FFR Vs Peak

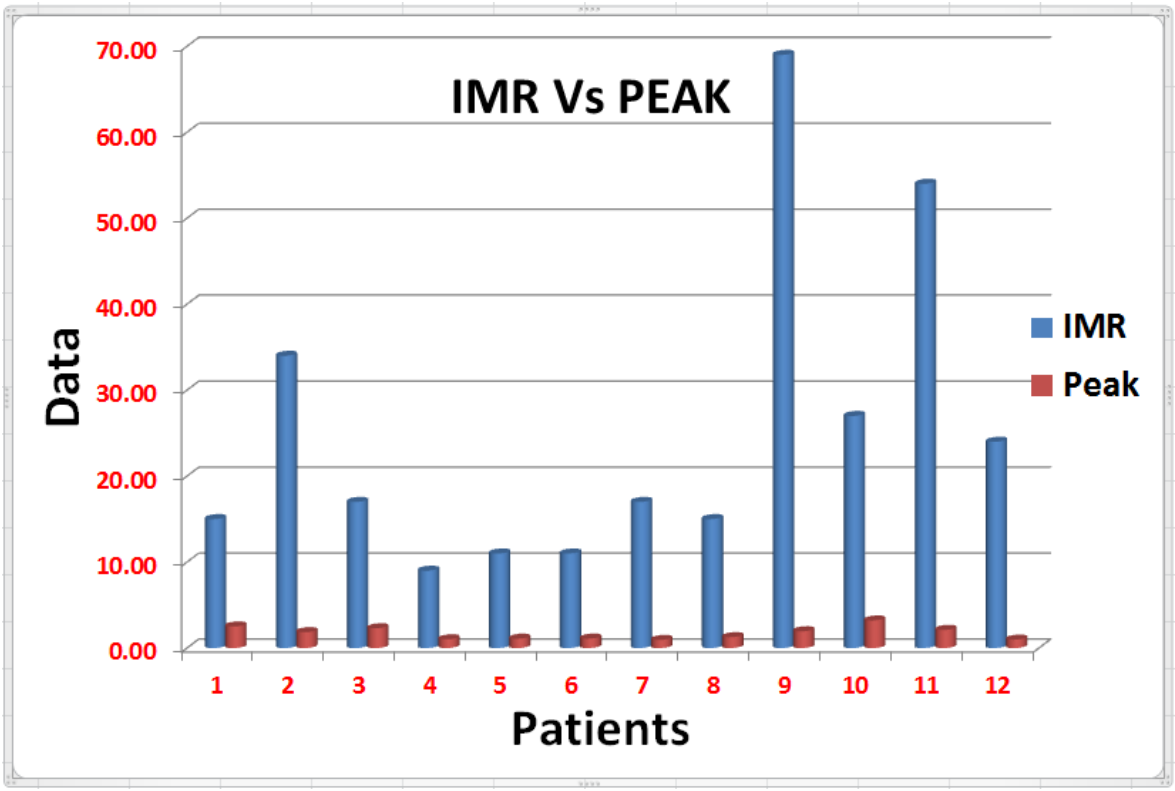

Figure 4.21: IMR Vs Peak

We then plotted the scatter graph to see the correlation between peak ratios and CFR, FFR and IMR and also calculated the value of correlation coefficient between them to check the relationship.

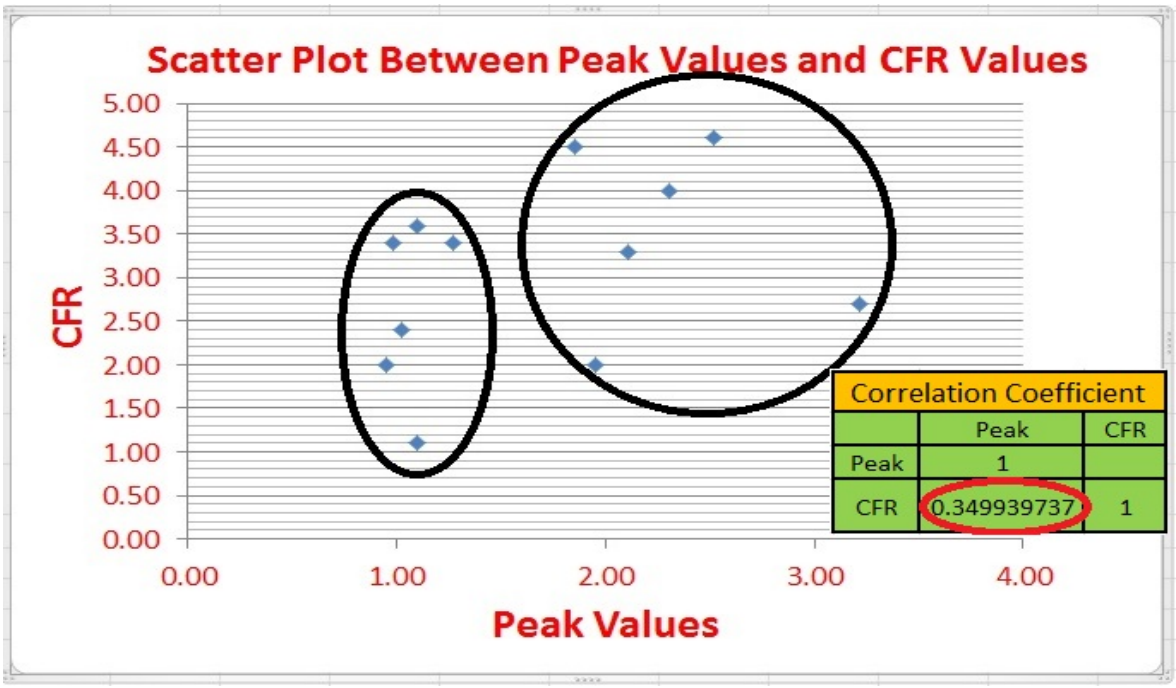

Figure 4.22: Scatter plot between CFR and peak values showing that there are two groups of cluster data with peak values > 1.5 and < 1.5

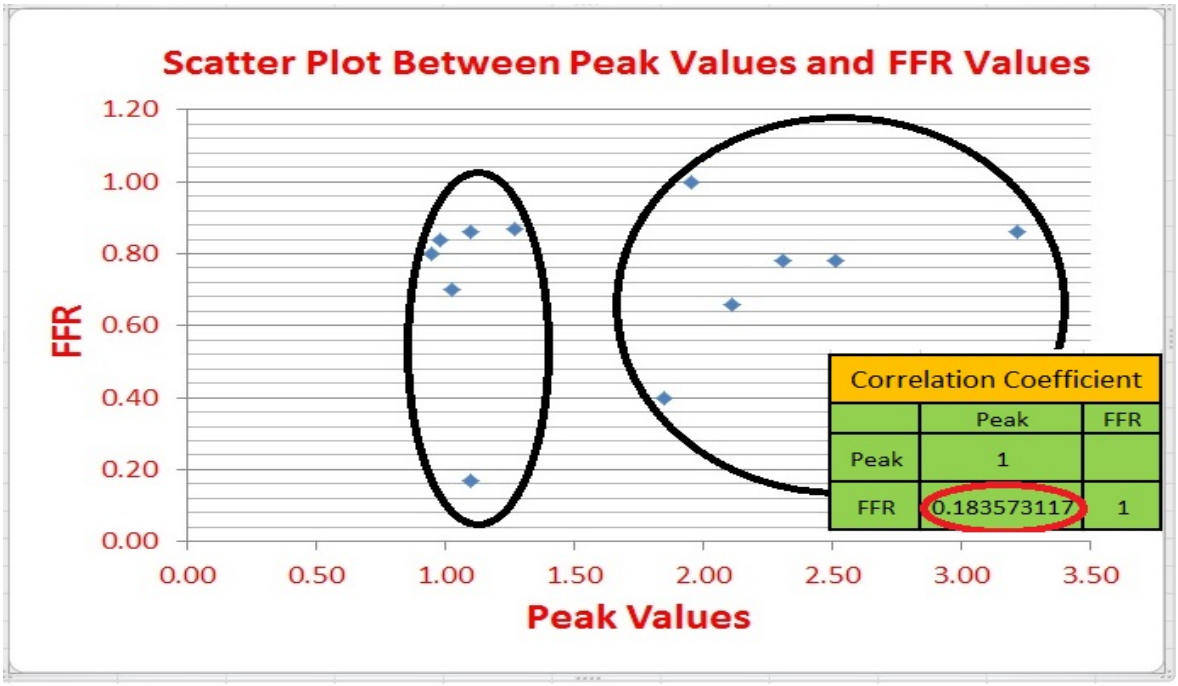

Figure 4.23: Scatter plot between FFR and peak values showing that there are two groups of cluster data with peak values > 1.5 and < 1.5

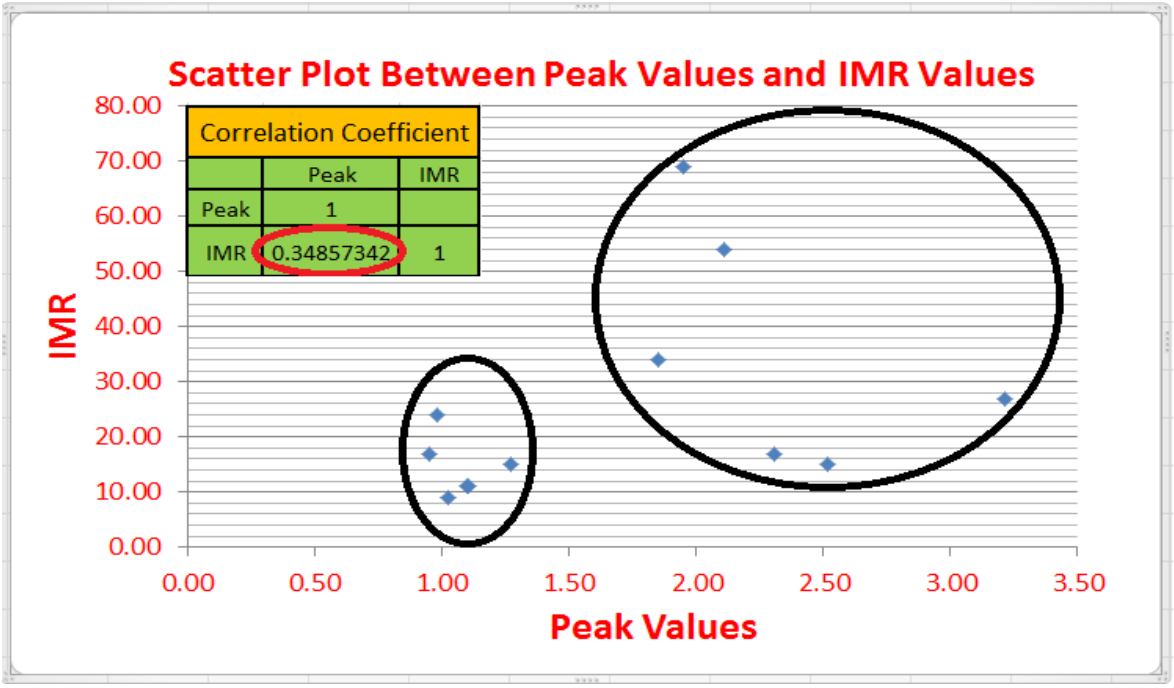

Figure 4.24: Scatter plot between IMR and peak values showing that there are two groups of cluster data with peak values > 1.5 and < 1.5

The value of correlation coefficient shows the week relationships between the peak values and CFR, FFR and IMR. However if we look at the scatter plots we can divide the data into two groups with peak values > 1.5 and < 1.5 as shown in Figures 4.22, 4.23 and 4.24. As coronary artery flow is pulsatile i.e. reduced in systole and increased

during diastole, we did not see any evidence of pulsatility in the thermodilution data.

4.5 Analysis of Data from CE-MARC2 Study

Following the analysis of the initial data sets of 12 patients, the study was extended to all of the large CE-MARC2 data set which has 66 patients including the unfixed 12 (Appendix B.1). CE-MARC2 study pressure wire data set is from a group of patients with stable anginal symptoms who attended for invasive coronary angiography. Thermodilution was performed in an epicardial artery > 2.5 mm diameter with a stenosis of 40% to 90%.

The data includes an excel spreadsheet in which next to each patient's study number was the coronary vessel from which the measurement was obtained (LAD = left anterior descending artery, Cx = circumflex artery, RCA = right coronary artery), the data obtained from the Radiview pressure wire recordings (eg. FFR, IMR, CFR). Additionally, some patients had thermodilution recordings repeated after coronary stenting (percutaneous coronary intervention, PCI) and these recordings were also noted in the spreadsheet.

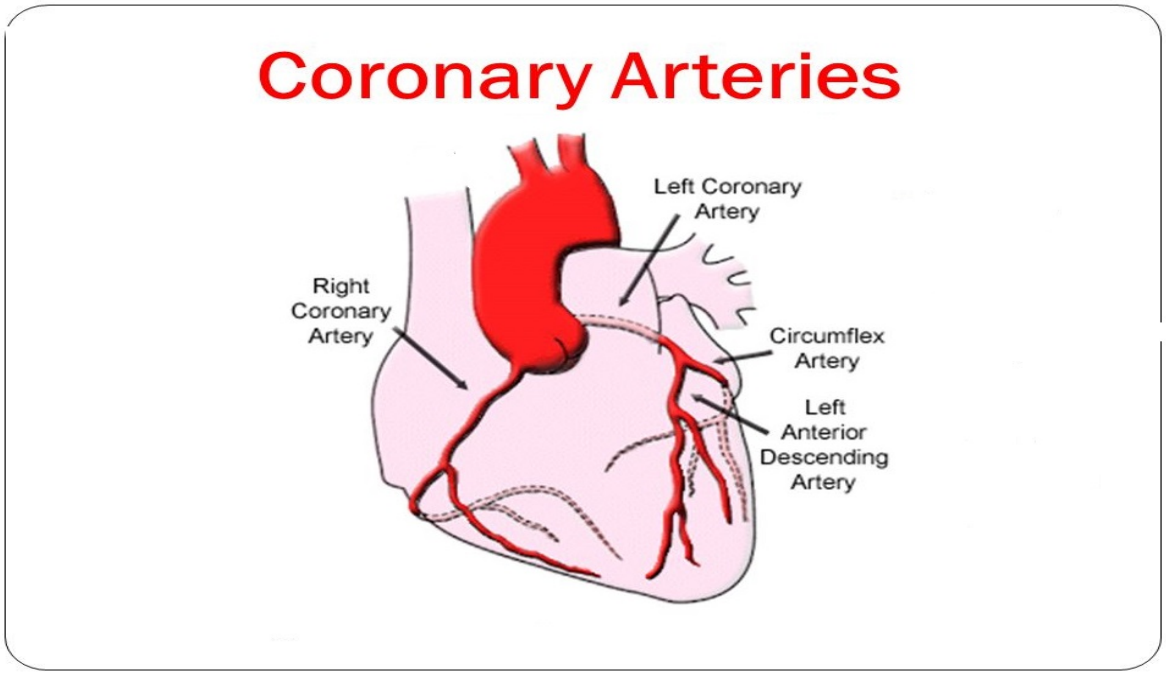

Figure 4.25: Coronary Arteries [48]

We converted thermodilution data of 66 patients into spreadsheets with the help

of Radiview software and loaded that data into Matlab program for further analysis. With the help of same, we calculated the values of peaks, width and the time at which the peaks occurs and the data was saved into separate spreadsheets (Appendix B).

We then separated the data of patients according to different coronary arteries (LAD, RCA and CX) in which thermodilution was performed and plotted the results.

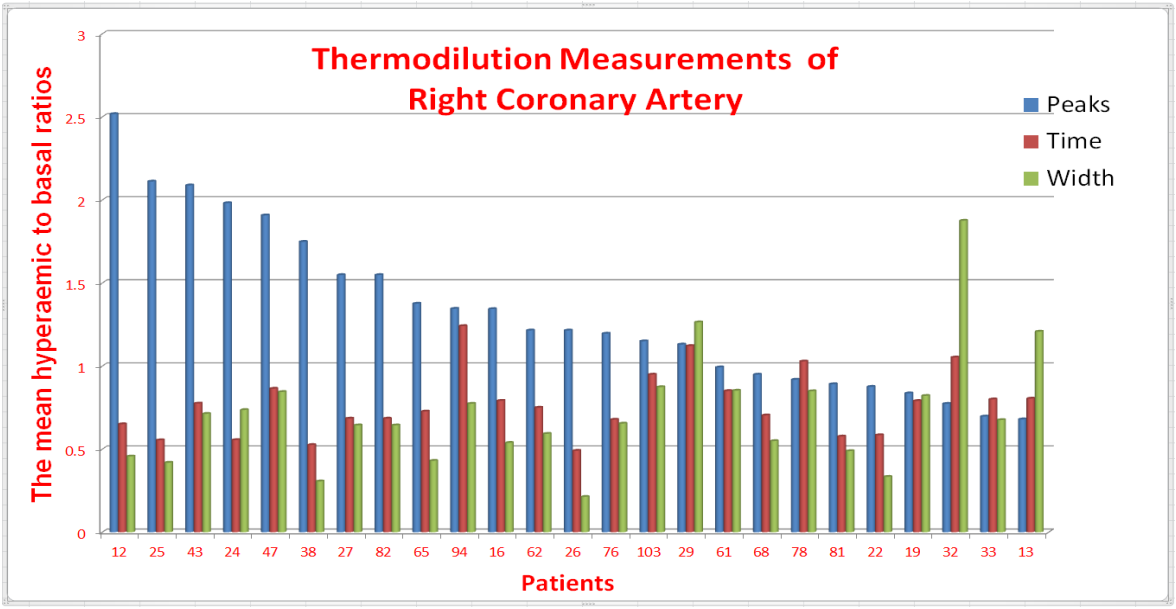

Figure 4.26: Comparison betweeen mean hyperaemic to basal ratio of peak, width and time in Right Coronary Artery

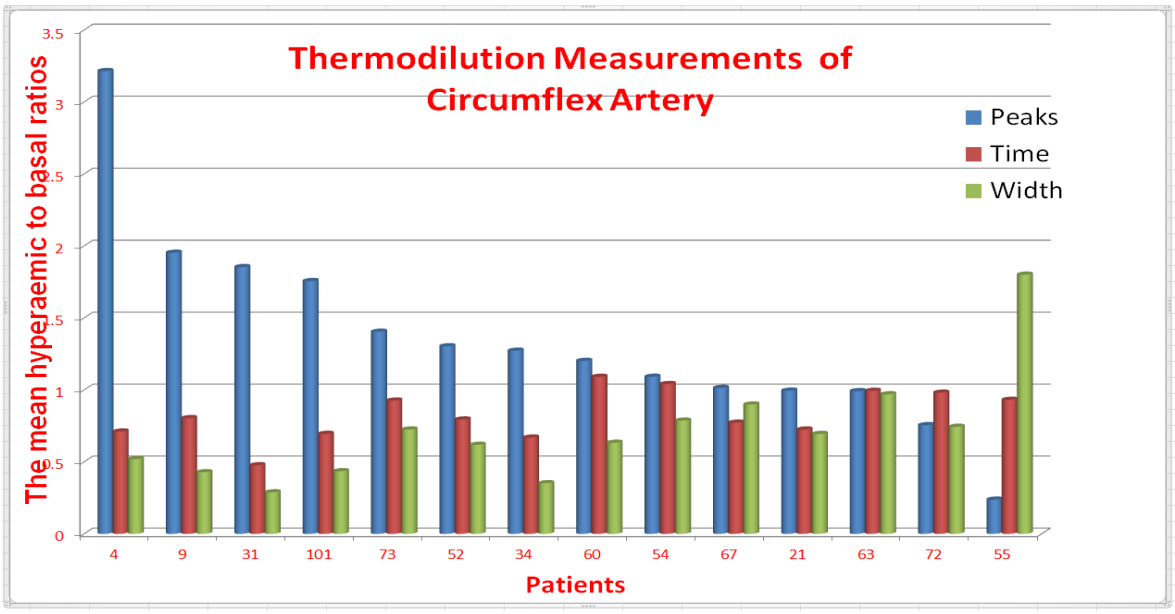

Figure 4.27: Comparison betweeen mean hyperaemic to basal ratio of peak, width and time in Circumflex Artery

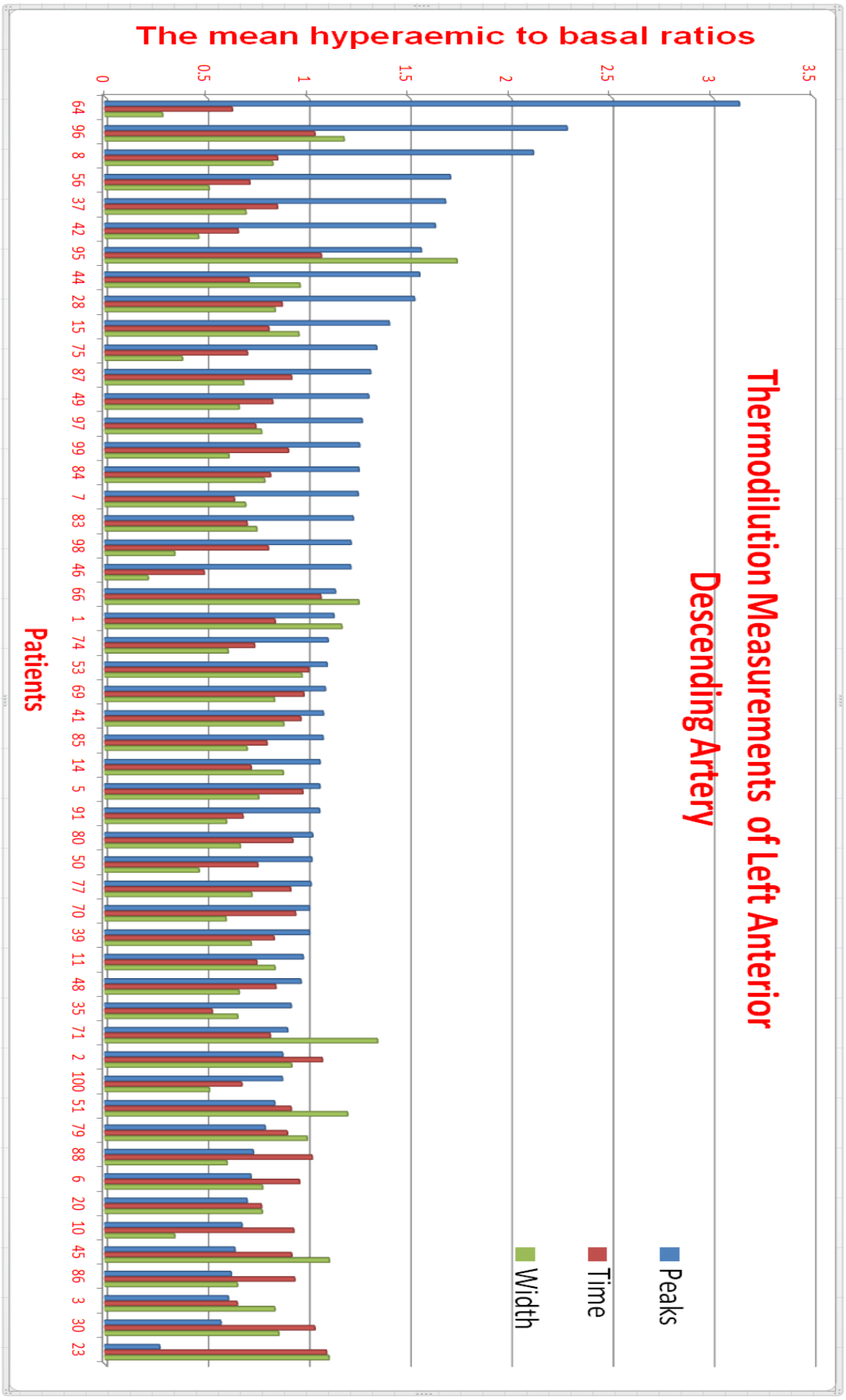

Figure 4.28: Comparison betweeen mean hyperaemic to basal ratio of peak, width and time in Left Anterior Decending Artery

Furthermore, some patients had thermodilution recordings repeated after coronary stenting (percutaneous coronary intervention, PCI). The plotted result is shown in Figure 4.29.

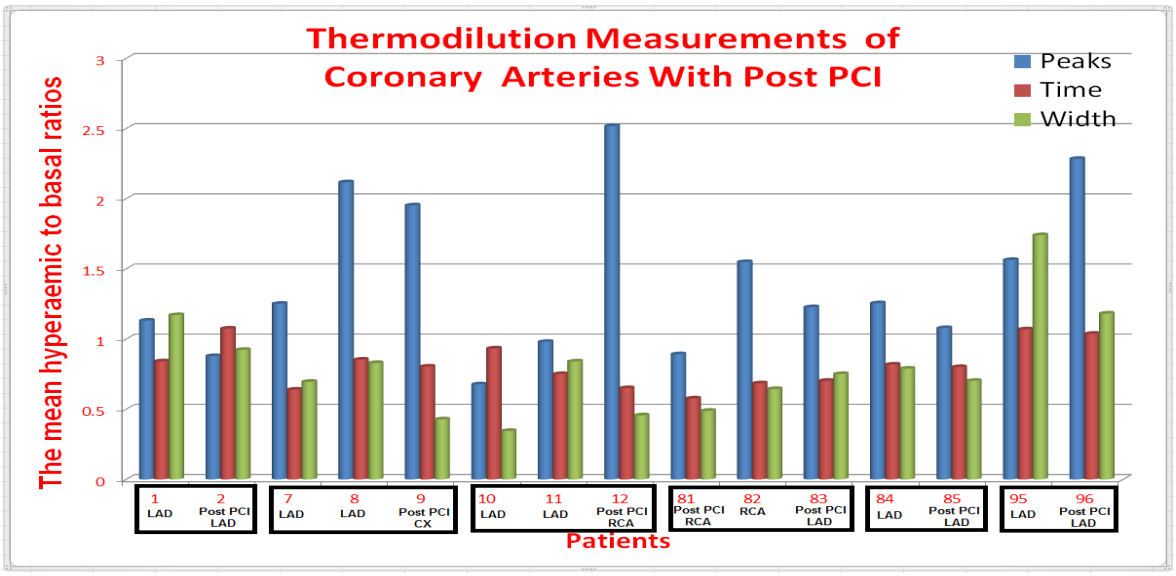

Figure 4.29: Comparison betweeen mean hyperaemic to basal ratio of peak, width and time in coronary arteries after PCI

After a careful observation of the shapes of the thermodilution data of 66 patients, we divided the sensor temperature data into different categories and plotted the results so that we can better analyse the data and can deduce some useful results.

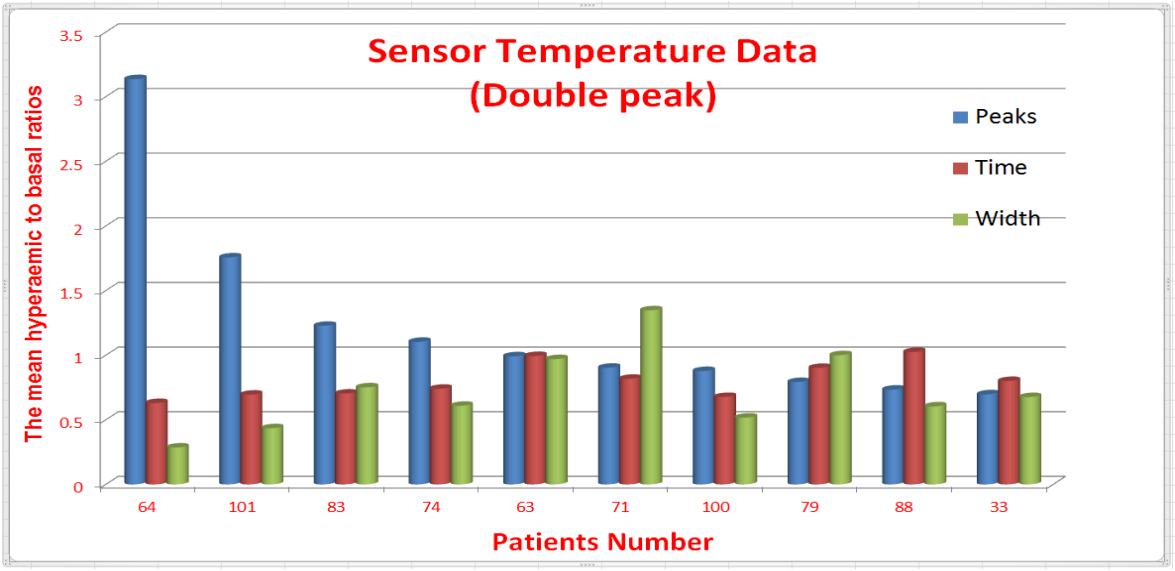

Figure 4.30: Sensor temperature data of the patients having double peak curves

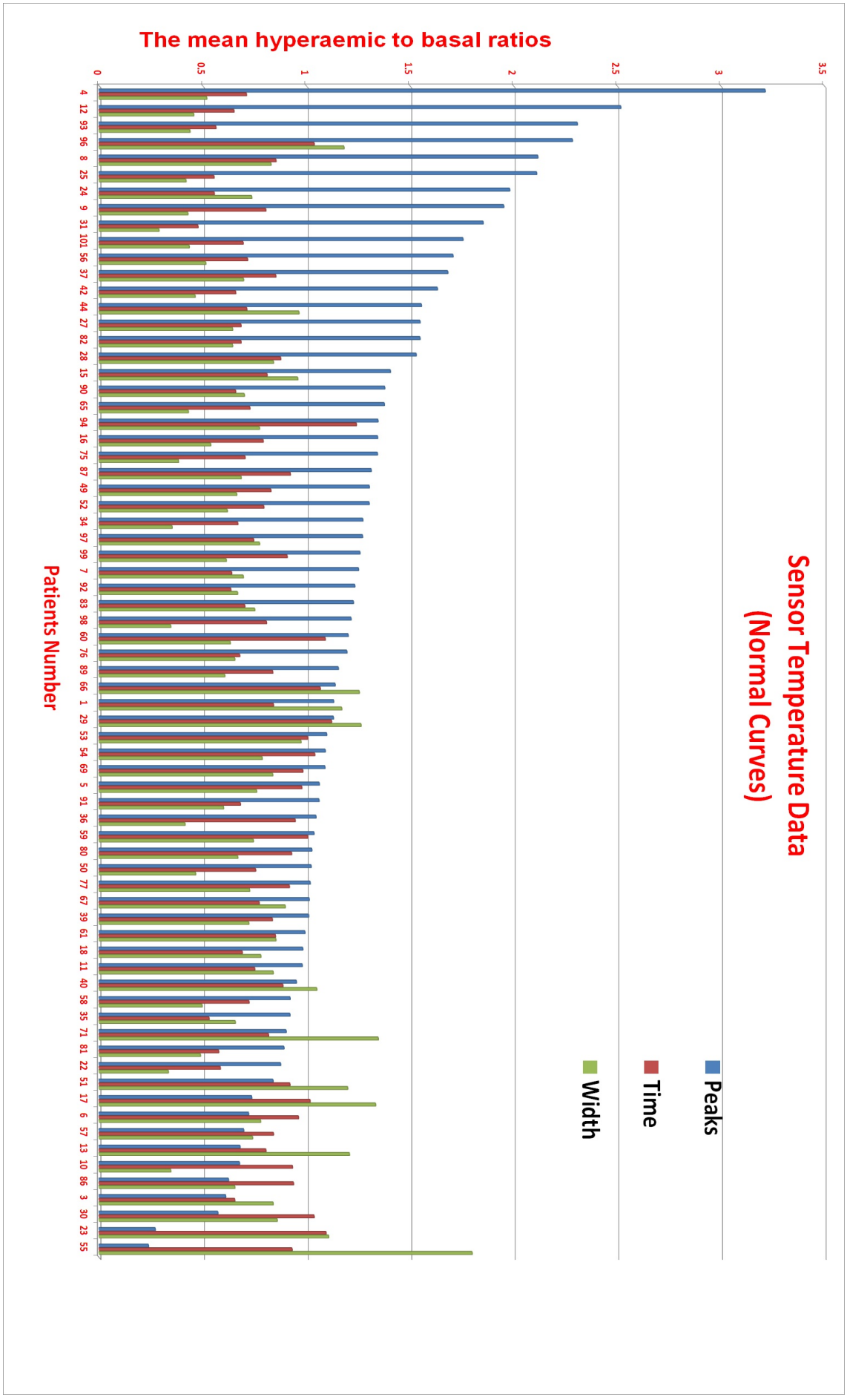

Figure 4.31: Sensor temperature data of the patients having normal thermodilution curves

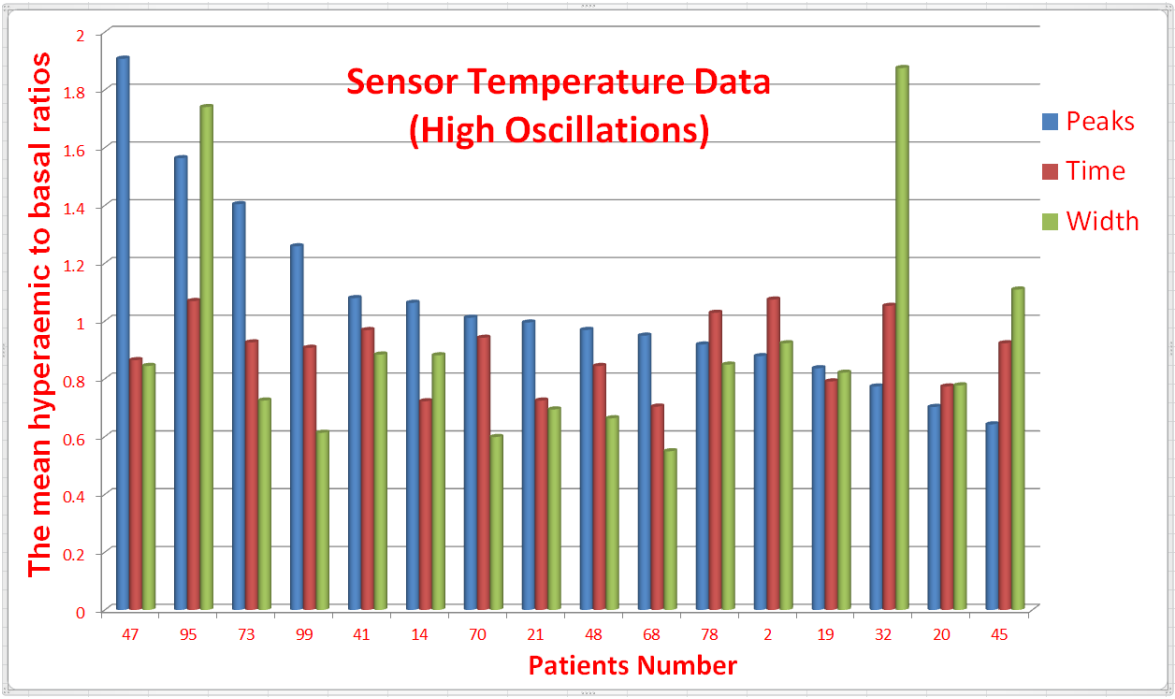

Figure 4.32: Sensor temperature data of the patients having high oscillation in the curves

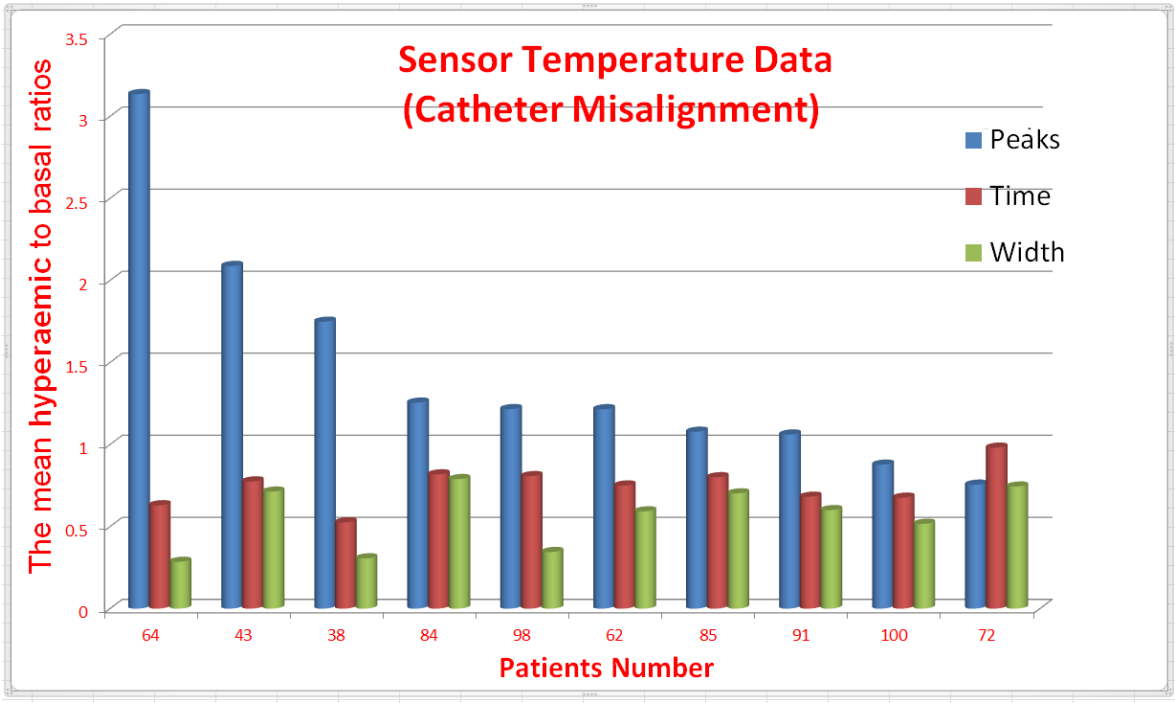

Figure 4.33: Sensor temperature data of the patients having abnormal curves that may be due to the catheter misalignment

We then calculated the correlation coefficient for the sensor temperature data of patients having normal curves without any double peak or oscillation and plotted the scatter plot to see the correlation between the peak and width hyperaemic to basal

ratios as shown in Figure 4.34.

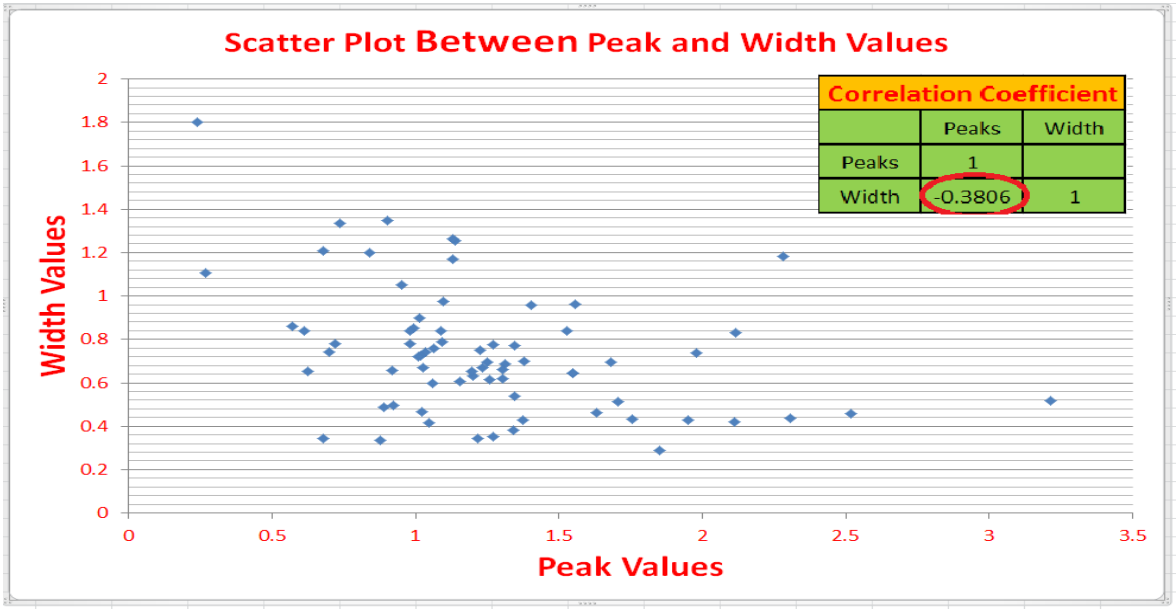

Figure 4.34: Scatter plot showing a weak relationship between the hyperaemic to basal ratios of peak and width of sensor temperature data of patients having normal curves

We also plotted the scatter plot between the peak ratios and CFR, FFR and IMR of the normal patients data but no significant correlation was found. The scatter plots are given below:-

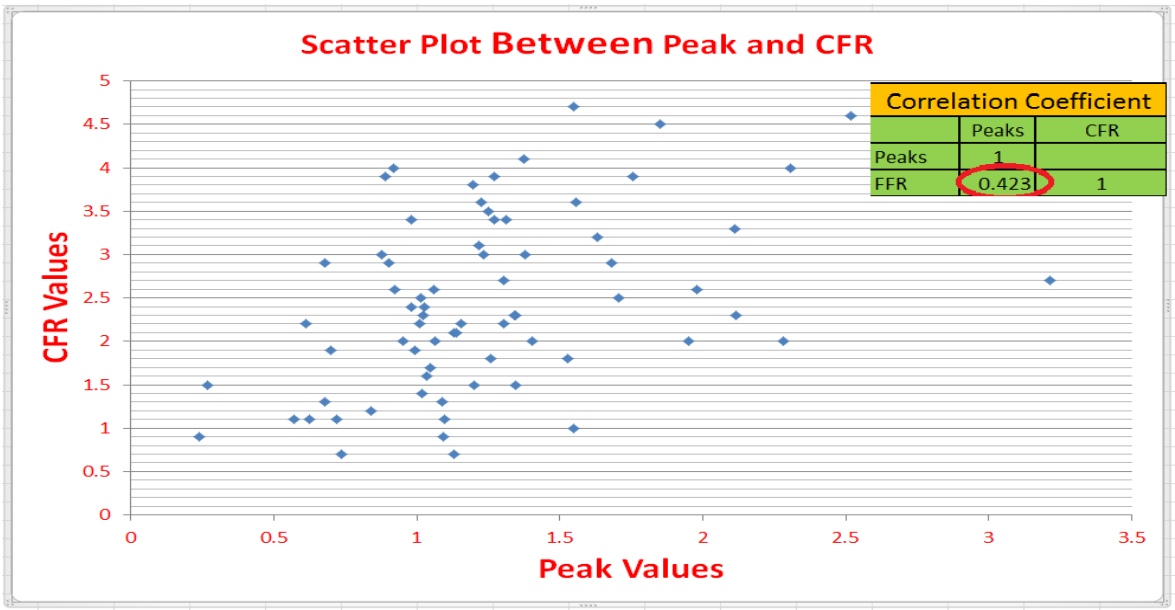

Figure 4.35: Scatter plot showing a weak relationship between between peak ratios and CFR values of sensor temperature data of patients having normal curves

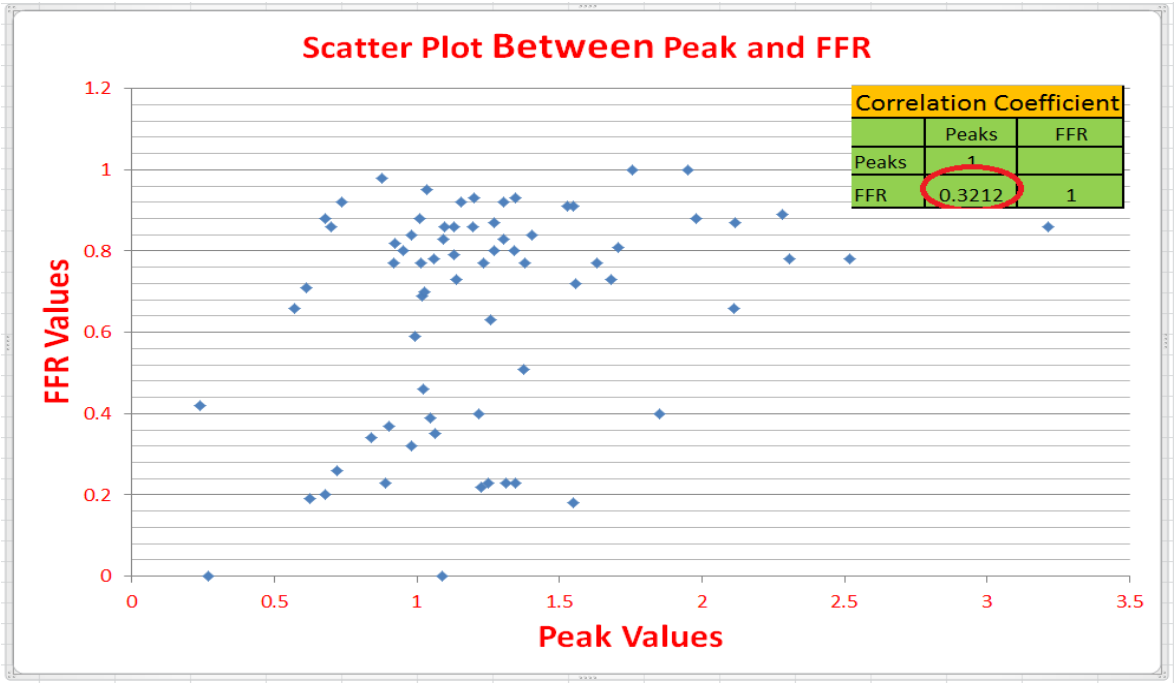

Figure 4.36: Scatter plot showing a weak relationship between peak ratios and FFR values of sensor temperature data of patients having normal curves

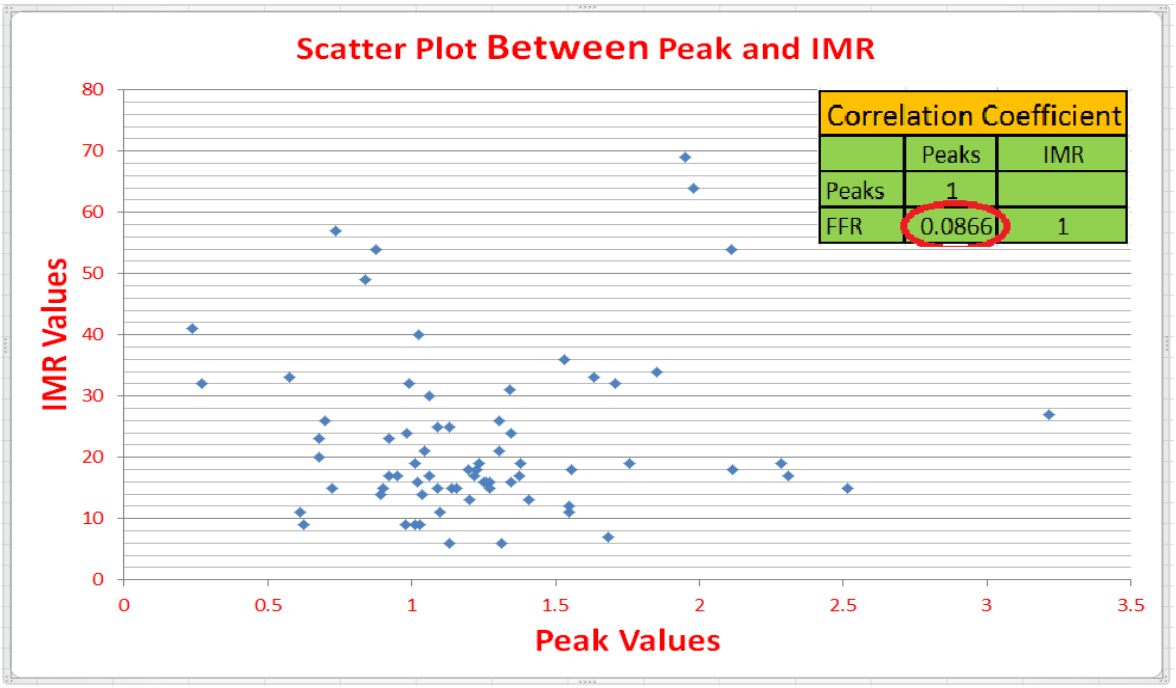

Figure 4.37: Scatter plot showing a weak relationship between peak ratios and IMR values of sensor temperature data of patients having normal curves

The analysis on the full data sets shows no significant correlation between peak and width ratios, peak and CFR, peak and FFR and peak and IMR values. The analysis of 66 patients'data shows no significant correlation between peakn and width ratios, peak and CFR, peak and FFR and peak and IMR values. The preliminary study

indicates that the patients are divided into two groups. However, if we analyse the whole data set, it does not divide the patients' data into two groups. This highlights the importance of testing the statistical hypothesis on larger data sets.

4.6 Curve Categories

Motivated by the suggestions from our clinical colleagues that particular features of some typical thermodilution curves are of clinical significance, we attempted to identify and analyse these features. After visualizing the data curves, we divided these into different categories:-

4.6.1 Normal Curve

We observed in most of the data sets that the curve has a smooth upstoke towards peak and a gradual downslope towards base line. There is no clear gap indicating compromise of the microcirculation but the relative height of the temperature peaks seems to be the strongest signal and one can set threshold values. Some typical results are shown in Figures 4.38, 4.39 and 4.40.

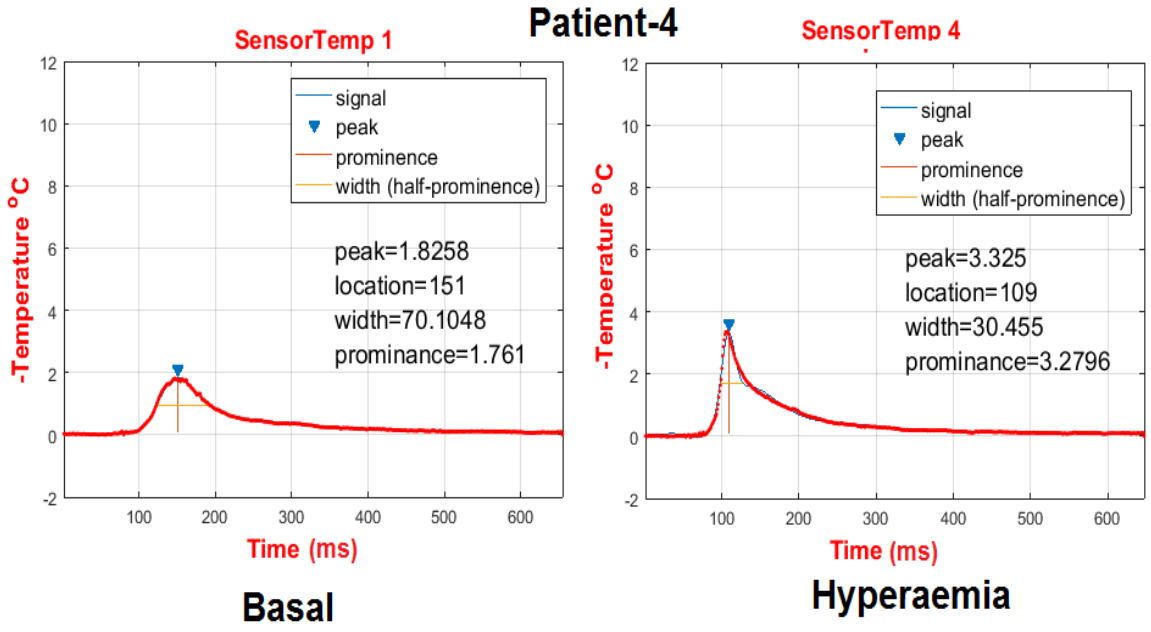

Figure 4.38: Sensor temperature data of patient-4 showing the increase in peak value during hyperaemic condition due to the increase in blood flow rate.

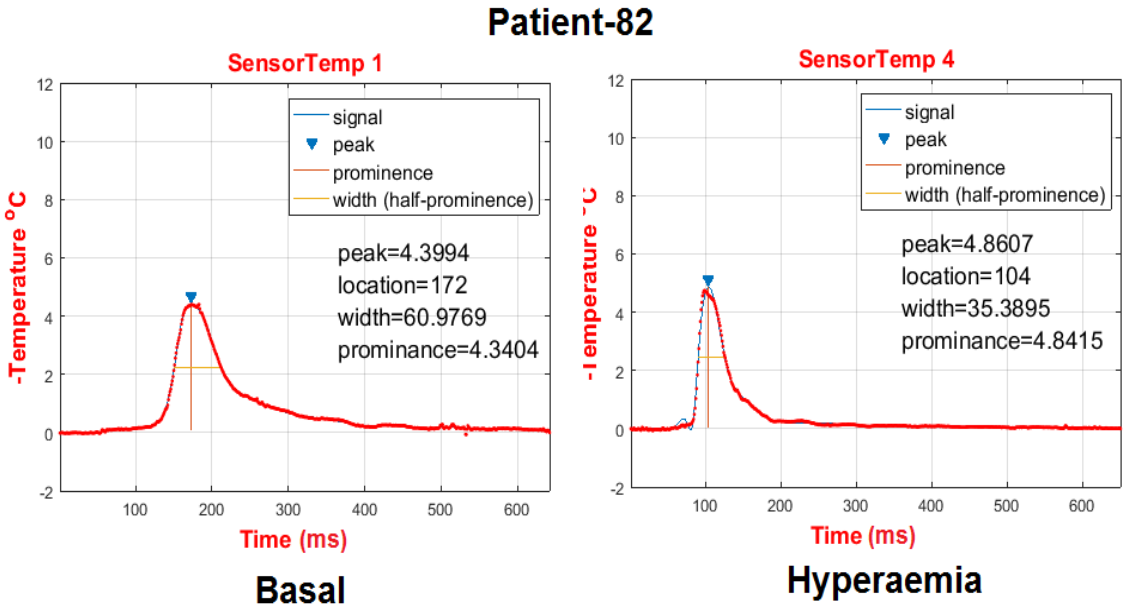

Figure 4.39: Sensor temperature data of patient-82 shows that there is not too much increase in peak value during hyperaemic condition

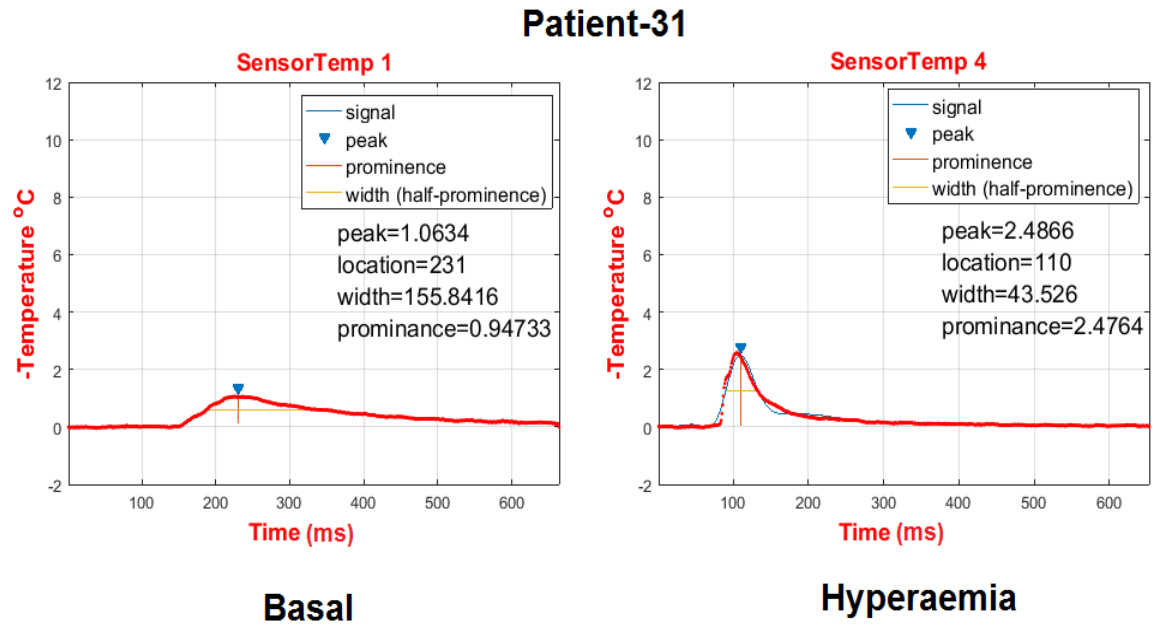

Figure 4.40: Sensor temperature data of patient-31 shows that the early arrival of the peak during hyperaemic condition due to the increase in blood flow rate.

4.6.2 Double Peak

We have observed a few with a double peak but these are not usually reproduced in all three tests in a set, so they do not seem to be significant as shown in Figures 4.41, 4.42 and 4.43.

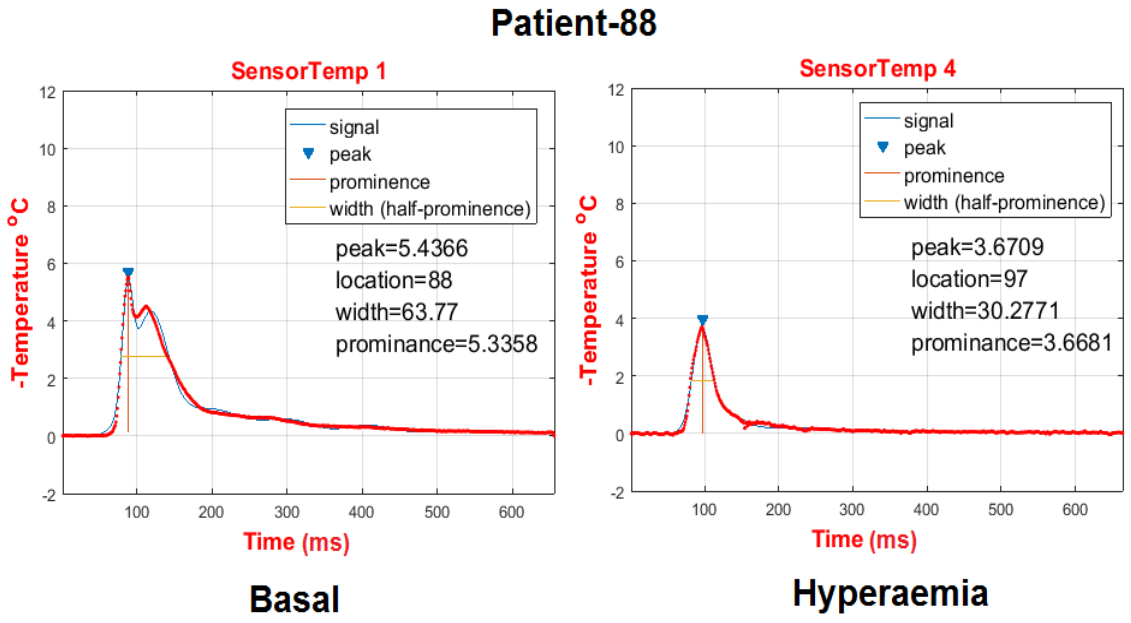

Figure 4.41: Sensor temperature data of patient-88 showing small double peak near the shoulder during basal condition but there is no double peak during hyperaemia.

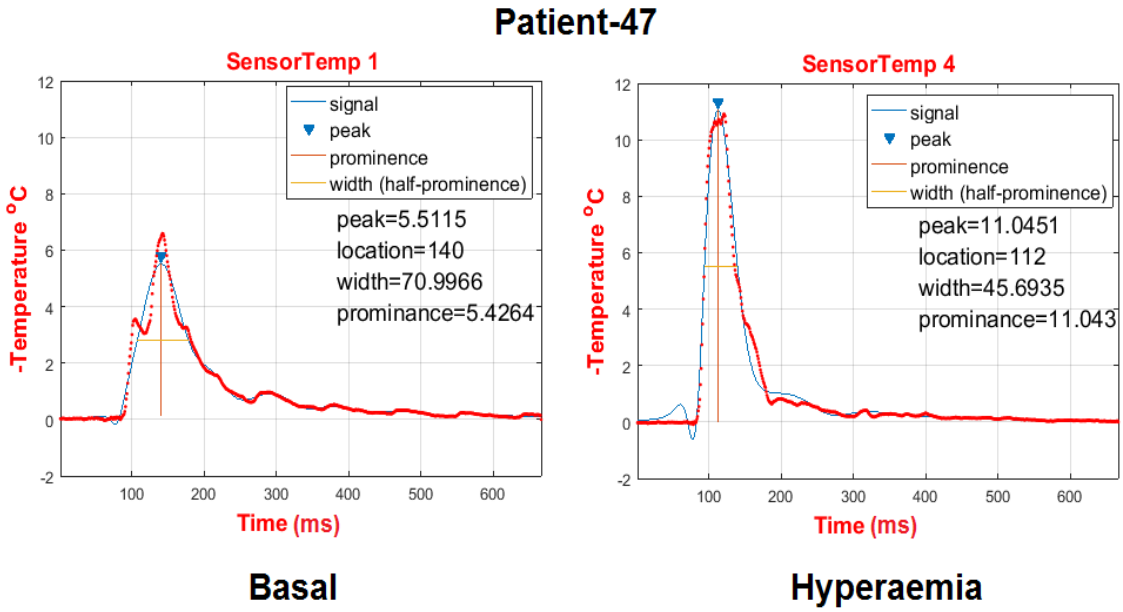

Figure 4.42: Sensor temperature data of patient-47 showing double peak during basal condition.

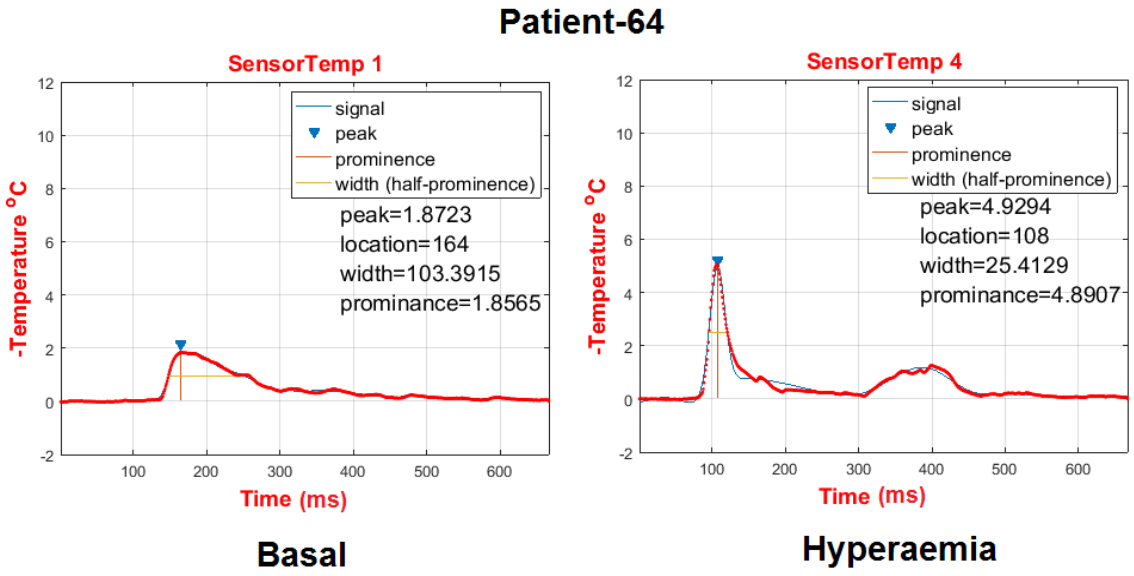

Figure 4.43: Sensor temperature data of patient-64 shows the double peak at the end of curve during hyperaemic condition.

4.6.3 Misalignment of Guide Catheter

We have observed high frequency oscillations in about 15 of the data sets. These look to be a fluid mechanical origin due to a misaligned outlet. Professor Colin Berry advised that it is a plausible sporadic set-up problem at the time of the thermodilution protocol with misalignment of guide catheter non-coaxial with the long axis of the coronary artery.

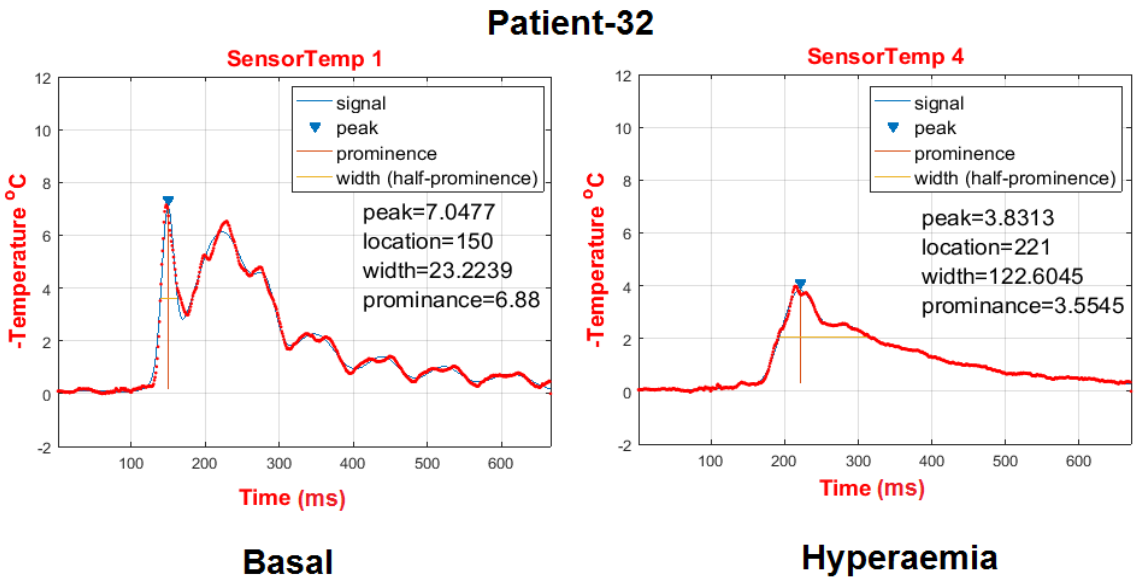

Figure 4.44: Sensor temperature data of patient-32 showing high oscillations due to the misalignment of the guide catheter.

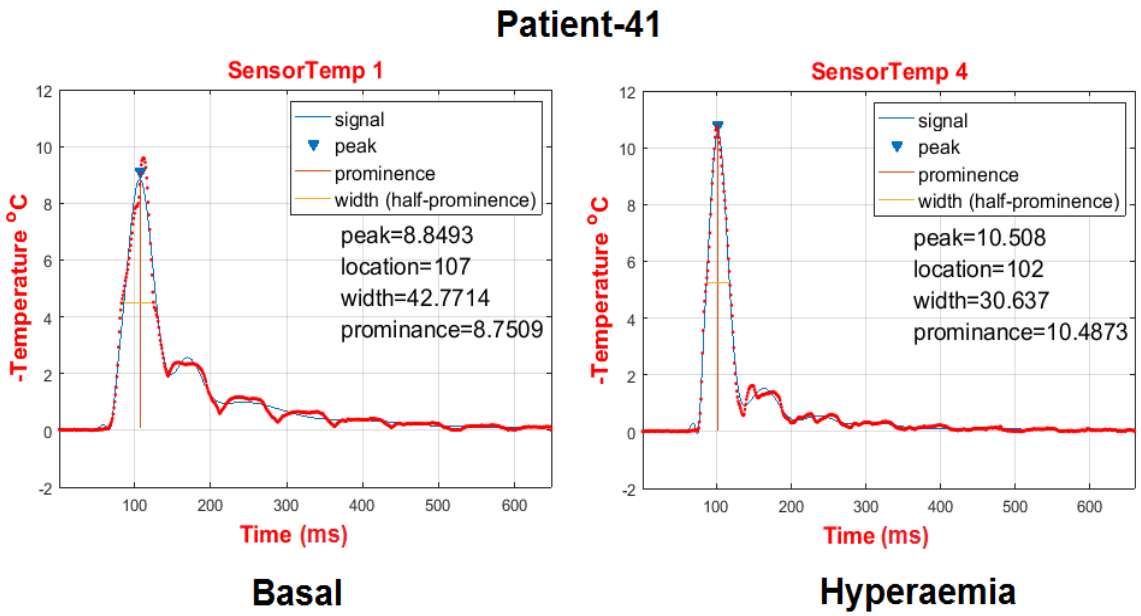

Figure 4.45: Sensor temperature data of patient-41 showing high oscillations at the down stream curve due to the misalignment of the guide catheter.

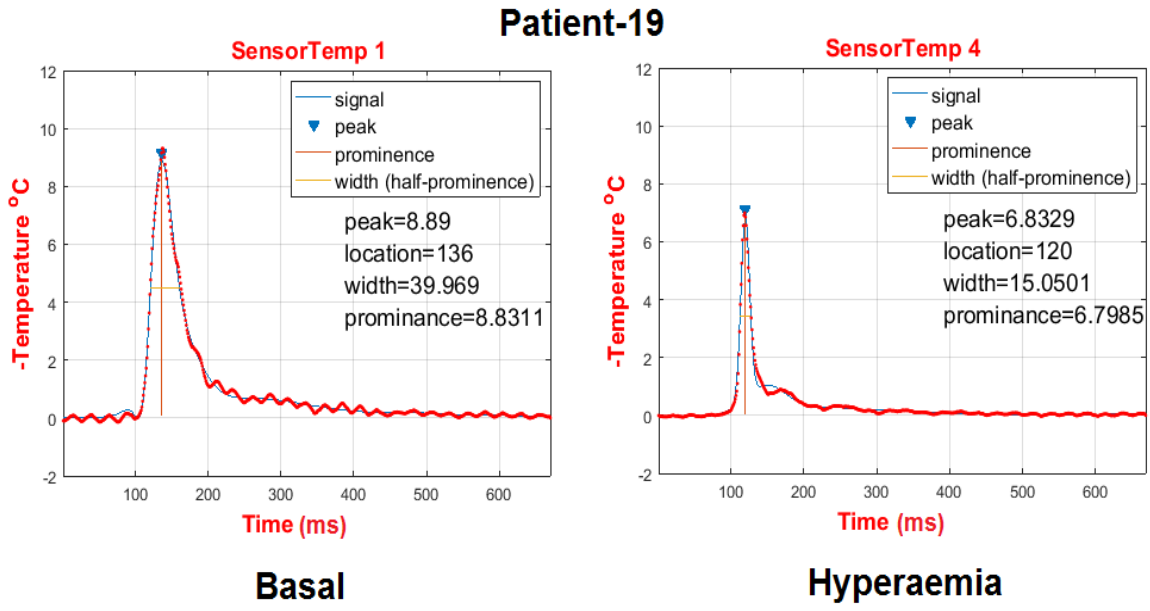

Figure 4.46: Sensor temperature data of patient-19 showing high oscillations at the start and the end of the curve due to the misalignment of the guide catheter.

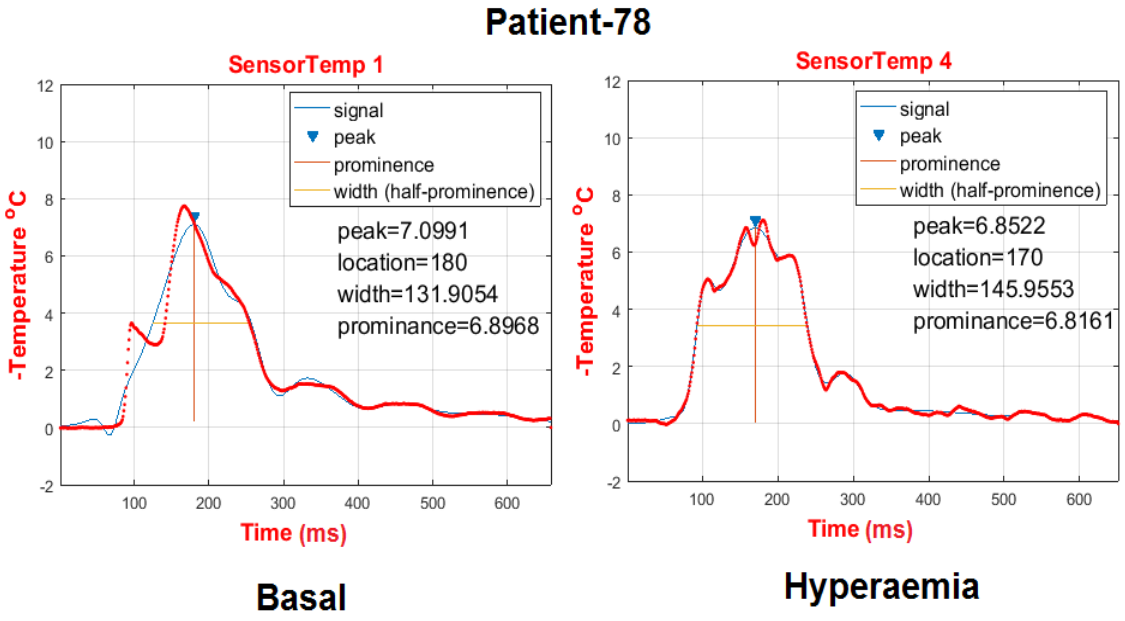

Figure 4.47: Sensor temperature data of patient-78 showing double peak and oscillations due to the wrong positioning of the guide catheter.

4.6.4 Curves with High/Low Starting/Final Temperature

Finally, we have also observed a few with high or low starting or final temperatures and discussed with Professor Colin Berry. He suggested that inadvertent spilling of a small amount of room temperature saline could explain a negative start point or spilling to cool then mixing of warm blood may explain a positive start point (reset of baseline with saline). Furthermore, he also explained that the artery is actually warmer at the location of the sensor.

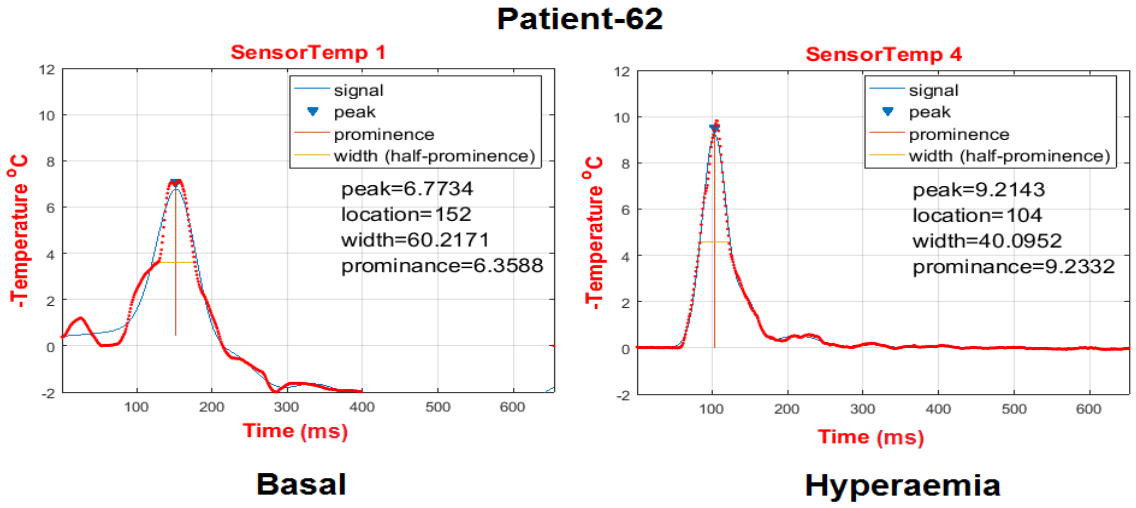

Figure 4.48: Sensor temperature data of patient-62 showing curves with high and low starting temperature

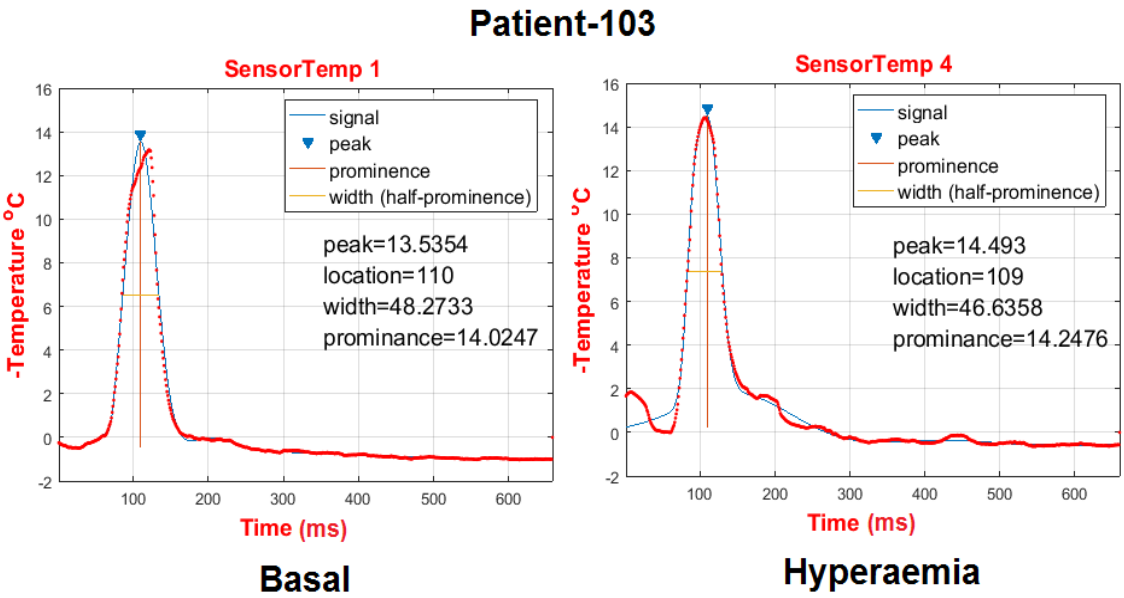

Figure 4.49: Sensor temperature data of patient-103 showing curves with high and low starting temperature

4.7 Conclusion

1. The data sets show no significant correlation between peak and width, CFR, FFR and IMR values.

2. Almost 70% of data sets have normal thermodilution profiles but a number have different features.

3. Double peaks are not reproduced in all of 3 readings, taken before hyperaemia or the 3 taken during hyperaemia, which might be caused by an error in the measurement technique.

4. High frequency variations in the thermodilution plot seem likely to have a fluid mechanical origin associated with e.g. vortex shedding or are associated with collapse of a vessel due to Bernoulli effects. This may occur when the catheter is positioned very close to a vessel wall.

To understand the possible causes for results with double peaks, we proceeded to a CFD study the clinical measurement which is reported in Chapter 5.

Chapter 5

Simulation of Coronary Artery Thermodilution

5.1 Introduction

Pressure and flow behaviour taking place in the coronary arteries has generally been under the discussion and being researched frequently as well. Generally, in order to determine the flow, a model based on coronary arteries is built through which the fluid is made to pass resembling with the flow during normal conditions. Calculations on the basis of empirical data are made for estimating the features of flow. If such experiment is carried out appropriately, it can produce accurate results. At the same time, due to the complexity of mentioned experiment, there are number of things that could go wrong and hence can affect the overall accuracy of results [229].

5.2 Governing Equations

Computational Fluid Dynamics (CFD) programs solve the fundamental equations of the fluid dynamics (continuity, momentum and energy equations). Blood flow through the coronary arteries is 3-dimensional. The unsteady incompressible Navier-Stokes equation holds for any 3-dimensional Newtonian fluid and the blood flowing the coronary arteries is thought to be well-approximated as a Newtonian fluid provided that the shear rate exceeds $100\,\mathrm{s}^{-1}$ [230].

The equation for the conservation of mass is

$$\frac{\partial u}{\partial x} + \frac{\partial v}{\partial y} + \frac{\partial w}{\partial z} = 0 \tag{5.1}$$

where u, v and w represent the component of velocity along x-, y- and z-axes. Further, the equations representing the conservation of momentum along x-, y- and z-axes respectively are:

$$\frac{\partial u}{\partial t} + u\frac{\partial u}{\partial x} + v\frac{\partial u}{\partial y} + w\frac{\partial u}{\partial z} = -\frac{1}{\rho}\frac{\partial p}{\partial x} + \nu\left(\frac{\partial^2 u}{\partial^2 x} + \frac{\partial^2 u}{\partial^2 y} + \frac{\partial^2 u}{\partial^2 z}\right) + F_x \tag{5.2}$$

$$\frac{\partial v}{\partial t} + u\frac{\partial v}{\partial x} + v\frac{\partial v}{\partial y} + w\frac{\partial v}{\partial z} = -\frac{1}{\rho}\frac{\partial p}{\partial y} + \nu\left(\frac{\partial^2 v}{\partial^2 x} + \frac{\partial^2 v}{\partial^2 y} + \frac{\partial^2 v}{\partial^2 z}\right) + F_y \tag{5.3}$$

$$\frac{\partial w}{\partial t} + u\frac{\partial w}{\partial x} + v\frac{\partial w}{\partial y} + w\frac{\partial w}{\partial z} = -\frac{1}{\rho}\frac{\partial p}{\partial z} + \nu\left(\frac{\partial^2 w}{\partial^2 x} + \frac{\partial^2 w}{\partial^2 y} + \frac{\partial^2 w}{\partial^2 z}\right) + F_z \tag{5.4}$$

In the above equations t represents time, p the pressure, ν kinematic viscosity and $F = (F_x, F_y, F_z)^T$ the external body force. Since in our case there is no external force, therefore it will be zero.

With $\mathbf{u} = (u, v, w)^T$, these equations can also be written as

$$\nabla \cdot \mathbf{u} = 0 \tag{5.5}$$

$$\frac{\partial \mathbf{u}}{\partial t} + (\mathbf{u} \cdot \nabla)\mathbf{u} = -\frac{1}{\rho}\nabla p + \nu\nabla^2\mathbf{u} \tag{5.6}$$

The energy equation for the heat transfer is given below

$$\rho C_p \frac{\partial T}{\partial t} + (\mathbf{u} \cdot \nabla)T = \nabla \cdot (K\nabla T) \tag{5.7}$$

where C_p is the specific heat of blood and T is the temperature in Kelvin and k is the thermal conductivity [231].

In order to non-dimensionalise Navier-Stokes equation (5.6), suppose l is the length of the artery (i.e. its diameter) and U is the velocity of the blood flow. As velocity has the dimension of length per time thus, $\frac{l}{U}$ has the dimension of time. Hence we can rescale x, $\mathbf{u}$ and t to obtain the dimensionless quantities [232–235].

$$\widetilde{x} = \frac{x}{l}$$

$$\widetilde{t} = \frac{tU}{l}$$

$$\widetilde{\mathbf{u}}(\widetilde{x},\widetilde{t}) = \frac{1}{U}\mathbf{u}(x(\widetilde{x}),t(\widetilde{t})) = \frac{1}{U}\mathbf{u}\left(l\widetilde{x},\frac{l}{U}\widetilde{t}\right)$$

From the above relation we can also rewrite

$$x = l\widetilde{x}$$

$$t = \frac{l}{U}\widetilde{t}$$

By taking the partial derivatives of $\widetilde{\mathbf{u}}$ with respect to $\widetilde{t}$, $\widetilde{x}$, $\widetilde{y}$ and $\widetilde{z}$, we get

$$\frac{\partial\widetilde{\mathbf{u}}}{\partial\widetilde{t}} = \frac{1}{U}\frac{\partial\mathbf{u}}{\partial t}\frac{\partial t}{\partial\widetilde{t}} = \frac{l}{U^2}\frac{\partial\mathbf{u}}{\partial t}$$

$$\frac{\partial\widetilde{\mathbf{u}}}{\partial\widetilde{x}} = \frac{1}{U}\frac{\partial\mathbf{u}}{\partial x}\frac{\partial x}{\partial\widetilde{x}} = \frac{l}{U}\frac{\partial\mathbf{u}}{\partial x}$$

$$\frac{\partial\widetilde{\mathbf{u}}}{\partial\widetilde{y}} = \frac{1}{U}\frac{\partial\mathbf{u}}{\partial y}\frac{\partial y}{\partial\widetilde{y}} = \frac{l}{U}\frac{\partial\mathbf{u}}{\partial y}$$

$$\frac{\partial\widetilde{\mathbf{u}}}{\partial\widetilde{z}} = \frac{1}{U}\frac{\partial\mathbf{u}}{\partial z}\frac{\partial z}{\partial\widetilde{z}} = \frac{l}{U}\frac{\partial\mathbf{u}}{\partial z}$$

From the above equation, we conclude that

$$\frac{\partial\widetilde{\mathbf{u}}}{\partial\widetilde{t}} = \frac{l}{U^2}\frac{\partial\mathbf{u}}{\partial t}$$

$$\bigtriangledown_{\widetilde{x}}\widetilde{\mathbf{u}} = \frac{l}{U}\bigtriangledown_x\mathbf{u}$$

$$\bigtriangledown^2_{\widetilde{x}}\widetilde{\mathbf{u}} = \frac{l^2}{U}\bigtriangledown^2_x\mathbf{u}$$

$$(\widetilde{\mathbf{u}}.\bigtriangledown_{\widetilde{x}})\widetilde{\mathbf{u}} = \frac{l}{U^2}(\mathbf{u}.\bigtriangledown_x)\mathbf{u}$$

We know that $\bigtriangledown_p$ has the same dimension as acceleration (i.e.$\frac{l}{t^2}$), therefore, the dimension of pressure is $\frac{l^2}{t^2}$ (i.e.U^2). Equation (5.8) represents the non-dimensional pressure.

$$\widetilde{p}(\widetilde{x},\widetilde{t}) = \frac{1}{U^2}p(x(\widetilde{x}),t(\widetilde{t})) \tag{5.8}$$

The pressure term in the dimensionless variable with the help of chain rule is

$$\bigtriangledown_{\widetilde{x}}\widetilde{p} = \frac{l}{U^2}\bigtriangledown_x p$$

Replacing all the above values in (5.6), we will get the Navier-Stokes equation in terms

of dimensionless quantities.

$$\frac{U^2}{l}\frac{\partial \widetilde{\mathbf{u}}}{\partial \widetilde{t}} + \frac{U^2}{l}(\widetilde{\mathbf{u}}.\bigtriangledown_{\widetilde{x}})\widetilde{\mathbf{u}} = -\frac{U^2}{l}\bigtriangledown_{\widetilde{x}}\widetilde{p} + \nu\frac{U}{l^2}\bigtriangledown^2_{\widetilde{x}}\widetilde{\mathbf{u}} \tag{5.9}$$

By dividing the equation (5.9) with $\frac{U^2}{l}$, we get

$$\frac{\partial \widetilde{\mathbf{u}}}{\partial \widetilde{t}} + (\widetilde{\mathbf{u}}.\bigtriangledown_{\widetilde{x}})\widetilde{\mathbf{u}} = -\bigtriangledown_{\widetilde{x}}\widetilde{p} + \frac{\nu}{lU}\bigtriangledown^2_{\widetilde{x}}\widetilde{\mathbf{u}} \tag{5.10}$$

The dimensionless quantity

$$\mathrm{R}_e = \frac{lU}{\nu} \quad \text{or} \quad \mathrm{R}_e = \frac{lU\rho}{\mu} \quad (\nu = \frac{\mu}{\rho}) \tag{5.11}$$

is called the Reynolds number of the flow. By replacing the value of Reynolds number in (5.10), the dimensionless Navier-stokes equation becomes

$$\frac{\partial \widetilde{\mathbf{u}}}{\partial \widetilde{t}} + (\widetilde{\mathbf{u}}.\bigtriangledown_{\widetilde{x}})\widetilde{\mathbf{u}} = -\bigtriangledown_{\widetilde{x}}\widetilde{p} + \frac{1}{\mathrm{R}_e}\bigtriangledown^2_{\widetilde{x}}\widetilde{\mathbf{u}} \tag{5.12}$$

The term $\frac{1}{\mathrm{R}_e}\bigtriangledown^2_{\widetilde{x}}\widetilde{\mathbf{u}}$ is called the diffusion or dissipation term and the term $(\widetilde{\mathbf{u}}.\bigtriangledown_{\widetilde{x}})\widetilde{\mathbf{u}}$ is called the inertia or convection term. Thus Reynolds number gives us a measure of the ratio between inertia term and the dissipation term. We have noticed by the definition of Reynolds number that R_e and ν have opposite tendencies [232–235].

1. $\mathrm{R}_e \gg 1$ corresponds to low viscosity flow. The fluid in this case is well approximated by an ideal fluid. Formally, for $\nu \ll 1$ Navier-Stokes equation reduces to the Euler equation and in this case the inertia term is dominant.

2. If $\mathrm{R}_e \ll 1$, then fluids are very viscous and the diffusion term is domination.

Blood flow is normally considered to be laminar in the body. However, in case of high flow especially in the ascending aorta, the flow can be disturbed and therefore becomes turbulent. For example, the blood flow in large arteries at branch point and in diseased and narrowed arteries can also be turbulent as shown in Figure 5.1 [236, 237].

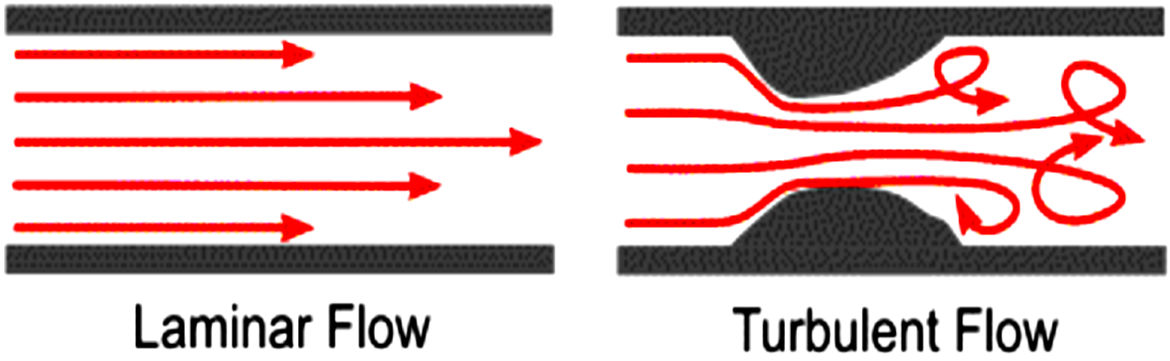

Figure 5.1: Laminar and Turbulent Flow. [236]

High velocity results the turbulence in the laminar flow of blood vessels. In fact, turbulence occurs when Reynolds number is exceeded to certain limit ($R_e > 2000$) [236, 237].

The critical Reynolds number is comparatively high in long, straight and smooth blood vessels under ideal conditions whereas low in case of branch vessels or the vessels with atherosclerotic plaques. The critical Reynolds number is lower which can result in turbulence even at normal physiological flow velocities [236].

5.2.1 Boundary Conditions

There is no blood flow through the wall and the flow satisfies the no slip boundary condition at the wall. Therefore at the wall:

$$u = 0 \quad \text{and} \quad v = 0 \quad \text{and} \quad w = 0$$

The boundary conditions at the inlets are:

$$\mathbf{u}(x, y, x, t) = \mathbf{u}_{in}(t) = \begin{cases} \mathbf{u}_{Main}(t) = 0.1 \times \sin(\pi t) \quad \text{and} \quad T = 300\text{K} \quad \text{if} \quad t \geq 0 \\ \mathbf{u}_{Catheter}(t) = 0.2 \times \sin\left(\frac{\pi}{2.0 \times (t-1.0)}\right) \quad \text{and} \quad T = 295\text{K} \quad \text{if} \quad 1 \leq t \leq 3 \end{cases}$$

The pressure is considered to be unidirectional and zero (constant) at the outlet. Therefore

$$p_{out} = 0 \quad \text{Pa}, \quad \text{and} \quad T = 300\,\text{K} \quad \text{and} \quad \frac{\partial \mathbf{u}}{\partial \mathbf{n}} = 0$$

where $\mathbf{n} = (n_x, n_y, n_z)$ is the normal pointing outward at the boundary. At the inlet the fluid will take time to be fully developed and flat profile will tend to become parabolic

(i.e. Poiseuille) in downstream.

5.2.2 Poiseuille Flow

Jean Louis Marie Poiseuille, a French physicist and physiologist who worked in the field of human blood flow and derived a law for the flow in the cylindrical pipes which is considered to be very useful for all kinds of hydrodynamics. Because of him, it is generally known as Poiseuille flow [238].

This is one of the special cases of the Navier-Stokes equation. Consider the flow between the plates is unidirectional, steady and incompressible. Thus $u = w = 0$ and $\frac{\partial u}{\partial t} = 0$. The geometry is shown in Figure 5.2 below [239]:

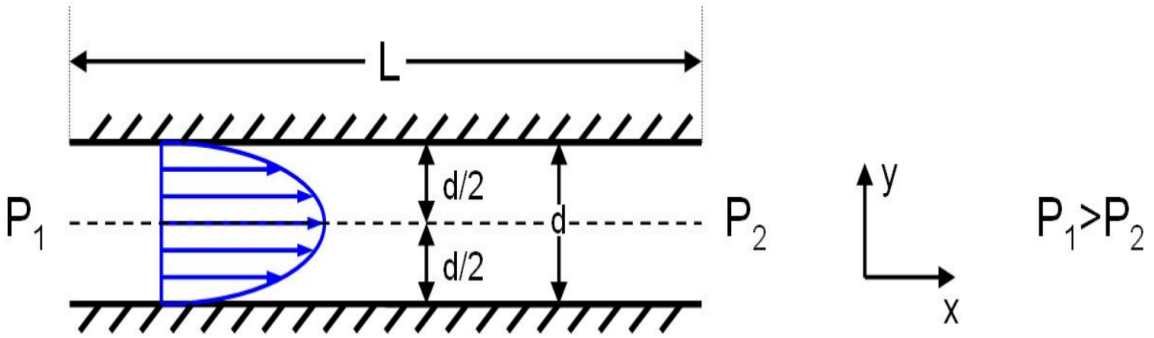

Figure 5.2: Poiseuille flow between parallel plates [239]

The continuity equation in this case is

$$\frac{\partial u}{\partial x} = 0 \quad u = u(y) \tag{5.13}$$

Thus the Navier-Stokes equation becomes

$$-\frac{\partial p}{\partial x} + \mu \frac{\partial^2 u}{\partial y^2} = 0 \quad \left(\frac{\partial p}{\partial y} = \frac{\partial p}{\partial z} = 0\right) \tag{5.14}$$

$$\frac{dp}{dx} = \mu \frac{d^2 u}{dy^2}$$

Also

$$\frac{dp}{dx} = 0 \quad \Rightarrow p = c_1 x + c_2 \tag{5.15}$$

The boundary conditions are [239]

$$\begin{aligned} x = 0, \quad p = p_1 \quad &\Rightarrow c_2 = p_1 \\ x = L, \quad p = p_2 \quad &\Rightarrow c_1 = -\tfrac{\Delta p}{L} \end{aligned} \tag{5.16}$$

Therefore,

$$p = p_1 - \frac{\Delta p_x}{L} \tag{5.17}$$

$$\mu \frac{\partial^2 u}{\partial y^2} = c_1 = -\frac{\Delta p}{L}$$

$$\frac{\partial^2 u}{\partial y^2} = -\frac{\Delta p}{\mu L}$$

$$\frac{\partial u}{\partial y} = -\left(\frac{\Delta p}{\mu L}\right) y + c_3$$

$$u = -\left(\frac{\Delta p}{\mu L}\right) y^2 + c_3 y + c_4 \tag{5.18}$$

The no slip boundary conditions at top and bottom plates are [239]

$$\begin{aligned} &\text{Top plate} \quad y = \tfrac{d}{2}, \quad u = 0 \\ &\text{Bottom plate} \quad y = -\tfrac{d}{2}, \quad u = 0 \end{aligned}$$

Replacing these values in the above equation, we get

$$0 = -\left(\frac{\Delta p}{8\mu L}\right) d^2 + c_3 \frac{d}{2} + c_4 \tag{5.19}$$

$$c_4 = \left(\frac{\Delta p}{8\mu L}\right) d^2 \quad (\text{as} \quad c_3 = 0)$$

$$u = \frac{\Delta p}{2\mu L}\left[\frac{d^2}{4} - y^2\right] \tag{5.20}$$

which is a parabolic profile [239].

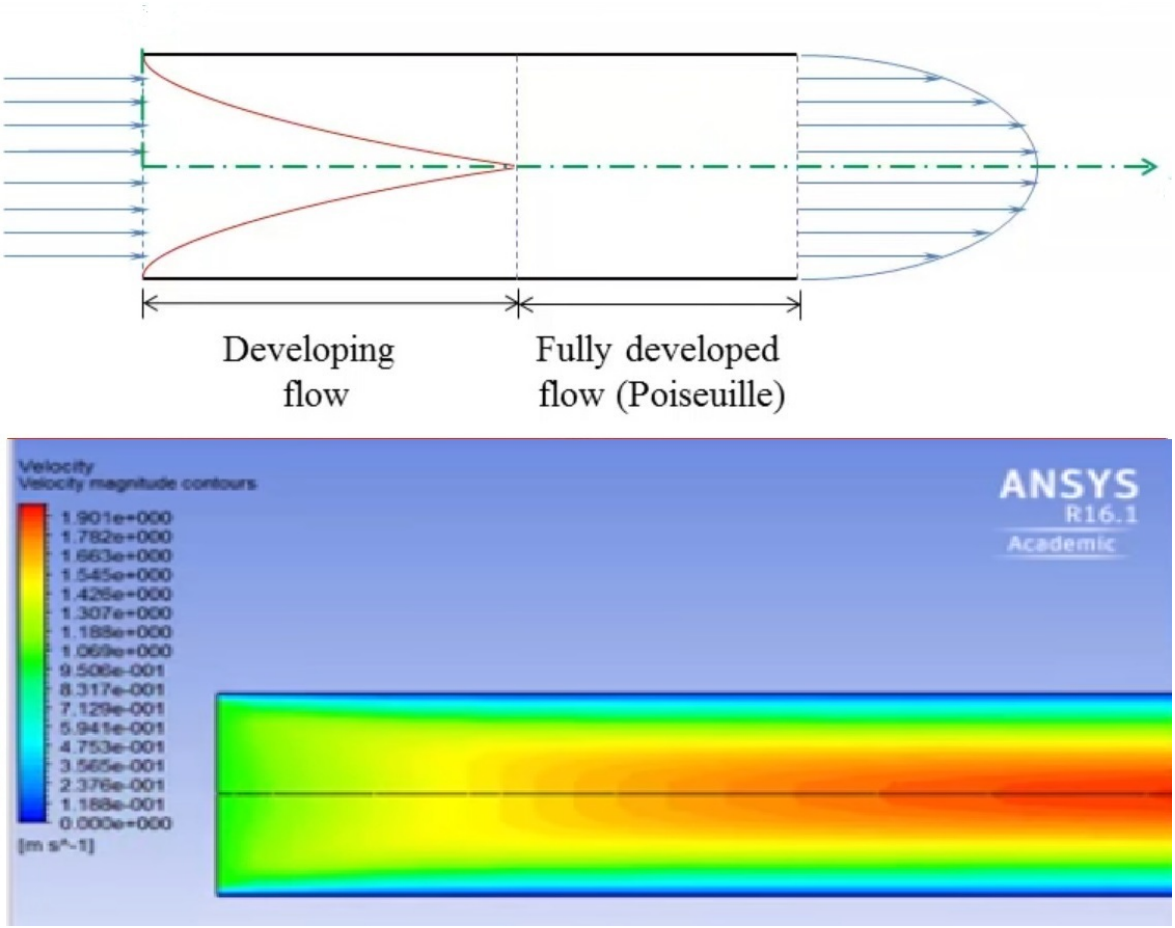

Figure 5.3: Laminar pipe flow - Numerical results [240]

Figure 5.3 shows the developing parabolic profile in which red colour shows the highest velocity which is at the centre of the pipe whereas blue colour represents the lowest velocity which is near the walls.

5.3 Simulation

The purpose of the study was to set out the physical conditions in an in silico experiment that might simulate the patterns of the thermodilution curves of the coronary arteries and to determine the validity by using CFD software Fluent to monitor or analyse flow patterns in coronary arteries. The first step in conducting the experiment was the creation of a physical model. After constructing the model, the next step was to determine the type of fluid and boundary conditions for simulating the flow through the model.

5.3.1 Numerical Procedure

After making the geometry, the second task is the numerical solution procedure to solve the mathematical model. The mathematical model as a boundary value problem is solved through the finite volume method in Fluent software which has a control volume analysis for each cell. It derives a set of algebraic equations and relating velocity and pressure at neighbouring cell-centred values. These algebraic equations are non-linear because these contain the terms like $\mathbf{u^2}$ arising from the non-linear terms in the Navier Stokes equation. To solve the non-linear algebraic equations, these equations are linearised about the guess values and then solved iteratively. The commercial software Fluent is based on the finite volume method which solves the equations automatically and displays the results. Figure 5.4 shows the numerical procedure to solve the mathematical model through finite volume method [240].

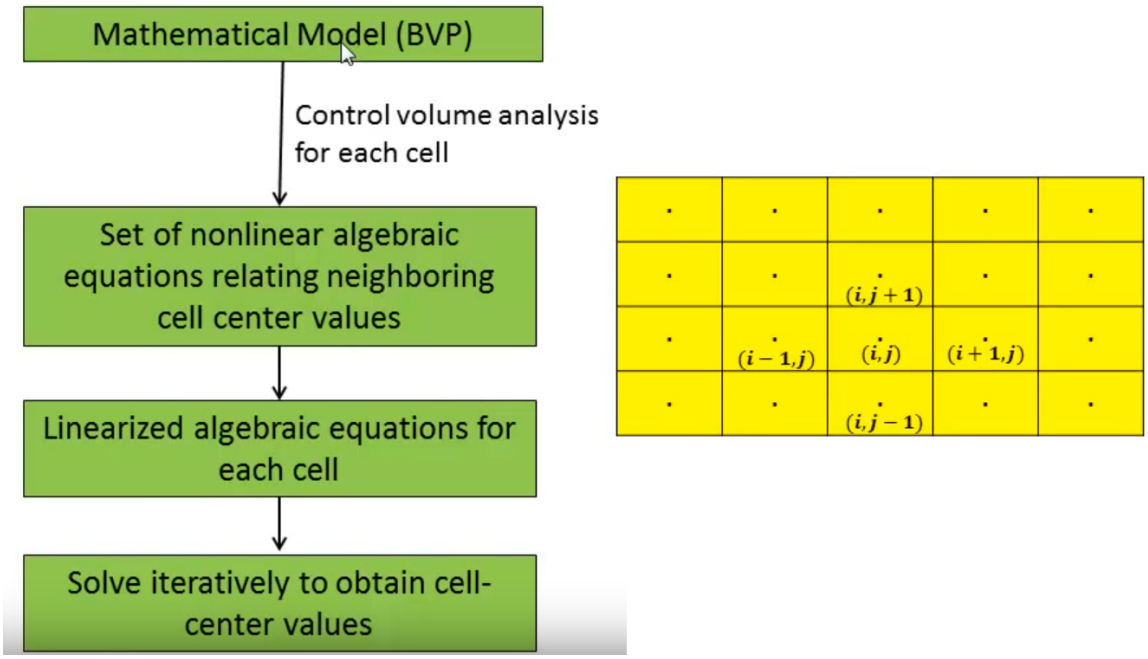

Figure 5.4: Numerical procedure to solve the mathematical model through finite volume method [240].

5.3.2 ANSYS Fluent

ANSYS fluent is the most reliable and powerful computaional fluid dynamics software which has the modelling capabilities and provides the accurate results of not only computational fluid dynamics applications but also multiphysics applications [241].

It contains the broad physical modeling capabilities needed to model flow, turbulence, heat transfer, and reactions for industrial applications ranging from air flow over an aircraft wing to combustion in a furnace, from bubble columns to oil platforms, from blood flow to semiconductor manufacturing, and from clean room design to wastewater treatment plants. Fluent covers a broad reach, including special models with capabilities to model in-cylinder combustion, aero-acoustics, turbomachinery and multiphase systems [241]. The above model can directly be solved in Fluent software as per the procedure shown in Figure 5.5.

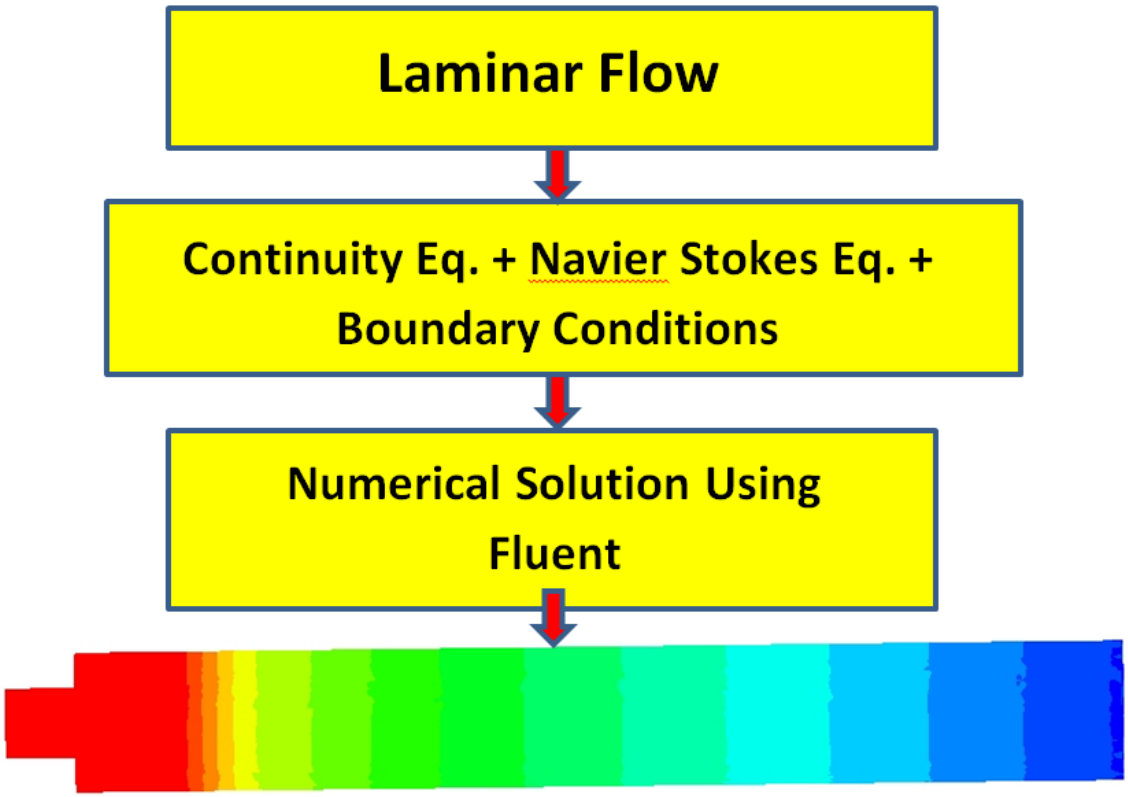

Figure 5.5: Procedure in Fluent software to solve the mathematical boundary value problem [240].

5.3.3 2D Geometry

First of all, a simple 2D geometry was created with dimensions 50 mm × 4 mm and then a mesh was generated with 9800 nodes and 9552 quadrilateral elements (Appendix C.1). The blood flow was taken to be unsteady, incompressible and laminar. The FLUENT software package was used for this simulation. Standard no-slip boundary conditions were set at the wall. A user defined function for unsteady velocity was used in the main inlet (Section 5.2) and zero outlet pressure was prescribed. The blood density

and viscosity were taken to be 1068 kg m^{-3} and 0.003 kg $m^{-1}s^{-1}$. The specific heat and thermal conductivity were assumed to be the same as of water i.e. 4182 J $kg^{-1}K^{-1}$ and 0.6 W $m^{-1}K^{-1}$ as shown in Figure 5.6.

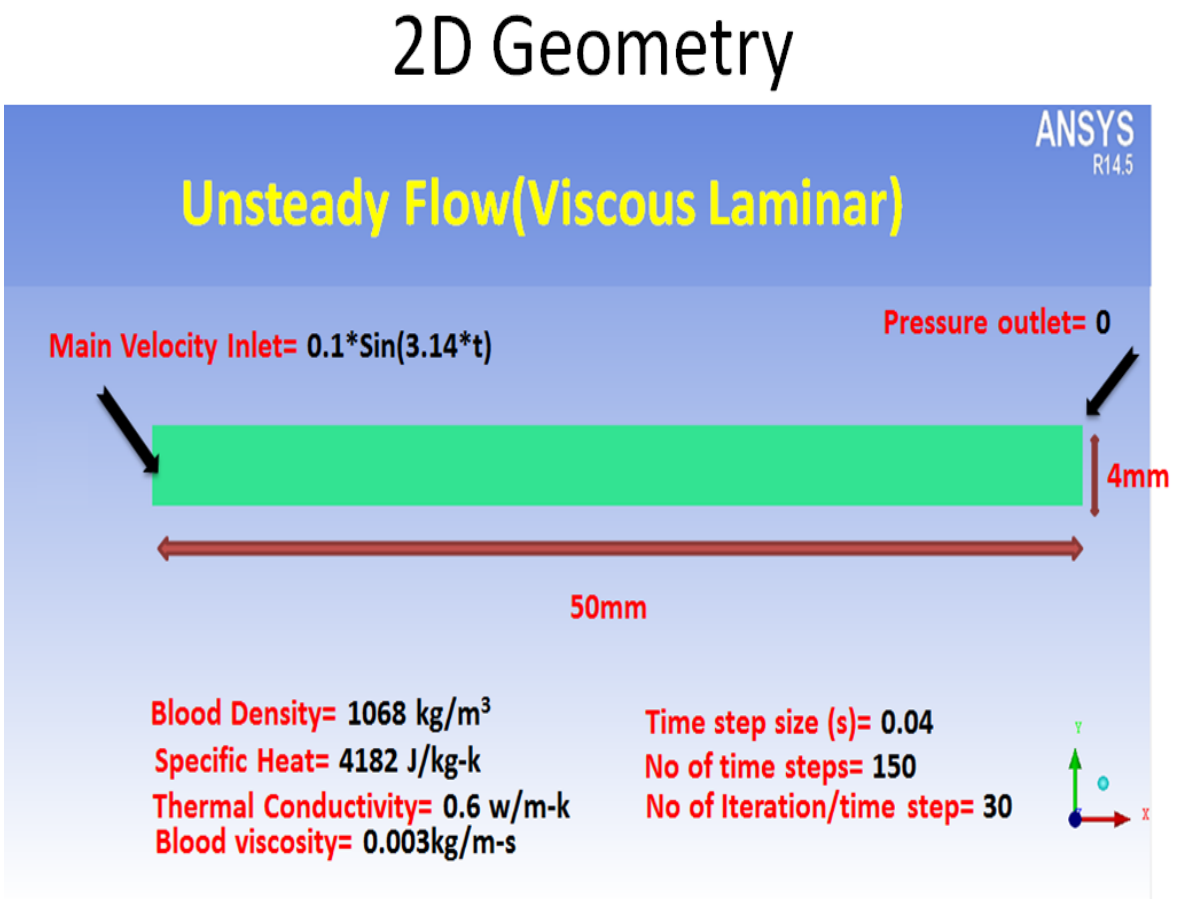

Figure 5.6: Computational geometry of 2D simple model without catheter.

The computational domain was solved using the solver settings for two-dimensional inlets and an unsteady state condition. The numerical simulation of the Navier-Stokes equations, which govern the fluid flow and heat transfer, make use of the finite volume method. The code was solved for temperature, pressure and flow velocity at every cell. Heat transfer was modelled through the energy equation. For this unsteady simulation, the residual criterion for convergence was set to 10^{-3}, except for the energy equation for which the residual convergence criterion was set to 10^{-6}. The calculations were run for 6 cycles with time step size of 0.04.

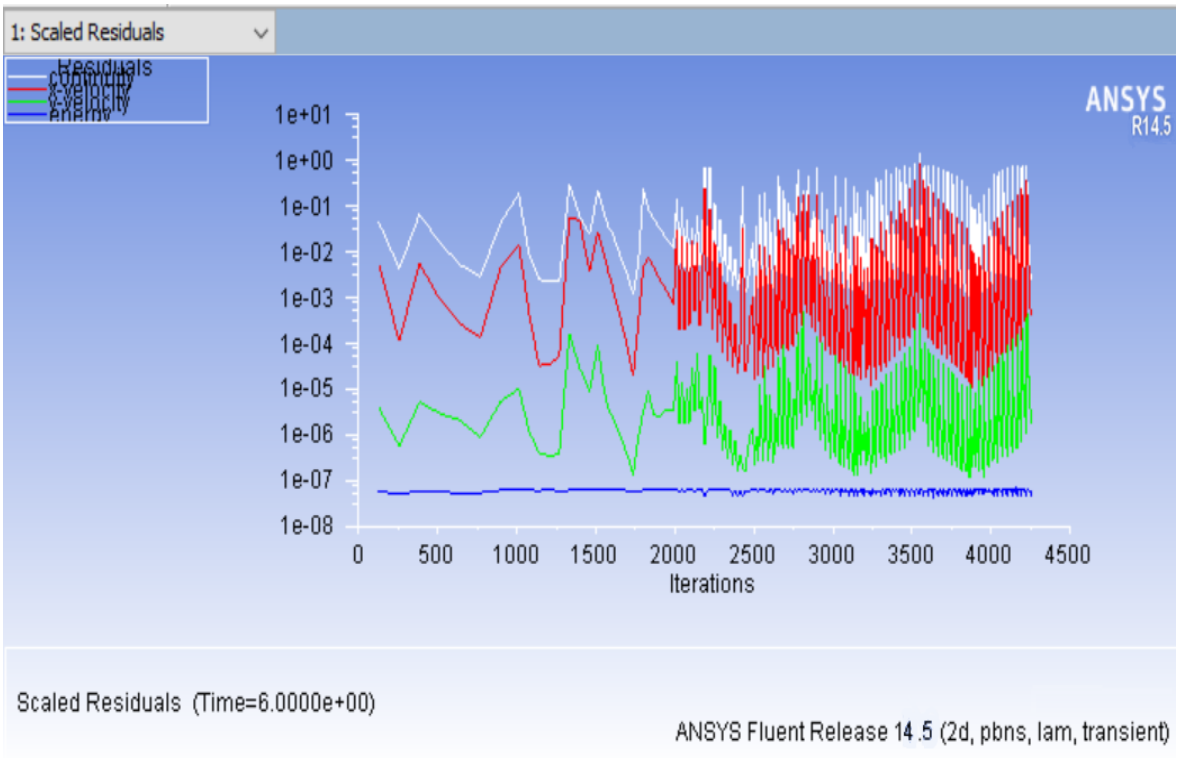

Figure 5.7: Scaled residuals for 2D unsteady flow

The simulation is deemed to have convergeal when the residuals decrease to 10^{-3} for continuity, u and v, and the energy residual is below 10^{-6}. In Figure 5.7, the residuals are plotted against the total iteration number, which is $\sum_i n_i$, i is the time step and n_i is the iteration number for a time step. When continuity, u and v residuals are below 10^{-3}, and energy residual is less than 10^{-6}, the simulation will step forward with updated boundary conditions. The peaks above the convergence criteria are at the beginning of a time step; with more iterations, the residuals decrease towards the specified values.

5.3.3.1 Residuals

Error magnitudes for the equations during the process of iterations are knows as residuals. The basic equations which are used during simulations include the momentum equations for each direction, the continuity equation (conservation of mass) and the energy equation, if the heat transfer is applicable. The equations of the turbulence model can also be included. The difference between the previous results and current result is also called the residual. If the equation's results are changing less and less due to the low residuals, the solution is said to be converged and if the errors start to increase, the solution is said to be diverged [242].

We calculated the velocity and pressure profiles with respect to time at four different locations with a difference of 10 mm distance at the centre of the 2D coronary artery model for six seconds to check the prescribed flow and pressure. Simulations were run in Fluent software and the data was plotted in Tecplot360 software which is very efficient, easy to use and produces visual powerful output results to analyse data more effectively. The profiles of velocity and pressure at 4 different locations are shown in Figure 5.8 and Figure 5.9 respectivily. The profile of velocity and pressure does not change as we go downstream.

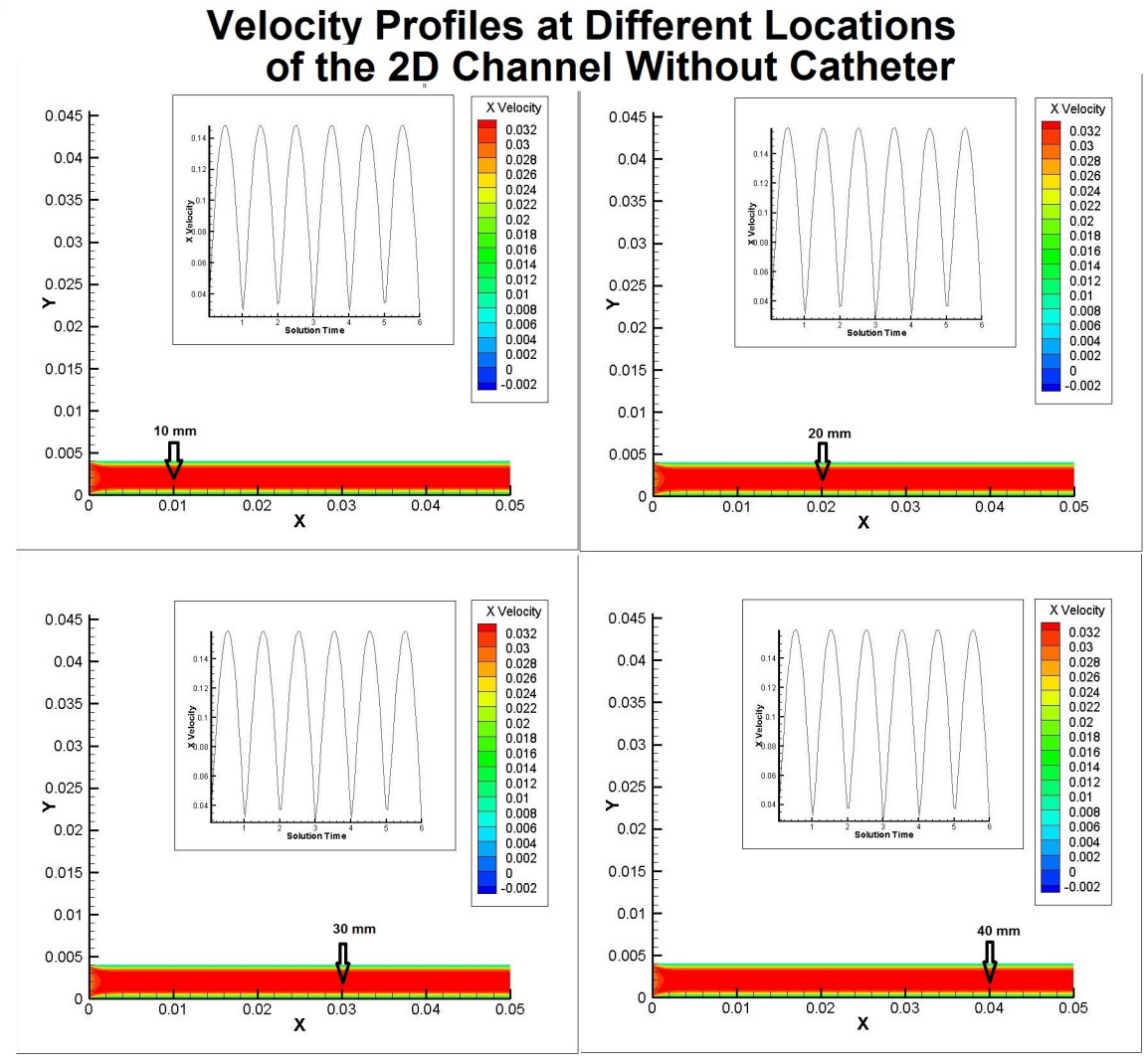

Figure 5.8: Velocity profiles at 4 different locations in the absence of catheter. The Poiseuille Flow is expected along the central axis of the channel for each heart beat.

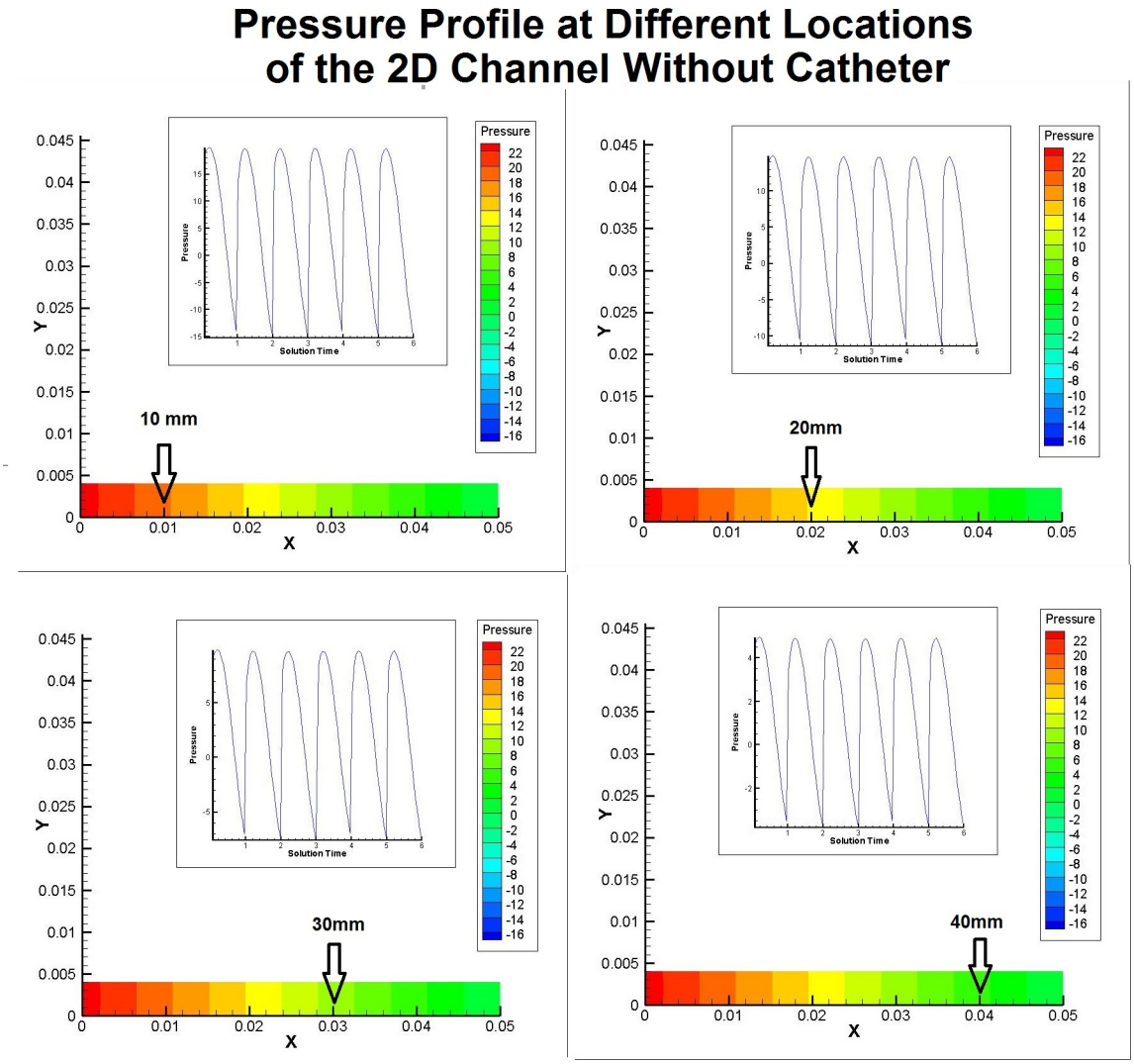

Figure 5.9: Pressure profiles at 4 different locations in the absence of catheter. The pressure decreases as we go down stream along the central axis.

5.3.4 2D Geometry With Catheter

We then modified the 2D geometry and inserted the catheter at the centre of artery. The blood is considered to be unsteady, incomressible and laminar. The diameter and length of the catheter is taken as D = 0.002 m and L = 0.012 m respectivily. The mesh was generated with 103602 number of cells, 208149 number of faces and 104546 number of nodes and applied the boundary conditions (Section 5.2).

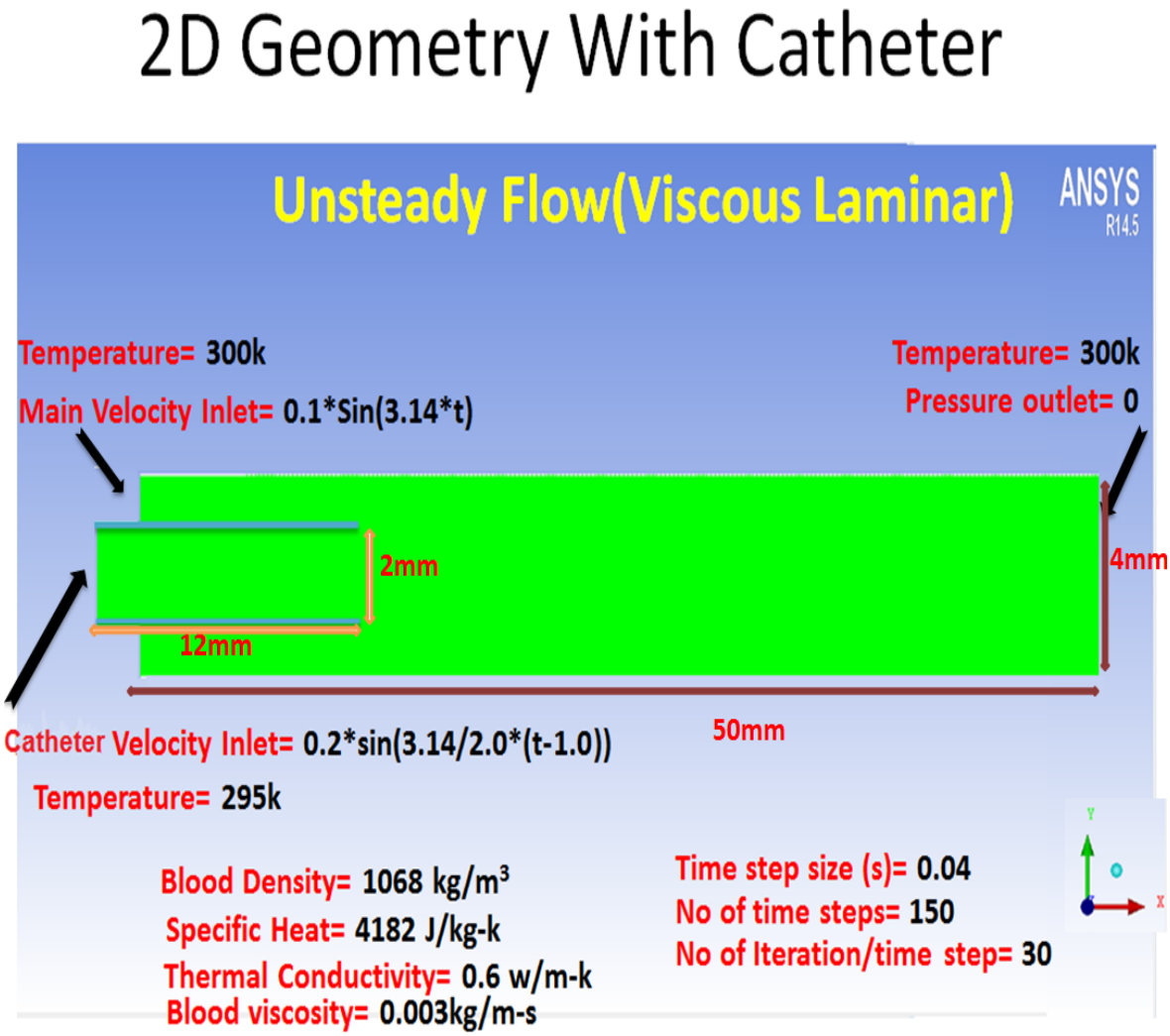

Figure 5.10: Diagram of the computational fluid domain of 2D channel with catheter inside the artery on the central axis for each heart beat.

In this case, we set the temperature of the catheter to be 295 K (i.e. room temperature) and 300 K in the main artery to see the temperature profiles between one and three seconds. The results of blood flow, pressure and temperature are shown in Figures 5.11, 5.12 and 5.12 respectivily.

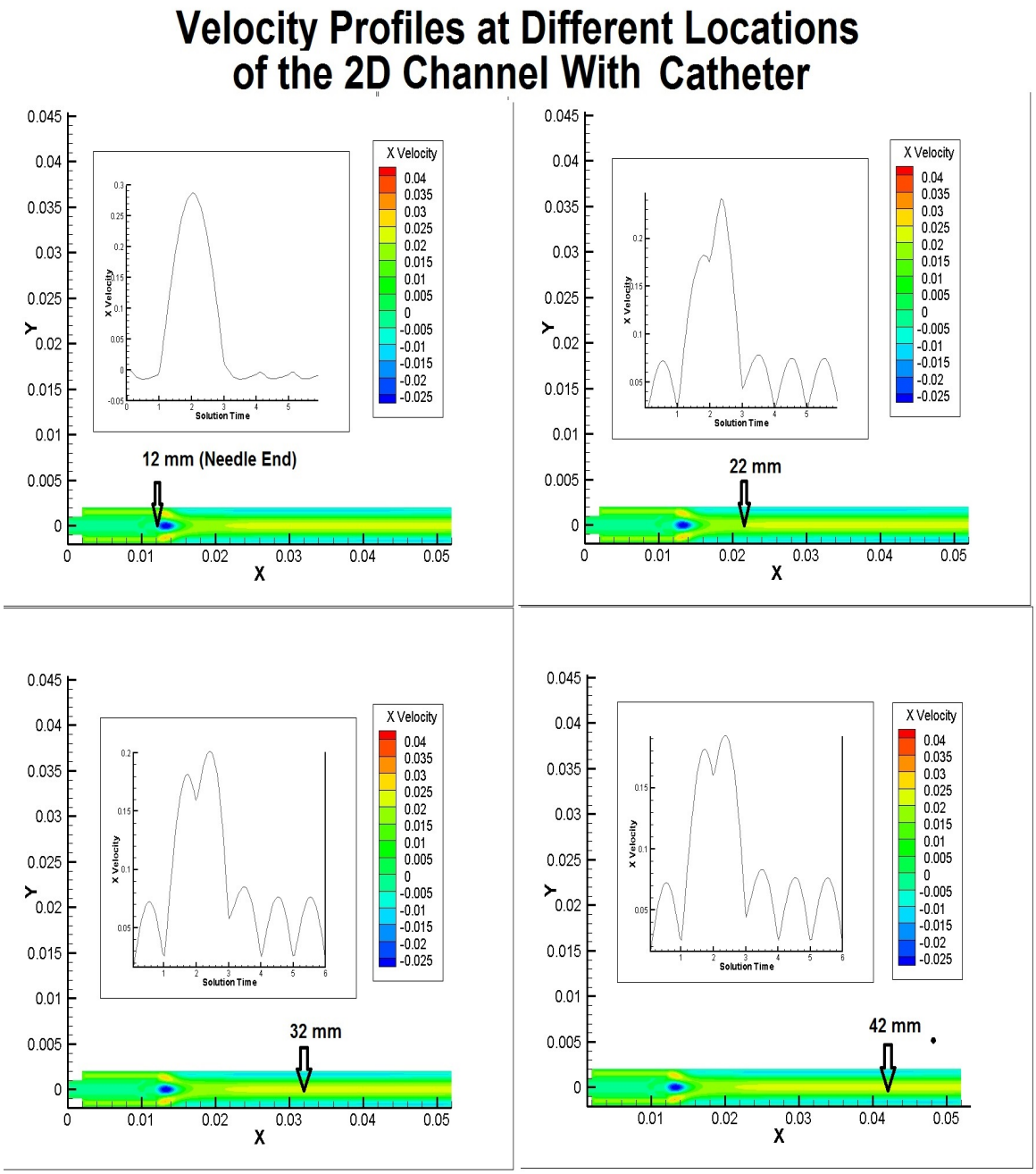

Figure 5.11: Velocity profiles at 4 different locations of the 2D channel with catheter along the central axis for each heart beat.

In Figure 5.11 we can observe the increase in velocity near the catheter end then with the passage of time it becomes smooth. Furthermore, the velocity also decreases as change in the location is given in the remaining three profiles. At the catheter end the peak velocity is almost $0.3\,\mathrm{m\ s^{-1}}$ whereas at a distance of 42 mm it becomes less than $0.2\,\mathrm{m\ s^{-1}}$.

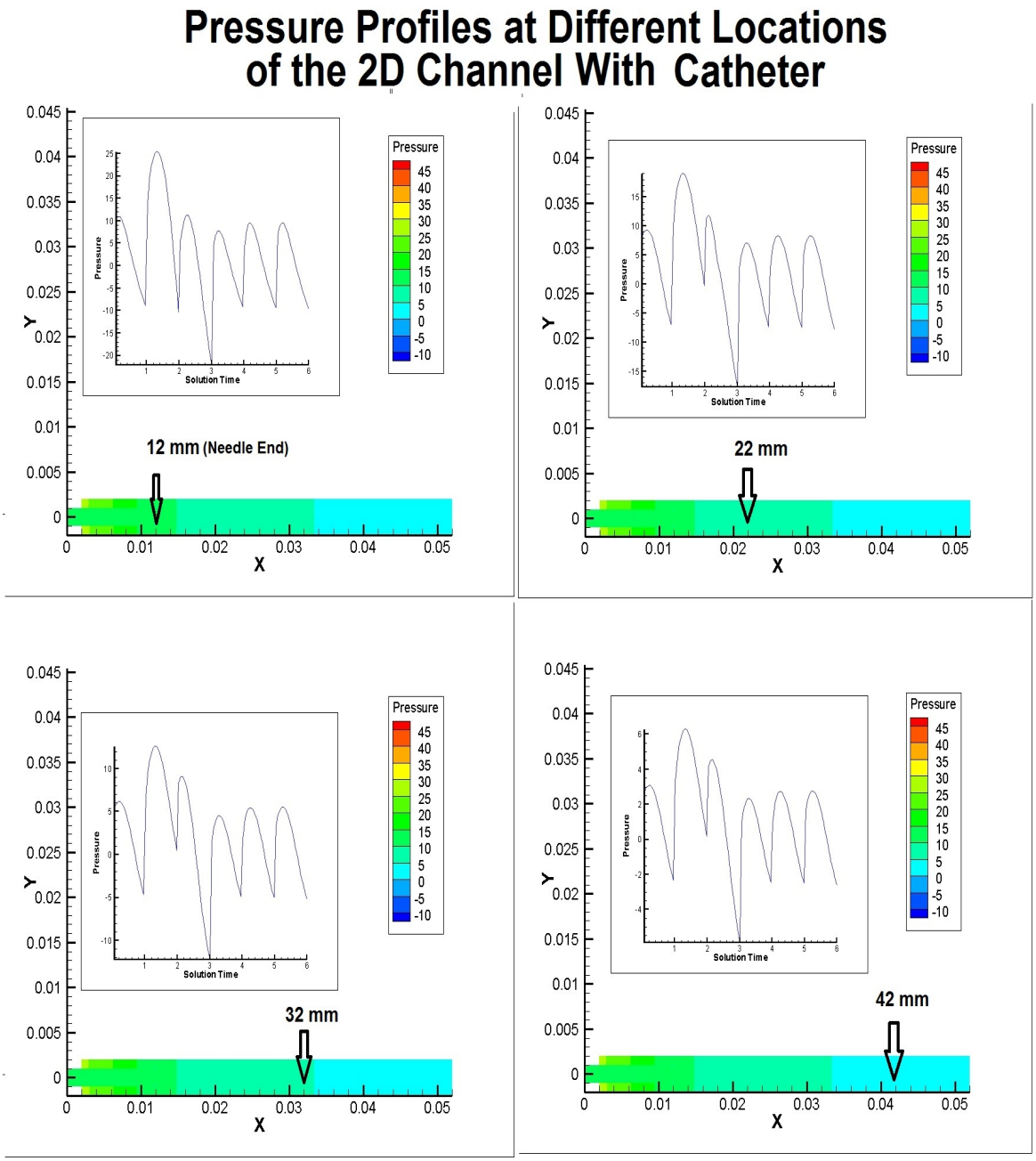

Figure 5.12: Pressure profiles at 4 different location of the 2D channel with catheter along the central axis for each heart beat.

We observe the increase in pressure at the catheter end but with the passage of time the pressure difference remain very less and profiles become smooth.

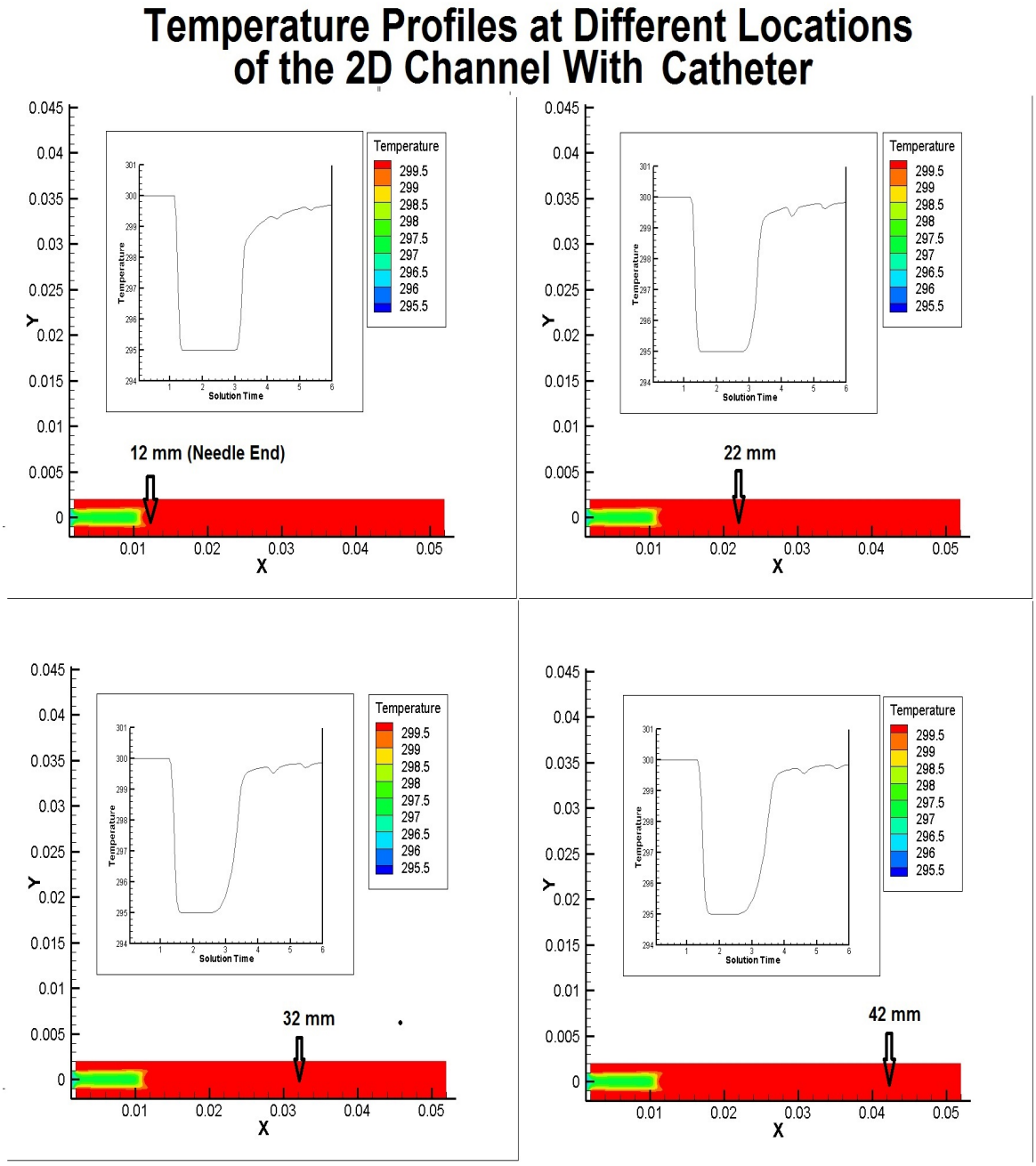

Figure 5.13: Temperature profiles at 4 different location of the 2D channel with catheter at the centre showing the rectangular shape near the catheter end whereas it becomes smooth down stream.

After visualising the temperature profiles shown in Figure 5.13, we can observe the sudden decrease in temperature after one second and then being smooth for two seconds and then increases sharply until it reaches at 300 K again.

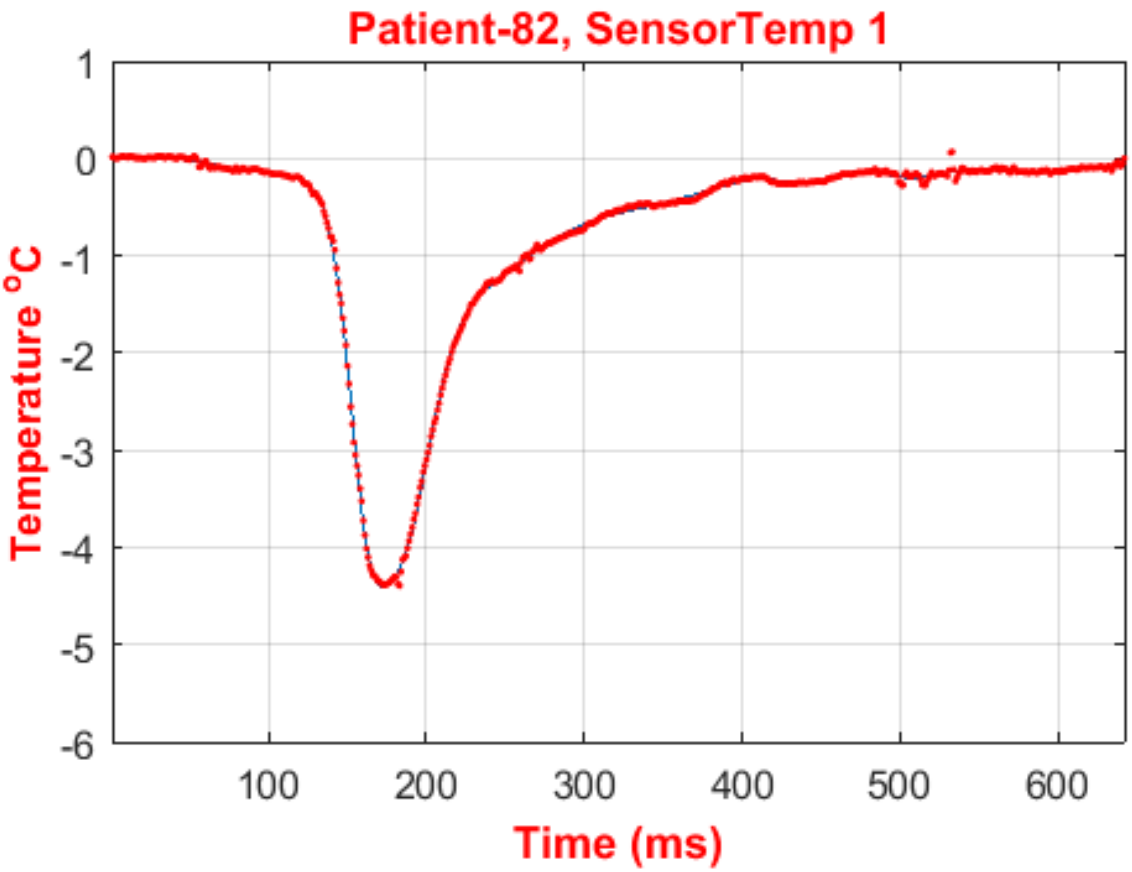

Figure 5.14: Thermodilution temperature profile of patient-82 showing the same curve as found during the CFD experiment (see Figure 5.13) with minnor differences.

If we compare the CFD results with the actual thermodilution data, there is no difference in the curves except the curve becomes smooth for a while in the CFR results as shown in Figure 5.14. If we compare the velocity and temperature profiles we can observe that as the velocity increases, the temperature decreases. Moreover, we did not see any pulsatility in the temperature profiles because the probe lies along the central axis and lies within the bolus of cold fluid over several periods. The conductivity of the fluid is sufficiently low that the bolus does not gain significant heat from the surrounding warm fluid.

5.3.5 3D Geometry

Thermodilution is performed in the cornonary arteries which are 3-dimensional. In order to do the same, we created a simple 3-dimensional computational model of the left coronary artery in the SolidWorks software which is very efficient tool for making complex geometries. We considered blood flowing through simple model of a typical left coronary artery, of constant diameter D = 0.004 m and length L = 0.050 m, to be

unsteady, incompressible and laminar. The diameter and length of the catheter is D = 0.002 m and L = 0.012 m respectivily. We set the temperature at the catheter inlet to be 295 K as the cold saline solution is injected into the artery through the catheter and the temperature inside the artery is considered to be 300 K. We used a simple velocity function at the artery and catheter inlet (Section 5.2.1) to see the behaviour of flow as shown in Figure 5.15 and and compared the results with 2D model.

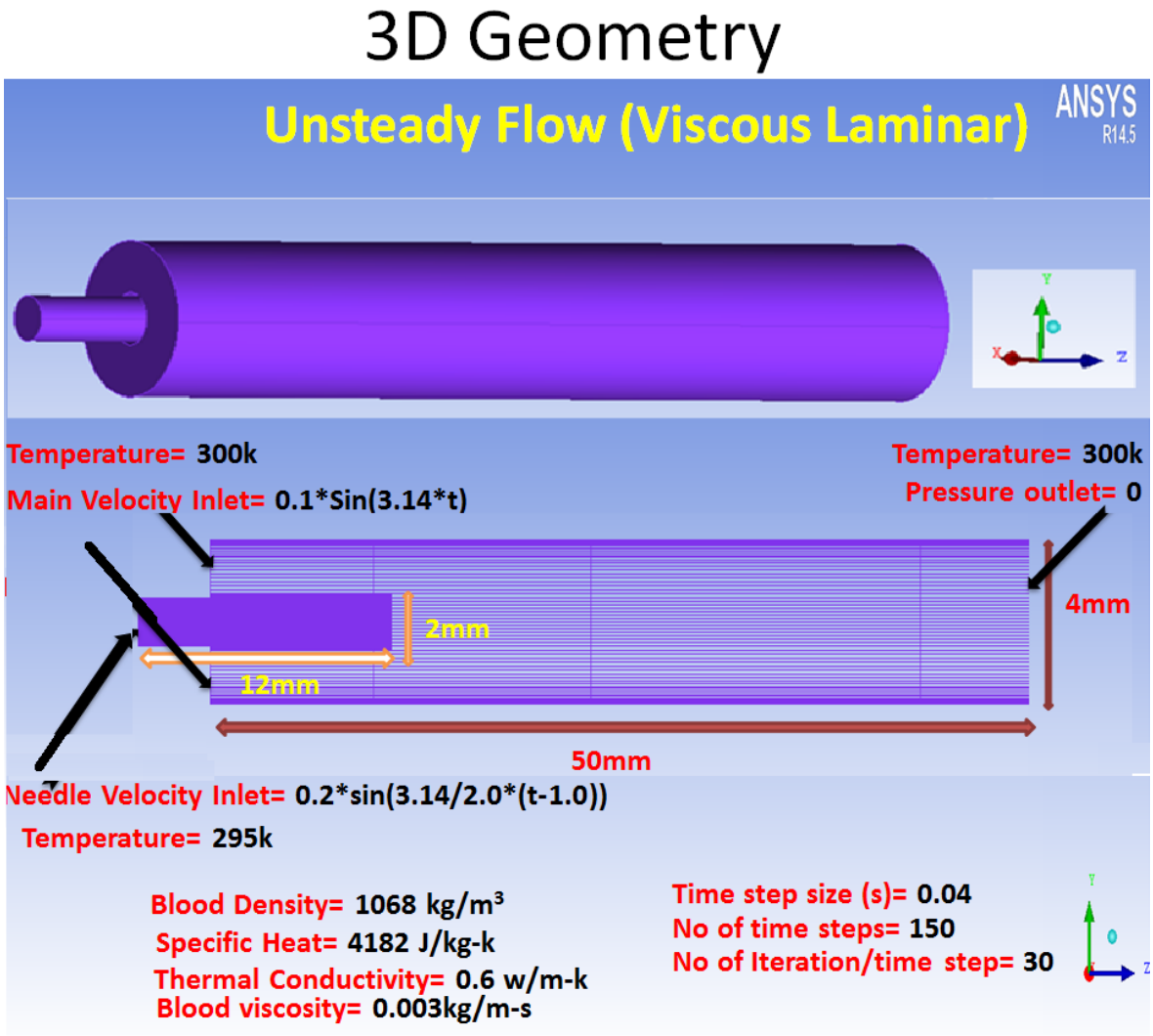

Figure 5.15: Diagram of the computational fluid domain.

The computations were performed in the Fluent software and the results of velocity, pressure and temperature were plotted in Tecplot software which is most efficient tool to visualise and analyse of CFD results. The profiles of velocity, pressure and temperature are shown in Figures 5.16, 5.17 and 5.18.

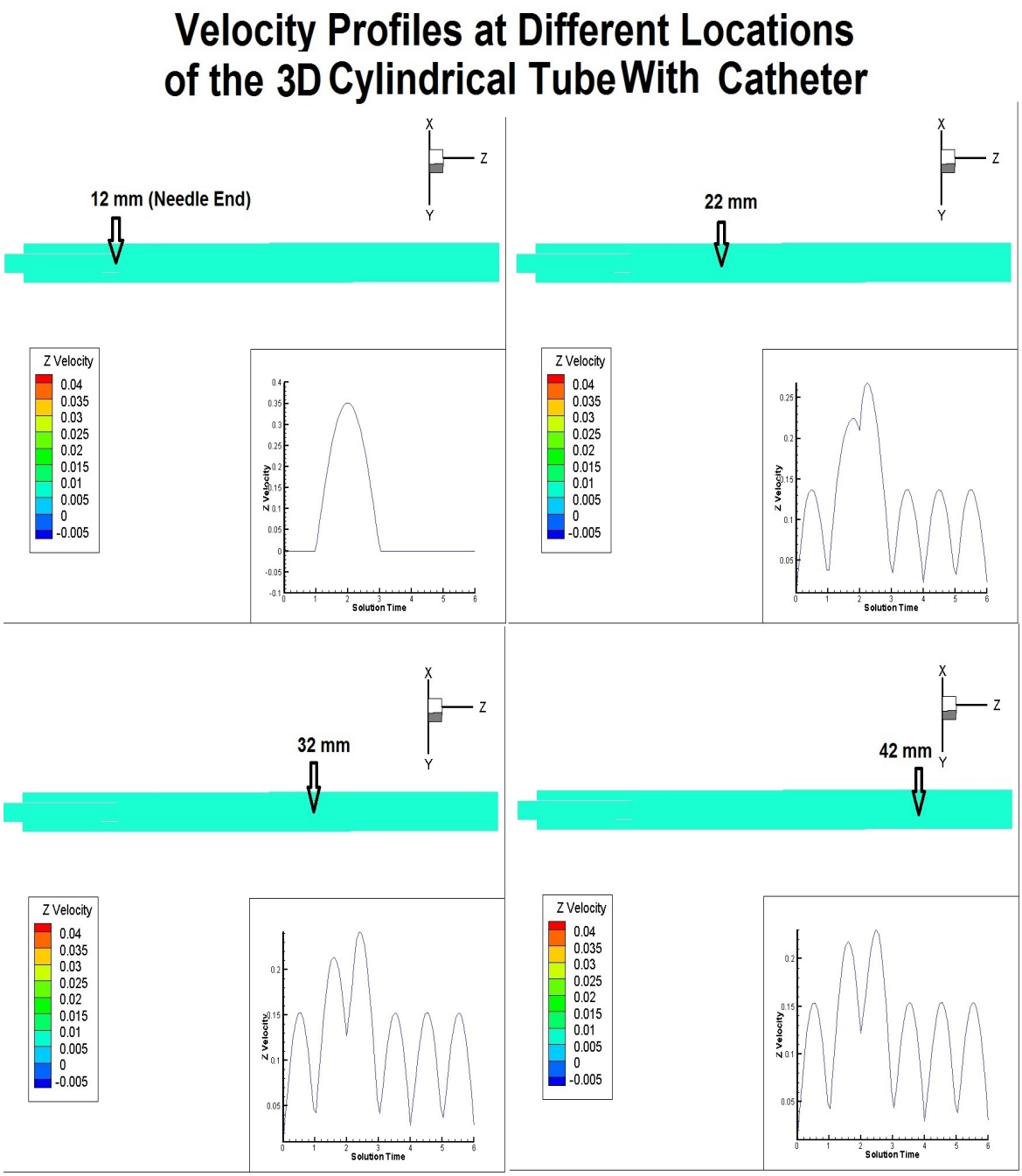

Figure 5.16: Velocity profiles at 4 different locations along the central axis of the tube in the presence of catheter for each heart beat.

The peak velocity at the end of the catheter along the central axix is $0.35\,\mathrm{m\ s^{-1}}$ however, the profiles become smooth after 3 s as we go downstream in the tube with constant peak velocity of $0.15\,\mathrm{m\ s^{-1}}$ which in case of 2D is $0.07\,\mathrm{m\ s^{-1}}$ (Figure 5.11). However, the shape for both the cases remains the same.

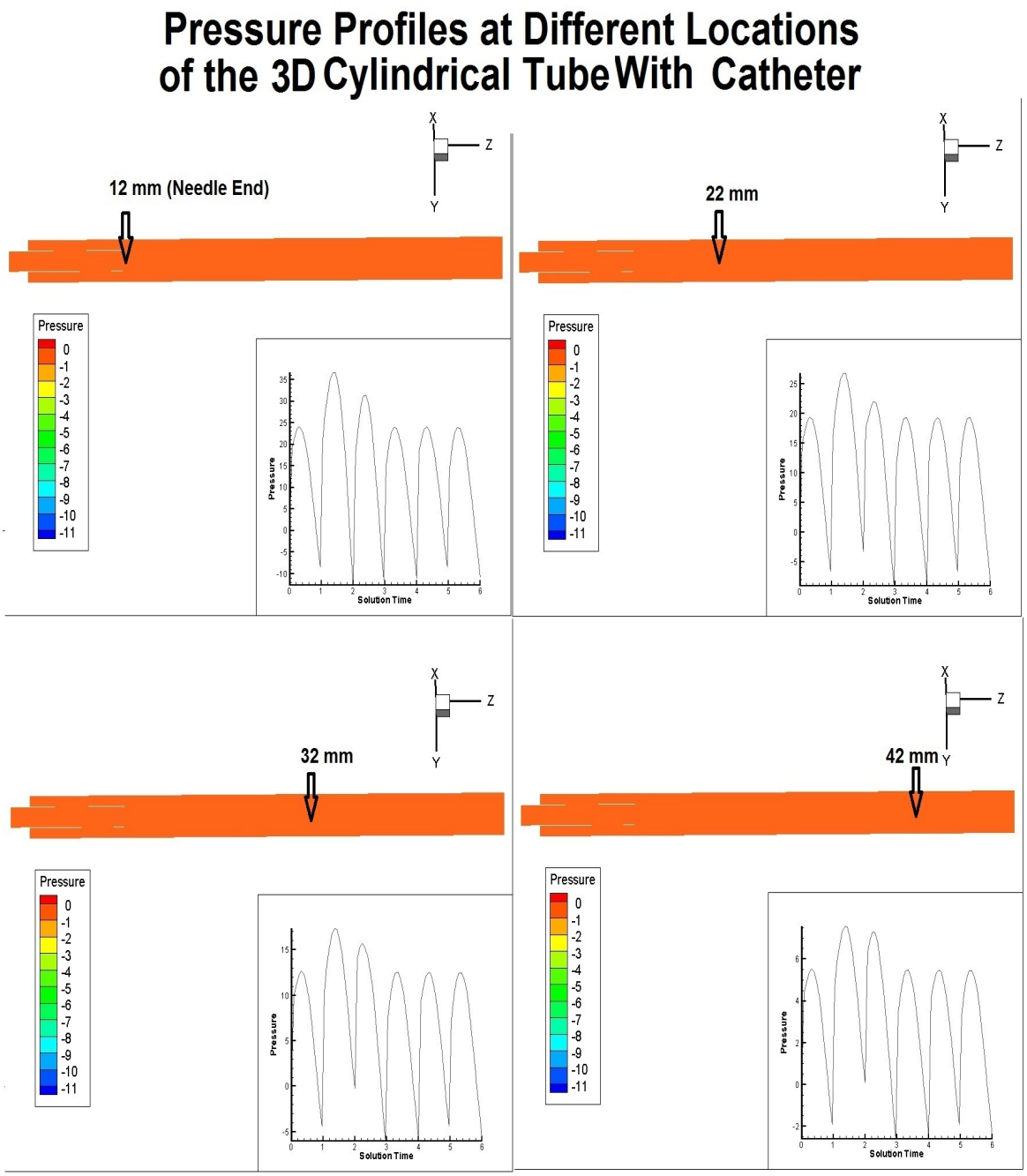

Figure 5.17: Pressure profiles at 4 different locations along the central axis of the tube in the presence of catheter showing the decrease in pressure as we go downstream.

The peak pressure near the catheter end is 35 Pa which decreases with the passage of time and the pressure difference remain very less near the end of the catheter and profiles become smooth. We did not observe the significant difference in the profiles of pressure in both cases of 2D and 3D geometries.

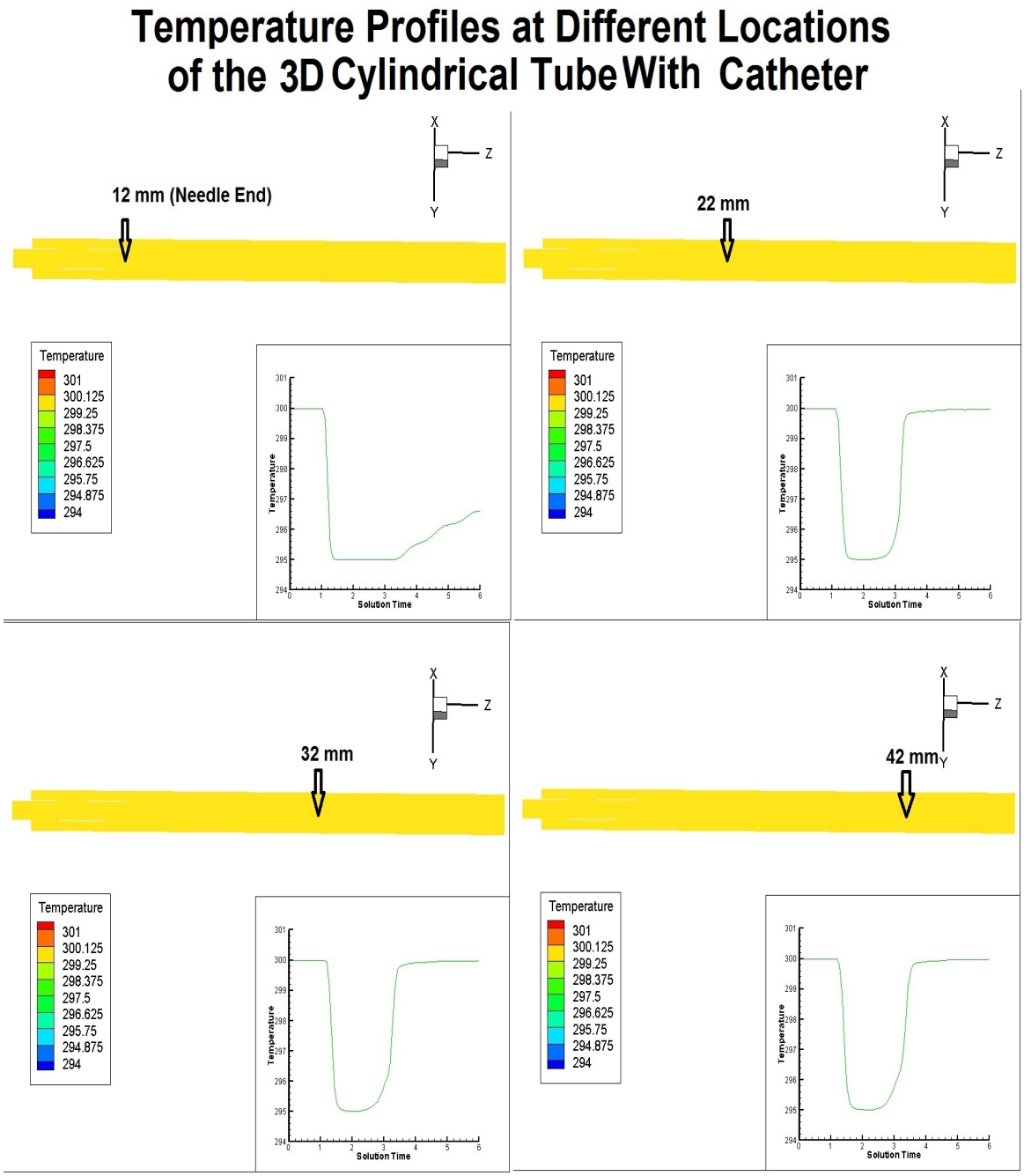

Figure 5.18: Temperature profiles at 4 different locations along the central axis of the tube in the presence of catheter for each heart beat.

Temperature profiles of 3D are also the same as in case of 2D geometry with a small difference of oscillations at the end. We did not see any oscillations at the end of the curves in 3D and the curves become straight line when temperature reaches back to 300 K.

5.4 Off-Axis Temperature Measurements in the 3D Tube

We observed the normal curves if the catheter remain at the central axis. To investigate the changes in temprature, we supposed that the probe is lying near the vessel wall instead of lying at the central axis. We then calculated the temperature at different position of the artery near the wall instead of centre to see the effects. We observed different shapes of the curves which also include the double peak. The temperature results are shown in Figures 5.20 and 5.22.

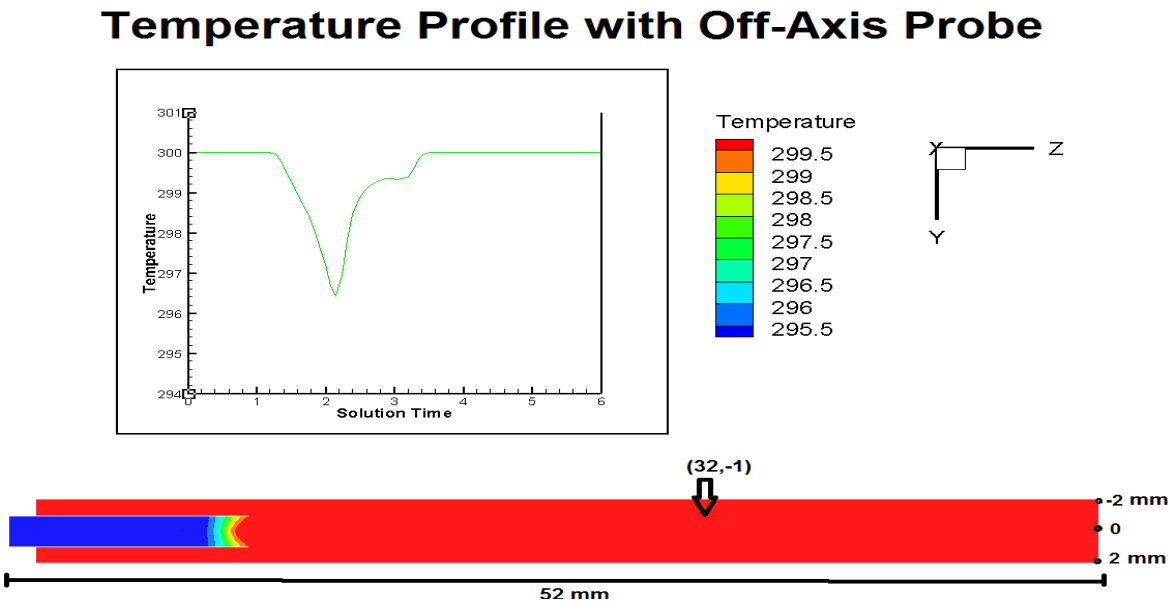

Figure 5.19: Temperature profile at a different location in the 3D coronary artery with probe away from the central axis. In this case the probe is in-line to the wall of the catheter at a distance of 32 mm.

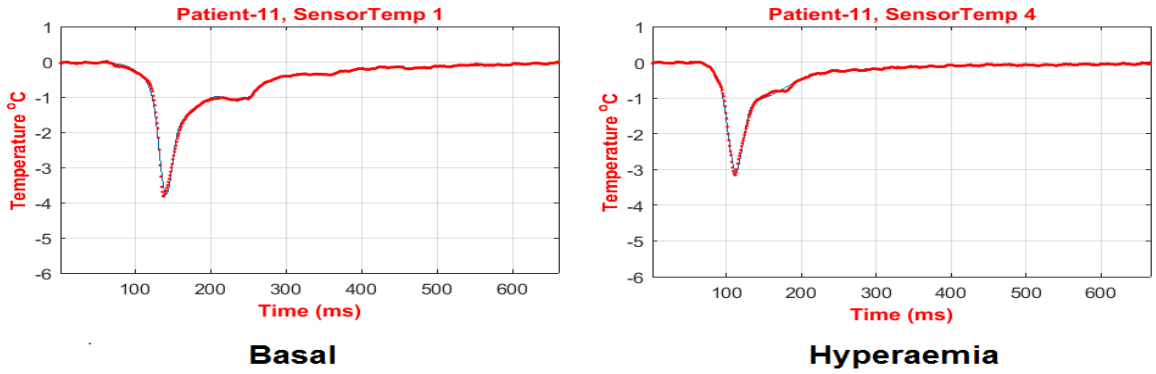

Figure 5.20: Thermodilution waveform of patient-11 showing the same double peak as we obtained during CFD simulations with an off-axis probe.

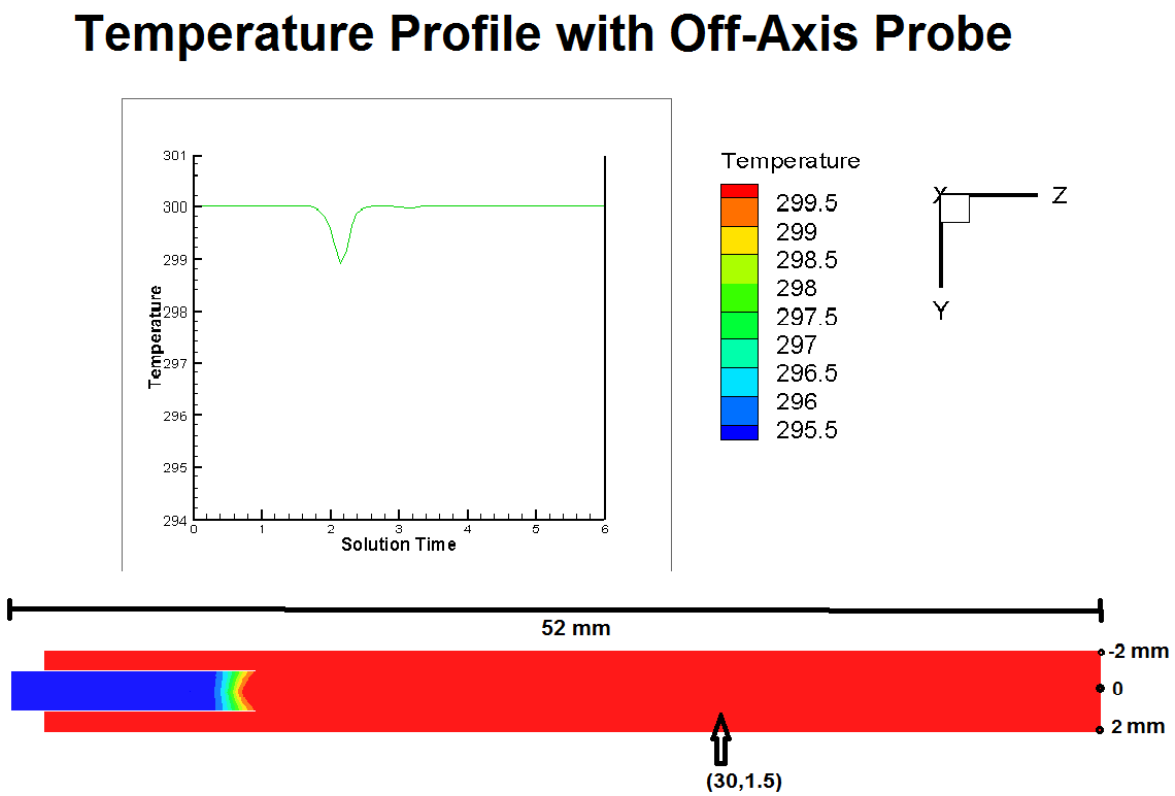

Figure 5.21: Temperature profile at a different location in the 3D coronary artery with probe away from the central axis. In this case the probe is closer to the vessel wall.

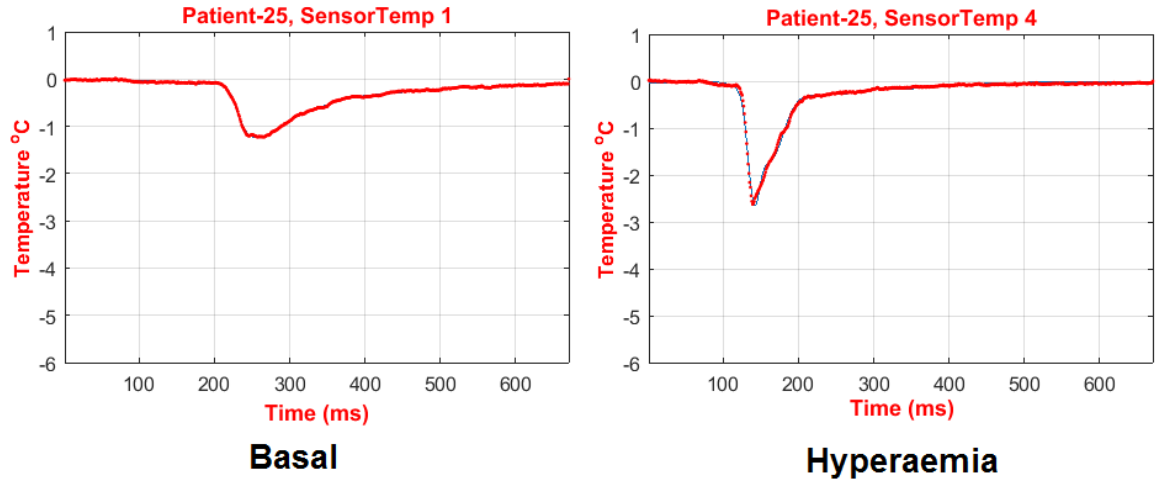

Figure 5.22: Thermodilution waveform of patient-25 showing the same result as we obtained during CFD simulations when the probe is closer to the vessel wall.

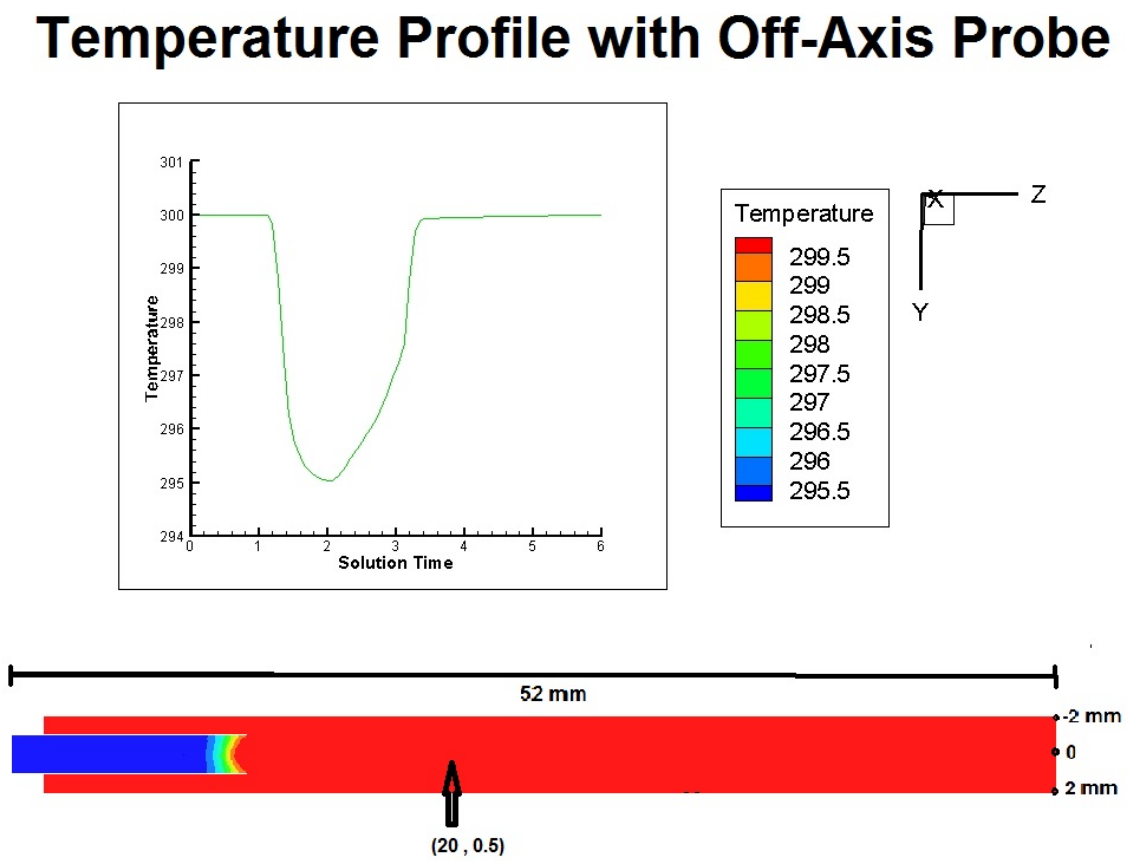

Figure 5.23: Temperature profile at a different location in the 3D coronary artery with probe near to the central axis showing the normal thermodilution curve (Section 4.6.1).

After analysing and correlating the results with the thermodilution waveforms, we can conclude that if we go near the vessel wall to calculate the temperature, double peak and other types of waveforms appear which we observed in Sections 4.6.2 and 4.6.1.

5.4.1 Flow in a Stenosed Channel

After finding some fruitful results, we decided to include 45% stenosis inside the 2D model coronary artery to further investigate the waveforms. The boundary conditions and the geometry were kept same as given in Section 5.3.4. The mesh was generated with 118561 number of nodes and 117257 number of quadrilaterals. The CFD silulations were run in the Fluent software and results were plotted using Tecplot software.

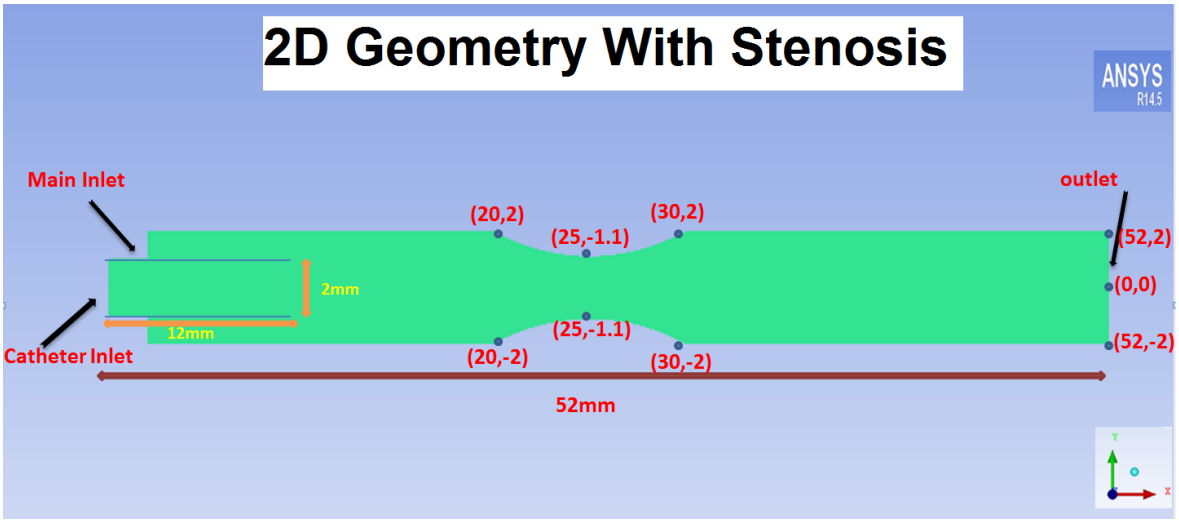

Figure 5.24: Computational geometry of 2D simple model in the presence of stenosis

We calculated the temperature on and off the central axis at different locations before and after stenosis. Few results are shown in Figure 5.25.

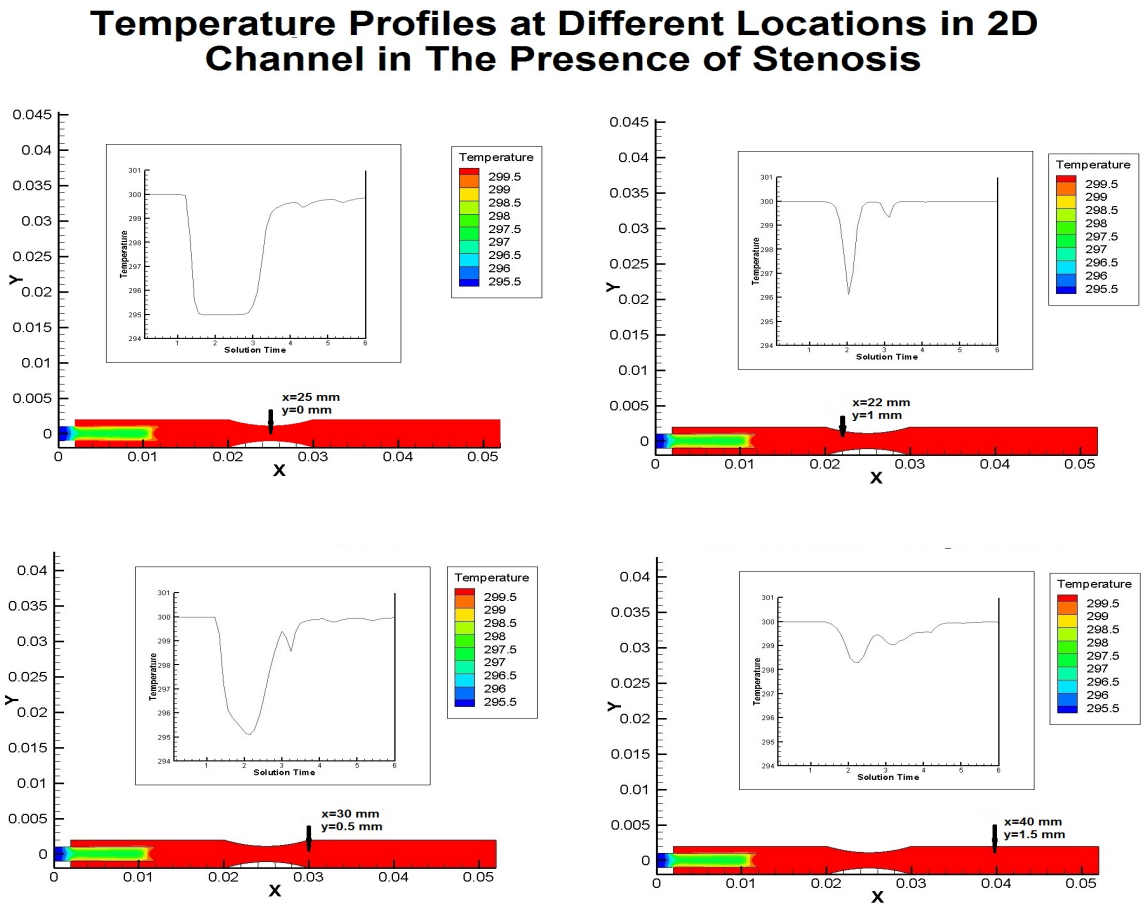

Figure 5.25: Temperature profiles at a different location in the 2D coronary artery with probe away from the central axis in the presence of stenosis shows double peaks and other shapes as we observed in Sections 4.6.2 and 4.6.3 whereas it remains normal at the central axis.

From Figure 5.25, we can observe that double peaks and other types of curves appear if the probe is away from the central axis or near the vessel wall and behaves normal at the central axis.

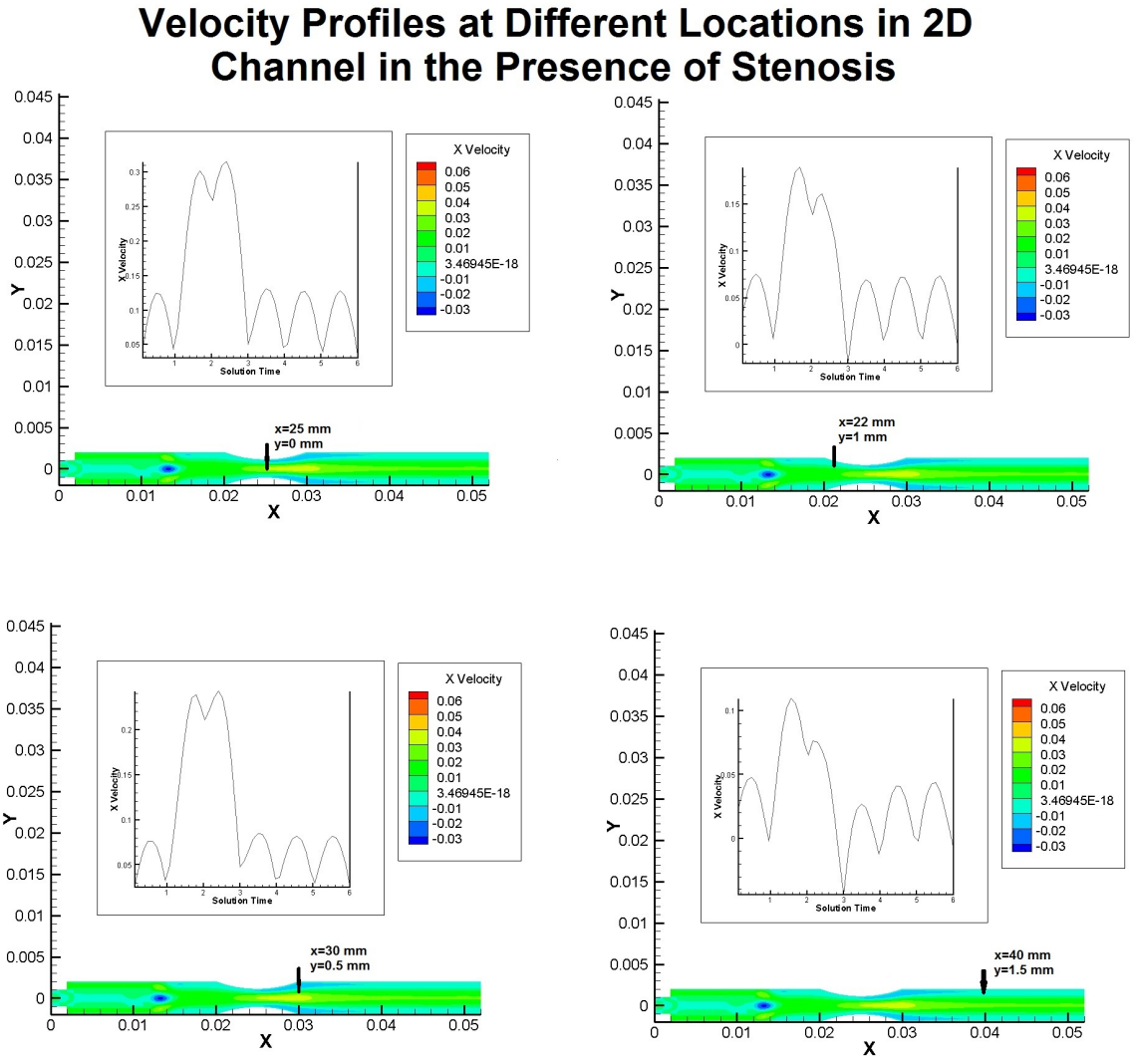

Figure 5.26: Velocity profiles at a different location in the 2D coronary artery with probe away from the central axis in the presence of stenosis shows the negative velocity profiles on the other side of the stenosis.

5.5 Results

The results of the simulations in the 2D and 3D model geometries are almost same at the centre of the artery and we have not seen any significant differences between the results of both geometries. If we compare the simulation results with the experimental results of thermodilution waveforms, we observed the same normal thermodilution curves if the probe remains at the centre of the coronary artery (see Section 4.6.1). However, if we calculate the temperature near the vessel wall, the shape of the curve

changes and it also shows the double peaks that are observed in some cases of actual thermodilution data in Section 4.6.2. Furthermore, we also observed the poor quality waveforms when the probe is off centre in case of 2D model geometry with stenosis (Section 4.6.3). Thus, we can say that the misalignment of the catheter inside the coronary artery affects badly on the thermodilution waveform's results which may affect clinical diagnosis.

Chapter 6

Discussion

6.1 Summary of Findings

A Matlab program was written to assess the thermodilution waveforms. We observed different shapes of waveforms in the thermodilution data. We tried to find the correlation between the thermodilution peak values and its half prominence but no strong relationship was found. Furthermore, we also tried to find the relationship between ratio of the mean values of the hyperaemic to basal peak temperature and CFR, FFR and IMR values for 66 patients but no statistically significant correlations were found. We observed few double peaks and high oscillations in the thermodilution curves and to investigate these curves, we set up a simple CFD model and experiments were performed using the commercial CFD software Fluent. We did not see pulsatility because the probe lies along the central axis and lies within the bolus of cold fluid over several periods and diffusion is too slow to affect the measurements. We observed normal thermodilution curves if the probe lies at the central axis but results with double peaks and other shapes if the probe lies off–axis or near the vessel wall. High frequency variations in the thermodilution plot seem likely to have a fluid mechanical origin associated with e.g. vortex shedding, or are associated with collapse of a vessel due to Bernoulli effects. This may occur when the catheter is positioned very close to a vessel wall. The misalignment of the catheter in case of stenosis badly affects the thermodilution waveforms which we also observed in the actual thermodilution data.

6.2 Suggestions for Future Research

In this project, different waveforms of thermodilution have been observed and critically analysed. We made a simple 3D cylindrical shape of the coronary artery with a catheter at the centre of artery and used the simple boundary conditions to provoke the pattern of the thermodilution waveforms and got some good results. We also include the stenosis inside the 2D model of coronary artery and found some fruitful results. However, further improvements can be made to observe the actual waveforms more critically. Following are some suggestions that can be adopted.

1. The stenosis can be incorporated with simple 3D geometry to get actual results as the patients were presented having a stenosis severity of $(45\% - 90\%)$.

2. An elasticity model can be included in the geometry as we have used simple 3D rigid cylindrical tube.

3. Boundary conditions can be improved which are more realistic in flow profiles.

4. The location of the catheter may be misaligned in the 3-dimensional model artery to see the difference in results.

6.3 Conclusion

Thermodilution technique is so far the best technique to measure the flow in the coronary arteries after myocardial infarction. However, intense care is needed during the procedure. The person who is performing thermodilution must be aware of the errors and pathalogical conditions of the patient. A misaligned catheter can result in incorrect flow estimate and hence incorrect treatment. The results obtained from the simple model can be further improved to better understand the different waveform results of thermodilution and the comparison of CFD results with the experimental thermodilution waveforms can improve the diagnostic procedures.

Appendix A

Radiview Software

Radiview software is used to convert and visualise the patients data for clinical use and research purposes. The thermodilution waveform data of patients is loaded into the Radiview software and following procedure is adopted to convert the data into spread sheets for further analysis.

1. The first procedure after the installation of software on the system is to load the data into software. For this very purpose, first of all we will go to start menu and will open the Radiview 2.2 software in the program menu. The window will appear on the screen as shown in Figure A.1.

Figure A.1: Step-1 after installation of software sackage

2. Click on 'SEARCH', the left most corner of Figure A.1, the screen will display as given in the right top corner side of Figure A.2. Then click on 'IMPORT' to

select the data you want to load which is already saved into your system. The window as given in Figure A.2 will appear when you will open the required folder.

Figure A.2: Step-2 Loading of data into Radiview Software package

3. Select the patient data from the screen and then click on export to convert into spread sheet or JPEG screen image.

Figure A.3: Step-3 Exporting and saving data into spreadsheet

4. When you will click export as given in Figure A.3, the following window will appear to save the data into desired location as shown in Figure A.4.

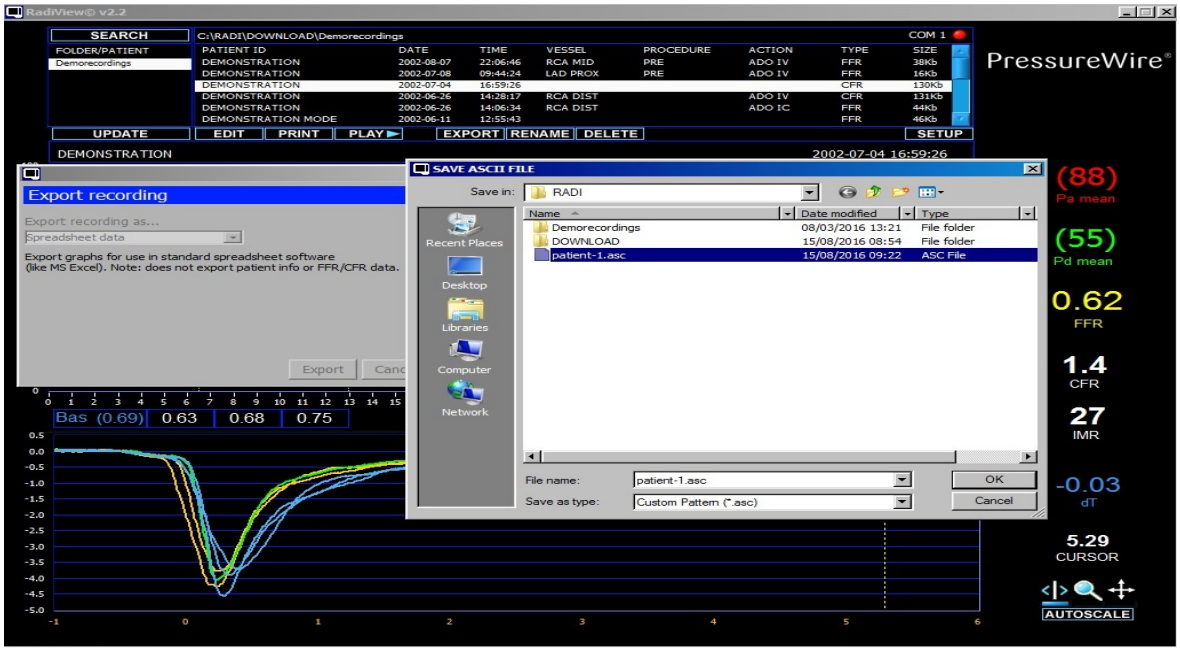

Figure A.4: Step-4 Exporting and saving data into spreadsheet

Appendix B

Matlab Program

Listing B.1: Matlab program which can load one patient data

```
clear all; close all; clc;
A=load('a (1).asc');
channel = ['SensorTemp 1';
'CableTemp 1  ';
'SensorTemp 2';
'CableTemp  2';
'SensorTemp 3';
'CableTemp  3';
'SensorTemp 4';
'CableTemp  4';
'SensorTemp 5';
'CableTemp  5';
'SensorTemp 6';
'CableTemp  6';
'Pa           ';
'Pa_{mean}    ';
'Pd           ';
'Pd_{mean}    ';
'Pd/Pa        '];
Size=size(A);
n=Size(1);
m=Size(2);
count=zeros(1,m);
R=count;
for j=1:12;
    for i=1:n-17
        if i+7>n
            [rows,columns] = size(A(:,j));
            count(j)=rows;
            break
        end
  if (A(i,j)==0 && A(i+1,j)==0 && A(i+2,j)==0 && A(i+3,j)==0 && A(i+4,j)==0 ...
        && A(i+5,j)==0 && A(i+6,j)==0 && A(i+7,j)==0 && A(i+8,j)==0 && A(i+9,j)==0
            ...
        && A(i+10,j)==0 && A(i+11,j)==0 && A(i+12,j)==0 && A(i+13,j)==0 && A(i+14,j)
            ==0 ...
        && A(i+15,j)==0 && A(i+16,j)==0 && A(i+17,j)==0 && A(i+18,j)==0 && A(i+19,j)
            ==0 ...
        && A(i+20,j)==0)
           count(j)=i-1;
        end
        if count(j)~=0;
            break
        end
    end


end
b=count;

for i = 1:12
    figure;
```

```
50      plot (-A(1:b(i),i)/1000);
51      xlabel('Time (ms)'); ylabel('-Temperature ^oC'); title(channel(i,:));
52  end;
```

Listing B.2: Input function which is used to calculate the values of Peak

```
1  clc;
2  clear all;
3  close all;
4  patnum=12;
5  data=zeros(12,4,patnum);
6  for i=1:patnum
7      str=['a (',num2str(i),').asc'];
8      A=load(str);
9      [data(:,1,i),data(:,2,i),data(:,3,i),data(:,4,i)]=heartdata(A);
10     xlswrite('data.xls',data(:,:,i),['Sheet',num2str(i)]);
11
12     i
13 end
```

```
1  function [pks, locs, width, prom] = heartdata(A)
2  pks=zeros(103,1);
3  locs=pks;
4  width=pks;
5  prom=pks;
6
7  channel = ['SensorTemp 1';
8  'CableTemp 1  ';
9  'SensorTemp 2';
10 'CableTemp  2';
11 'SensorTemp 3';
12 'CableTemp  3';
13 'SensorTemp 4';
14 'CableTemp  4';
15 'SensorTemp 5';
16 'CableTemp  5';
17 'SensorTemp 6';
18 'CableTemp  6';
19 'Pa          ';
20 'Pa_{mean}   ';
21 'Pd          ';
22 'Pd_{mean}   ';
23 'Pd/Pa       '];
24 Size=size(A);
25 n=Size(1);
26 m=Size(2);
27 count=zeros(1,m);
28 R=count;
29 for j=1:12;
30     for i=1:n-20
31         if i+7>n
32             [rows,columns] = size(A(:,j));
33             count(j)=rows;
34             break
35         end
36   if (A(i,j)==0 && A(i+1,j)==0 && A(i+2,j)==0 && A(i+3,j)==0 && ...
37           A(i+4,j)==0 && A(i+5,j)==0 && A(i+6,j)==0 && A(i+7,j)==0 ...
38           && A(i+8,j)==0 && A(i+9,j)==0 && A(i+10,j)==0 && A(i+11,j)==0 ...
39           && A(i+12,j)==0 && A(i+13,j)==0 && A(i+14,j)==0 && A(i+15,j)==0 ...
40           && A(i+16,j)==0 && A(i+17,j)==0 && A(i+18,j)==0 && A(i+19,j)==0 ...
41           && A(i+20,j)==0)
42
43             count(j)=i-1;
44         end
45         if count(j)~=0;
46             break
47         end
48     end
49
50
51 end
52 b=count;
53
54 for i = 1:12
55 %     figure;
56 %     plot (-A(1:b(i),i)/1000);
```

```
57      %xlabel('Time (ms)'); ylabel('-Temperature ^oC'); title(channel(i,:));
58      % print -djpeg ...;
59        xdata=-A(1:b(i),i)/1000;
60         ydata=[1:b(i)]';
61 %% Fit: 'untitled fit 1'.
62 [xData, yData] = prepareCurveData( ydata, xdata );
63
64 % Set up fittype and options.
65 ft = fittype( 'gauss8' );
66 opts = fitoptions( 'Method', 'NonlinearLeastSquares' );
67 opts.Display = 'Off';
68 opts.Lower = [-Inf -Inf 0 -Inf -Inf 0 -Inf -Inf 0 -Inf -Inf ...
69      0 -Inf -Inf 0 -Inf -Inf 0 -Inf -Inf 0 -Inf -Inf 0];
70 opts.StartPoint = [0 74.4444444444444 73.4444444444444 0 ...
71      147.888888888889 73.4444444444444 0 221.333333333333 ...
72      73.4444444444444 0 294.777777777778 73.4444444444444 0 ...
73      368.222222222222 73.4444444444444 0 441.666666666667 ...
74      73.4444444444444 0 515.111111111111 73.4444444444444 0 ...
75      588.555555555556 73.4444444444444];
76
77 % Fit model to data.
78 [fitresult, gof] = fit( xData, yData, ft, opts );
79
80 % Plot fit with data.
81 % figure( 'Name', 'untitled fit 1' );
82 % h = plot( fitresult, xData, yData );
83 % legend( h, 'xdata vs. ydata', 'untitled fit 1', 'Location', 'NorthEast' );
84 % % Label axes
85 % xlabel( 'ydata' );
86 % ylabel( 'xdata' );
87 % grid on
88 % %      figure(2*i);
89 [pks(i),locs(i),width(i),prom(i)] =findpeaks(fitresult(xData),...
90      'MinPeakProminence',0.7,'NPeaks',1);
91 % [pks(i),locs(i),width(i),prom(i)] =findpeaks(fitresult(xData),...
92 'Annotate','extents','MinPeakDistance',310,'MinPeakProminence',0.7);%-A(1:b(i),i)/1000
93 % hold on
94 % findpeaks(-A(1:b(i),i)/1000,'Annotate','extents','MinPeakDistance',20.0,...
95 'MinPeakProminence',0.5)
96 % hold off
97
98 %pks = findpeaks(-A(1:662,i)/1000,'MinPeakDistance',20.0,'MinPeakHeight', 0.5)
99
100 end;
101
102 end
```

Listing B.3: Function used to find the mean hyperaemic to basal ratios of peak

```
1  clc;
2  clear all;
3  close all;
4  patnum=103;
5  data=zeros(103,4,patnum);
6  RatioS=zeros(patnum,5);
7  RatioS(:,1)=linspace(1,patnum,patnum)';
8  RatioC=RatioS;
9   for i=1:patnum
10 %  i=103
11      str=['a (',num2str(i),').asc'];
12      A=load(str);
13      [data(:,1,i),data(:,2,i),data(:,3,i),data(:,4,i)]=heartdata(A);
14      M=data(:,:,i);
15      B = M(1:2:end,:);  % odd matrix
16      C = M(2:2:end,:);  % even matrix
17      O1=mean(B(1:3,:));
18      O2=mean(B(4:6,:));
19      E1=mean(C(1:3,:));
20      E2=mean(C(4:6,:));
21      RatioS(i,2:5)=O2./O1;
22      RatioC(i,2:5)=E2./E1;
23
24      xlswrite('patientdata',RatioS,'Sheet1');
25      xlswrite('patientdata',RatioC,'Sheet2');
26      i
27  end
```

Listing B.4: A function used to find the pictorial view of thermodilution curves of own choice.

```
function [ output_args ] = drawGraphs( patientNum, Columns )
%% --load patient file--
str=['a (',num2str(patientNum),').asc'];
A=load(str);

%% --determine the rows and columns--
Size=size(A);
cutoff=Size(1);
for k=1:Size(1)-20
    if (A(k,Columns)==0 && A(k+1,Columns)==0 && A(k+2,Columns)==0 ...
            && A(k+3,Columns)==0 && A(k+4,Columns)==0 && A(k+5,Columns)==0 ...
            && A(k+6,Columns)==0 && A(k+7,Columns)==0 && A(k+8,Columns)==0 ...
            && A(k+9,Columns)==0 && A(k+10,Columns)==0 && A(k+11,Columns)==0 ...
            && A(k+12,Columns)==0 && A(k+13,Columns)==0 && A(k+14,Columns)==0 ...
            && A(k+15,Columns)==0 && A(k+16,Columns)==0 && A(k+17,Columns)==0 ...
            && A(k+18,Columns)==0 && A(k+19,Columns)==0 && A(k+20,Columns)==0)
        cutoff=k;
        break;
    end
end
Temp=-A(1:cutoff,Columns)/1000;
Time=[1:cutoff]';

%% Fit: 'untitled fit 1'.
[Temp, Time] = prepareCurveData( Time, Temp );

%% Set up fittype and options.
ft = fittype( 'gauss8' );
opts = fitoptions( 'Method', 'NonlinearLeastSquares' );
opts.Display = 'Off';
opts.Lower = [-Inf -Inf 0 -Inf -Inf 0 -Inf -Inf 0 -Inf -Inf ...
    0 -Inf -Inf 0 -Inf -Inf 0 -Inf -Inf 0];
opts.StartPoint = [0 74.4444444444444 73.4444444444444 0 147.888888888889 ...
    73.4444444444444 0 221.333333333333 73.4444444444444 0 294.777777777778 ...
    73.4444444444444 0 368.222222222222 73.4444444444444 0 441.666666666667 ...
    73.4444444444444 0 515.111111111111 73.4444444444444 0 588.555555555556 ...
    73.4444444444444];


%%
switch Columns
    case 1
        titl='SensorTemp 1';
    case 2
        titl='CableTemp 1';
    case 3
        titl='SensorTemp 2';
    case 4
        titl='CableTemp  2';
    case 5
        titl='SensorTemp 3';
    case 6
        titl='CableTemp 3';
    case 7
        titl='SensorTemp 4';
    case 8
        titl='CableTemp  4';
    case 9
        titl='SensorTemp 5';
    case 10
        titl='CableTemp  5';
    case 11
        titl='SensorTemp 6';
    otherwise
        titl='CableTemp 6';
end


%%
[fitresult, gof] = fit( Temp, Time, ft, opts );
[pks,locs,width,prom] =findpeaks(fitresult(Temp),'Annotate','extents','MinPeakDistance
    ',320,'MinPeakProminence',0.5);
% findpeaks(fitresult(Temp),'Annotate','extents','MinPeakDistance',450,'
    MinPeakProminence',0.5)
findpeaks(fitresult(Temp),'Annotate','extents','MinPeakProminence',0.7,'NPeaks',1)
```

```
74 hold on
75 plot(Temp,Time,'.r');
76 title(titl);
77 ylim([-2 12]);
78 %legend('actual data','fitted data');
79 str = {['peak=',num2str(pks)],['location=',num2str(locs)],['width=',num2str(width)],['
       prominance=',num2str(prom)]};
80 text(cutoff-250,7.0,0,str);
81 % Label axes
82 xlabel( 'Time (msec)' );
83 ylabel( '-Temperature ^oC' );
84 grid on
85 hold off
```

Listing B.5: Function used to find the subgraphs and show 6 curves at a time.

```
1
2 function [ output_args ] = Subplot( PatNum )
3
4 % figure('Name','Patient Number','NumberTitle','off')
5 scrsz = get(groot,'ScreenSize');
6 F1=figure('Position',[1 1 scrsz(3) scrsz(4)]);
7 subplot(2,3,1);
8 drawGraphs(PatNum,1);
9
10 subplot(2,3,2);
11 drawGraphs(PatNum,2);
12
13 subplot(2,3,3);
14 drawGraphs(PatNum,3);
15
16 subplot(2,3,4);
17 drawGraphs(PatNum,4);
18
19 subplot(2,3,5);
20 drawGraphs(PatNum,5);
21
22 subplot(2,3,6);
23 drawGraphs(PatNum,6);
24 saveas(F1,['Patient',num2str(PatNum),'-1'],'jpg');
25
26 % figure('Name','Patient Number','NumberTitle','off')
27
28 F2=figure('Position',[1 1 scrsz(3) scrsz(4)]);
29 subplot(2,3,1);
30 drawGraphs(PatNum,7);
31
32 subplot(2,3,2);
33 drawGraphs(PatNum,8);
34
35 subplot(2,3,3);
36 drawGraphs(PatNum,9);
37
38 subplot(2,3,4);
39 drawGraphs(PatNum,10);
40
41 subplot(2,3,5);
42 drawGraphs(PatNum,11);
43
44 subplot(2,3,6);
45 drawGraphs(PatNum,12);
46 saveas(F2,['Patient',num2str(PatNum),'-2'],'jpg');
47 end
```

B.1 CE-MARC2 Study Folder

Thermodilution Data of Patients with Their Study Number					
Sr.No	Study Number	Patient Number	Sr. No	Study Number	Patient Number
1	CEMARC2 AB00435	1,2	34	CEMARC2 LP00825	51
2	CEMARC2 AB01096	3	35	CEMARC2 LW00259	52
3	CEMARC2 AC00086	4	36	CEMARC2 MA00856	53,54
4	CEMARC2 APM00604	5,6	37	CEMARC2 MAE00304	55
5	CEMARC2 AW00127	7,8,9	38	CEMARC2 MG00613	56
6	CEMARC2 BC01097	10,11,12	39	CEMARC2 MG00613 RCA	57,58
7	CEMARC2 BH00017	13	40	CEMARC2 MH01192	59,60
8	CEMARC2 BV00132	14	41	CEMARC2 MJP00266	61
9	CEMARC2 CD00020	15,16	42	CEMARC2 MN00630	62
10	CEMARC2 CM01158	17,18	43	CEMARC2 MW00469	63,64
11	CEMARC2 CT00315	19,20,21	44	CEMARC2 MY00486	65
12	CEMARC2 DC00378	22	45	CEMARC2 NH00666	66,67
13	CEMARC2 DC00623	23	46	CEMARC2 PJ00360	68
14	CEMARC2 DG00014	24,25	47	CEMARC2 PP00541	69,70
15	CEMARC2 DJ00059	26	48	CEMARC2 RGP00581	71
16	CEMARC2 DK00118	27	49	CEMARC2 RH00730	72,73
17	CEMARC2 DL01118	28	50	CEMARC2 RH00922	74,75
18	CEMARC2 EH01095	29	51	CEMARC2 SG00459	76,77
19	CEMARC2 FDH00775	30	52	CEMARC2 SP00245	78
20	CEMARC2 GB01136	31	53	CEMARC2 SQ00684	79
21	CEMARC2 GF00429	32	54	CEMARC2 SR00923	80
22	CEMARC2 GJS00402	33,34,35,36	55	CEMARC2 SS00156	81,82,83
23	CEMARC2 GM00565	37	56	CEMARC2 SVR00745	84,85
24	CEMARC2 GSR00471	38	57	CEMARC2 TB00068	86,87
25	CEMARC2 IC01055	39	58	CEMARC2 TB00468	88,89
26	CEMARC2 JD00818	40,41	59	CEMARC2 TK01133	90,91,92,93
27	CEMARC2 JEC00718	42,43	60	CEMARC2 TLH00506	94
28	CEMARC2 JL00636	44	61	CEMARC2 VAP00551	95,96
29	CEMARC2 JMcA00233	45	62	CEMARC2 WG00496	97
30	CEMARC2 JMcM00758	46,47	63	CEMARC2 WH00458	98,99
31	CEMARC2 JW00614	48	64	CEMARC2 WL00559	100,101
32	CEMARC2 LA00519	49	65	CEMARC2 WW00013	102
33	CEMARC2 LAS00491	50	66	CEMARC2 ZI00808	103

Figure B.1: Thermodilution data of 66 patients with their study number

Appendix C

Computational Fluid Domains

C.1 2-Dimensional Geometry

C.1.1 Fluid Domain (Geometry)

Following procedure was adopted to make 2D model geometry for blood flow in arteries.

1. Go to the start menu and open the ICEM CFD 14.5.7. Figure C.1 will appear.

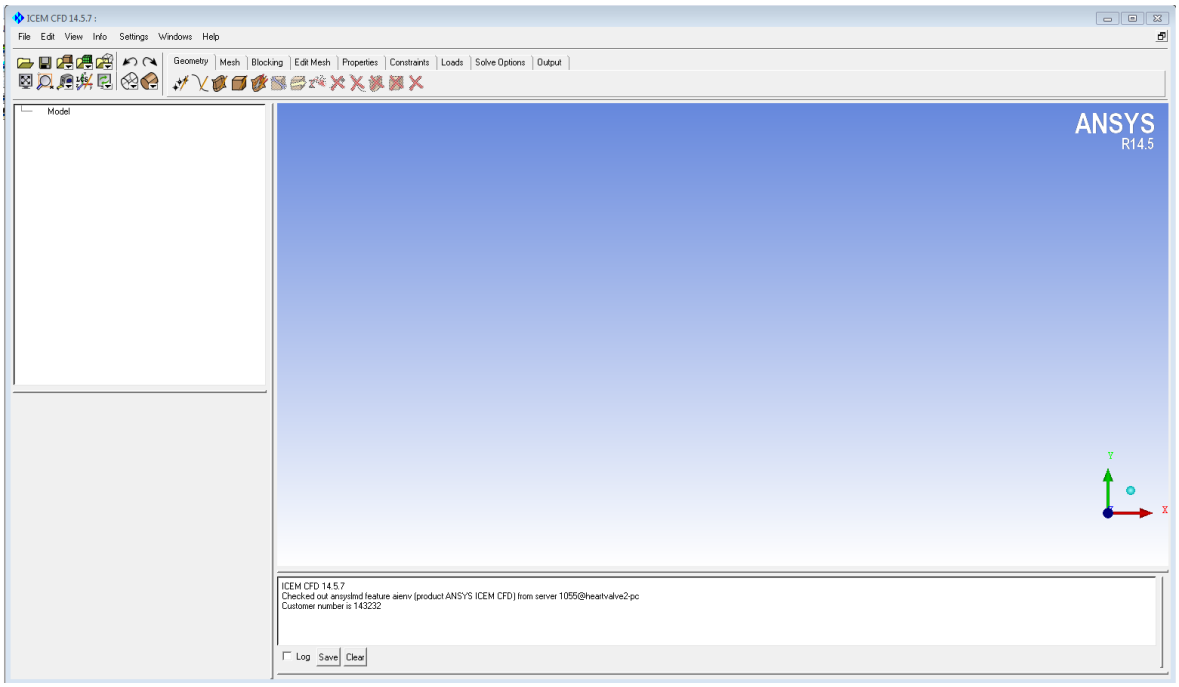

Figure C.1

2. Right click on model and click on geometric units. At the bottom of window, select the appropriate unit i.e. millimetre in our case.

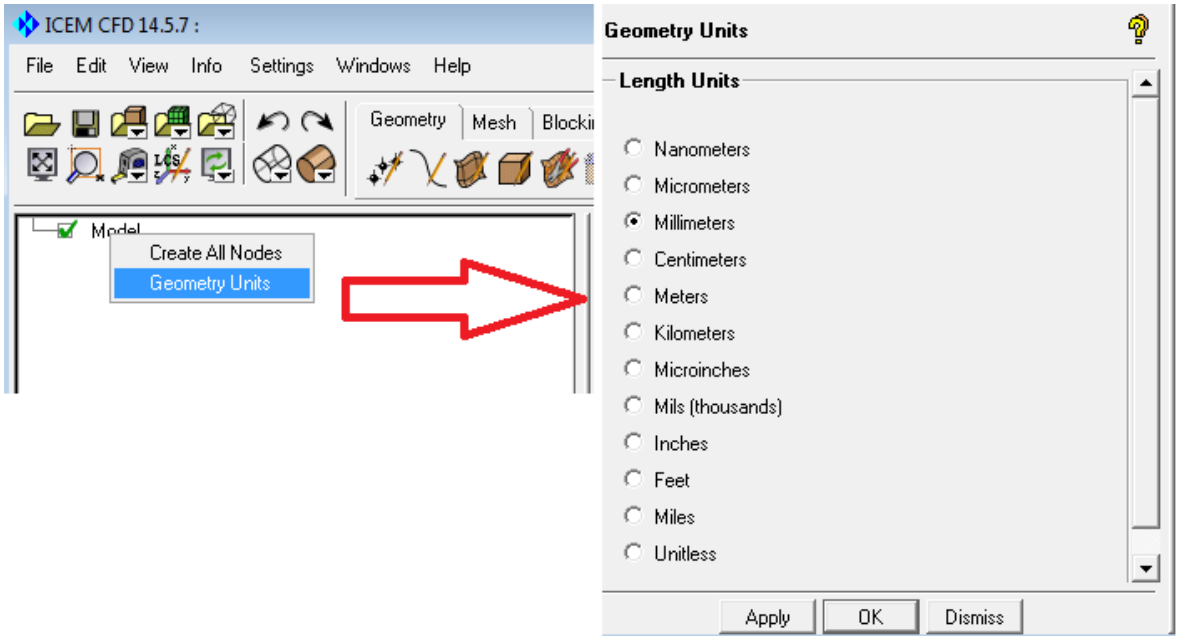

Figure C.2

3. Go to the file menu and click on the change working directory and save the file as shown in Figure C.3.

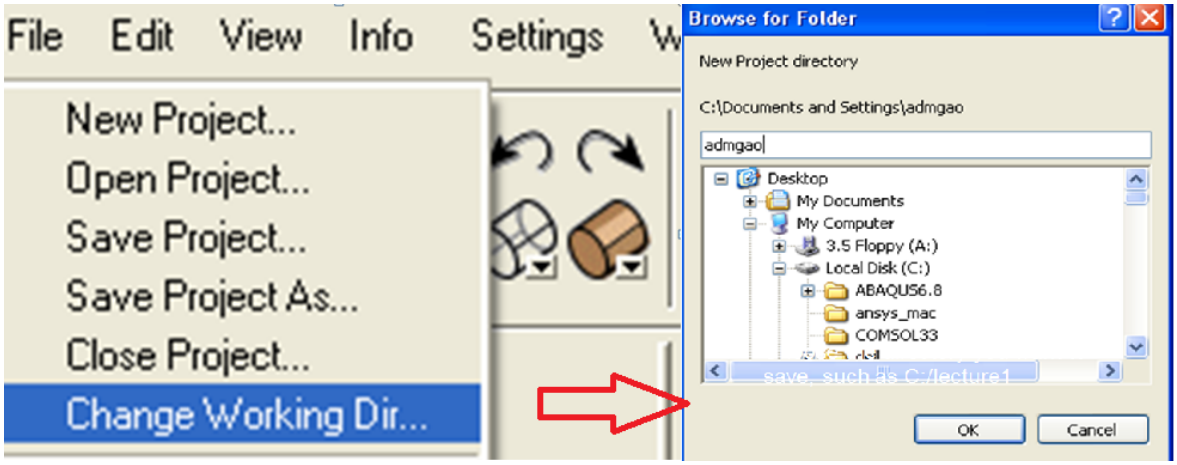

Figure C.3

4. Create the initial points by using following procedure.

   - Click on Geometry tab.
   - Click on create point icon under the Geometry tab for creating points.
   - Part name GEOM will remain same.
   - Select locations
   - Choose Create 1 Point in the list.
   - Input x y z coordinates. In this case it is 2-dimensional (i.e. x, y).
   - Click on apply for creation of one point.
   - Create other points using steps.

- Click dismiss after creating all points.
- The coordinates for the 4 points are in mm: P1: 0, -2 P2: 0, 2 P3: 50, -2 P4: 50, 2

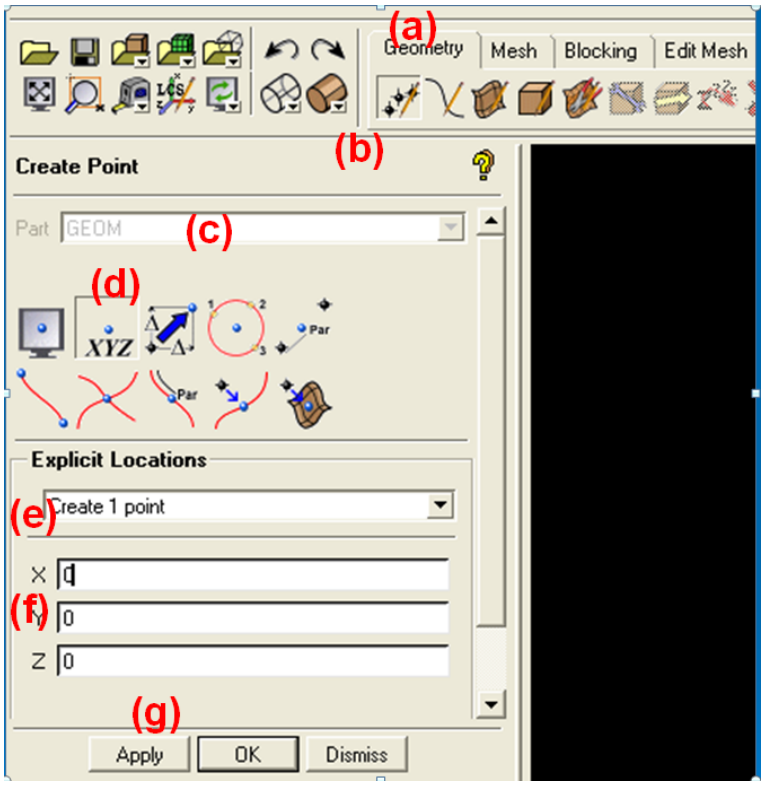

Figure C.4

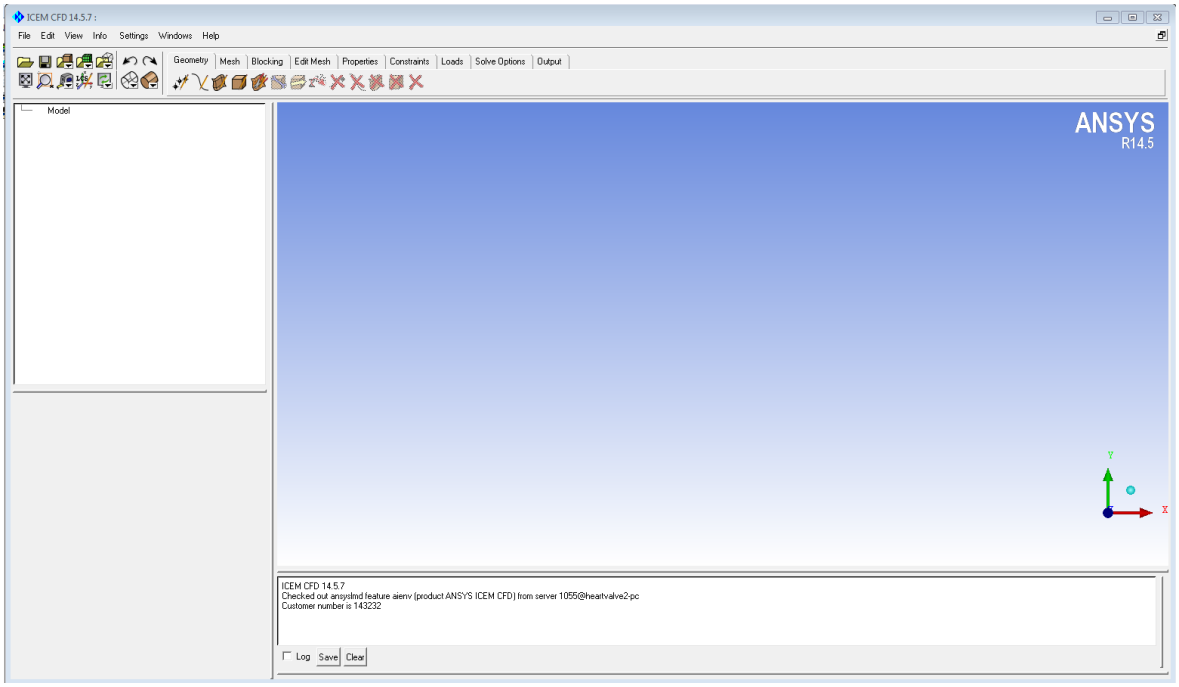

Figure C.5

5. The points will appear on screen as shown in Figure C.6 (Note: Click on fit window icon if points are not visible).

Figure C.6

6. Create the lines by adopting following steps.

   - Click on geometry.
   - Go to the lines.
   - GEOM part will remain as it is.
   - Select the point icon.
   - Click on points and choose any two points from the main window.
   - Click apply and repeat this step for the four points. Figure C.8 will appear.

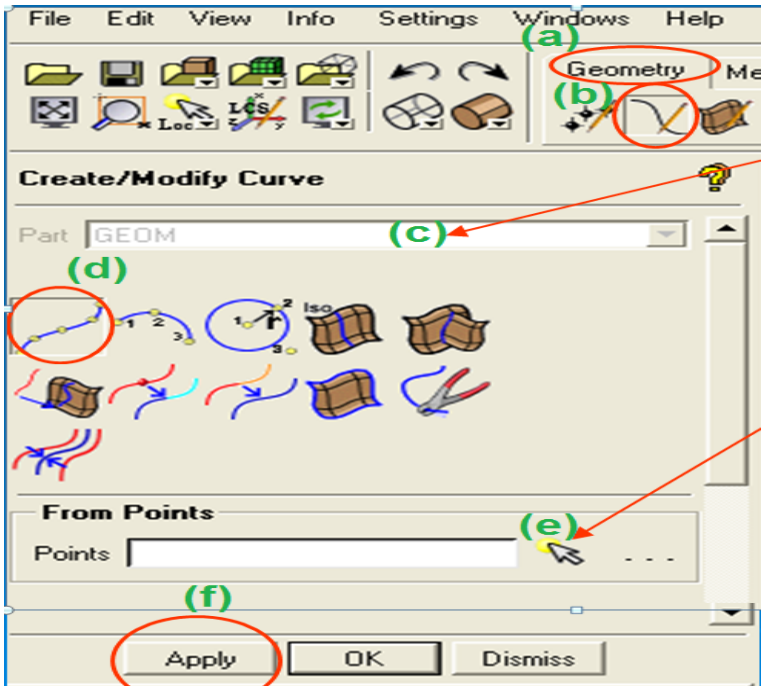

Figure C.7

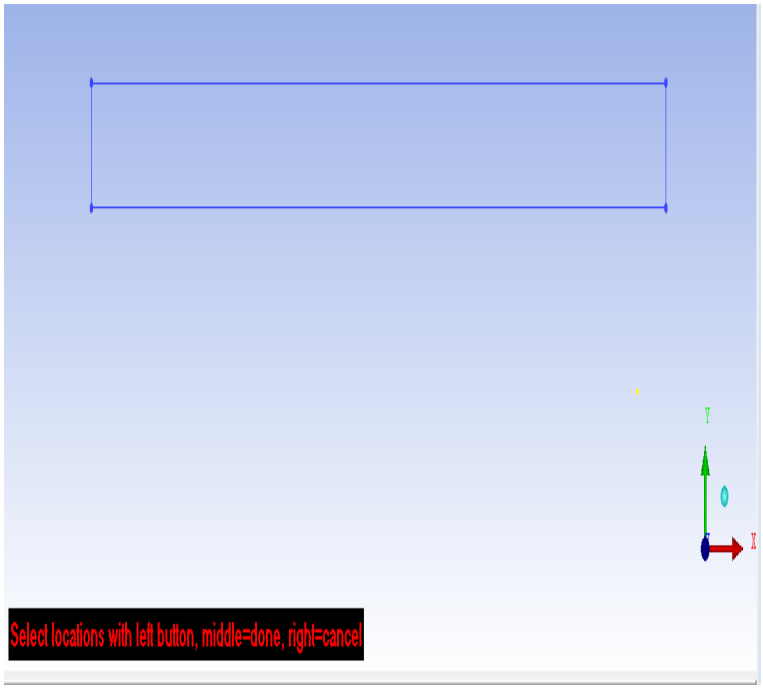

Figure C.8

7. Define the fluid domain by choosing the body icon from the geometry tab.
    - Change the name of BODY.
    - Click on the material points.
    - Select the any two locations on the window screen.
    - Click on apply to create body.

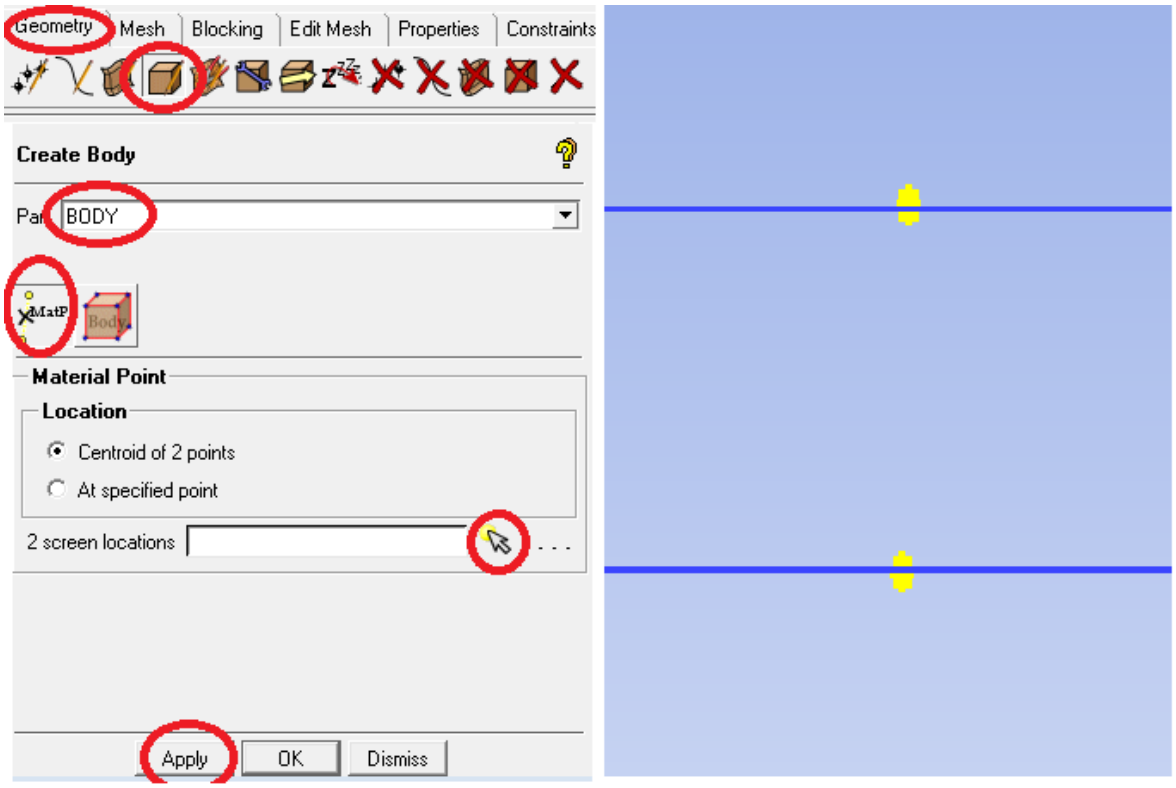

Figure C.9

8. In model control tree view, right click on the parts.
    - Figure C.10 will appear at the bottom of the screen.
    - Write inlet in parts.
    - Click on entities and select the line of inlet from the main screen and then apply.
    - Repeat this procedure to give the name of other parts.

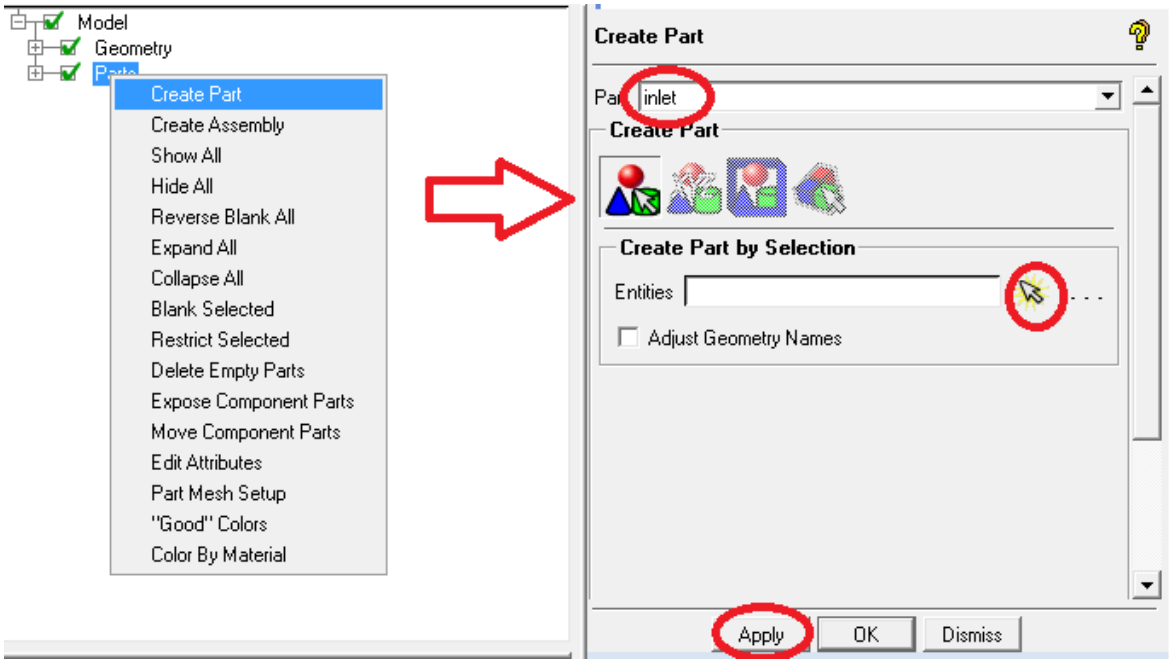

Figure C.10

9. Click on the model tree to view to confirm that all parts have been created as shown in Figure C.11 and then save the geometry.

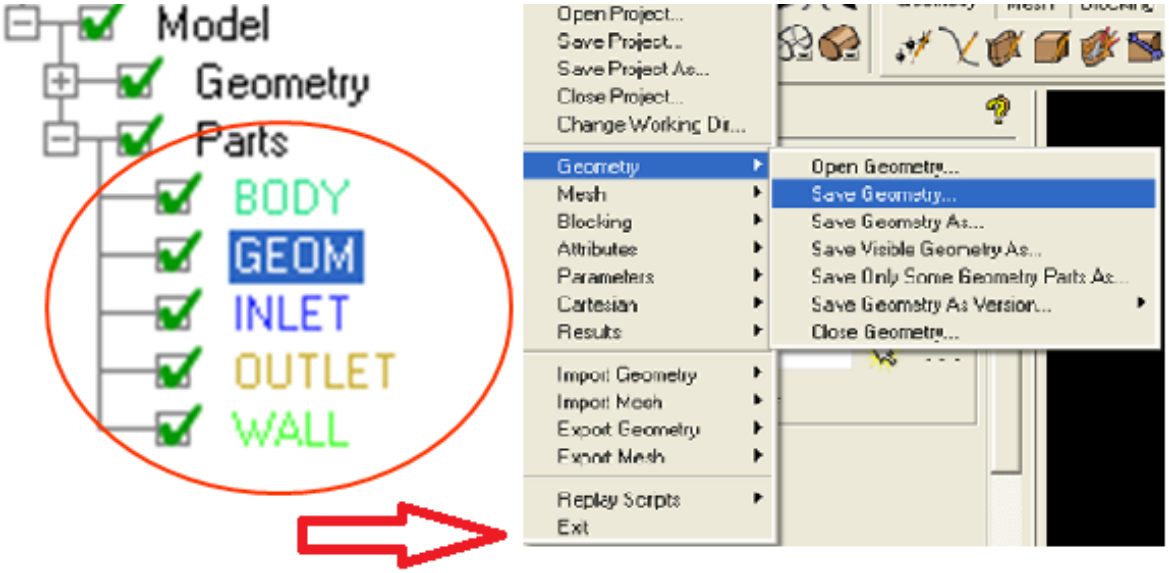

Figure C.11

C.1.2 Mesh Generation

Following procedure was implemented to generate the mesh.

1. Click on the block icon under the geometric tab.
    - Choose BODY from the list.
    - Click on initialise block icon
    - Select 2D Planer type and click ok.

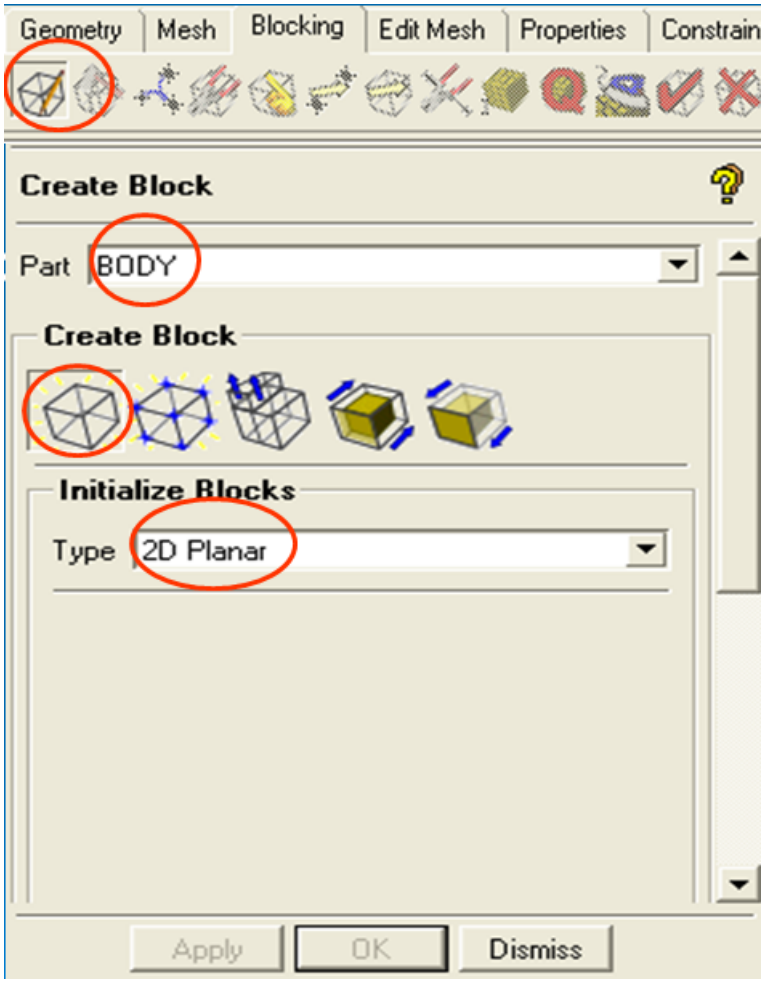

Figure C.12

2. Associate the created block with geometry, a one to one map was made for the edges in block and curves in the geometry. Procedure is shown in Figure C.13.
    - Choose associate icon.
    - Choose associate edge to Curve.
    - Click on edge icon and then select the edge in the main window and press the middle button of mouse.
    - Click the curve icon and then select the same edge which was selected before. When it is highlighted then press the middle button of mouse to associate.
    - Click on apply and repeat the same procedure for the remaining edges.

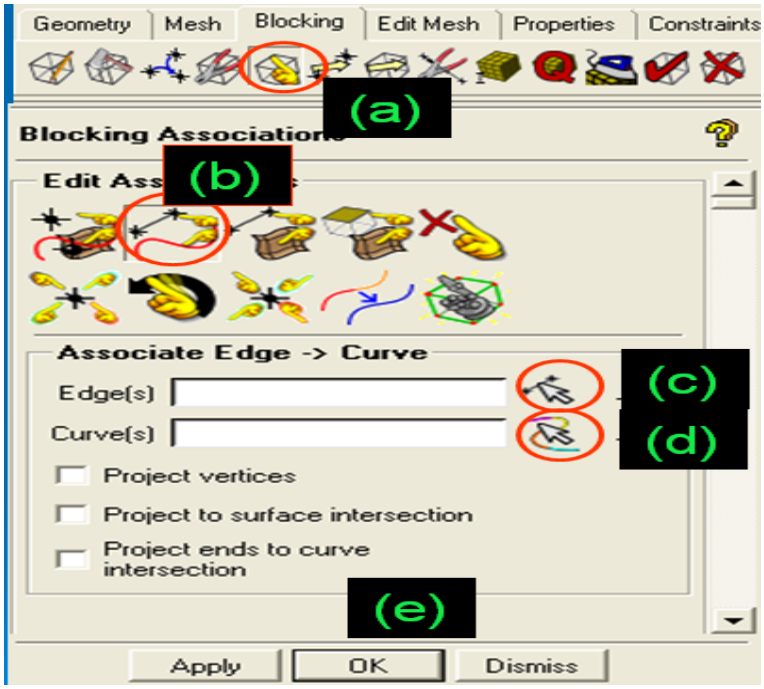

Figure C.13

3. Apply the mesh as described and shown in Figure C.14

   - Choose the curve mesh set up
   - Method will remain General
   - Select the curve icon and then click on the any edge of geometry in the main window and press the middle button of mouse. The name will appear in the window.
   - Insert the number of nodes (i.e. 50).
   - Click ok and repeat the same procedure for all edges.

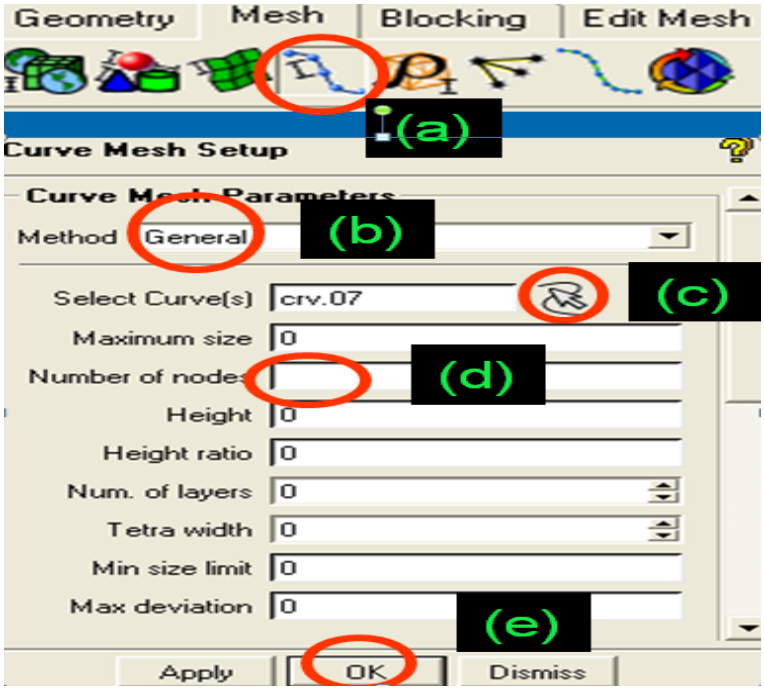

Figure C.14

4. Initialize the mesh generation

   - Choose the pre-mesh icon from the blocking tab.
   - Choose the update size
   - Select update all and then click on apply.

Figure C.15

5. Go to the blocking tree and turn on the pre-mesh. When you will click on the pre-mesh, a new window will appear. Select yes when the message appears to re-compute. Further, to view the mesh, switch off edges and vertices from the display control tree.

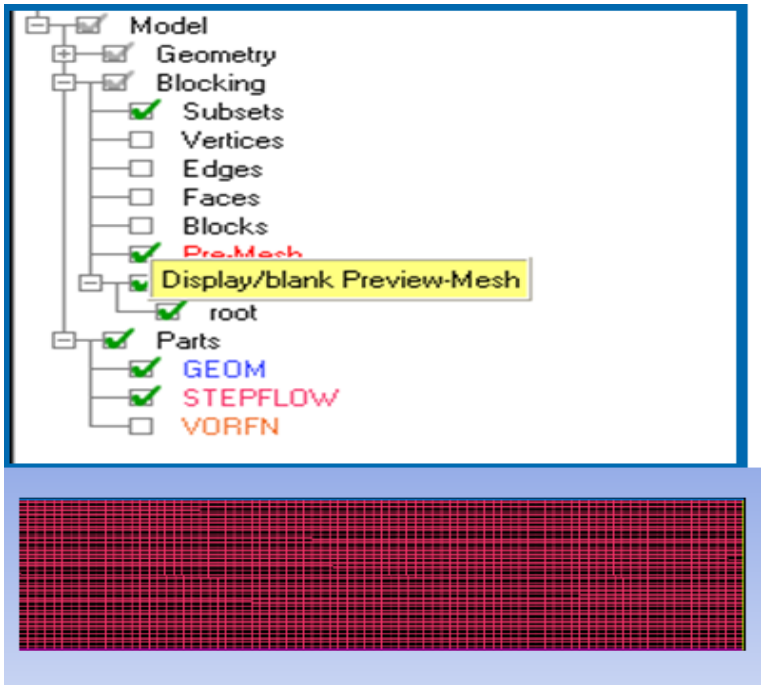

Figure C.16

6. Go to the blocking display control tree and right click on pre-mesh and select the un-structured mesh to generate the domain file and save the project file.

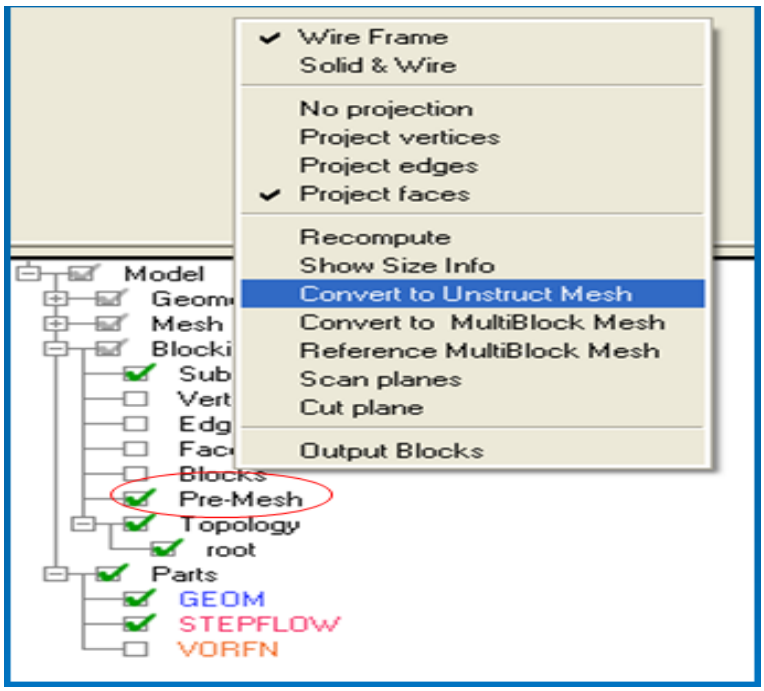

Figure C.17

7. To export the mesh, go to output tab and select solver. Select the output solver as Fluent V6 and common structural solver with remain ANSYS (Figure B.22).

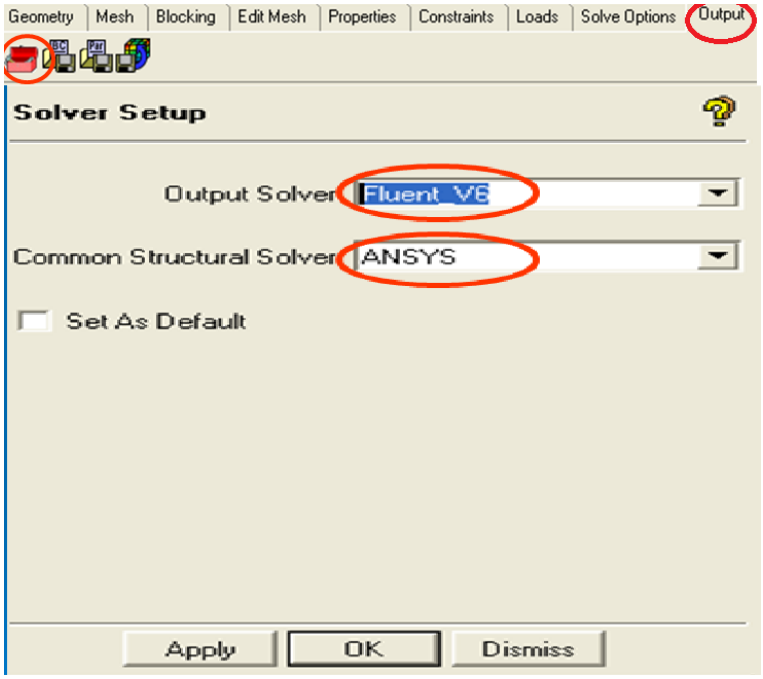

Figure C.18

8. Click on write input icon and save the project first. Then a file open window will appear. Save the mesh file (*.uns), which is the same name as the project name saved earlier as shown in Figure C.19

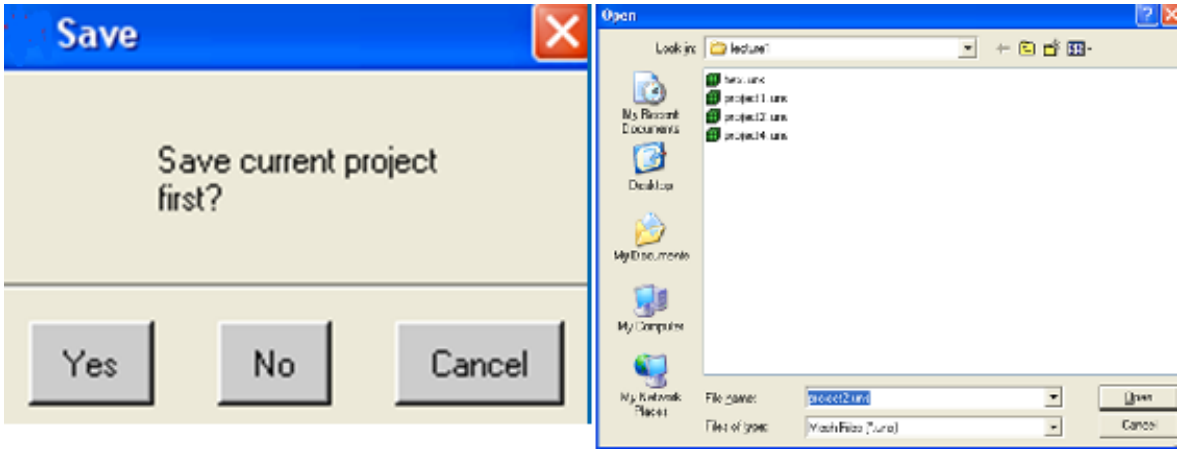

Figure C.19

9. Select 2D and change the name of the output mesh file as shown in Figure C.20

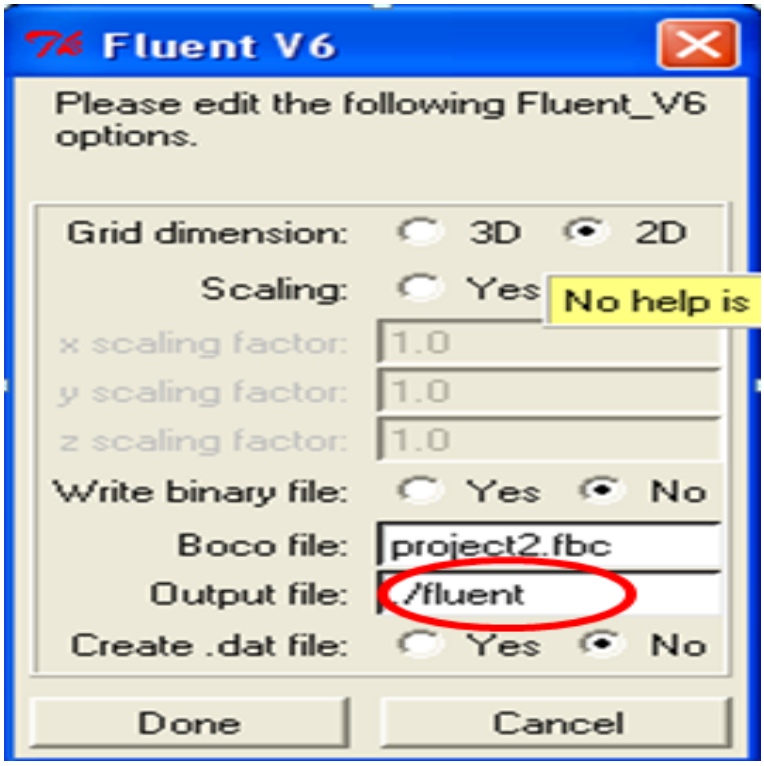

Figure C.20

10. The mesh file will be saved in the working directory with .msh extension .

C.1.3 Simulation in Fluent Software

11. Go to the All programs option in the start menu and click on the FLUENT in the ANSYS folder. A FLUENT Launcher window will appear as shown in Figure C.21.

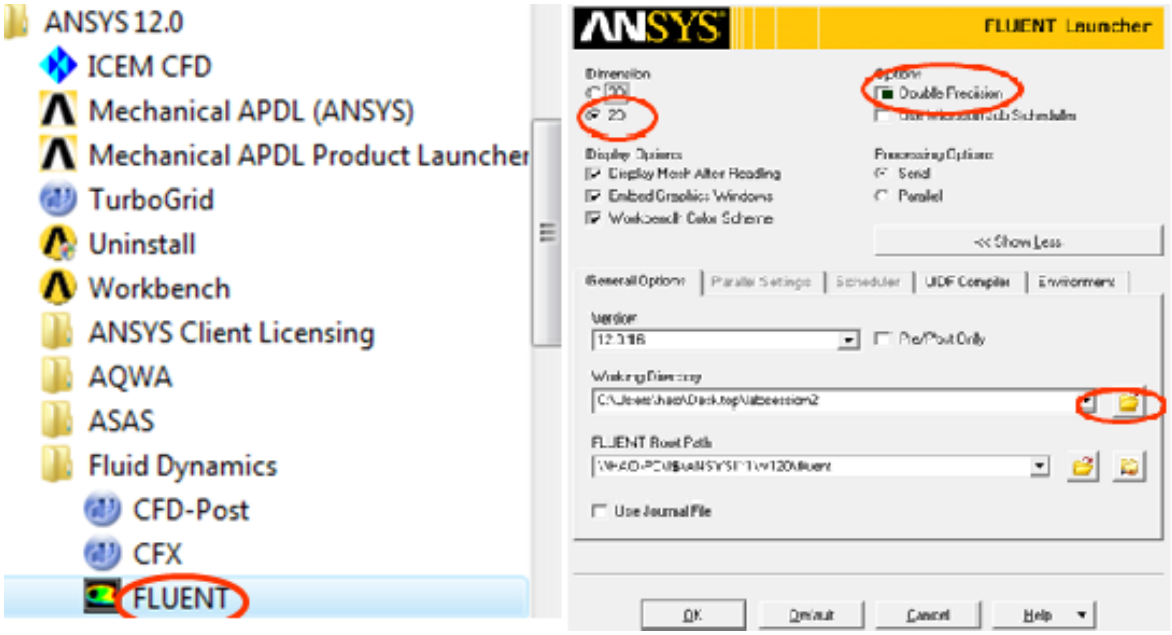

Figure C.21

12. Click on 2D and Double Percesion for more accurate results. Select the working directory to save the data at the specific location.

13. Figure C.22 will appear when we click ok

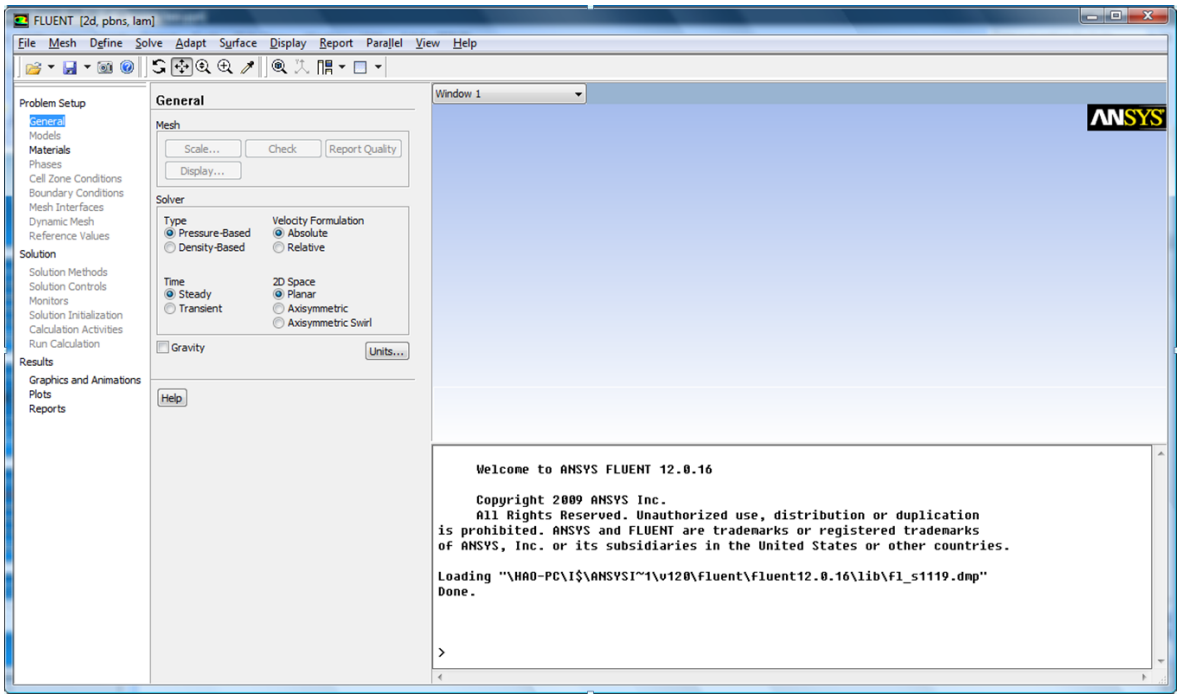

Figure C.22

14. Go to the file menu and click read the mesh as shown in Figures B.29 and B.30.

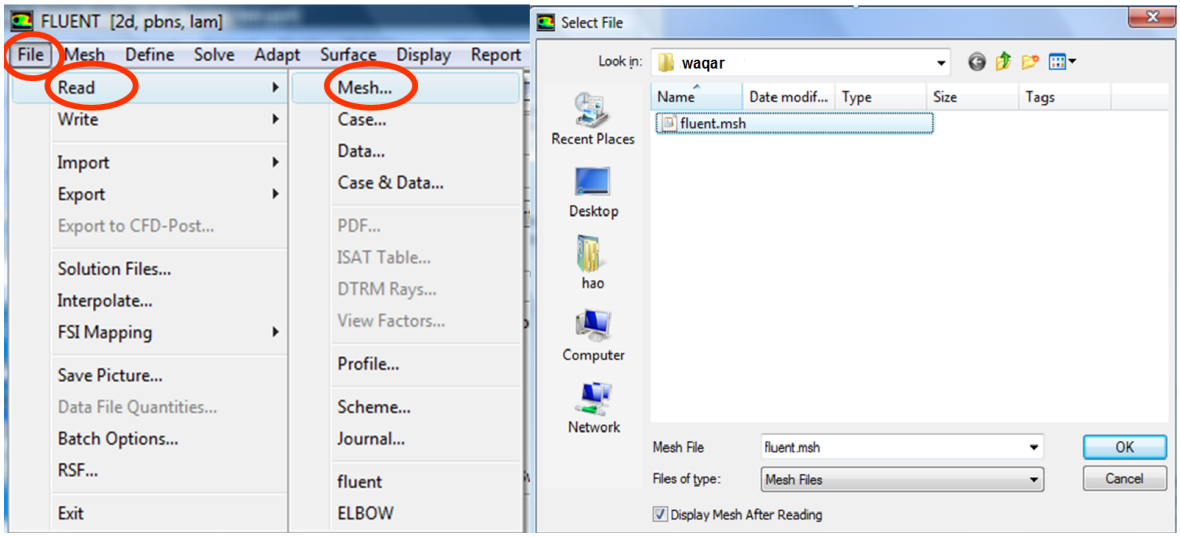

Figure C.23

15. Go to the display menu and click on mesh and select all surfaces, the mesh will be displayed on the main screen as shown in Figure C.25

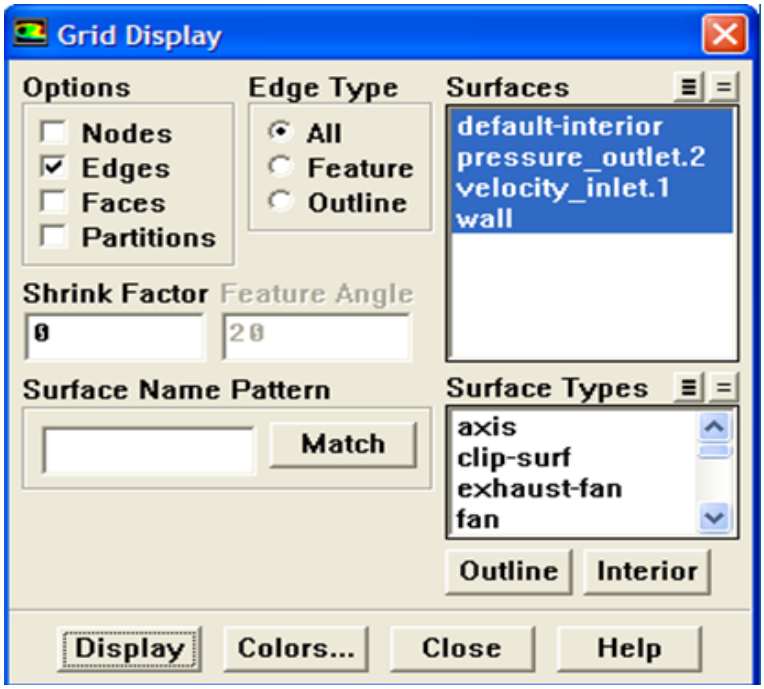

Figure C.24

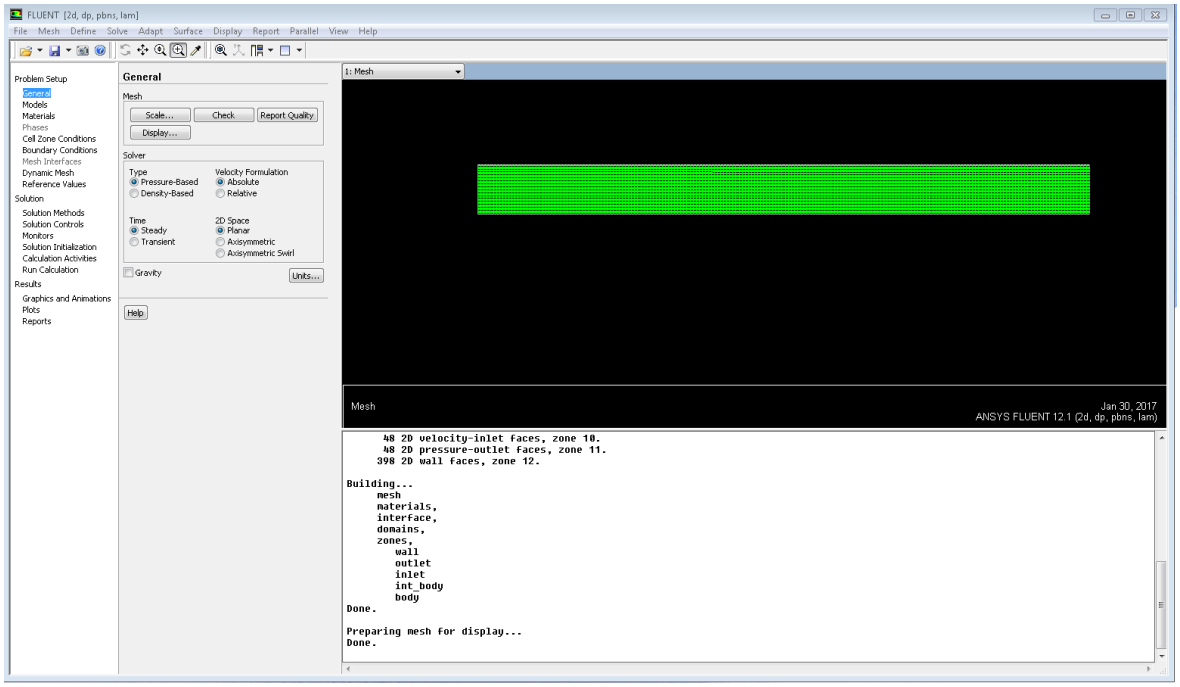

Figure C.25

16. Click on General and change the steady flow to transient flow as shown in Figure C.26

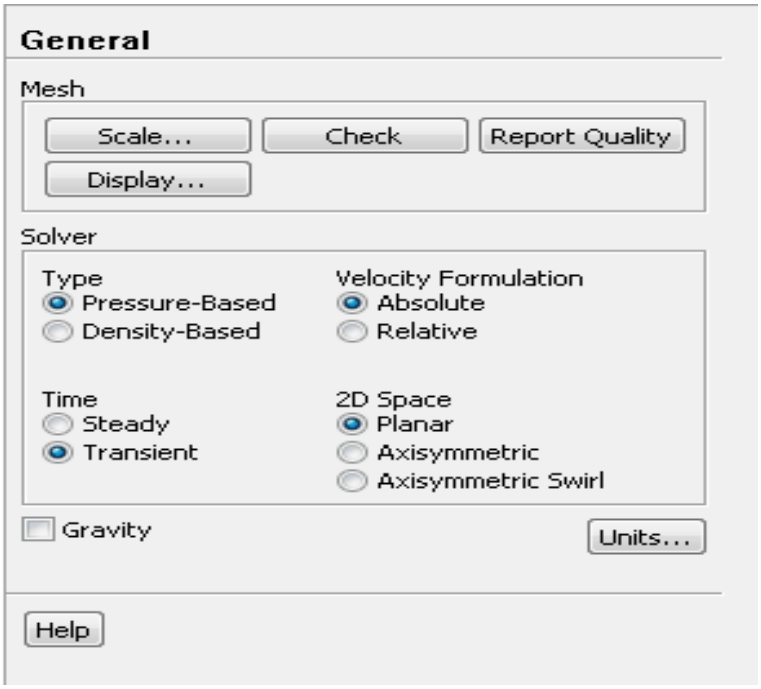

Figure C.26

17. Go to Viscous-Laminar model and then click on edit and select the Laminar as shown in Figure C.27

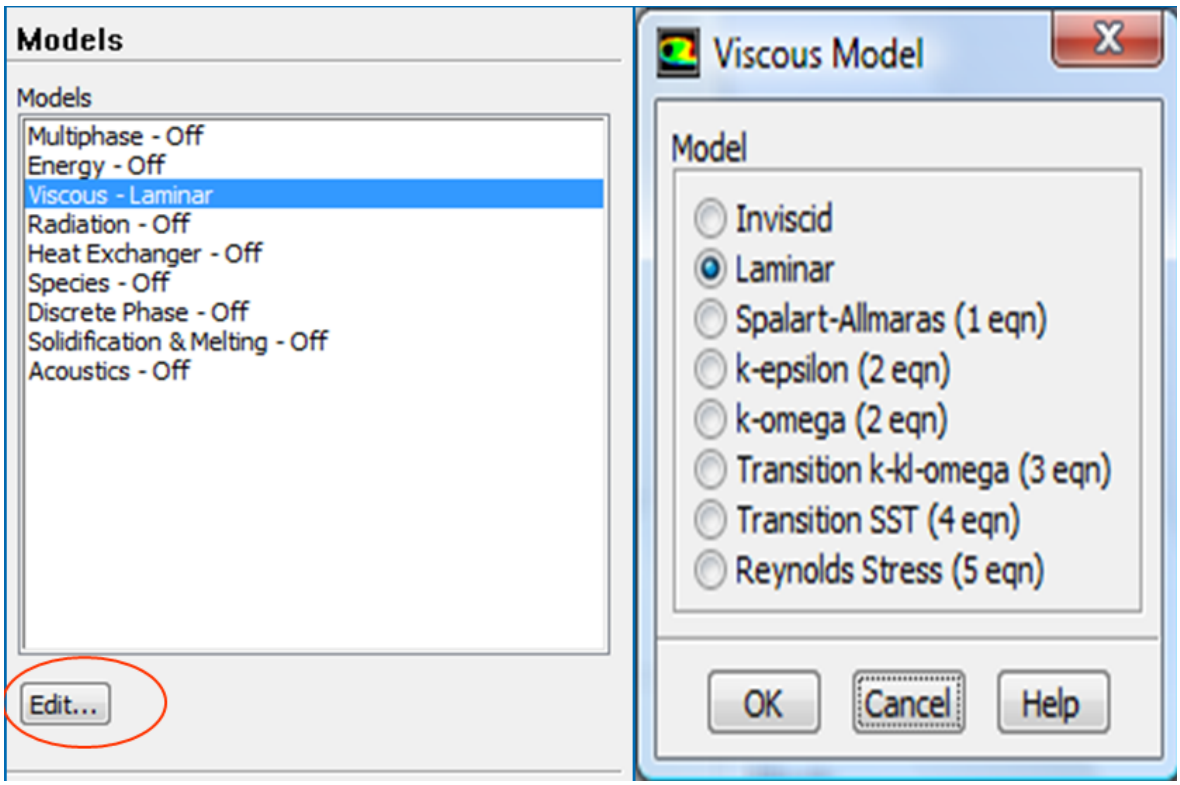

Figure C.27

18. Define material as blood using the procedure shown in Figure C.28. When we click on change, a new window will appear. Click no to save both the settings.

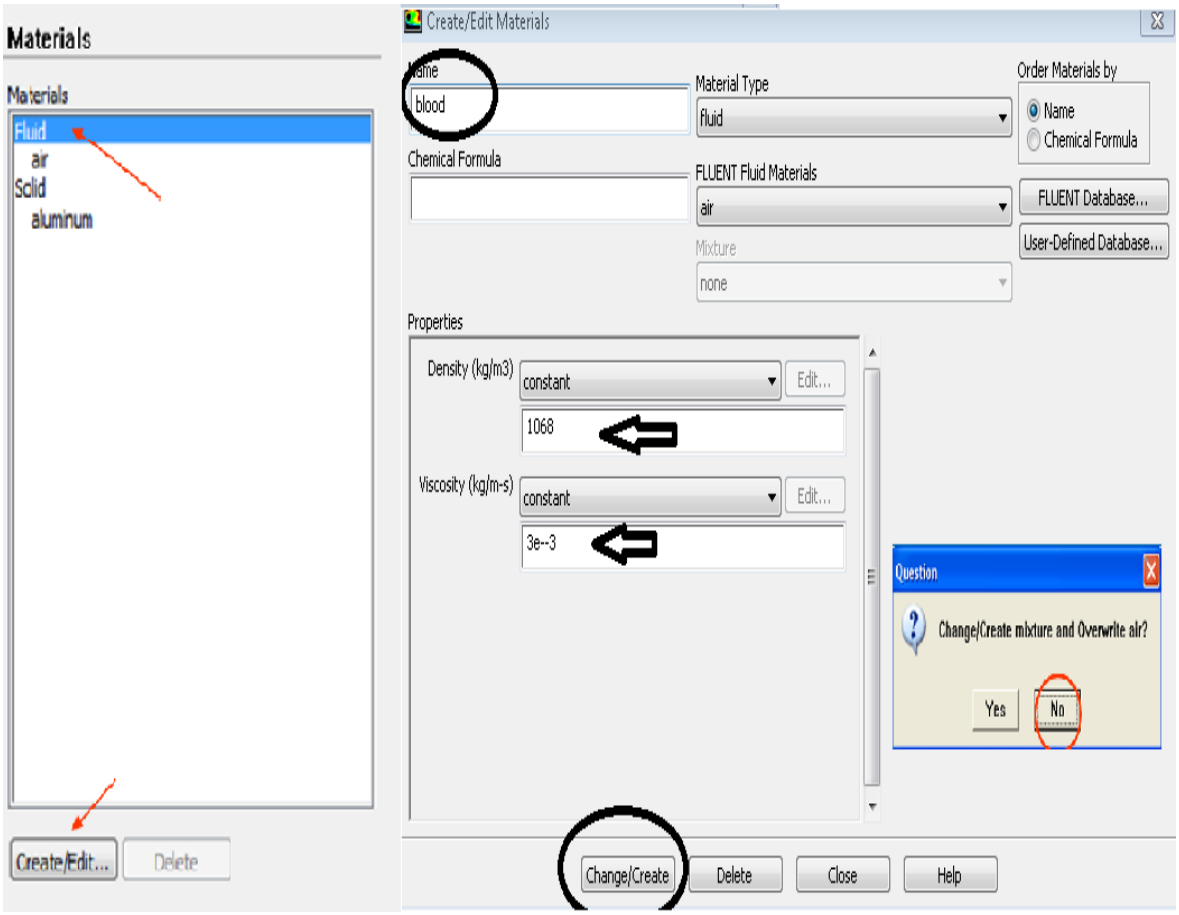

Figure C.28

19. Define the cell zone conditions as shown in Figure C.29

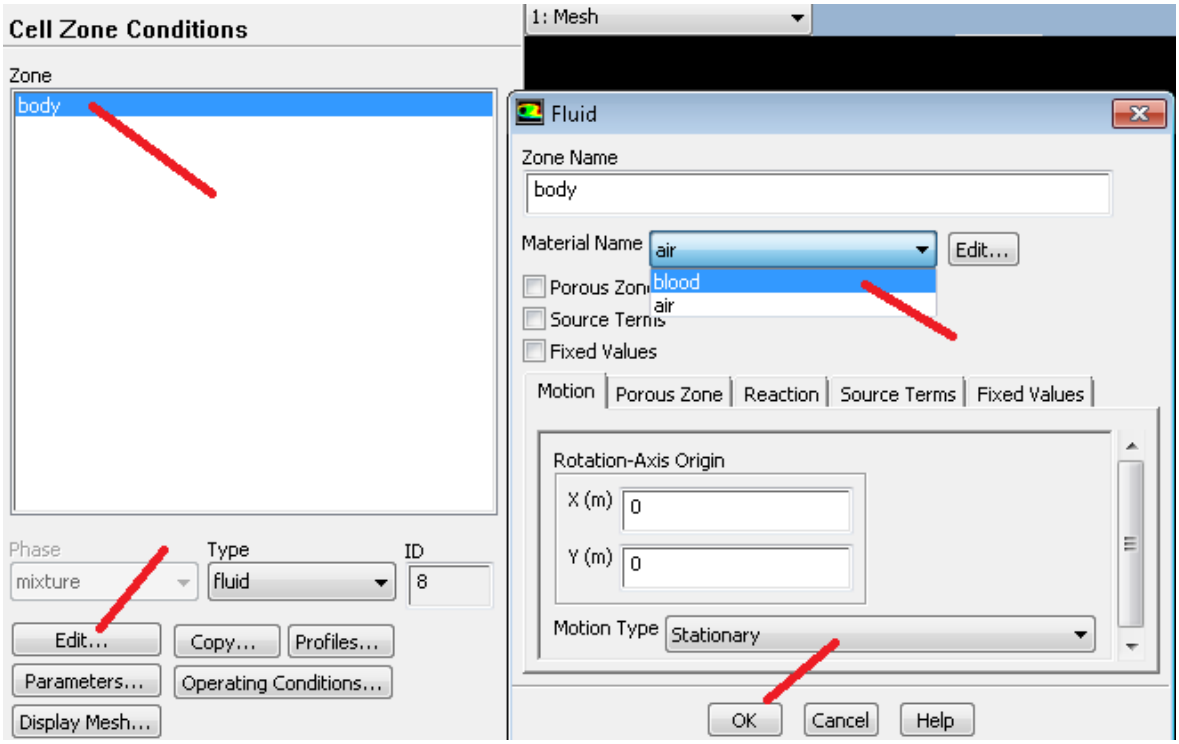

Figure C.29

20. Define the boundary conditions. First of all upload the user defined function which we have made for the unsteady flow in the main artery as shown in Figure C.30.

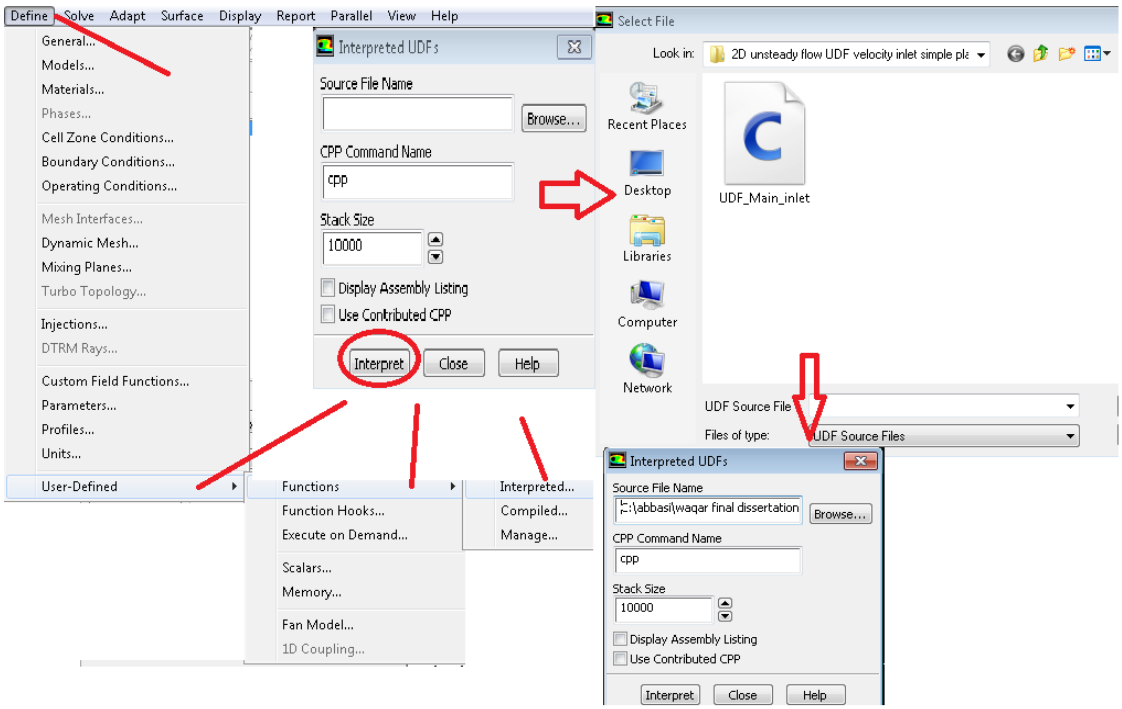


```
Building...
     mesh
     materials,
     interface,
     domains,
     zones,
        wall
        outlet
        inlet
        int_body
        body
Done.

Preparing mesh for display...
Done.

cpp -I"C:\Users\heartvalve\Workspace\CFDandFEM\fluent\fluent12.1.4/src" -I"C:\Users\heartvalve\Workspace\CFDandFEM\fluent\fluent12.
\CFDandFEM\fluent\fluent12.1.4/multiport/src" -I. -DUDFCONFIG_H="<udfconfig.h>" "C:\abbasi\waqar final dissertation\2D unsteady flo
```

Figure C.30

21. Set the boundary conditions for the fluid flow as shown in Figure C.31. The inlet velocity is defined by UDF and shown in Figure C.32.

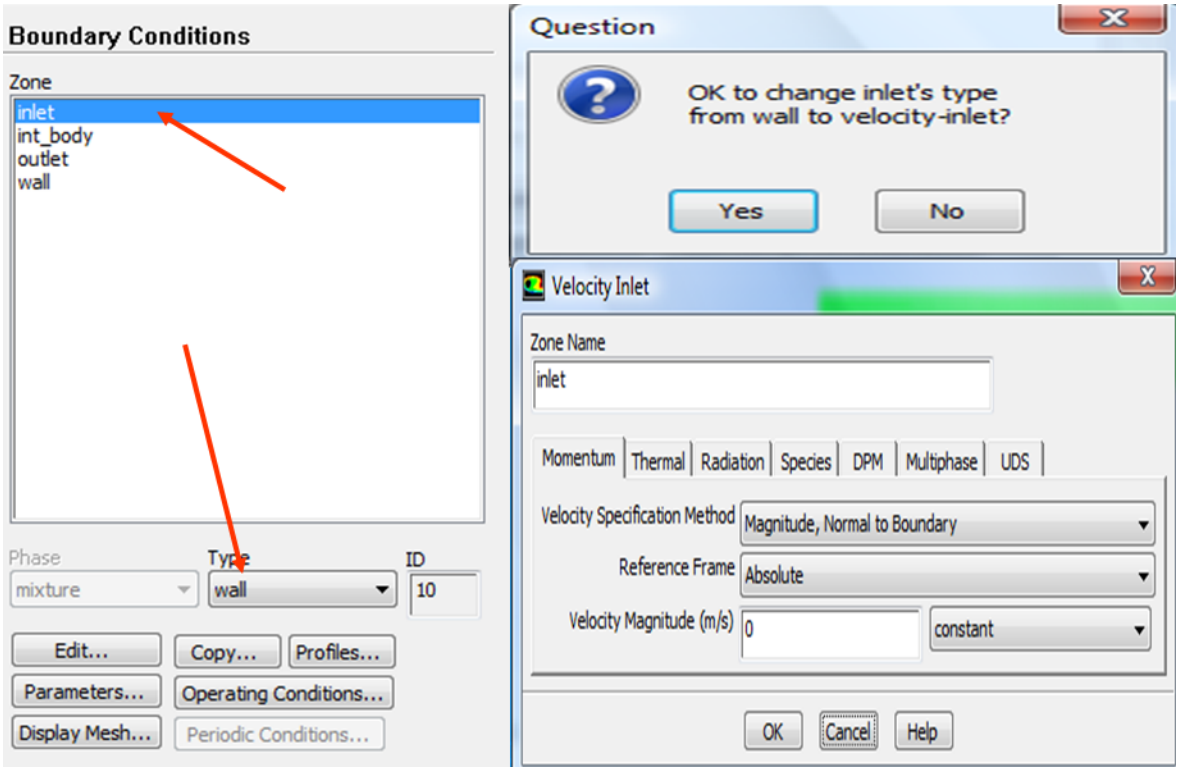

Figure C.31

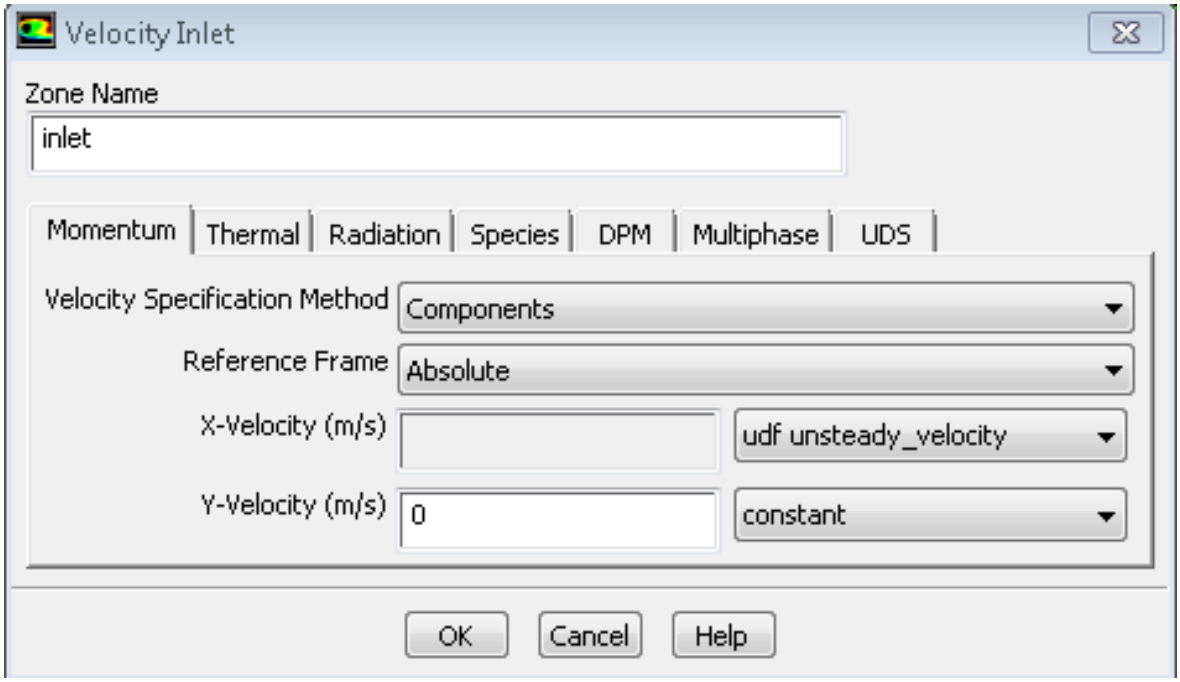

Figure C.32

22. The boundary conditions at outlet are shown in Figure C.33.

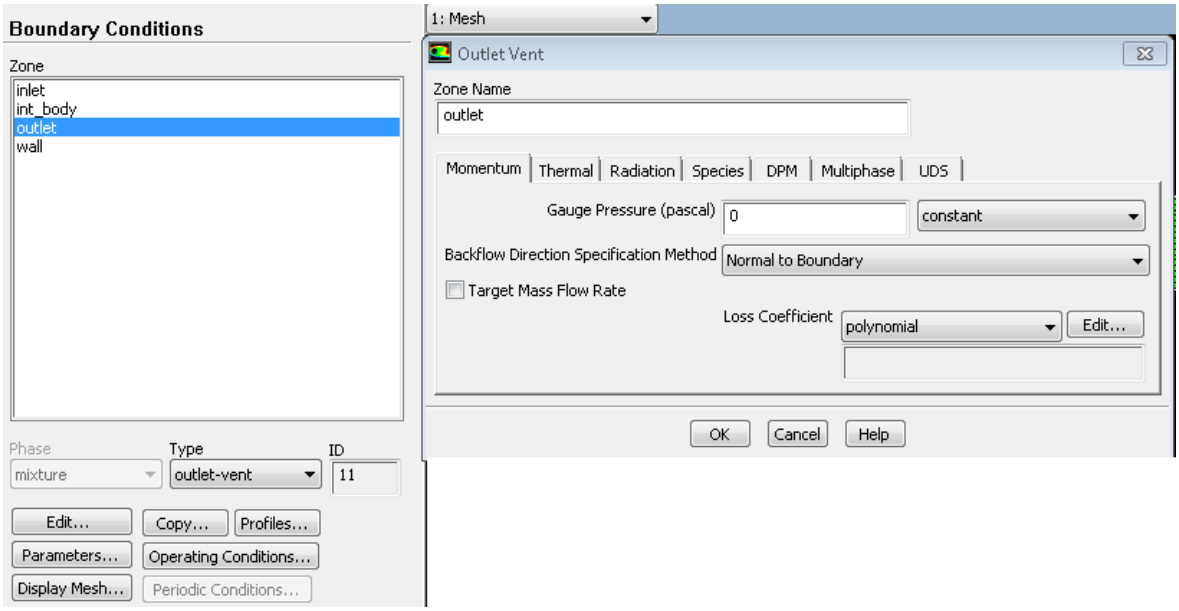

Figure C.33

23. No slip and stationary boundary conditions are applied at the wall (C.34).

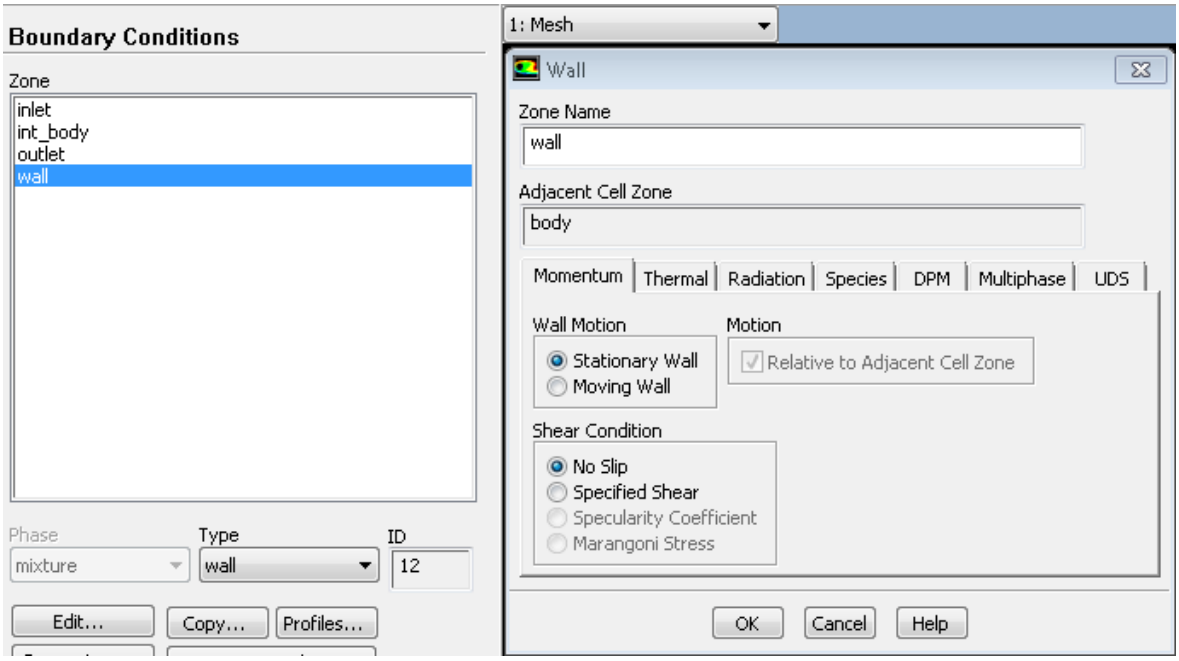

Figure C.34

24. We used the simple solver method, one can change the method to get high resolution results.

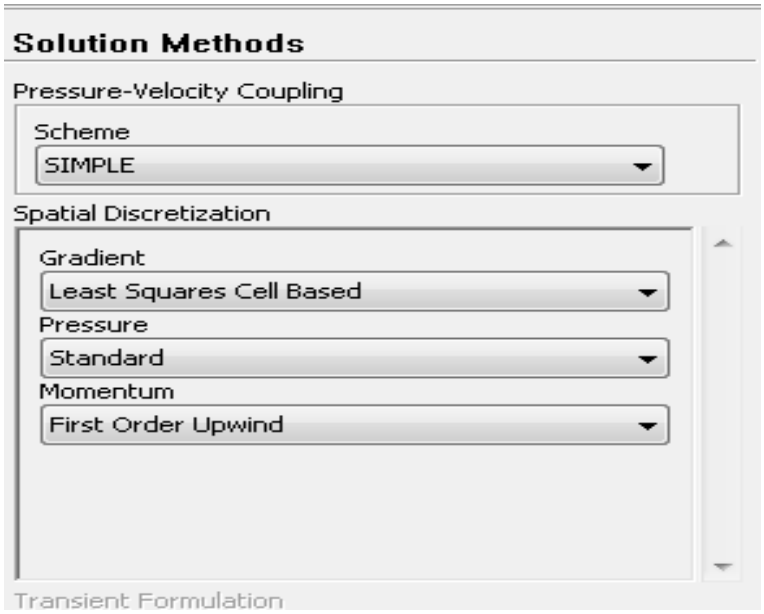

Figure C.35

25. Set up the solver control and use the default setting.

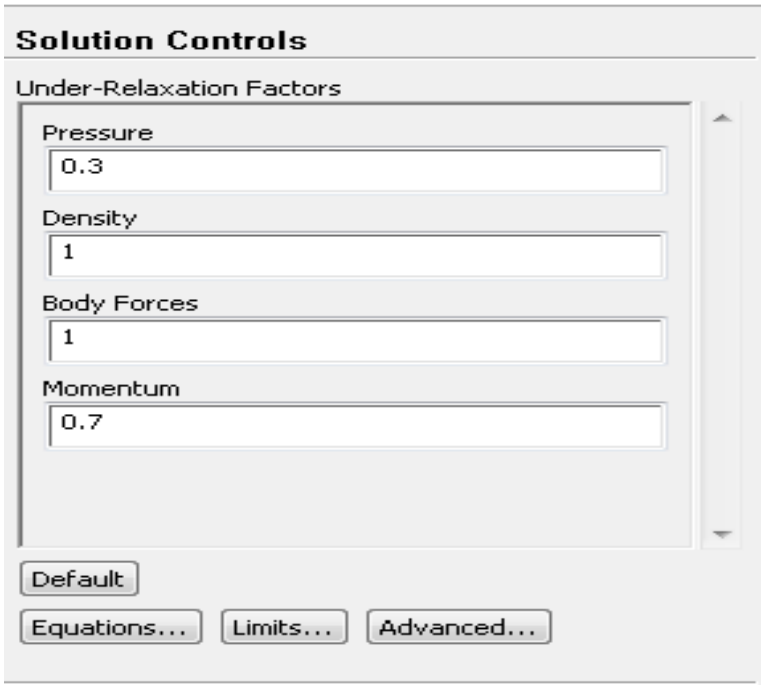

Figure C.36

26. Set the solver monitors and keep the default settings.

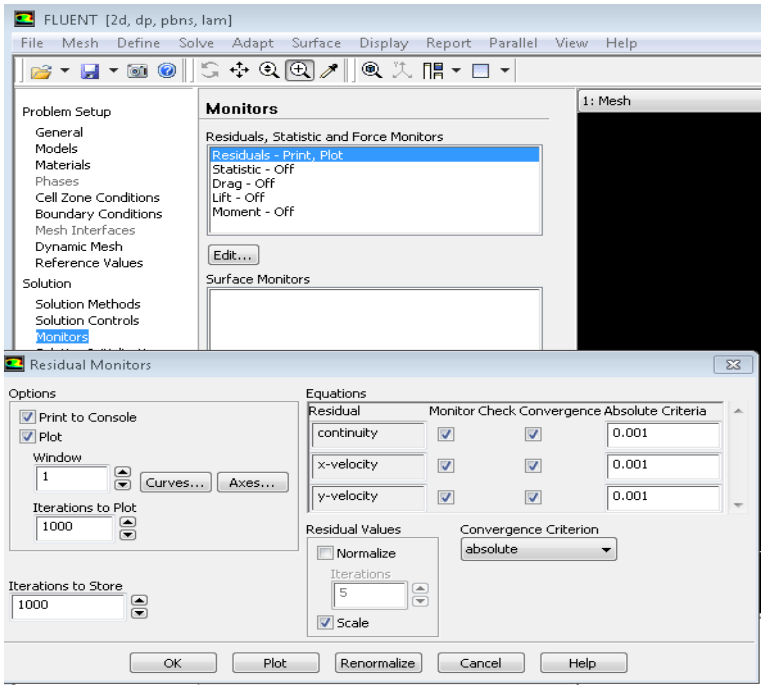

Figure C.37

27. Initialise the flow field by using the boundary conditions at the inlet which is the starting point.

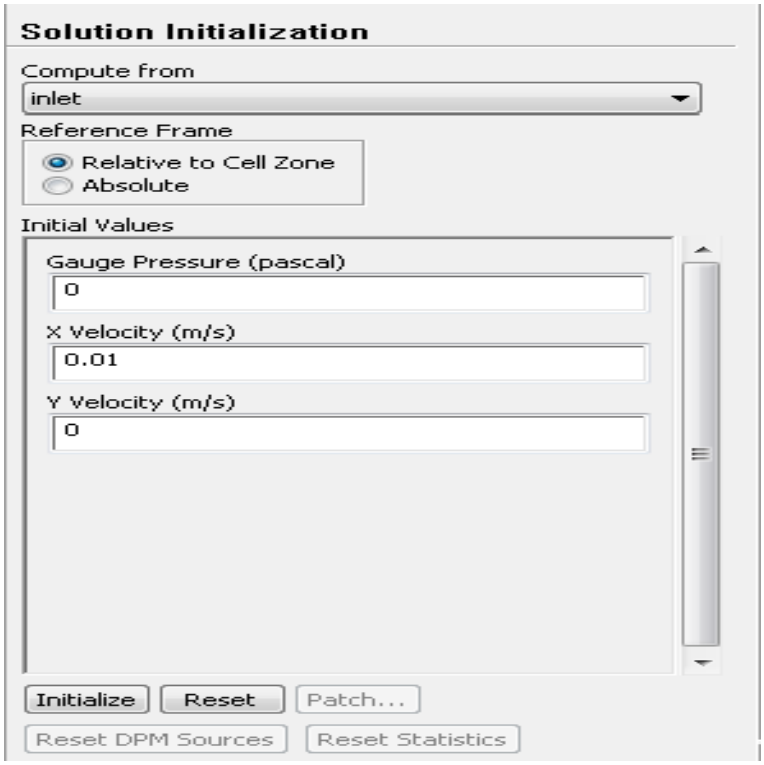

Figure C.38

28. Data is auto saved for every three iterations as shown in C.39.

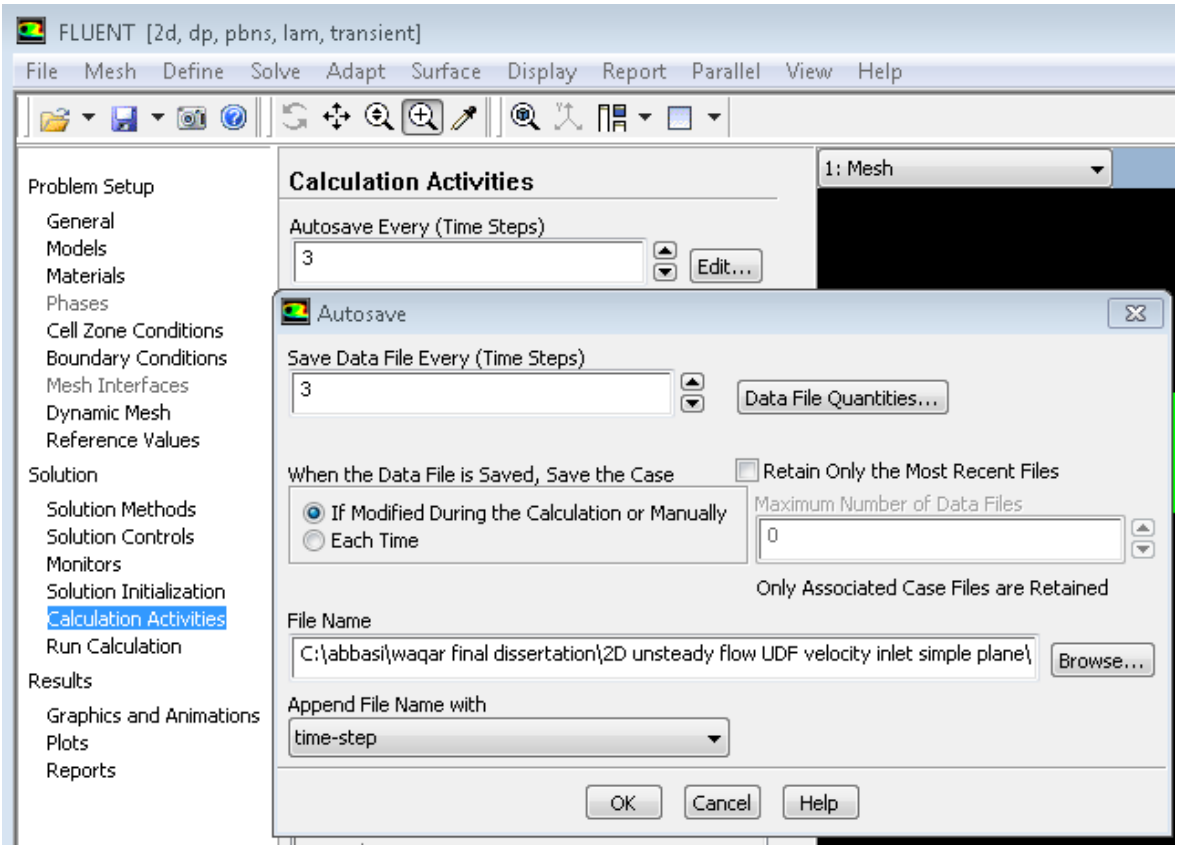

Figure C.39

29. We run the calculation for six cycles as shown in C.40.

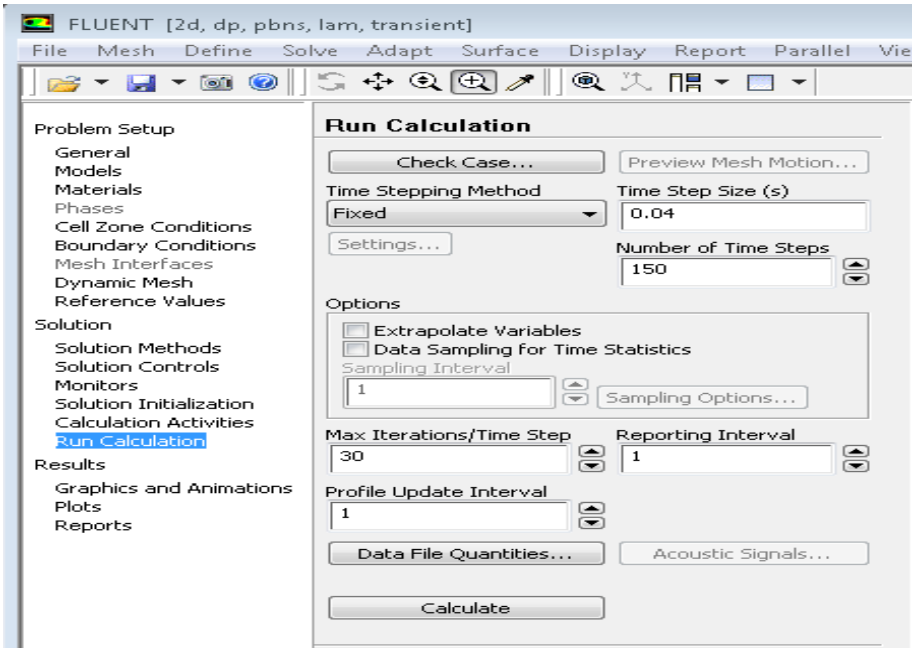

Figure C.40

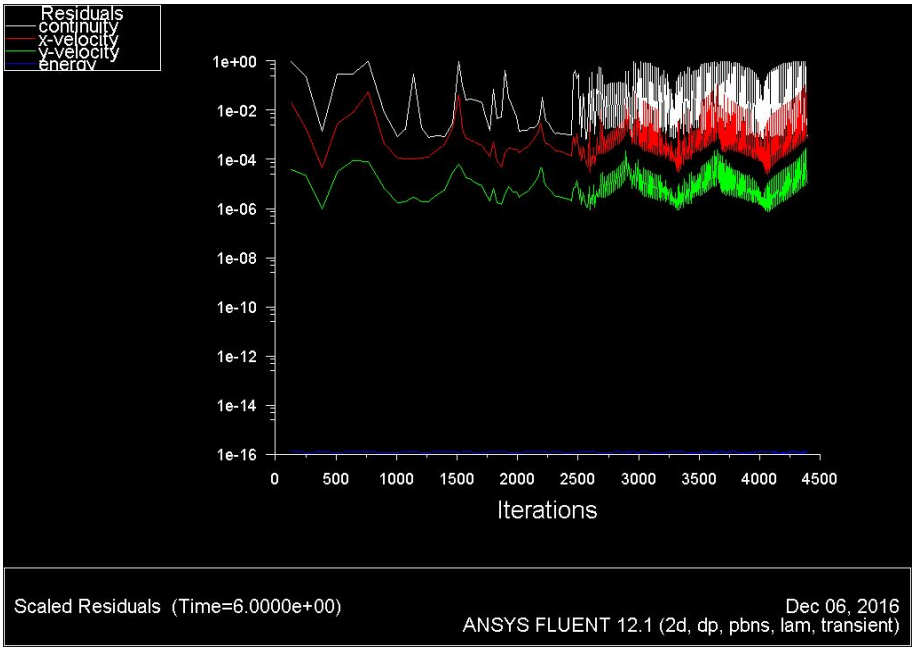

Figure C.41

30. We saved the case and data files and the results were plotted in Tecplot 360 Software for better visualisation [243].

C.2 2-Dimensional Geometry with Catheter

C.2.1 Fluid Domain (Geometry)

Following procedure was adopted to make 2D model geometry with catheter at the central axis for blood flow in the arteries in addition to 2D geometry.

The points will appear on screen as shown in C.43 (Note: Click on fit window if points are not visible. Following are the points P1: 0, -1 P2: 0, 1 P3: 2, -1 P4: 2, 1 P5: 2, -2 P6: 2, 2 P7: 12, -1 P8: 12, 1 P9: 52, 2 P10: 52, -2

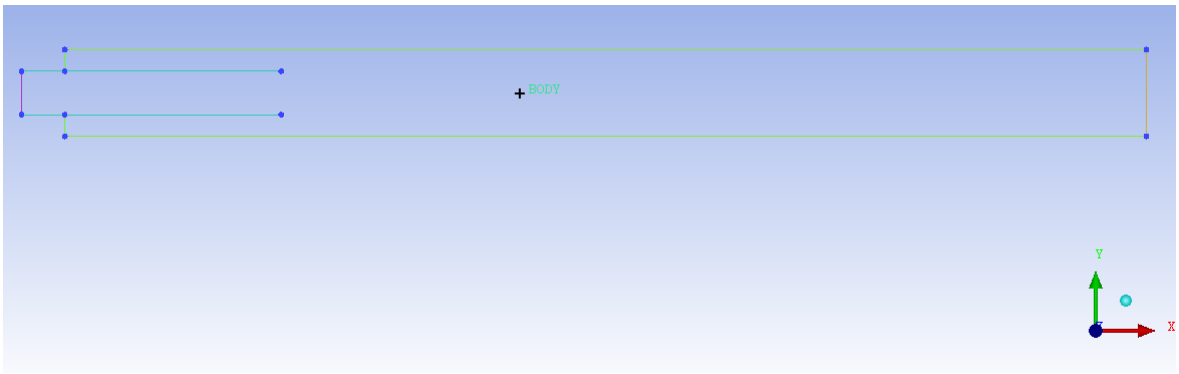

Figure C.42

C.2.2 Meshing Procedure

(a) In order to delete these extra block, we used the following procedure.

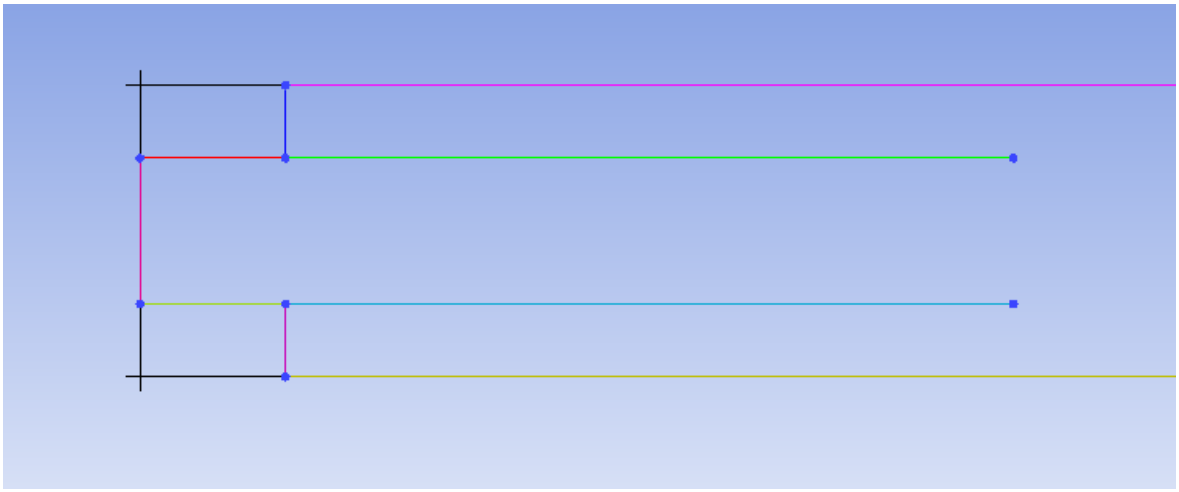

Figure C.43

- Select the split block from the Blocking tab.
- Choose the split block icon
- Click to All visible option
- Click on the edge option and then click on the upper line on the main window and drag it until it comes equal to the block where you want to split and then click on the middle button of mouse to accept the creation. Same procedure is done on the left line as well.

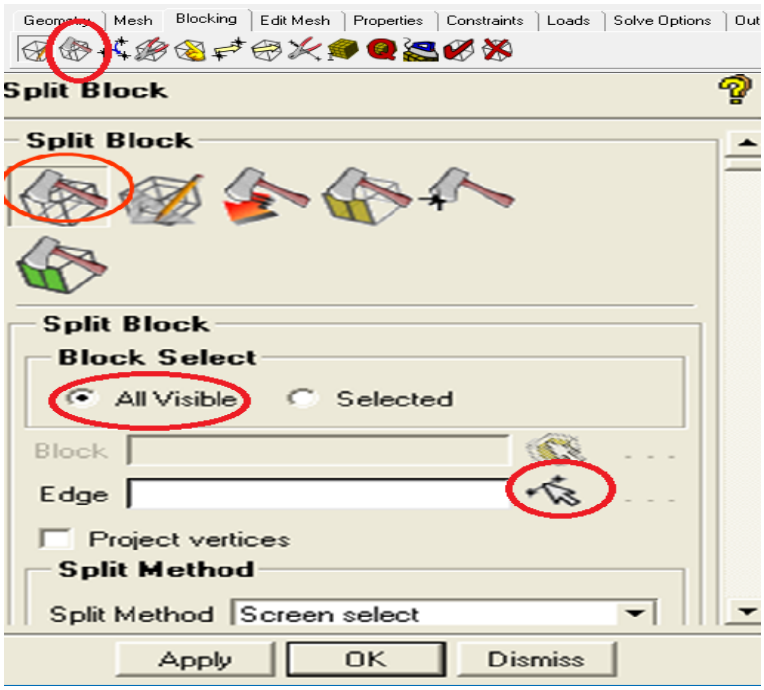

Figure C.44

(b) Go to the delete block option of Blocking tab and select the icon. After selecting click on the block which you want to delete. When you will click the block, it will be highlighted then press the middle button of mouse to delete the blocks.

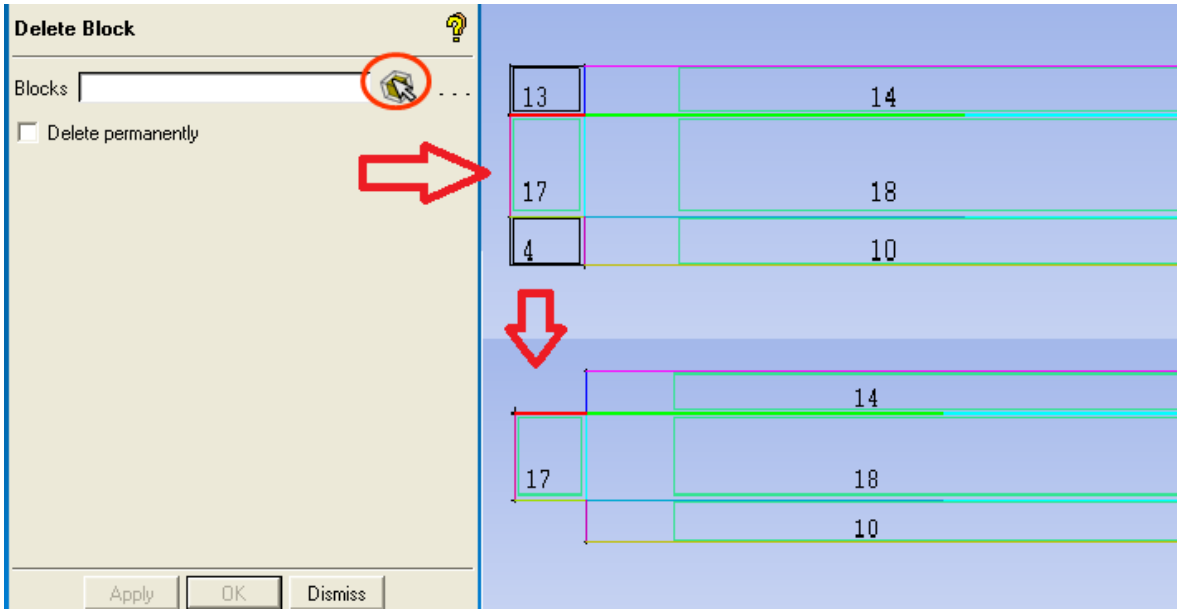

Figure C.45

(c) The remaining procedure of meshing is same as described in 2D Geometry.

C.2.3 Simulation in Fluent Software

Following changes will be adopted along with the 2D Catheter geometry procedure.

(a) 1. The energy equation is turned on.

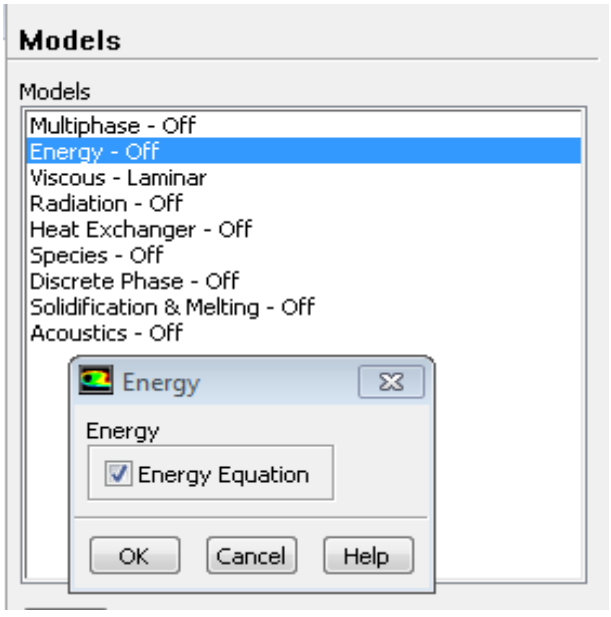

Figure C.46

(b) Because of the energy equation, specific heat and thermal conductivity values have been added.

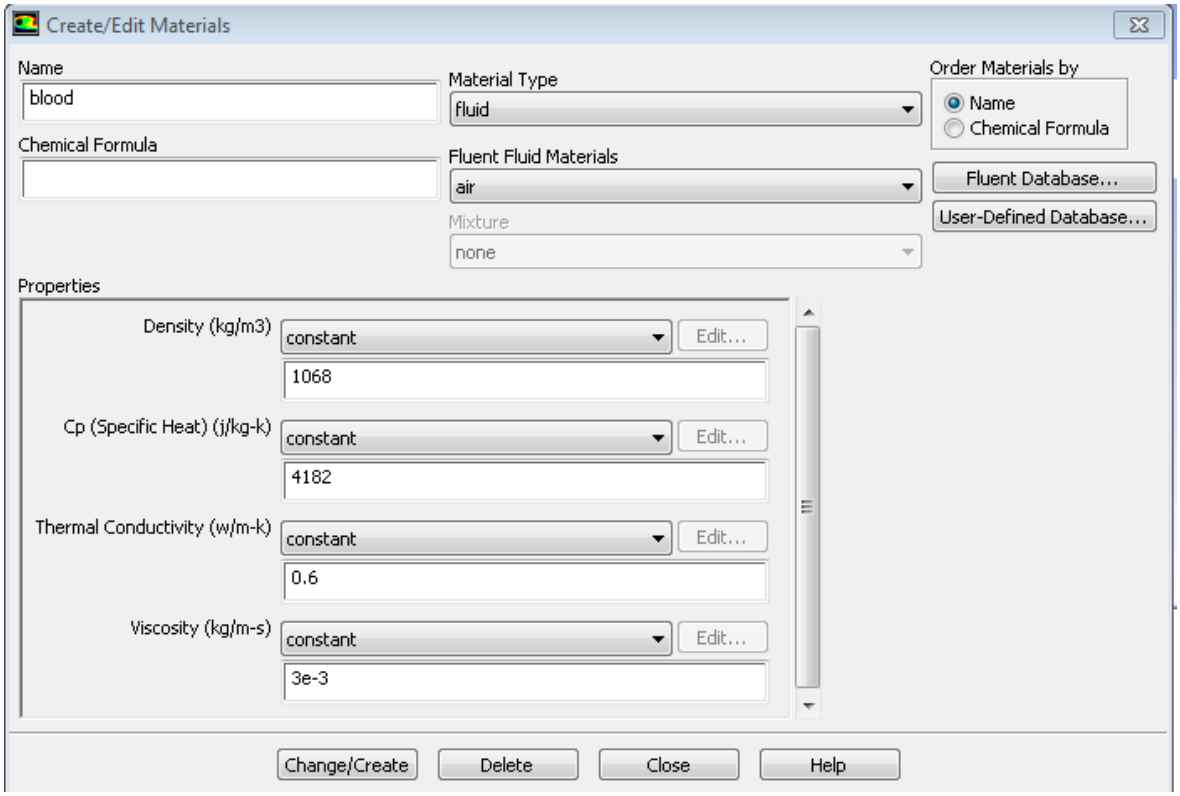

Figure C.47

(c) UDF have been modified for the catheter inlet whereas the UDF for main inlet is same as we used previously. Further, the values of temperature have been included.

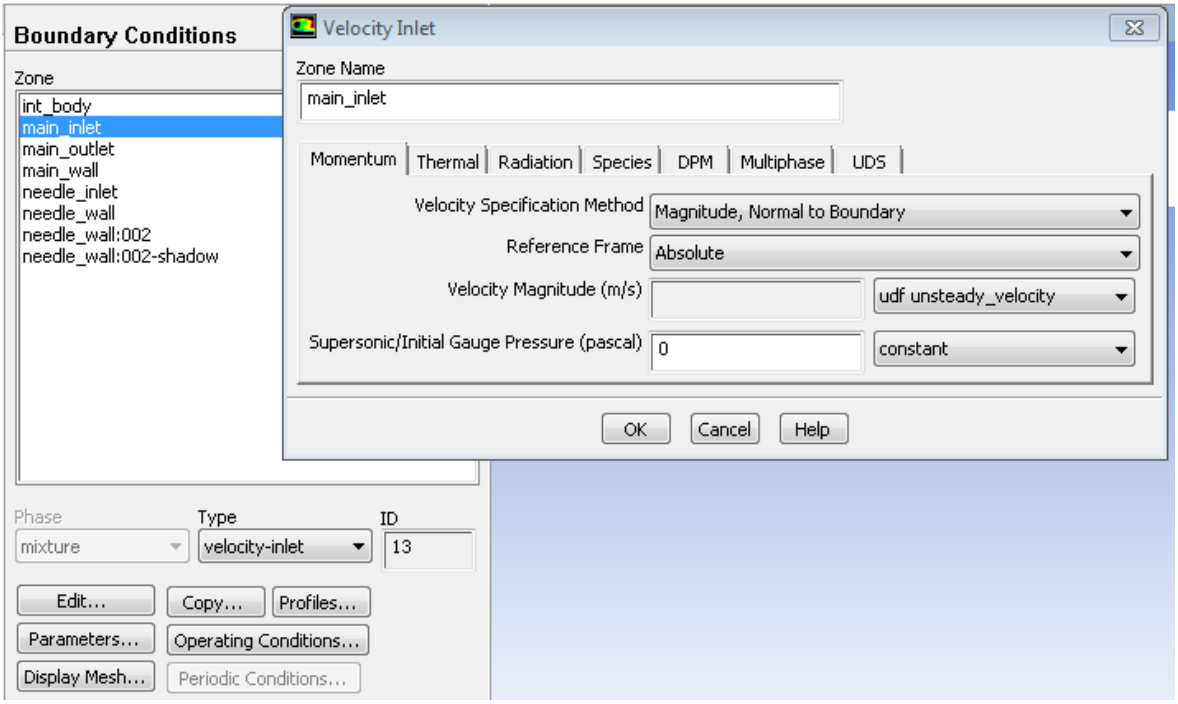

Figure C.48

(d) The velocity and temperature at the catheter is also included.

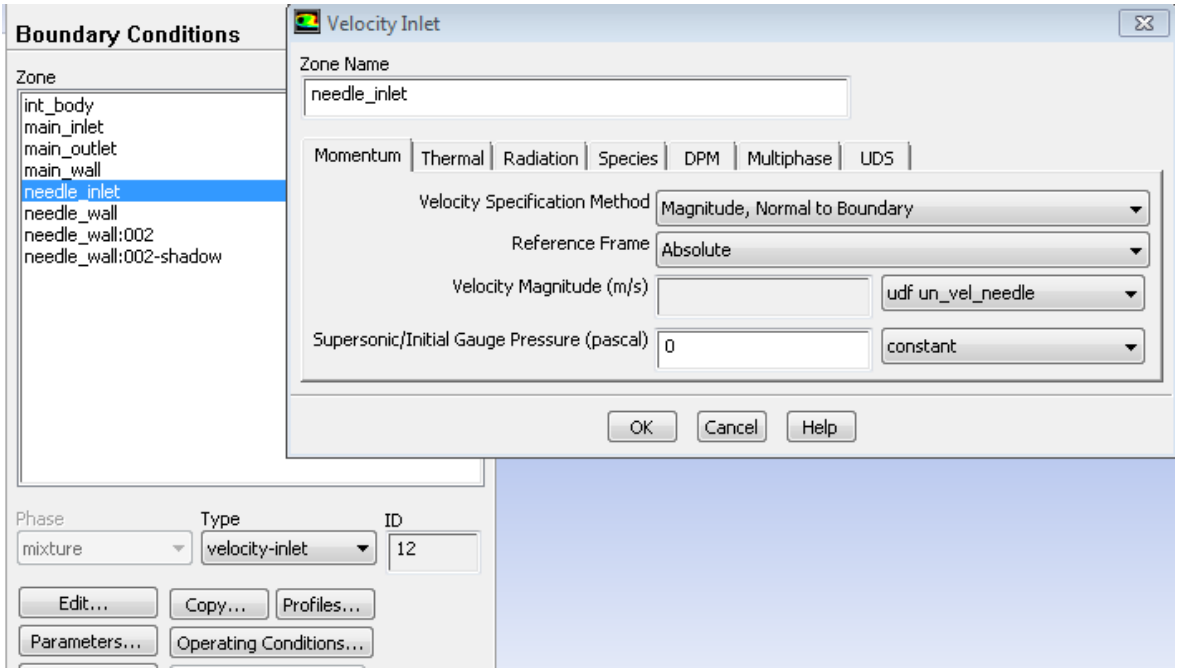

Figure C.49

(e) The remaining procedure remains the same as 2D Geometry.

C.3 Flow In Stenosed Channel

C.3.1 Fluid Domain (Geometry)

Following procedure was adopted to include 45% stenosis to 2D geometry with catheter in addition to the previously done.

(a) The points will appear on screen as shown in Figure B.1 (Note: Click on fit window if points are not visible. Following are the points P1: 0, -1 P2: 0, 1 P3: 2, -1 P4: 2, 1 P5: 2, -2 P6: 2, 2 P7: 12, -1 P8: 12, 1 P9: 52, 2 P10: 52, -2 P11: 20, 2 P12: 20, -2 P13: 25, -1.1 P14: 25, 1.1 P15: 30, 2 P16: 30, -2

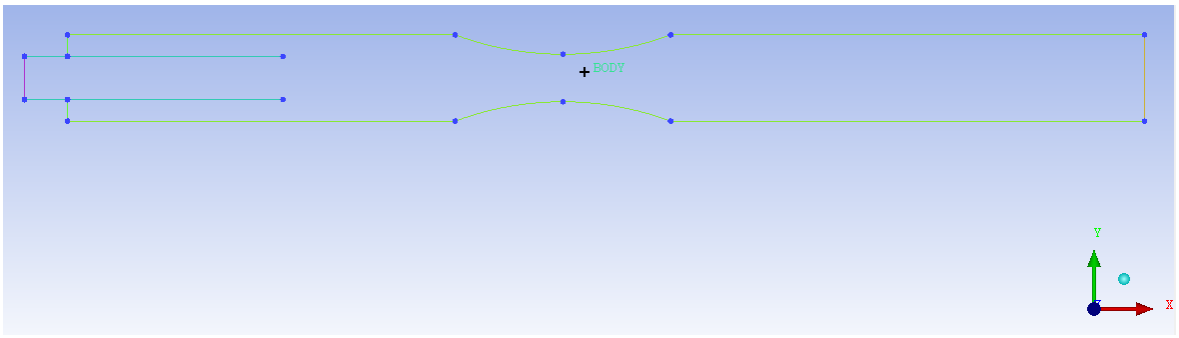

Figure C.50

(b) We used arc to join three points instead of straight line curve to make stenosis.

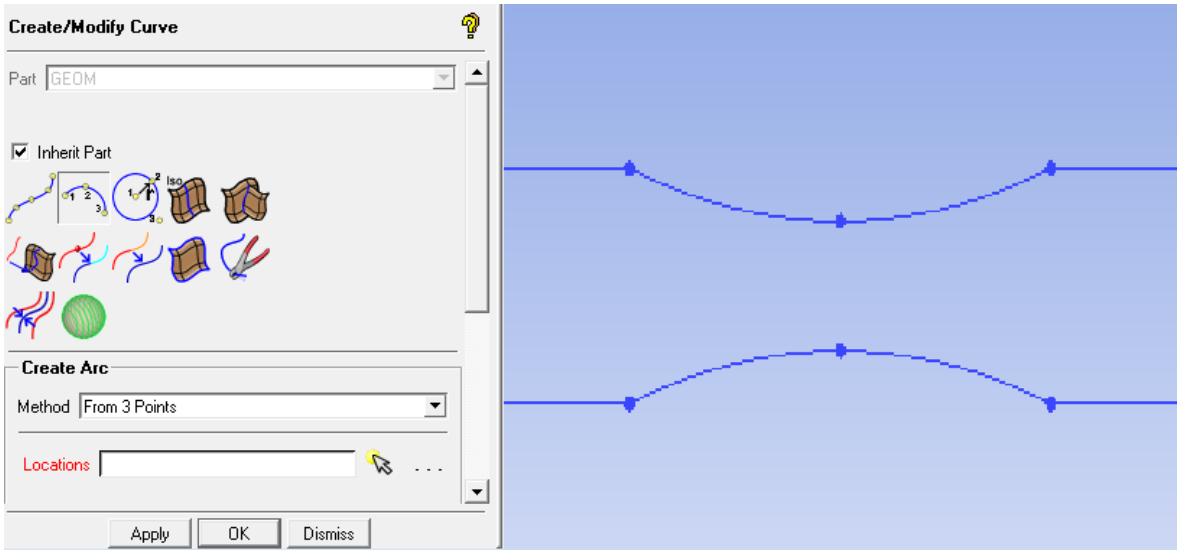

Figure C.51

(c) The remaining procedure is same for meshing and for simulations.

C.4 3-Dimensional Geometry with Catheter

C.4.1 Fluid Domain (Geometry)

Following procedure was adopted to make 3D geometry with catheter at the central axis to measure the blood flow in the arteries.

(a) 3D cylinderically tube was created in SolidWorks software with length of 50 mm and diameter 2 mm.

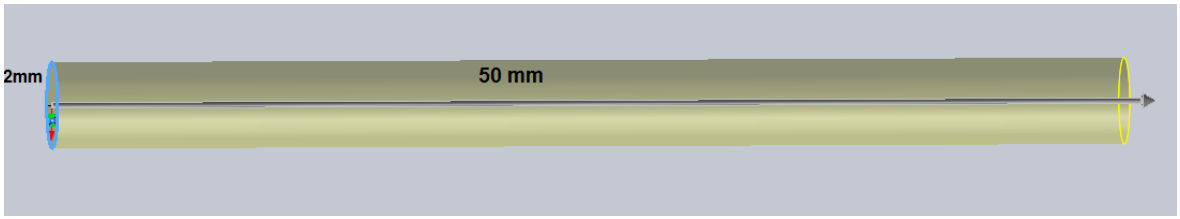

Figure C.52

(b) A small cylinder of length 10 mm with diameter 1 mm is inserted into that cylinderical tube and intersection was created between them.

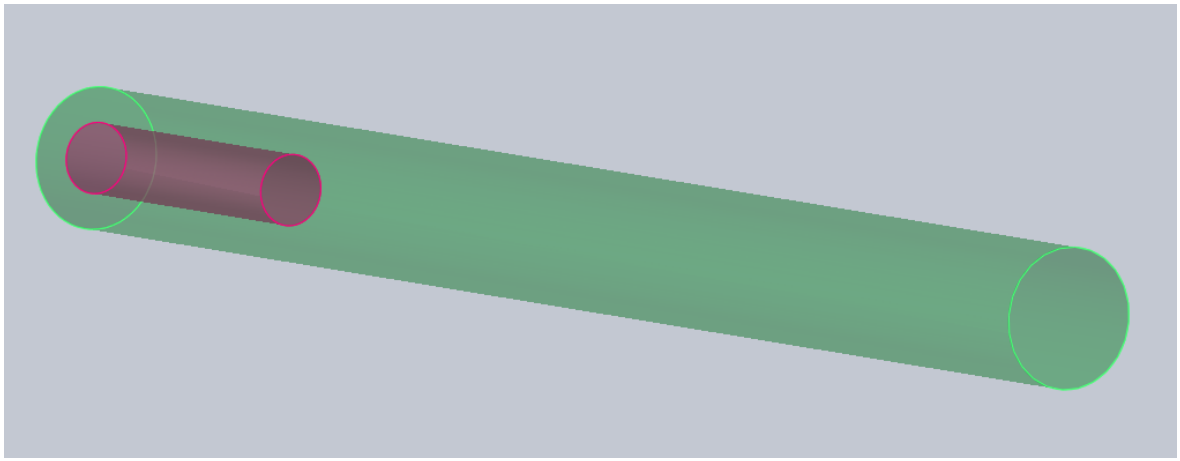

Figure C.53

(c) After making the intersection, a catheter of length 12 mm was also inserted.

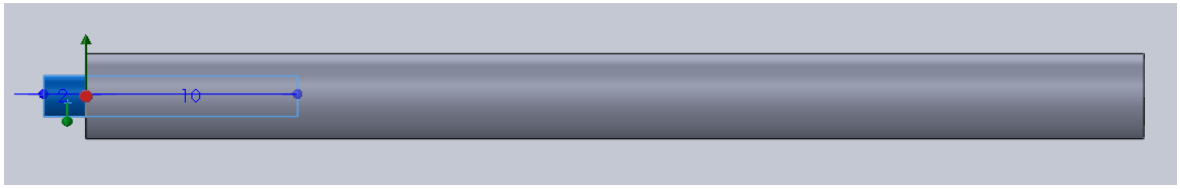

Figure C.54

(d) The geometry was saved and opened in ICEM where we gave the names of different parts of geometry.

C.4.2 Meshing Procedure)

(a) Mesh was created using options shown in C.56.

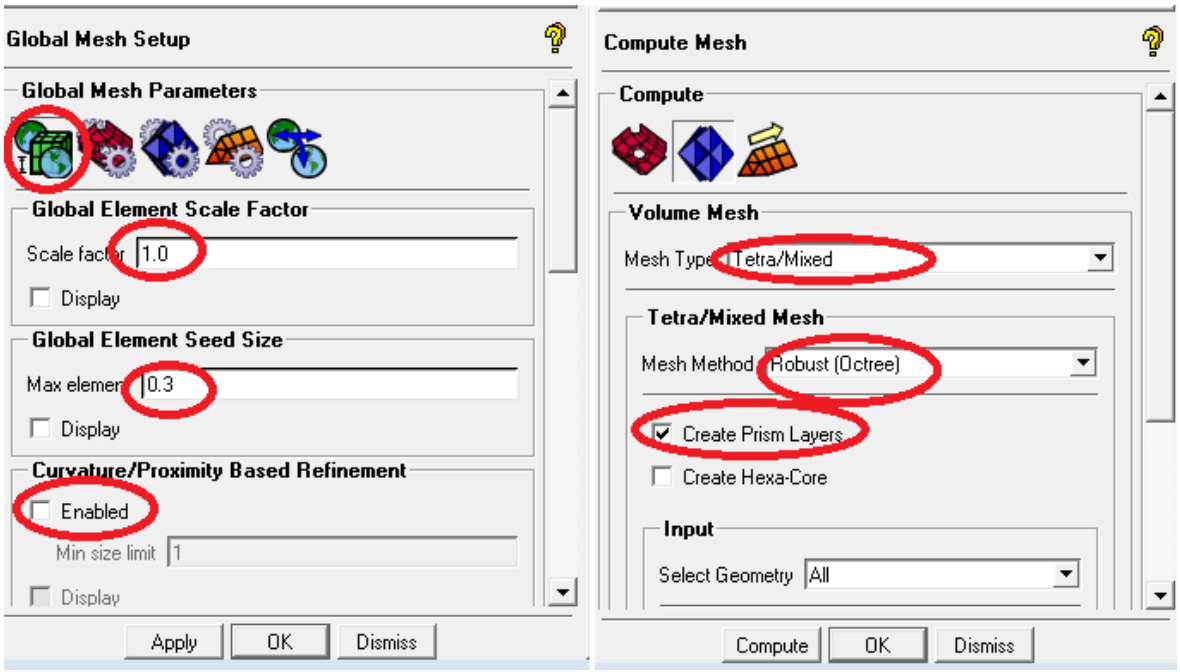

Figure C.55

Figure C.56

(b) There is no change in the procedure of simulations expect the geometry was selected 3D.

Bibliography

[1] Gilles Montalescot, Udo Sechtem, Stephan Achenbach, Felicita Andreotti, Chris Arden, Andrzej Budaj, Raffaele Bugiardini, Filippo Crea, Thomas Cuisset, Carlo Di Mario, et al. 2013 esc guidelines on the management of stable coronary artery disease. *European heart journal*, 34(38):2949–3003, 2013.

[2] Angela Cooper, Adam Timmis, and Jane Skinner. Assessment of recent onset chest pain or discomfort of suspected cardiac origin: summary of nice guidance. *BMJ: British Medical Journal*, 340, 2010.

[3] Stephan D Fihn, James C Blankenship, Karen P Alexander, John A Bittl, John G Byrne, Barbara J Fletcher, Gregg C Fonarow, Richard A Lange, Glenn N Levine, Thomas M Maddox, et al. 201 acc/aha/aats/pcna/scai/sts focused update of the guideline for the diagnosis and management of patients with stable ischemic heart disease. *Circulation*, 2014.

[4] Angina nhs choices. `http://www.nhs.uk/conditions/Angina/Pages/Introduction.aspx`. [Online; accessed 04 January, 2017].

[5] Ana Ruigómez, Luis Alberto García Rodríguez, Mari-Ann Wallander, Saga Johansson, and Roger Jones. Chest pain in general practice: incidence, comorbidity and mortality. *Family practice*, 23(2):167–174, 2006.

[6] Staffan Nilsson, Morten Scheike, David Engblom, Lars-Göran Karlsson, Sigvard Mölstad, I Akerlind, K Ortoft, and Eva Nylander. Chest pain and ischaemic heart disease in primary care. *Br J Gen Pract*, 53(490):378–382, 2003.

[7] NF Murphy, K MacIntyre, S Capewell, S Stewart, J Pell, J Chalmers, A Redpath, S Frame, J Boyd, and JJV McMurray. Hospital discharge rates for suspected acute coronary syndromes between 1990 and 2000: population based analysis. *Bmj*, 328(7453):1413–1414, 2004.

[8] Mario Marzilli, C Noel Bairey Merz, William E Boden, Robert O Bonow, Paola G Capozza, William M Chilian, Anthony N DeMaria, Giacinta Guarini, Alda Huqi, Doralisa Morrone, et al. Obstructive coronary atherosclerosis and ischemic heart disease: an elusive link! *Journal of the American College of Cardiology*, 60(11):951–956, 2012.

[9] Sanjiv Kaul and Ananda R Jayaweera. Myocardial capillaries and coronary flow reserve. pages 1399–1401, 2008.

[10] Paolo G Camici and Filippo Crea. Coronary microvascular dysfunction. *New England Journal of Medicine*, 356(8):830–840, 2007.

[11] Joerg Herrmann, Juan Carlos Kaski, and Amir Lerman. Coronary microvascular dysfunction in the clinical setting: from mystery to reality. *European heart journal*, page ehs246, 2012.

[12] Ali Yilmaz and Udo Sechtem. Angina pectoris in patients with normal coronary angiograms: current pathophysiological concepts and therapeutic options. *Heart*, 98(13):1020–1029, 2012.

[13] Barry L Sharaf, Carl J Pepine, Richard A Kerensky, Steven E Reis, Nathaniel Reichek, William J Rogers, George Sopko, Sheryl F Kelsey, Richard Holubkov, Marian Olson, et al. Detailed angiographic analysis of women with suspected ischemic chest pain (pilot phase data from the nhlbi-sponsored womens ischemia syndrome evaluation [wise] study angiographic core laboratory). *The American journal of cardiology*, 87(8):937–941, 2001.

[14] William Wijns, Philippe Kolh, Nicolas Danchin, Carlo Di Mario, Volkmar Falk, Thierry Folliguet, Scot Garg, Kurt Huber, Stefan James, Juhani Knuuti, et al. Guidelines on myocardial revascularization. *European heart journal*, 31(20):2501–2555, 2010.

[15] Joe V Selby, Bruce H Fireman, Robert J Lundstrom, Bix E Swain, Alison F Truman, Candice C Wong, Erika S Froelicher, Hal V Barron, and Mark A Hlatky. Variation among hospitals in coronary-angiography practices and outcomes after myocardial infarction in a large health maintenance organization. *New England Journal of Medicine*, 335(25):1888–1896, 1996.

[16] Carl W White, Creighton B Wright, Donald B Doty, Loren F Hiratza, Charles L Eastham, David G Harrison, and Melvin L Marcus. Does visual interpretation of the coronary arteriogram predict the physiologic importance of a coronary stenosis? *New England Journal of Medicine*, 310(13):819–824, 1984.

[17] David Carrick, Miles Behan, Fiona Foo, Jim Christie, William S Hillis, John Norrie, Keith G Oldroyd, and Colin Berry. Usefulness of fractional flow reserve to improve diagnostic efficiency in patients with non-st elevation myocardial infarction. *The American journal of cardiology*, 111(1):45–50, 2013.

[18] K Lance Gould, Kirk Lipscomb, and Glen W Hamilton. Physiologic basis for assessing critical coronary stenosis: instantaneous flow response and regional distribution during coronary hyperemia as measures of coronary flow reserve. *The American journal of cardiology*, 33(1):87–94, 1974.

[19] K Lance Gould and Kirk Lipscomb. Effects of coronary stenoses on coronary flow reserve and resistance. *The American journal of cardiology*, 34(1):48–55, 1974.

[20] K Lance Gould. Pressure-flow characteristics of coronary stenoses in unsedated dogs at rest and during coronary vasodilation. *Circulation research*, 43(2):242–253, 1978.

[21] Nico HJ Pijls, Bernard de Bruyne, Kathinka Peels, Pepijn H van der Voort, Hans JRM Bonnier, Jozef Bartunek, and Jacques J Koolen. Measurement of fractional flow reserve to assess the functional severity of coronary-artery stenoses. *New England Journal of Medicine*, 334(26):1703–1708, 1996.

[22] K Lance Gould. Does coronary flow trump coronary anatomy? *JACC: Cardiovascular Imaging*, 2(8):1009–1023, 2009.

[23] Morton J Kern and Habib Samady. Current concepts of integrated coronary physiology in the catheterization laboratory. *Journal of the American College of Cardiology*, 55(3):173–185, 2010.

[24] Atsushi Yamamuro, Takashi Akasaka, Koichi Tamita, Kenji Yamabe, Minako Katayama, Tsutomu Takagi, and Shigefumi Morioka. Coronary flow velocity pattern immediately after percutaneous coronary intervention as a predictor of complications and in-hospital survival after acute myocardial infarction. *Circulation*, 106(24):3051–3056, 2002.

[25] Masashi Fukunaga, Kenichi Fujii, Daizo Kawasaki, Hisashi Sawada, Koujiro Miki, Hiroto Tamaru, Takahiro Imanaka, Toshihiro Iwasaku, Tsuyoshi Nakata, Masahiko Shibuya, et al. Thermodilution-derived coronary blood flow pattern immediately after coronary intervention as a predictor of microcirculatory damage and midterm clinical outcomes in patients with st-segment–elevation myocardial infarction. *Circulation: Cardiovascular Interventions*, 7(2):149–155, 2014.

[26] Silvia G Priori, Etienne Aliot, C Bløms trom-Lundqvist, Leo Bossaert, Gunther Breithardt, Pedro Brugada, John A Camm, Riccardo Cappato, Stuart M Cobbe, Carlo Di Mario, et al. Task force on sudden cardiac death, european society of cardiology. *Europace*, 4(1):3–18, 2002.

[27] Kleio Fragkouli and Theodore Vougiouklakis. Sudden cardiac death: an 11-year postmortem analysis in the region of epirus, greece. *Pathology-Research and Practice*, 206(10):690–694, 2010.

[28] Alessandra Doolan, Neil Langlois, Christopher Semsarian, et al. Causes of sudden cardiac death in young australians. *Medical Journal of Australia*, 180(3):110–112, 2004.

[29] Rajesh Puranik, Clara K Chow, Johan A Duflou, Michael J Kilborn, and Mark A McGuire. Sudden death in the young. *Heart Rhythm*, 2(12):1277–1282, 2005.

[30] Yaacov Drory, Yoseph Turetz, Yehuda Hiss, Boaz Lev, Enrique Z Fisman, Amos Pines, and Mordechai R Kramer. Sudden unexpected death in persons¡ 40 years of age. *The American journal of cardiology*, 68(13):1388–1392, 1991.

[31] Swedish national board of health and welfare guidelines for cardiac medical care. *Medical Facts Document*, 2004.

[32] Douglas L Mann, Douglas P Zipes, Peter Libby, and Robert O Bonow. *Braunwald's heart disease: a textbook of cardiovascular medicine*. Elsevier Health Sciences, 2014.

[33] MJ Davies. The composition of coronary-artery plaques, 1997.

[34] Gaetano Antonio Lanza. Cardiac syndrome x: a critical overview and future perspectives. *Heart*, 93(2):159–166, 2007.

[35] Cardiovascular diseases. `https://www1.msjc.edu/hs/hs121/hs121_unit4a_lecture.html`. [Online; accessed 12 December, 2016].

[36] Bio nanotechnology develops nanocontainers for effective treatment of atherosclerosis. `http://www.quantumday.com/2012/06/bio-nanotechnology-develops.html`. [Online; accessed 12 December, 2016].

[37] Alexander W Clowes. Intimal hyperplasia and graft failure. *Cardiovascular Pathology*, 2(3):179–186, 1993.

[38] Andrew C Newby and Alla B Zaltsman. Molecular mechanisms in intimal hyperplasia. *The Journal of pathology*, 190(3):300–309, 2000.

[39] Merce Roque, Lina Badimon, and Juan Jose Badimon. Pathophysiology of unstable angina. *Thrombosis research*, 95(3):V5–V14, 1999.

[40] Curtis M. Rimmerman. Coronary artery disease. http://www.clevelandclinicmeded.com/medicalpubs/diseasemanagement/cardiology/coronary-artery-disease/. [Online; accessed 12 December, 2016].

[41] A Chait. Pathogenesis of macrovascular disease in diabetes. *Joslin's diabetes mellitus*, pages 648–664, 1994.

[42] Y.C. Fung. Biomechanics:. *Circulation, Springer-Verlag,*, pages 446–509., 1997.

[43] Julius M Guccione, Ghassan Sleewa Kassab, Mark B Ratcliffe, et al. *Computational Cardiovascular Mechanics*. Springer, 2010.

[44] Gerard J Tortora and Kevin Petti. *Principles of human anatomy*. John Wiley & Sons, 2002.

[45] YC Fung. Motion, flow, stress, and growth,. In *Biomechanics*. Springer–Verlag, 1990.

[46] Hematology; the study of blood. http://www.seplessons.org/files/take_home_reading_0.pdf. [Online; accessed 12 December, 2016].

[47] Boundless. the aorta and its branches. boundless anatomy and physiology boundless. https://www.boundless.com/physiology/textbooks/boundless-anatomy-and-physiology-textbook/cardiovascular-system-blood-vessels-19/circulatory-routes-189/the-aorta-and-its-branches-936-632/. [Online; accessed 07 January, 2017].

[48] Coronary artery spasm @ONLINE. http://www.texasheart.org/HIC/Topics/Cond/CoronaryArterySpasm.cfm. [Online; accessed 07 January, 2017].

[49] Arteries; the morphology of healthy arteries. http://www.infarktforschung.de/arteries_uk.html. [Online; accessed 07 January, 2017].

[50] Arteries. http://www.teachpe.com/anatomy/arteries.php. [Online; accessed 07 January, 2017].

[51] Elastic arteries. https://www.boundless.com/physiology/textbooks/boundless-anatomy-and-physiology-textbook/cardiovascular-system-blood-vessels-19/arteries-180/elastic-arteries-899-6161/images/anatomy-of-the-arterial-wall/. [Online; accessed 07 January, 2017].

[52] Coronary artery dominance. http://www.wikidoc.org/index.php/Coronary_artery_dominance. [Online; accessed 12 December, 2016].

[53] Left anterior descending artery. http://www.wikidoc.org/index.php/Left_anterior_descending_artery. [Online; accessed 12 December, 2016].

[54] Coronary artery; circumflex artery. http://www.vhlab.umn.edu/atlas/coronary-arteries/circumflex-artery/. [Online; accessed 12 December, 2016].

[55] Understanding and managing high blood pressure. https://www.heart.org/idc/groups/heart-public/@wcm/@hcm/documents/downloadable/ucm_461840.pdf. [Online; accessed 12 December, 2016].

[56] Blood pressure. http://www.heart.org/idc/groups/heart-public/@wcm/@hcm/documents/downloadable/ucm_300310.pdf. [Online; accessed 12 December, 2016].

[57] Angina. http://www.heart.org/HEARTORG/Conditions/HeartAttack/SymptomsDiagnosisofHeartAttack/Angina-Chest-Pain_UCM_450308. [Online; accessed 12 December, 2016].

[58] Coronary artery disease symptoms: Angina types. http://my.clevelandclinic.org/health/articles/cad-symptoms/angina-types. [Online; accessed 07 January, 2017].

[59] Stenosis; dorlands medical dictionary. http://dictionnaire.sensagent.leparisien.fr/Stenosis/en-en/. [Online; accessed 12 December, 2016].

[60] Stenosis. https://en.wikipedia.org/wiki/Stenosis. [Online; accessed 12 December, 2016].

[61] Coronary stenosis. https://http://coronarystenosis.com/left-coronary-artery-stenosis/. [Online; accessed 11 November, 2017].

[62] Nstemi - non-st-segment myocardial infarction. https://www.verywell.com/non-st-segment-elevation-myocardial-infarction-nstemi-1746017. [Online; accessed 12 December, 2016].

[63] Types of heart attacks. http://www.secondscount.org/heart-condition-centers/info-detail-2/types-of-heart-attacks#.WHIb0E1DSJB. [Online; accessed 12 December, 2016].

[64] What is a stemi? https://www.ecgmedicaltraining.com/what-is-a-stemi/. [Online; accessed 12 December, 2016].

[65] Stemi. http://myheart.net/articles/stemi/. [Online; accessed 12 December, 2016].

[66] Percutaneous coronary intervention. https://www.nhlbi.nih.gov/health/health-topics/topics/angioplasty. [Online; accessed 12 December, 2016].

[67] M Lavdaniti. Invasive and non-invasive methods for cardiac output measurement. *International Journal of Caring Sciences*, 1(3):112, 2008.

[68] Eric EC de Waal, Bart WL De Boeck, Cas LJJ Kruitwagen, Maarten JM Cramer, and Wolfgang F Buhre. Effects of on-pump and off-pump coronary artery bypass grafting on left ventricular relaxation and compliance: a comprehensive perioperative echocardiography study. *European Heart Journal-Cardiovascular Imaging*, 11(9):732–737, 2010.

[69] Electrocardiogram (ecg or ekg). http://www.heart.org/HEARTORG/Conditions/HeartAttack/DiagnosingaHeartAttack/Electrocardiogram-ECG-or-EKG_UCM_309050_Article.jsp#.WHL7QlOLSJA. [Online; accessed 10 September, 2016].

[70] DANIEL D Savage, STUART F Seides, Chester E Clark, WALTER L Henry, Barry J Maron, Felipe C Robinson, and Stephen E Epstein. Electrocardiographic findings in patients with obstructive and nonobstructive hypertrophic cardiomyopathy. *Circulation*, 58(3):402–408, 1978.

[71] Gerold Mönnig, Lars Eckardt, Horst Wedekind, Wilhelm Haverkamp, Joachim Gerss, Peter Milberg, Kristina Wasmer, Paulus Kirchhof, Gerd Assmann, Günter Breithardt, et al. Electrocardiographic risk stratification in families with congenital long qt syndrome. *European heart journal*, 27(17):2074–2080, 2006.

[72] Frank I Marcus, William J McKenna, Duane Sherrill, Cristina Basso, Barbara Bauce, David A Bluemke, Hugh Calkins, Domenico Corrado, Moniek GPJ Cox, James P Daubert, et al. Diagnosis of arrhythmogenic right ventricular cardiomyopathy/dysplasia: Proposed modification of the task force criteria. *European heart journal*, pages 806–814, 2010.

[73] Martin Borggrefe Josep Brugada Ramon Brugada Domenico Corrado Ihor Gussak Herve LeMarec Koonlawee Nademanee Andres Ricardo Perez Riera Wataru Shimizu Eric Schulze-Bahr Hanno Tan Arthur Wilde Charles Antzelevitch, Pedro Brugada et al. Brugada sydrome:report of the second consensus conference:. *Circulation*, pages 659–670, 2005.

[74] Derval N. Sacher F. Jesal L. Deisenhofer I. de Roy L. Haissaguerre, M. et al. Sudden cardiac arrest associated with early repolarization. *The New England Journal of Mdicine*, pages 2016–2023, 2008.

[75] Patrick J Fitzsimmons, Paul D McWhirter, David W Peterson, and William B Kruyer. The natural history of wolff-parkinson-white syndrome in 228 military aviators: a long-term follow-up of 22 years. *American heart journal*, 142(3):530–536, 2001.

[76] Ecg: Medlineplus medical encyclopedia image. `https://medlineplus.gov/ency/imagepages/1135.htm`. [Online; accessed 10 September, 2016].

[77] RAF Linton, DM Band, and KM Haire. A new method of measuring cardiac output in man using lithium dilution. *British journal of anaesthesia*, 71(2):262–266, 1993.

[78] Charles Garcia-Rodriguez, James Pittman, Cynthia H Cassell, John Sum-Ping, Habib El-Moalem, Christopher Young, and Jonathan B Mark. Lithium dilution cardiac output measurement: a clinical assessment of central venous and peripheral venous indicator injection. *Critical care medicine*, 30(10):2199–2204, 2002.

[79] Rupert Pearse, Deborah Dawson, Jayne Fawcett, Andrew Rhodes, R Michael Grounds, and E David Bennett. Early goal-directed therapy after major surgery reduces complications and duration of hospital stay. a randomised, controlled trial [isrctn38797445]. *Critical care*, 9(6):R687–R693, 2005.

[80] Duane J Funk, Eugene W Moretti, and Tong J Gan. Minimally invasive cardiac output monitoring in the perioperative setting. *Anesthesia & Analgesia*, 108(3):887–897, 2009.

[81] Christoph K Hofer, Maurizio Cecconi, Gernot Marx, and Giorgio della Rocca. Minimally invasive haemodynamic monitoring. *European Journal of Anaesthesiology (EJA)*, 26(12):996–1002, 2009.

[82] SL King, MS Lim, et al. The use of the oesophageal doppler monitor in the intensive care unit. *Critical Care and Resuscitation*, 6(2):113–122, 2004.

[83] Barry M Chamberlain and Richard J Willshire. Oesophageal doppler monitor (odm) guided individualised goal directed fluid management (igdfm) in surgery-a technical review. *surgery*, 19:21.

[84] Kevin B Laupland and Colin J Bands. Utility of esophageal doppler as a minimally invasive hemodynamic monitor: a review. *Canadian Journal of Anesthesia*, 49(4):393–401, 2002.

[85] Susan Sinclair, Sally James, and Mervyn Singer. Intraoperative intravascular volume optimisation and length of hospital stay after repair of proximal femoral fracture: randomised controlled trial. *Bmj*, 315(7113):909–912, 1997.

[86] Michael Gerard Mythen and Andrew Roy Webb. Perioperative plasma volume expansion reduces the incidence of gut mucosal hypoperfusion during cardiac surgery. *Archives of Surgery*, 130(4):423–429, 1995.

[87] Jeetendra Sharma, Milind Bhise, Ajmer Singh, Yatin Mehta, and Naresh Trehan. Hemodynamic measurements after cardiac surgery: transesophageal doppler versus pulmonary artery catheter. *Journal of cardiothoracic and vascular anesthesia*, 19(6):746–750, 2005.

[88] Duane J Funk, Eugene W Moretti, and Tong J Gan. Minimally invasive cardiac output monitoring in the perioperative setting. *Anesthesia & Analgesia*, 108(3):887–897, 2009.

[89] JN Karnegis, WG Kubicek, RH Mattson, RP Patterson, and DA Witsoe. Development and evaluation of an impedance cardiac output system. 37:1208–1212, 1966.

[90] Bruce D Spiess, Muhammad A Patel, Louise O Soltow, and Ian H Wright. Comparison of bioimpedance versus thermodilution cardiac output during cardiac surgery: evaluation of a second-generation bioimpedance device. *Journal of cardiothoracic and vascular anesthesia*, 15(5):567–573, 2001.

[91] Pierre Squara, Dominique Rotcajg, Dominique Denjean, Philippe Estagnasie, and Alain Brusset. Comparison of monitoring performance of bioreactance vs. pulse contour during lung recruitment maneuvers. *Critical Care*, 13(4):R125, 2009.

[92] Hanan Keren, Daniel Burkhoff, and Pierre Squara. Evaluation of a noninvasive continuous cardiac output monitoring system based on thoracic bioreactance. *American Journal of Physiology-Heart and Circulatory Physiology*, 62(1):H583, 2007.

[93] Ecom endotracheal cardiac output monitor (2004). `http://www.cardiacengineering.com/ECOM.pdf`. [Online; accessed 10 September, 2016].

[94] Peter R. Lichtenthal. Quick guide to cardiopulmonary care. 2002.

[95] Dexter L. Cardiac catheterization in the diagnosis of congenital heart disease. *Bull N Y Acad Med.*, 26:93–102, 1950.

[96] HJC Swan, William Ganz, James Forrester, Harold Marcus, George Diamond, and David Chonette. Catheterization of the heart in man with use of a flow-directed balloon-tipped catheter. *New England Journal of Medicine*, 283(9):447–451, 1970.

[97] Allison J Lee, Jennifer Hochman Cohn, and J Sudharma Ranasinghe. Cardiac output assessed by invasive and minimally invasive techniques. *Anesthesiology research and practice*, 2011, 2011.

[98] Yatin Mehta and KK Sharma. Double knot with formation of a double loop of pulmonary artery catheter. *Journal of cardiothoracic anesthesia*, 4(1):149–150, 1990.

[99] Posner KL Spitellie PH Lee LA Cheney FW. Domino KB, Bowdle TA. Injuries and liability related to central vascular catheters: A closed claims analysis. *Survey of Anesthesiology*, 100:144–1418, 2004.

[100] Joel M Gore, Robert J Goldberg, David H Spodick, Joseph S Alpert, and James E Dalen. A community-wide assessment of the use of pulmonary artery catheters in patients with acute myocardial infarction. *Chest*, 92(4):721–727, 1987.

[101] Eugene D Robin. Death by pulmonary artery flow-directed catheter. time for a moratorium? *CHEST Journal*, 92(4):727–731, 1987.

[102] C Binanay, RM Califf, V Hasselblad, CM O'Connor, MR Shah, G Sopko, LW Stevenson, GS Francis, CV Leier, and LW Miller. Evaluation study of congestive heart failure and pulmonary artery catheterization effectiveness: the escape trial. *Jama*, 294(13):1625–1633, 2005.

[103] Fractional flow reserve. `https://en.wikipedia.org/wiki/Fractional_flow_reserve`. [Online; accessed 06 June, 2016].

[104] Nico HJ Pijls, Berry Van Gelder, Pepijn Van der Voort, Kathinka Peels, Frank ALE Bracke, Hans JRM Bonnier, and Mamdouh IH El Gamal. Fractional flow reserve. *Circulation*, 92(11):3183–3193, 1995.

[105] Berry Colin. Fractional flow reserve, coronary flow reserve and the index of microvascular resistance in clinical practice. *Radcliffe Cardiology*, pages 3183–3193, 2014.

[106] Andy S Yong, Jamie Layland, William F Fearon, Michael Ho, Maulik G Shah, David Daniels, Robert Whitbourn, Andrew MacIsaac, Leonard Kritharides, Andrew Wilson, et al. Calculation of the index of microcirculatory resistance without coronary wedge pressure measurement in the presence of epicardial stenosis. *JACC: Cardiovascular Interventions*, 6(1):53–58, 2013.

[107] Michalis Hamilos, Aaron Peace, George Kochiadakis, Emmanuel Skalidis, Argirios Ntalianis, Bernard De Bruyne, and Panos Vardas. Fractional flow reserve: an indispensable diagnostic tool in the cardiac catheterisation laboratory. *Hellenic J Cardiol*, 51(2):133–141, 2010.

[108] Otto M Hess, Mark J McGillem, Scott F Deboe, Ibraim Mf Pinto, Kim P Gallagher, and GB Mancini. Determination of coronary flow reserve by parametric imaging. *Circulation*, 82(4):1438–1448, 1990.

[109] Nico HJ Pijls, Bernard De Bruyne, Leif Smith, Wilbert Aarnoudse, Emanuele Barbato, Jozef Bartunek, G Jan Willem Bech, and Frans Van De Vosse. Coronary thermodilution to assess flow reserve. *Circulation*, 105(21):2482–2486, 2002.

[110] Nico HJ Pijls, Gerard JH Uijen, Albert Hoevelaken, Theo Arts, WR Aengevaeren, Hans S Bos, Jules H Fast, KL Van Leeuwen, and T Van der Werf. Mean transit time for the assessment of myocardial perfusion by videodensitometry. *Circulation*, 81(4):1331–1340, 1990.

[111] Wilbert Aarnoudse, Petra van den Berg, Frans van de Vosse, Maartje Geven, Marcel Rutten, Mark van Turnhout, William Fearon, Bernard De Bruyne, and Nico Pijls. Myocardial resistance assessed by guidewire-based pressure-temperature measurement: In vitro validation. *Catheterization and cardiovascular interventions*, 62(1):56–63, 2004.

[112] William F Fearon, Leora B Balsam, HM Omar Farouque, Robert C Robbins, Peter J Fitzgerald, Paul G Yock, and Alan C Yeung. Novel index for invasively assessing the coronary microcirculation. *Circulation*, 107(25):3129–3132, 2003.

[113] William F Fearon. Index of microcirculatory resistance.

[114] William F Fearon, Wilbert Aarnoudse, Nico HJ Pijls, Bernard De Bruyne, Leora B Balsam, David T Cooke, Robert C Robbins, Peter J Fitzgerald, Alan C Yeung, and Paul G Yock. Microvascular resistance is not influenced by epicardial coronary artery stenosis severity. *Circulation*, 109(19):2269–2272, 2004.

[115] Wilbert Aarnoudse, William F Fearon, Ganesh Manoharan, Maartje Geven, Frans van de Vosse, Marcel Rutten, Bernard De Bruyne, and Nico HJ Pijls. Epicardial stenosis severity does not affect minimal microcirculatory resistance. *Circulation*, 110(15):2137–2142, 2004.

[116] Andy SC Yong, Michael Ho, Maulik G Shah, Martin KC Ng, and William F Fearon. Coronary microcirculatory resistance is independent of epicardial stenosis. *Circulation: Cardiovascular Interventions*, 5(1):103–108, 2012.

[117] Jamie Layland, Andrew I MacIsaac, Andrew T Burns, Jithendra B Somaratne, George Leitl, Robert J Whitbourn, and Andrew M Wilson. When collateral supply is accounted for epicardial stenosis does not increase microvascular resistance. *Circulation: Cardiovascular Interventions*, 5(1):97–102, 2012.

[118] Anna Gawlinski. Measuring cardiac output: intermittent bolus thermodilution method. *Critical Care Nurse*, 24(5):74–78, 2004.

[119] Nico HJ Pijls, Bernard De Bruyne, Leif Smith, Wilbert Aarnoudse, Emanuele Barbato, Jozef Bartunek, G Jan Willem Bech, and Frans Van De Vosse. Coronary thermodilution to assess flow reserve. *Circulation*, 105(21):2482–2486, 2002.

[120] Measurement of cardiac output. `http://www.cvphysiology.com/Cardiac%20Function/CF021`. [Online; accessed 10 September, 2016].

[121] K. A. Watson, S: Gorski. *Invasive Cardiology*. Jones & Bartlett Learning Publishing, 3 edition, 2001.

[122] Pim AL Tonino, Bernard De Bruyne, Nico HJ Pijls, Uwe Siebert, Fumiaki Ikeno, Marcel vant Veer, Volker Klauss, Ganesh Manoharan, Thomas Engstrøm, Keith G Oldroyd, et al. Fractional flow reserve versus angiography for guiding percutaneous coronary intervention. *New England Journal of Medicine*, 360(3):213–224, 2009.

[123] Eugene Evonuk, Charles J Imig, Wilbert Greenfield, and John W Eckstein. Cardiac output measured by thermal dilution of room temperature injectate. *Journal of applied physiology*, 16(2):271–275, 1961.

[124] William Ganz, Roberto Donoso, Harold S Marcus, James S Forrester, and Harold JC Swan. A new technique for measurement of cardiac output by thermodilution in man. *The American journal of cardiology*, 27(4):392–396, 1971.

[125] Uri Elkayam, Robert Berkley, Stanley Azen, Laura Weber, Boaz Geva, and Walter L Henry. Cardiac output by thermodilution technique: Effect of injectate's volume and temperature on accuracy and reproducibility in the critically iii patient. *Chest*, 84(4):418–422, 1983.

[126] Ronald G Pearl, Myer H Rosenthal, Lis Nielson, JP Ashton, and BW Brown Jr. Effect of injectate volume and temperature on thermodilution cardiac output determination. *Anesthesiology*, 64(6):798–801, 1986.

[127] Thomas V Bilfinger, Chung-Yuan Lin, and Constantine E Anagnostopoulos. In vitro determination of accuracy of cardiac output measurements by thermal dilution. *Journal of Surgical Research*, 33(5):409–414, 1982.

[128] Christian W Stetz, Rupert G Miller, Gabriel E Kelly, and Thomas A Raffin. Reliability of the thermodilution method in the determination of cardiac output in clinical practice 1, 2. *American Review of Respiratory Disease*, 126(6):1001–1004, 1982.

[129] FG Shellock and MS Riedinger. Reproducibility and accuracy of using room-temperature vs. ice-temperature injectate for thermodilution cardiac output determination. *Heart & lung: the journal of critical care*, 12(2):175–176, 1983.

[130] CV Vennix, DH Nelson, and GL Pierpont. Thermodilution cardiac output in critically ill patients: comparison of room-temperature and iced injectate. *Heart & lung: the journal of critical care*, 13(5):574–578, 1984.

[131] Loren D Nelson and Hans B Anderson. Patient selection for iced versus room temperature injectate for thermodilution cardiac output determinations. *Critical care medicine*, 13(3):182–184, 1985.

[132] Neil Buchbinder and William Ganz. Hemodynamic monitoringinvasive techniques. *The Journal of the American Society of Anesthesiologists*, 45(2):146–155, 1976.

[133] WB Runciman, AH Ilsley, and JG Roberts. An evaluation of thermodilution cardiac output measurement using the swan-ganz catheter. *Anaesthesia and intensive care*, 9(3):208–220, 1981.

[134] RH Woog and DB McWilliam. A comparison of methods of cardiac output measurement. *Anaesthesia and intensive care*, 11(2):141–146, 1983.

[135] Replogle RL. Levett JM. Thermodilution cardiac output: a critical analysis and review of the literature. 27:392–404., 1979.

[136] Kenneth L Zierler et al. Theoretical basis of indicator-dilution methods for measuring flow and volume. *Circ Res*, 10(3):393–407, 1962.

[137] A FRONĚ and V Ganz. Measurement of flow in single blood vessels including cardiac output by local thermodilution. *Circulation Research*, 8(1):175–182, 1960.

[138] Toshiaki Nlshikawa and Shuji Dohi. Slowing of heart rate during cardiac output measurement by thermodilution. *The Journal of the American Society of Anesthesiologists*, 57(6):538–539, 1982.

[139] Andrew Harris, Clair F Miller, CHARLES Beattie, GILBERT I Rosenfeld, and Mark Charles Rogers. The slowing of sinus rhythm during thermodilution cardiac output determination and the effect of altering injectate temperature. *Anesthesiology*, 63(5):540–541, 1985.

[140] Toshiaki Nishikawa and Shuji Dohi. Hemodynamic status susceptible to slowing of heart rate during thermodilution cardiac output determination in anesthetized patients. *Critical care medicine*, 18(8):841–844, 1990.

[141] Toshiaki Nishikawa and Akiyoshi Namiki. Mechanism for slowing of heart rate and associated changes in pulmonary circulation elicited by cold injectate during thermodilution cardiac output determination in dogs. *Anesthesiology*, 68(2):221–225, 1988.

[142] Powner DJ. Thermodilution technic for cardiac output (correspondence). *N Engl J Med*, 293:1210–1211, 1975.

[143] WB Runciman, AH Ilsley, and JG Roberts. Thermodilution cardiac output–a systematic error. *Anaesthesia and intensive care*, 9(2):135–139, 1981.

[144] H Meisner, S Glanert, B Steckmeier, E Gams, S Hagl, W Heimisch, F Sebening, and K Messmer. Indicator loss during injection in the thermodilution system. *Research in Experimental Medicine*, 159(3):183–196, 1973.

[145] MA Branthwaite and RD Bradley. Measurement of cardiac output by thermal dilution in man. *Journal of Applied Physiology*, 24(3):434–438, 1968.

[146] M Bredgaard Sorensen, NE Bille-Brahe, and HC Engell. Cardiac output measurement by thermal dilution: reproducibility and comparison with the dye-dilution technique. *Annals of surgery*, 183(1):67, 1976.

[147] William Ganz and HJC Swan. Measurement of blood flow by thermodilution. *The American journal of cardiology*, 29(2):241–246, 1972.

[148] Richard D Weisel, Louis Vito, Richard C Dennis, Robert L Berger, and Herbert B Hechtman. Clinical applications of thermodilution cardiac output determinations. *The American Journal of Surgery*, 129(4):449–454, 1975.

[149] Richard D Weisel, Robert L Berger, and Herbert B Hechtman. Measurement of cardiac output by thermodilution. *New England Journal of Medicine*, 292(13):682–684, 1975.

[150] M Woods, RN Scott, and AH Harken. Practical considerations for the use of a pulmonary artery thermistor catheter. *Surgery*, 79(4):469–475, 1976.

[151] HANS U Wessel, Milton H Paul, Gordon W James, and ALLAN R Grahn. Limitations of thermal dilution curves for cardiac output determinations. *Journal of applied physiology*, 30(5):643–652, 1971.

[152] Skoda Afonso, JF Herrick, WB Youmans, GG Rowe, and CW Crumpton. Temperature variations in the venous system of dogs. *American Journal of Physiology–Legacy Content*, 203(2):278–282, 1962.

[153] Hans U Wessel, Gordon W James, and Milton H Paul. Effects of respiration and circulation on central blood temperature of the dog. *American Journal of Physiology–Legacy Content*, 211(6):1403–1412, 1966.

[154] MS Riedinger and FG Shellock. Technical aspects of the thermodilution method for measuring cardiac output. *Heart & lung: the journal of critical care*, 13(3):215–222, 1984.

[155] E Enghoff and S Sjögren. Thermal dilution for measurement of cardiac output in the pulmonary artery in man in relation to choice of indicator volume and injection time. *Upsala journal of medical sciences*, 78(1):33, 1973.

[156] A Saadjian, JE Quercy, and J Torresani. Cardiac output measurement by thermodilution: methodologic problems. *Medical progress through technology*, 3(4):161–167, 1976.

[157] A Versprille. Thermodilution in mechanically ventilated patients. *Intensive care medicine*, 10(5):213–215, 1984.

[158] Loren D Nelson and Bruce A Houtchens. Automatic vs manual injections for thermodilution cardiac output determinations. *Critical care medicine*, 10(3):190–192, 1982.

[159] RC WETZELL and Terry W Latson. Major errors in thermodilution cardiac output measurement during rapid volume infusion. *Anesthesiology*, 62(5):684–687, 1985.

[160] Frank G Shellock and Mary S Riedinger. Hemodynamic measurement errors caused by catheter introducers. *Catheterization and Cardiovascular Interventions*, 8(3):319–319, 1982.

[161] Douglas S Moodie, Robert H Feldt, Michael P Kaye, David A Strelow, and Lois J van der Hagen. Measurement of cardiac output by thermodilution: development of accurate measurements at flows applicable to the pediatric patient. *Journal of Surgical Research*, 25(4):305–311, 1978.

[162] Susan L Norris, E Garner King, Michael Grace, and Bryce Weir. Thermodilution cardiac output-an in vitro model of low flow states. *Critical care medicine*, 14(1):57–59, 1986.

[163] Sophie Nadeau and William H Noble. Limitations of cardiac output measurements by thermodilution. *Canadian Journal of Anesthesia/Journal canadien d'anesthésie*, 33(6):780–784, 1986.

[164] Fulachier V Setbon F Gouin E Martin C. Saux P, Auffray JP. Thermodilution cardiac output measurements by injection in pulmonary artery vs cvp catheter. *Anesthesia & Analgesia*, (11):460–461, 1983.

[165] David G Bjoraker and Thomas R Ketcham. Catheter thrombus artifactually decreases thermodilution cardiac output measurements. *Anesthesia & Analgesia*, 62(11):1031–1034, 1983.

[166] Gene R Pesola and Graziano C Carlon. Thermodilution cardiac output: Proximal lumen versus right ventricular port. *Critical care medicine*, 19(4):563–565, 1991.

[167] Mark G Bearss, David N Yonutas, and William T Allen. A complication with thermodilution cardiac outputs in centrally-placed pulmonary artery catheters. *CHEST Journal*, 81(4):527b–527, 1982.

[168] Joseph Curley, Francis Harte, and Farhan Sheikh. Erroneous cardiac output determination due to pulmonary artery catheter proximal port dysfunction. *The Journal of the American Society of Anesthesiologists*, 64(5):662–662, 1986.

[169] James K Stoller, Timothy J Herbst, William Hurford, and Michael A Rie. Spuriously high cardiac output from injecting thermal indicator through an ensheathed port. *Critical care medicine*, 14(12):1064–1065, 1986.

[170] M Andreen. Computerized measurement of cardiac output by thermodilution: methodological aspects. *Acta Anaesthesiologica Scandinavica*, 18(4):297–305, 1974.

[171] A Landais, JP Morin, A Roche, C Cornec, and N Sansoy. Measurement of cardiac output by the thermodilution method during left thoracotomy in the lateral position in the dog. *Acta Anaesthesiologica Scandinavica*, 34(2):158–161, 1990.

[172] Faysal M Hasan, Anthony Malanga, William M Corrao, and Sidney S Braman. Effect of catheter position on thermodilution cardiac output during continuous positive-pressure ventilation. *Critical care medicine*, 12(4):387–390, 1984.

[173] Fred Morady, Bruce H Brundage, and Harris J Gelberg. Rapid method for determination of shunt ratio using a thermodilution technique. *American heart journal*, 106(2):369–373, 1983.

[174] Gunnel Hedvall. The applicability of the thermodilution method for determination of pulmonary blood flow and pulmonary vascular resistance in infants and children with ventricular septal defects. *Scandinavian journal of clinical and laboratory investigation*, 38(6):581–585, 1978.

[175] Eric D Silove, MJ Tynan, and AJ Simcha. Thermal dilution measurement of pulmonary and systemic blood flow in secundum atrial septal defect, and transposition of great arteries with intact interventricular septum. *British heart journal*, 34(11):1142, 1972.

[176] Peeter Jögi and Olof Werner. Left-to-right shunt assessed by thermodilution during surgery for congenital heart disease. *Scandinavian journal of thoracic and cardiovascular surgery*, 21(3):203–206, 1987.

[177] Corey A Burchman and Demetrios G Lappas. Thermodilution cardiac output provides unanticipated intraoperative diagnosis. *Journal of cardiothoracic anesthesia*, 2(4):584–585, 1988.

[178] SM McGuirk, FH Welker, WW Muir, and BL Hull. Thermodilution curves for diagnosis of ventricular septal defect in cattle. *Journal of the American Veterinary Medical Association*, 184(9):1141–1145, 1984.

[179] Fred Kahan, Joseph Profeta, and Daniel Thys. High cardiac output measurements in a patient with congestive heart failure. *Journal of cardiothoracic anesthesia*, 1(3):234–236, 1987.

[180] Ronald G Pearl and Lawrence C Siegel. Thermodilution cardiac output measurement with a large left-to-right shunt. *Journal of Clinical Monitoring and Computing*, 7(2):146–153, 1991.

[181] Michael D Freed and John F Keane. Cardiac output measured by thermodilution in infants and children. *The Journal of pediatrics*, 92(1):39–42, 1978.

[182] Jurgen Beyer, John J Lamberti, Robert L Replogle, Helmut Kundler, and Diane Schwarz. Validity of thermodilution cardiac output determination: experimental studies with and without pulmonary insufficiency. *Journal of Surgical Research*, 21(5):313–317, 1976.

[183] B Olsson, J Pool, P Vandermoten, E Varnauskas, and R Wassen. Validity and reproducibility of determination of cardiac output by thermodilution in man. *Cardiology*, 55(3):136–148, 1970.

[184] Scott W Sharkey. Beyond the wedge: clinical physiology and the swan-ganz catheter. *The American journal of medicine*, 83(1):111–122, 1987.

[185] H Ohteki, H Nagara, J Wada, Y Inoue, and S Kimata. Measurement of cardiac output by thermodilution and fick methods in man–problems in case of tricuspid regurgitation (author's transl). *Kokyu to junkan. Respiration & circulation*, 29(4):433, 1981.

[186] Hillel I Kashtan, Andrew Maitland, Tomas A Salerno, Samual V Lichtenstein, and Robert J Byrick. Effects of tricuspid regurgitation on thermodilution cardiac output: studies in an animal model. *Canadian journal of anaesthesia*, 34(3):246–251, 1987.

[187] L David Hillis, Brian G Firth, and Michael D Winniford. Analysis of factors affecting the variability of fick versus indicator dilution measurements of cardiac output. *The American journal of cardiology*, 56(12):764–768, 1985.

[188] Shahbudin H Rahimtoola and HJC Swan. Calculation of cardiac output from indicator-dilution curves in the presence of mitral regurgitation. *Circulation*, 31(5):711–718, 1965.

[189] Philip Samet, William H Bernstein, and Cesar Castillo. Validity of indicator-dilution determinations of cardiac output in patients with mitral regurgitation. *Circulation*, 33(3):410–416, 1966.

[190] Philip Samet, Cesar Castillo, and William H Bernstein. Validity of indicator-dilution determination of cardiac output in patients with aortic regurgitation. *circulation*, 34(4):609–610, 1966.

[191] SD Wyse, J Pfitzner, A Rees, JC Lincoln, and MA Branthwaite. Measurement of cardiac output by thermal dilution in infants and children. *Thorax*, 30(3):262–265, 1975.

[192] M Mathur, EA Harris, S Yarrow, and BG Barratt-Boyes. Measurement of cardiac output by thermodilution in infants and children after open-heart operations. *The Journal of thoracic and cardiovascular surgery*, 72(2):221–225, 1976.

[193] Frank J Colgan and Scott Stewart. An assessment of cardiac output by thermodilution in infants and children following cardiac surgery. *Critical care medicine*, 5(5):220–225, 1977.

[194] Ottavio Alfieri and S Subramanian. Cardiac output determination in infants and small children after open intracardiac operations. *The Annals of thoracic surgery*, 19(3):322–326, 1975.

[195] Gary F Maruschak, Alan M Potter, James F Schauble, and MARK C Rogers. Overestimation of pediatric cardiac output by thermal indicator loss. *Circulation*, 65(2):380–383, 1982.

[196] Hans Meisner, Siegfried Hagl, Werner Heimisch, Norbert Mayr, Nikolaus Mendler, Eberhard Struck, Volker Walther, and Fritz Sebening. Evaluation of the thermodilution method for measurement of cardiac output after open-heart surgery. *The Annals of thoracic surgery*, 18(5):504–515, 1974.

[197] Joel D Baskoff and Gary F Maruschak. Correction factor for thermodilution determination of cardiac output in children. *Critical care medicine*, 9(12):870–872, 1981.

[198] Hiroshi Kanai, Masahiko Iizuka, and Katsuyuki Sakamoto. One of the problems in the measurement of blood pressure by catheter-insertion: Wave reflection at the tip of the catheter. *Medical and biological engineering*, 8(5):483–496, 1970.

[199] Nico HJ Pijls, Morton J Kern, Paul G Yock, and Bernard De Bruyne. Practice and potential pitfalls of coronary pressure measurement. *Catheterization and cardiovascular interventions*, 49(1):1–16, 2000.

[200] Herman L Falsetti, Robert E Mates, Robyn J Carroll, Ramji L Gupta, and Adam C Bell. Analysis and correction of pressure wave distortion in fluid-filled catheter systems. *Circulation*, 49(1):165–172, 1974.

[201] L Jerome Krovetz, Rufus B Jennings, and Stephen D Goldbloom. Limitation of correction of frequency dependent artefact in pressure recordings using harmonic analysis. *Circulation*, 50(5):992–997, 1974.

[202] Reed M Gardner. Direct arterial pressure monitoring. *Current Anaesthesia & Critical Care*, 1(4):239–246, 1990.

[203] JK Li, AG van Brummelen, and ABRAHAM Noordergraaf. Fluid-filled blood pressure measurement systems. *Journal of applied physiology*, 40(5):839–843, 1976.

[204] MWB Allan, WM Gray, and AJ Asbury. Measurement of arterial pressure using catheter-transducer systems improvement using the accudynamic. *British journal of anaesthesia*, 60(4):413–418, 1988.

[205] BC Taylor and FM Donovan. Hydraulic resistance and damping in catheter-transducer systems. *IEEE Engineering in Medicine and Biology Magazine*, 11(4):72–78, 1992.

[206] NR Gaddum, J Alastruey, P Beerbaum, P Chowienczyk, and T Schaeffter. A technical assessment of pulse wave velocity algorithms applied to non-invasive arterial waveforms. *Annals of biomedical engineering*, 41(12):2617–2629, 2013.

[207] Damien Kenny, Jaimie W Polson, Robin P Martin, Massimo Caputo, Dirk G Wilson, John R Cockcroft, Julian FR Paton, and Andrew R Wolf. Relationship of aortic pulse wave velocity and baroreceptor reflex sensitivity to blood pressure control in patients with repaired coarctation of the aorta. *American heart journal*, 162(2):398–404, 2011.

[208] Kohichiro Iwasaki and Shozo Kusachi. Coronary pressure measurement based decision making for percutaneous coronary intervention. *Current cardiology reviews*, 5(4):323–333, 2009.

[209] Lawrence A Garcia and Joseph P Carrozza. Physiologic evaluation of translesion pressure gradients in peripheral arteries: Comparison of pressure wire and catheter-derived measurements. *Journal of interventional cardiology*, 20(1):63–65, 2007.

[210] LH Back. Estimated mean flow resistance increase during coronary artery catheterization. *Journal of biomechanics*, 27(2):169–175, 1994.

[211] Angelika Costard-Jäckle and Michael B Fowler. Influence of preoperative pulmonary artery pressure on mortality after heart transplantation: testing of potential reversibility of pulmonary hypertension with nitroprusside is useful in defining a high risk group. *Journal of the American College of Cardiology*, 19(1):48–54, 1992.

[212] Nicholas R Banner, Robert S Bonser, Andrew L Clark, Stephen Clark, Peter J Cowburn, Roy S Gardner, Paul R Kalra, Theresa McDonagh, Chris A Rogers, Lorna Swan, et al. Uk guidelines for referral and assessment of adults for heart transplantation. *Heart*, 97(18):1520–1527, 2011.

[213] Thermodilution: Methods and applications. https://intensivecareunit.wordpress.com/2008/09/20/thermodilution-methods-and-applications/. [Online; accessed 05 Semtember, 2016].

[214] JUNICHI TAJIRI, HIROTADA KATSUYA, KAZUFUMI OKAMOTO, KENJI URATA, and TATSUO SATO. The effects of the respiratory cycle by mechanical ventilation on cardiac output measured using the thermodilution method. *Japanese circulation journal*, 48(4):328–330, 1984.

[215] Edward J Reininger and Bart L Troy. Error in thermodilution cardiac output measurement caused by variation in syringe volume. *Catheterization and Cardiovascular Interventions*, 2(4):415–417, 1976.

[216] KE Hammermeister and John Vandamme. A simple, new system for maintaining measured quantities of saline cold and sterile for thermodilution cardiac output measurement. *Catheterization and cardiovascular diagnosis*, 5(1):95–99, 1979.

[217] Rajindar Singh, Alfred J Ranieri, H Ryland Vest, Donald L Bowers, and J Francis Dammann. Simultaneous determinations of cardiac output by thermal dilution, fiberoptic and dye-dilution methods. *The American journal of cardiology*, 25(5):579–587, 1970.

[218] Joseph Armengol, Godfrey CW Man, Aras J Balsys, and Allan L Wells. Effects of the respiratory cycle on cardiac output measurements: Reproducibility of data enhanced by timing the thermodilution injections in dogs. *Critical care medicine*, 9(12):852–854, 1981.

[219] JUNICHI TAJIRI, HIROTADA KATSUYA, KAZUFUMI OKAMOTO, KENJI URATA, and TATSUO SATO. The effects of the respiratory cycle by mechanical ventilation on cardiac output measured using the thermodilution method. *Japanese circulation journal*, 48(4):328–330, 1984.

[220] Kazufumi Okamoto, Toru Komatsu, Vijaya Kumar, Vajubhai Sanchala, Keshav Kubal, Ramesh Bhalodia, and Kinichi Shibutani. Effects of intermittent positive-pressure ventilation on cardiac output measurements by thermodilution. *Critical care medicine*, 14(11):977–980, 1986.

[221] John H Stevens, Thomas A Raffin, Frederick G Mihm, Myer H Rosenthal, and Christian W Stetz. Thermodilution cardiac output measurement: Effects of the respiratory cycle on its reproducibility. *Jama*, 253(15):2240–2242, 1985.

[222] James V Snyder and David J Powner. Effects of mechanical ventilation on the measurement of cardiac output by thermodilution. *Critical care medicine*, 10(10):677–682, 1982.

[223] JR Jansen, JJ Schreuder, JM Bogaard, W Van Rooyen, and A Versprille. Thermodilution technique for measurement of cardiac output during artificial ventilation. *Journal of Applied Physiology*, 51(3):584–591, 1981.

[224] Tim Fisher. What is a dat file? https://www.lifewire.com/what-is-a-dat-file-2620550. [Online; accessed 25 January, 2017].

[225] Gaussian models: Mathworks. https://www.mathworks.com/help/curvefit/gaussian.html. [Online; accessed 25 October, 2017].

[226] Evaluating goodness of fit: Mathworks. https://www.mathworks.com/help/curvefit/evaluating-goodness-of-fit.html?

searchHighlight=r-SQUARE&s_tid=doc_srchtitle&requestedDomain=www.mathworks.com. [Online; accessed 25 October, 2017].

[227] Chiu David Chiu Yu-Wei. *Machine learning with R cookbook*. Packt Publishing Ltd, 2015.

[228] Nina Zumel, John Mount, and Jim Porzak. *Practical data science with R*. Manning, 2014.

[229] Richard H Pletcher, John C Tannehill, and Dale Anderson. *Computational fluid mechanics and heat transfer*. CRC Press, 2012.

[230] Timothy J Pedley. *The fluid mechanics of large blood vessels*, volume 1. Cambridge University Press Cambridge, 1980.

[231] Fluent 6.3 user's guide - 13.2.1 heat transfer theory. https://www.sharcnet.ca/Software/Fluent6/html/ug/node568.htm. [Online; accessed 05 January, 2017].

[232] DJ Acheson. Elementary fluid dynamics: Oxford applied mathematics and computing science series, 1990.

[233] Alexandre Joel Chorin, Jerrold E Marsden, and Jerrold E Marsden. *A mathematical introduction to fluid mechanics*, volume 3. Springer, 1990.

[234] Paul K Newton. *The N-vortex problem: analytical techniques*, volume 145. Springer Science & Business Media, 2013.

[235] Peter. S. Stewart. Fluid mechanics notes, 28 September, 2015.

[236] Turbulent flow. http://www.cvphysiology.com/Hemodynamics/H007. [Online; accessed 05 January, 2017].

[237] Blood circulation. http://fblt.cz/en/skripta/x-srdce-a-obeh-krve/2-krevni-obeh/. [Online; accessed 05 January, 2017].

[238] Poiseuille flow. http://mahi.ucsd.edu/guy/sio224/stokes-part2.pdf. [Online; accessed 05 January, 2017].

[239] Water flow in a pipe. http://zeus.plmsc.psu.edu/~manias/MatSE447/04_FlowInVariedGeometries.pdf. [Online; accessed 05 January, 2017].

[240] Laminar pipe flow: Numerical results. https://confluence.cornell.edu/display/SIMULATION/Laminar+Pipe+Flow+-+Numerical+Results. [Online; accessed 15 November, 2017].

[241] Ansys fluent: Cfd simulation. http://www.ansys.com/Products/Fluids/ANSYS-Fluent. [Online; accessed 05 January, 2017].

[242] Residuals. https://www.cfd-online.com/Forums/fluent/28009-residuals.html. [Online; accessed 05 January, 2017].

[243] Hao Gao. Fluent tutorial presentations; university of glasgow. 2016.